The University of Nottingham

Department of Chemical and Environmental Engineering

Film Behaviour of Vertical Gas-Liquid Flow in a Large Diameter Pipe

By

Mohammed Haseeb Sedeeq Zangana, MSc, BSc.

Thesis submitted to The University of Nottingham

for the degree of Doctor of Philosophy,

May 2011

Abstract

Gas-liquid flow commonly occurs in oil and gas production and processing system. Large diameter vertical pipes can reduce pressure drops and so minimize operating costs. However, there is a need for research on two-phase flow in large diameter pipes to provide confidence to designers of equipments such as deep water risers.

In this study a number of experimental campaigns were carried out to measure pressure drop, liquid film thickness and wall shear in 127mm vertical pipe. Total pressure drop were studied systematically through a data bank of 600 experimental runs. Magnitude and directional wall shear stress measurements have been made selectively using commercial non-directional probes and directional hot films. The latter were produced at Nottingham University during this study. Experimental data on liquid film characteristics were obtained by measuring total pressure drop, wall shear stress and film thickness simultaneously. In addition, the data were supported by some high speed video images through a visualization campaign.

The pressure drop profile (time-averaged total pressure drop as a function of gas flow rate) introduced is visibly different from that for smaller pipes as it does not show a clear minima in the churn-annular transition region and not in both bubble-slug and slug-churn region.

No completely unidirectional upward flow has been observed in the range of the conditions studied from the results of directional wall shear stress measurement which provided information on both time-varying and time-averaged wall shear stress. A condition of zero wall shear stress not reached

However, there was a minimum observed in the plot of mean wall shear stress against dimensionless gas velocity. This minimum occurred at the same dimensionless velocity for the present data at those from small diameter pipes. The change in the direction of the liquid film also supported by the measurements of local film thickness and high speed video images which have shown waves move both upward and downward and not purely in axial direction.

To my brothers Mariwan and Kamaran and all my relatives who lost their lives during the Anfal process

To my parents

To my wife and my son

Acknowledgements

I would like to express my gratitude to my supervisor Professor B.J. Azzopardi for his guidance, support, patience and encouragement. I greatly appreciate that he devoted time to my queries and was forthcoming with advice and suggestions. I would also like to acknowledge Dr.Christopher Mellor and Jasbinder Chauhan from the school of Physics and Astronomy for their work with enthusiasm on the manufacture of the directional wall shear stress probes.

Very special thanks and appreciation are due to the Ministry of Higher Education in the Kurdistan Regional Government (KRG) of Iraq for providing me the financial support to carry out my PhD. My special thanks are also go to Koya University; in particular I would like to thank the university president Professor Khidir Hawrami for his support and encouragement during my study. Thanks to all my friends and colleagues at College of Engineering - Koya University for their understanding and staying in touch while far away which meant a lot to me. I also owe a great deal of thanks to Kareem Hassan for his encouragement and constant support throughout my study.

Thanks to the UK Engineering and Physical Sciences Research Council (EPSRC) and the following: - Advantica; BP Exploration; CD-adapco; Chevron; ConocoPhillips; ENI; ExxonMobil; FEESA; IFP; Institutt for Energiteknikk; Norsk Hydro; PDVSA (INTERVEP); Petrobras; PETRONAS;

Scandpower PT; Shell; SINTEF; Statoil and TOTAL for their contributions to this project.

My sincere thanks to the technical staff in the Department of Chemical and Environmental Engineering: Fred, Phil, Paul, David Clift, Jim, Marion, Mel, Mick, Reg and Terry for their support and help during my experimental work, particularly the electronic technician Fred who was very helpful in the preparations of the measurement techniques and Paul for the rig construction.

I would specially like to thank all the members of Multiphase group here at Nottingham University: Lokman, Peter, Safa, Nazrul, Mukhtar, Abdulahi, Ezekiel, Kajero, Bayo, Kaji, Dr.Valenti, Dr.Donglin and the visitor Professor Azzi, for their help and friendship throughout my Ph.D study.

Finally, I should not forget to thank my parents, my wife, my brothers and my sisters for their understanding, patience and support.

Table of Contents

List of Figures

List of Tables

Chapter 1

Introduction

1.1 Two-Phase Gas-Liquid Flow

Two-phase gas-liquid flow occurs most frequently in well tubing and flow lines in oil and gas production systems. In off-shore production; this type of flow occurs in large diameter risers connecting the sea bed to a platform or floating production, storage and offloading (FPSO) units. It also occurs in pipelines during the transportation of gas and liquid phases together over long distances before separation (Figures 1.1 and 1.2). Two phase flow is more complicated than single phase flow due to the complex nature of the interface between the two phases. Therefore an accurate design of these facilities with minimum cost and high operation efficiency requires a good understanding of the behavior of such flows. In particular those parameters that known as an important designing elements, e.g., pressure drop. Gas-liquid flow is not unique to the petroleum industry as occurs also in chemical processing equipments such as condensers, heat exchangers and reactors. The flow may be vertical, horizontal or inclined. Vertical upward two phase flow known as one of the common types of flow in the mentioned fields of industry hence this is the focus of the present study. Gas and liquid with different physical

properties when they flow together inside a pipe they arrange themselves at different geometrical configurations called flow patterns or flow regimes. For co-current gas and liquid up-flow in vertical pipe, there are in general four main flow patterns; ***Bubbly, Slug, Churn*** and ***Annular flow*** (Figure 1.3). Detail of this classification can be found in many of the text books on two phase flow, e.g., Hewitt and Hall-Taylor (1970), Brill and Mukherjee (1999) and Azzopardi (2006) which can be summarized in terms of increasing gas flow rate as given below:

Bubbly flow: The liquid phase is continuous while the gas phase dispersed as bubbles within the liquid continuum.

Slug (or plug) flow: This flow pattern occurs when coalescence begins, and the bubble size tends towards that of the channel. Characteristically consists of a large bullet-shaped (Taylor) bubbles which have nearly the same cross-section as the channel, separated by slugs of liquid containing smaller bubbles. An important feature of this regime is the liquid phase surrounding the large bubbles in the form of a falling film.

Churn flow: It is an oscillatory flow in which parts of the liquid travel alternatively upward and downward. Churn flow with its characteristic oscillations is an important pattern and, often covering a fairly wide range of gas flow rate. At its higher range of gas velocity, the liquid consists mainly of a thick film on the pipe wall covered with large waves. Therefore, in that sense the term semi-annular can be used for this flow pattern. However, researchers, e.g., Hewitt and Hall-Taylor (1970), prefer the more general term "churn" to cover the whole region.

Annular flow: In this flow pattern the gas flows in the centre as a central core

and the liquid flows upwards as a film on the pipe wall and entrained in the gas core as small droplets and it is also possible for the liquid film to contain some of the gas bubbles. There are usually waves on the gas-film interface and a continuous exchange of liquid between the core and the film.

In most of the flow regimes as described above the liquid phase is travelling partly as a film on the pipe wall regardless of its direction, thickness and the roughness of its surface. In annular type flow the thickness of liquid film on the pipe wall is related to both the liquid film flow rate and wall shear stress according to the triangular relationship (Hewitt and Hall-Taylor, 1970). For same type of flow a close relationship between the liquid film thickness and wall shear stress were reported by Martin and Whalley (1983). Both shear stress and liquid film thickness are strongly related to the total pressure drop and the latter consists of three components which are frictional, gravitational and acceleration pressure drop (Hewitt and Whalley, 1989, Brill and Mukherjee, 1999 and Azzopardi, 2006) (see Section 2.2). The frictional term of pressure drop is represented by shear stress. The gravitational term corresponds to the weight of fluid per unit length of channel which is dominated by the liquid holdup; in annular flow, the liquid holdup is, in turn, dominated by the liquid film (the holdup in the entrained drops is usually small). Besides, the acceleration component of total pressure drop is normally negligible in adiabatic flows. Therefore, in the semi-annular and annular flow patterns the total pressure drop in vertical gas-liquid flow is significantly affected by the liquid film properties such as the thickness of the film, the interfacial roughness of the surface of the film and the shear stress on the pipe

wall. Therefore the measurements of such parameters, i.e., liquid film thickness, wall shear stress and total pressure drop can provide very useful information on the liquid film behavior and the overall behavior of the flow.

1.2 Gas-liquid flow in large diameter vertical pipes

Arguably large diameter pipes are nowadays being used much more by industry, particularly in oil and gas offshore production as there is a real challenge due to the pressure drop during transportation of gas and liquid together from the sea bed to the platforms. This is especially so because of the move into deeper water. Therefore the large diameter risers have been employed in order to reduce the production costs. The majority of the work carried out in the past was on pipe diameters smaller than 100 mm. There are only few works known in larger pipes. The above classification of flow patterns described in Section 1.1 is based generally on experimental measurements and visualization studies carried out in small diameter pipes. However, the conventional slug flow does not occur clearly in vertical two phase flow for large diameter pipes according to work by Cheng et al (1998) and Ohnuki et al (2000). There appears to be a direct transition from bubble flow to churn flow. Omebere-Iyari (2006) also did not observe the traditional Taylor bubble of slug flow within the range of his work. These were not the only differences in the behavior of gas and liquid flow in large diameter pipes. Further different characteristics have been reported. For instance, Azzopardi et al (1983) studied disturbance waves in a vertical 125 mm pipe and showed that they are not coherent around the pipe circumference, in contrast to the

findings of Hewitt and Lovegrove (1969) for small (32 mm) diameter tubes. Therefore it is worth mentioning that in spite of their scarcity the studies carried out in large diameter pipes show clearly an important influence of pipe diameter on flow behavior.

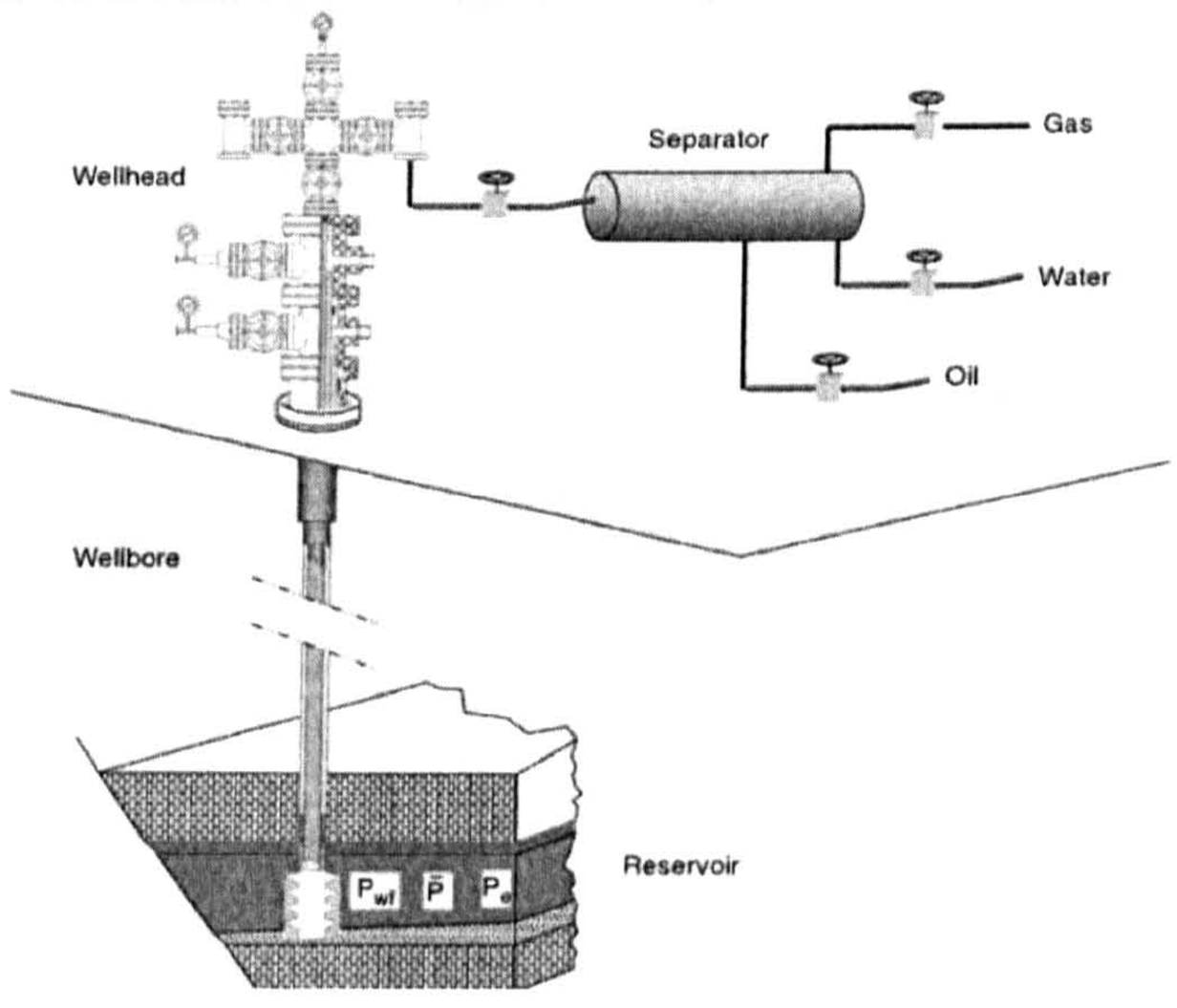

Figure 1.1 Sketch of a petroleum production system (Guo Boyun et al, 2007)

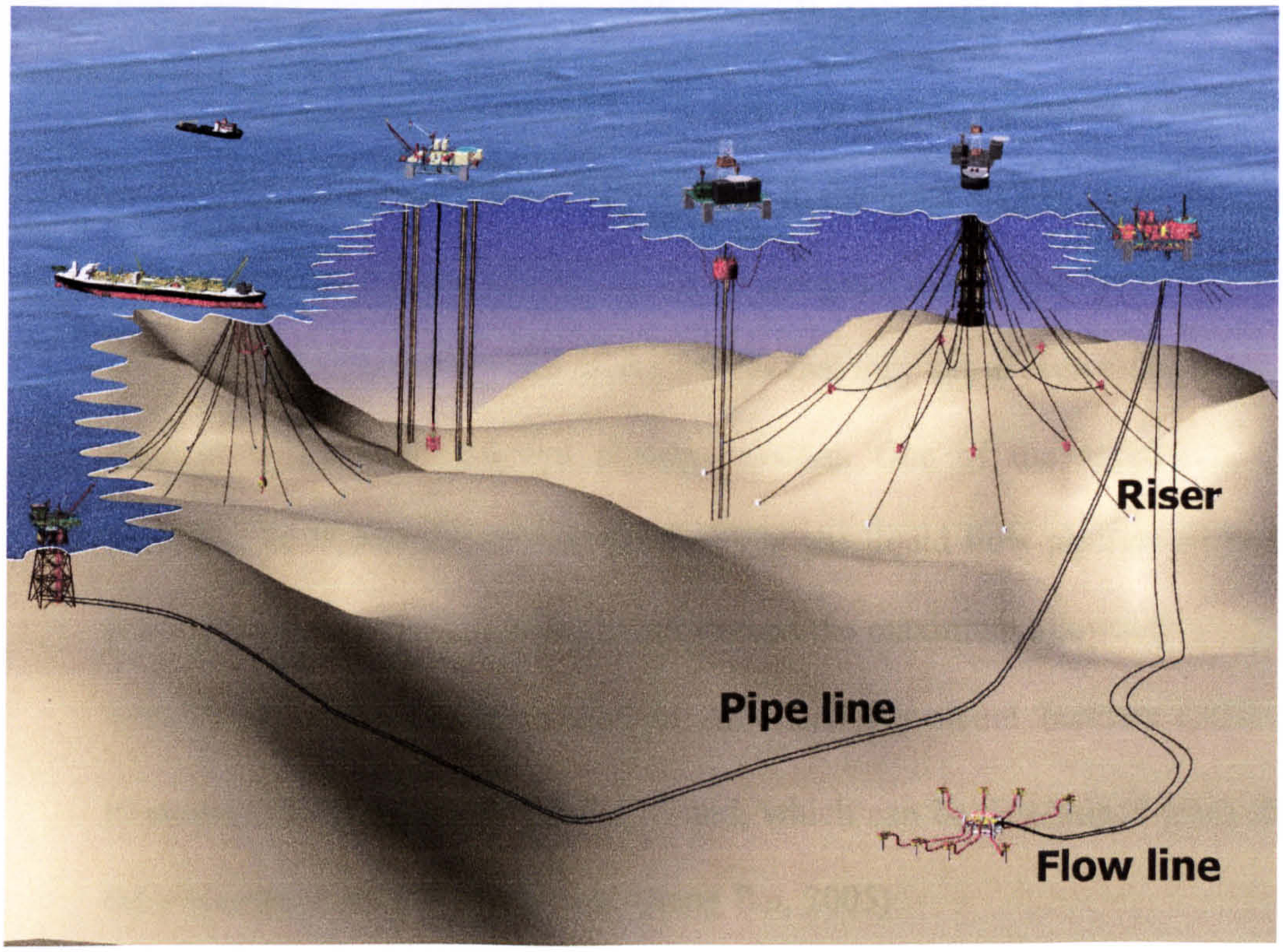

Figure 1.2 Flow line/Pipe line/ Riser System (Jaeyoung Lee, 2009)

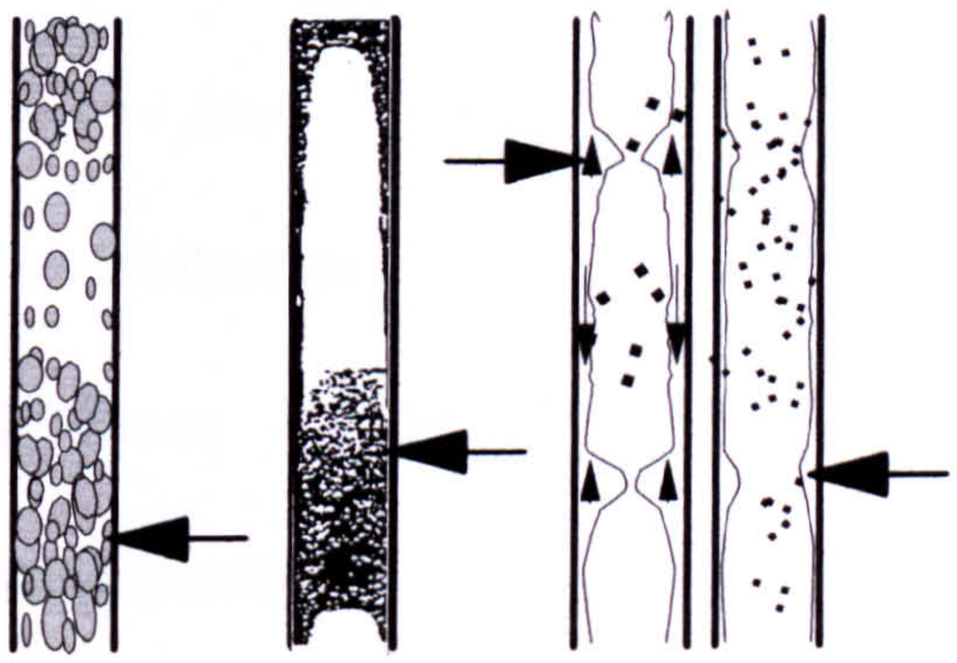

Figure 1.3 Flow patterns in vertical upward flow (Azzopardi, 2006).

1.3 Erosion related problems in gas-liquid flow

One of the mechanical problems that flow can cause in pipeline systems is erosion, which can lead to a severe damage in the inner wall of pipes, fittings, valves and other process equipment. In oil and gas industry, the fluid produced from the reservoir can contain sand particles that may cause even more erosion damage to the transportation pipeline system. One of the approaches to minimize or control the erosion problems in gas-liquid flow pipeline systems is by reducing the flow velocity to not exceed the maximum allowable erosion velocity (V_{max}), as recommended in American Petroleum Institute (API) - Recommended Practice API RP 14E and, which can be determined from the following equation (Yong Bai and Qiang Bai, 2005):

$$V_{max} = \frac{C}{\sqrt{\rho_m}} \tag{1.1}$$

Where C : is the empirical constant equal to 100 for continuous services.

ρ_m : is the density of the gas-liquid mixture (Ibm/ft^3) and defined as;

$$\rho_m = \varepsilon_g \rho_g + (1 - \varepsilon_g)\rho_l \tag{1.2}$$

Where ε_g : is the gas void fraction

ρ_g : is the gas density

ρ_l : is the liquid density

According to Costigan and Whalley (1997), the annular type flow in vertical pipes occurs at gas void fractions above 0.8 and, from Equations 1.1 and 1.2 the erosion velocity for the fluids used in this study are calculated as shown in Table 1.1:

Table 1.1: Erosion velocity (V_{max}) at operation conditions of this study

ε_g	V_{max} (m/s)
0.80	8.58
0.85	9.88
0.90	12.03
0.95	16.72

Although details of erosion related problems in gas-liquid flow are beyond the scope of this study and Equation 1.1 is the simplest model to predict the erosion velocity limit in the gas-liquid flow lines. Equation 1.1 can nevertheless provide a very useful guideline specially for selecting the range of the conditions to be studied during this work.

1.4 Aims and Objectives

It is clear from the above discussion that there are a lack of experimental data in large diameter vertical pipes, i.e., in pipe sizes similar or close to those typical of industry applications and especially on important parameters such as pressure drop which is known as a key design parameter and on liquid film properties such as liquid film thickness and wall shear stress which over all have a significant effect on the flow behavior. It might be more practical to pay attention to erosion velocity limit in the range of conditions to be studied. Therefore, the main objectives of this study can be summarized as the following:

- Obtain experimental data on total pressure drop in 127 mm diameter vertical pipe over a wide range of gas and liquid superficial velocities aiming to investigate the effect of liquid and gas flow rate on total pressure drop in such diameter pipes. Also to compare the data obtained with those available in the literature for smaller pipes so as to investigate the effect of pipe diameter on total pressure drop.
- Manufacture a directional wall shear stress probe that is needed to measure the wall shear stress during this study. This will be based on a review of the published wall shear stress measurement techniques specially those known to be used in two phase flow.
- Investigate the liquid film properties through an experimental campaign to measure the total pressure drop, liquid film thickness and wall shear stress simultaneously and selectively based on the results from the previous campaigns in this study. The interpretation of the data obtained also to be supported with some high speed images.

1.5 Structure of the thesis:

The contents of this thesis are structured as the following:

Chapter 2 is a literature review which contains a critical examination of published work that provides a background of this research program.

Chapter 3 describes the experimental arrangements; the large scale two-phase flow closed loop facility (127 mm) at Nottingham University and techniques used for the measurements of total pressure drop and liquid film thickness including the necessary preparation process involved. It also describes the

instrumentation and data acquisition arrangement. Finally this chapter summarizes the conditions studied in each of the experimental campaigns carried out.

Chapter 4 presents results of 600 experimental runs obtained during this study on total pressure drop in 127 mm diameter vertical pipe. Also in this chapter, the effects of pipe diameter on total pressure are investigated by comparing the data presented with data reported in the literature for pipes of different diameter. In addition the results of this campaign are examined against a number of models and correlations.

Chapter 5 Methods for wall shear stress measurement are presented in this chapter. The focus has been on hot film techniques. The construction steps of the directional wall shear stress probe that was produced during this study are summarized and compared with those commercially available through an experimental campaign presented. The chapter also discusses the potential of micro pillar sensors as a two-dimensional directional wall shear stress probe with some suggestions for the probe to be employed in two phase flow.

Chapter 6 presents the results of two experimental campaigns; firstly, the liquid film thickness measured by conductance ring probes is compared with those measured locally by pin probes and secondly, the simultaneously measured total pressure drop, liquid film thickness and wall shear stress data are presented and the relationship between these parameters are investigated through the time-averaged and time-varying results. In addition the direction of flow of the liquid film examined based on the results of locally measured liquid film thickness and directional wall shear stress together with some high speed video images.

Chapter 7 Brings together the key conclusions from each chapter and suggests the future work.

Chapter 2

Literature Review

The behavior of two-phase gas-liquid flow can be affected by a number of parameters or variables including; the flow rate of each phase and the pipe diameter (Hewitt and Hall Taylor, 1970, Brill and Beggs, 1991, Taitel, 1999 and Azzopardi, 2006). Researchers agree that the experimental data are the main sources of understanding such flow. Due to the complex nature of two phase flow these data are valid only in the range of the conditions studied. Not surprisingly, extensive studies on gas-liquid flow have been carried out in the past. However the majority of the work in gas-liquid vertical flow was conducted in pipes of small diameter. Most of the empirical correlations that have been developed over the last few decades have been based on these data. The amount of information available in the literature for large diameter pipes (e.g., Table 2.1) compared to that for smaller pipes should be an incentive for researchers to put more efforts in the former, given that they have different flow characteristics from behavior in smaller pipes as explained in Chapter 1. The main focus of most of available studies in large diameter pipes is on void fraction. Moreover, they have tended to concentrate on gas velocities < 5 m/s. This resulted in the flows studied being expected to be in the bubble and slug

Reference	Pipe Diameter (mm)	Fluids Studied	Range of		Parameter Measured
			ugs (m/s)	uls (m/s)	
Hills (1976)	150	Air-Water	0.07-3.5	0-2.7	Gas holdup
Azzopardi et al (1983)	125	Air-Water	30-51	0.002-0.02	Film Flow rate, Drop size Distribution and Pressure drop over a limited range of conditions
Hashemi et al (1986)	305	Air-Water	0.01-1.16	0-0.06	Void Fraction, Pressure Drop
Cheng et al (1998)	150	Air-Water	0.42 and 0.73	0, 0.32, 0.64 and 1.25	Void Fraction, Bubble size and Bubble velocity
	28.9	Air-Water	0.14-0.96	0.65	Void Fraction
Ohnuki and Akimoto (2000)	200	Air-Water	0.03-4.7	0.06-1.06	Axial Pressure Drop, Void Fraction, Bubble size and Bubble velocity
Shoukri et al (2003)	200	Air-Water	0.02-0.1	0-0.4	Void Fraction, Bubble size, Bubble velocity and Pressure Drop
Kobayashi et al (2004)	230	Air-Water	0.05-0.2	0.1-0.7	Void Fraction
Zhu et al (2004)	200	Air-Water	0.02-0.24	0.25-0.45	Void Fraction, Bubble size and Bubble velocity
Ombebere-Iyari (2006)	127	Air-Water	1.5-16.7	0.03, 0.05, 0.1 and 0.3	Void Fraction
	189	Nitrogen-Naphtha	0.1-14	0.004-4	Void Fraction, Pressure Drop
	5	Air-Water	0.07-50	0.02-0.67	Void Fraction
Omebere-Iyari et al (2008)	189	Nitrogen-Naphtha	0.09-1.48	0.01, 0.1 and 0.65	Void Fraction
	194	Steam-Water			

Table 2.1 From the literature; Experimental studies of gas-liquid two phase flow in large diameter vertical pipe

flow patterns. However churn-turbulent flow was observed instead of slug flow. Data on other important parameters such as pressure drop and film properties, e.g., the thickness of the film and shear stress in that geometry are very sparse. For instance the two-phase pressure drop data obtained by Hashemi et al (1986), Ohnuki and Akimoto (2000) and Shoukri et al (2003) is only for low gas velocity as stated above and although Azzopardi et al (1983) studied annular flow in 125 mm vertical pipe they have only introduced limited data points on total pressure drop. In addition, no data on wall shear stress in large diameter vertical pipe appear to exist in the literature. Therefore, in pursuance of the main objectives of this study, a number of experimental campaigns to measure total pressure drop, wall shear stress and liquid film thickness were carried out in 127 mm vertical pipe. Although experimentally obtained information on these parameters for large diameter pipes are rare as mentioned previously, nevertheless, considerable studies especially on pressure drop and film thickness in smaller pipes can be found in the literature which can provide an important basis for the discussion of the results of current work. Thus, in what follows in this chapter, findings based mainly on data and analysis for small diameter pipes are presented, concentrating on pressure drop (Section 2.1) and liquid film characteristics (Section 2.2). Section 2.1 includes a discussion of the minimum pressure phenomenon. Also because of their importance in the analysis of two-phase flow and as a basis of empirical correlations, Section 2.2 presents the separated flow conservation equations and then discusses the Triangular relationship which links above parameters , i.e., total pressure drop or wall shear stress with liquid film thickness and liquid film flow rate in annular type flow. Wall shear stress

however, as a difficult parameter to measure is presented in better detail in Chapter 5, including methods of measurement, the principles of each measurement technique, their limitations and necessary precautions required during the measurement.

2.1 Pressure Drop

Pressure drop is a key parameter in pipeline design. Information on this parameter is very important to determine the pumping power needed for the movement of the fluids through pipelines and through other equipment such as heat exchangers. Therefore researchers have placed significant effort into this topic over recent decades and pressure drop has become one of the common measurements in two phase flow.

2.1.1 Experimental two-phase vertical pressure drop

The majority of the experimental data on gas-liquid two-phase pressure drop in vertical pipes as described previously in this chapter were obtained in pipes with inner diameters smaller than 100 mm. Examples on the available studies in such pipes in the literature are Hewitt et al (1961), Martin (1983), Owen (1986), Holt (1996), Sawai et al (2004) and Kaji (2008). Lists of the published work on the topic can also be found in the literature, e.g., Spedding et al (1998) and Kaji and Azzopardi (2010).

The available pressure drop data in the literature may vary from one study to another in terms of range of gas and liquid flow rates studied, pipe diameter, number of data point, and operating system pressure under which the data

were obtained. For instance, some researchers obtained total pressure drop data over a wide range of gas velocities covering the full range of the flow patterns that exist in vertical pipes and some others only studied a certain flow pattern, e.g., Owen (1986) and Sawai et al (2004) respectively. In relation to the pipe diameter, the data obtained by Kaji (2008) was for a pipe with 19 mm diameter and Holt (1996) for pipes with 5 and 10 mm. However Martin (1983) studied 3 different pipe sizes with inner diameters of 10, 32 and 58 mm. The variation of pressure drop with gas flow rates can be linked to flow patterns and their transitions in vertical upward gas-liquid flow. For instance, the well known pressure drop profile(Figure 2.1 and 2.2) for air-water flow in 31.8 mm vertical pipe that was introduced by Owen (1986) are marked with various flow regimes that had been detected visually. The non-dimensional pressure gradient is plotted in Figure 2.1 and 2.2 against the non-dimensional superficial air flow. It can be seen that the transitions from bubbly and slug flow regimes are fairly sharp, while those from churn to annular are spread over a broad range of gas flow rates. Jayanti and Hewitt (1992) used this data of Owen (1986) to examine number of models for prediction of transition from slug to churn flow and as it is clear from Figures 2.1 and 2.2 that the transition from slug to churn flow is accompanied by a large and sudden increase in the pressure gradient for the liquid mass fluxes of 5.3 and 111.8 kg/m^2s. Also another change in the trend of pressure drop profile is clear at the transition from churn to annular flow as a minimum can be seen in that region. In the literature a number of approaches can be found on this transition, i.e., churn to annular transition. According to Taitel et al (1980) the transition can be determined when the gas velocity is sufficient to suspend the entrained

droplets and the condition for which the transition occurs can be found from Kutateladze number (Ku_g):

$$Ku_g = U_g \left(\frac{\rho_g^{\ 2}}{g\sigma(\rho_l - \rho_g)} \right)^{0.25} > 3.2 \qquad (2.1)$$

Where :

U_g : is the gas superficial velocity(m/s)

g : is the gravitational acceleration (m/s^2)

σ : is the surface tension(N/m)

ρ_g : is the gas phase density (kg/m^3)

ρ_l : is the liquid phase density (kg/m^3)

The second approach of transition to annular flow is the flow reversal of the falling film in slug or churn flow. The "flow reversal" point as described by Hewitt et al (1965), gives the gas velocity that is sufficient to carry all the liquid around the circumference upward as a climbing film. Then if the gas velocity is reduced a point will be reached at which the liquid phase, in addition to flowing upward, begins to creep down. That is, the point at which the liquid film starts to fluctuate between upward and downward flow in an oscillatory manner. So if the gas velocity is above the flow reversal point, upward annular flow will be expected. The gas velocity of flow reversal is commonly expressed as the dimensionless gas velocity which is known also as Wallis parameter as the following:

$$U_g^{\ *} = U_g \left(\frac{\rho_g}{g d_o (\rho_l - \rho_g)} \right)^{0.5} > 1 \qquad (2.2)$$

Where $U_g^{\ *}$: is the dimensionless gas velocity

d_o : is the pipe diameter

From the work by Hewitt et al (1965), it is seen that the pressure drop data in the climbing film region show a minimum (Figure 2.3). The pressure drop falls through a minimum on reducing the gas velocity and raised again until the flow reversal point was reached. Same characteristic also been observed by Hewitt et al (1985). The value of U_g^* at which the minimum pressure drop occurred was 1.12. Above this value annular flow expected to exist. According to Hewitt and Taylor (1970) at lower gas flow rate annular may still exist and is very probable down to U_g^* of 0.8. Although there is no exact value of U_g^* at which the transition from churn to annular might occur, however, the value of 1 appears to be the most popular by the researchers.

The minima and maxima in pressure drop data were also reported by other researchers, e.g., Spedding et al (1998) and Kaji and Azzopardi (2010). Based on what have been mentioned, the data on pressure drop in addition to its great importance for design purposes can provide very useful information on two-phase flow behaviors.

A pressure drop profile for the large diameter vertical pipes similar to what has been presented previously for smaller pipes does not appear to exist in the literature and hence it is not appear also that the transition of flow patterns in former pipes based on the variation of pressure gradient with the gas flow rate has been investigated so far and this is not surprising with the limited data that available in such diameter pipes.

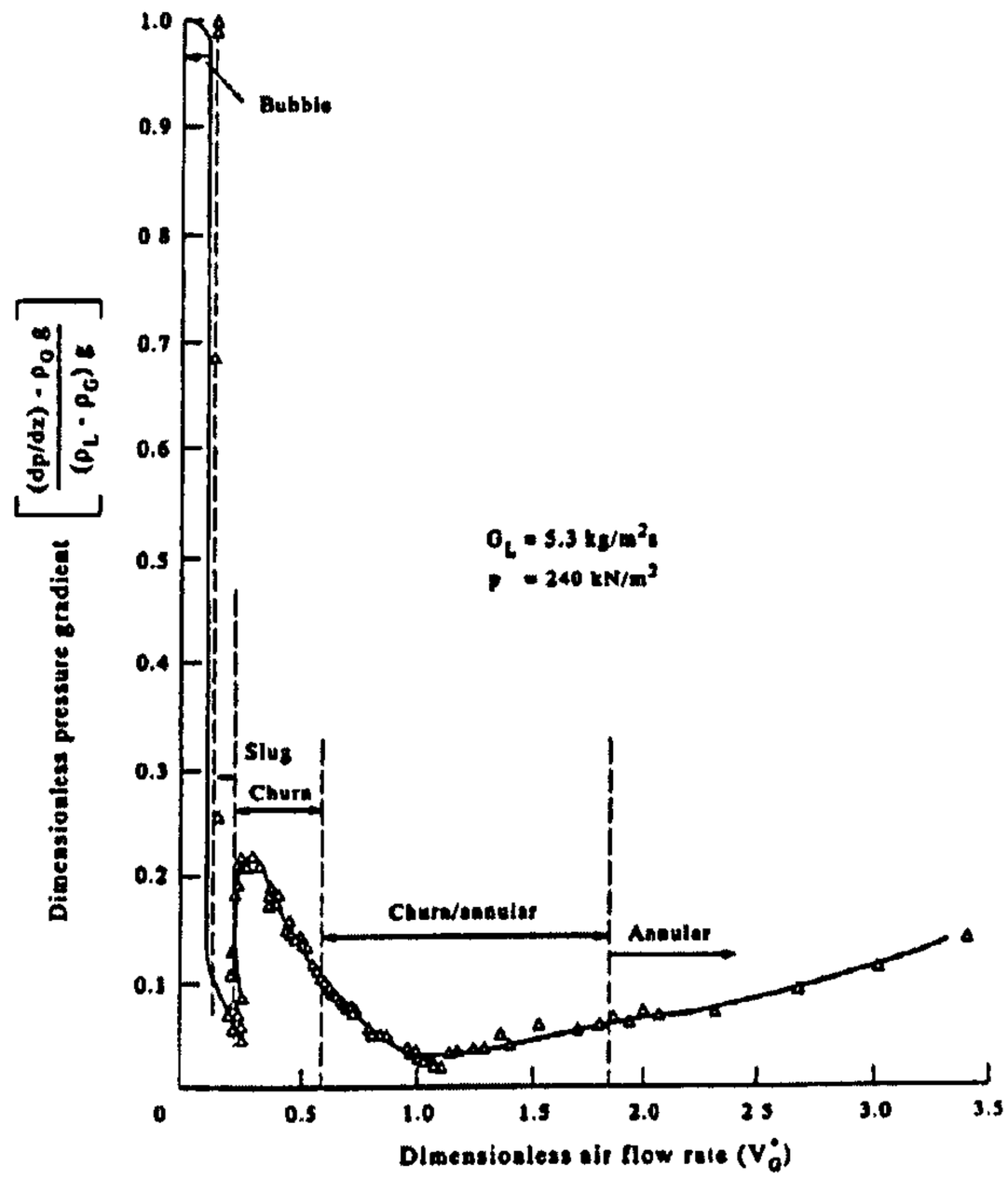

Figure 2.1 Measured pressure gradient as a function of gas flow rate in vertical two-phase flow; experimental results of Owen (1986) at low liquid flow rates (Jayanti and Hewitt, 1992)

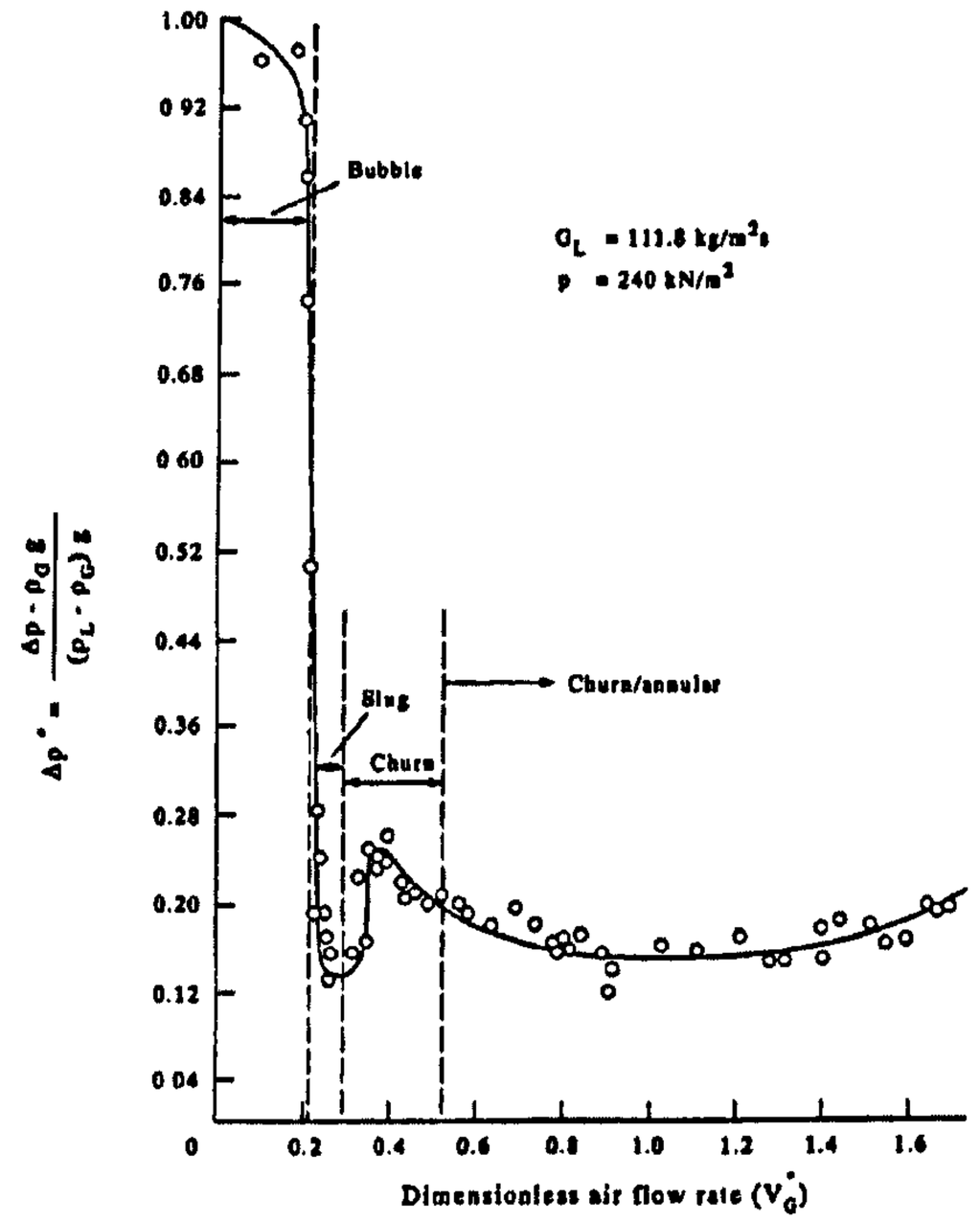

Figure 2.2 Measured pressure gradient as a function of gas flow rate in vertical two-phase flow; experimental results of Owen (1986) at intermediate liquid flow rates (Jayanti and Hewitt, 1992)

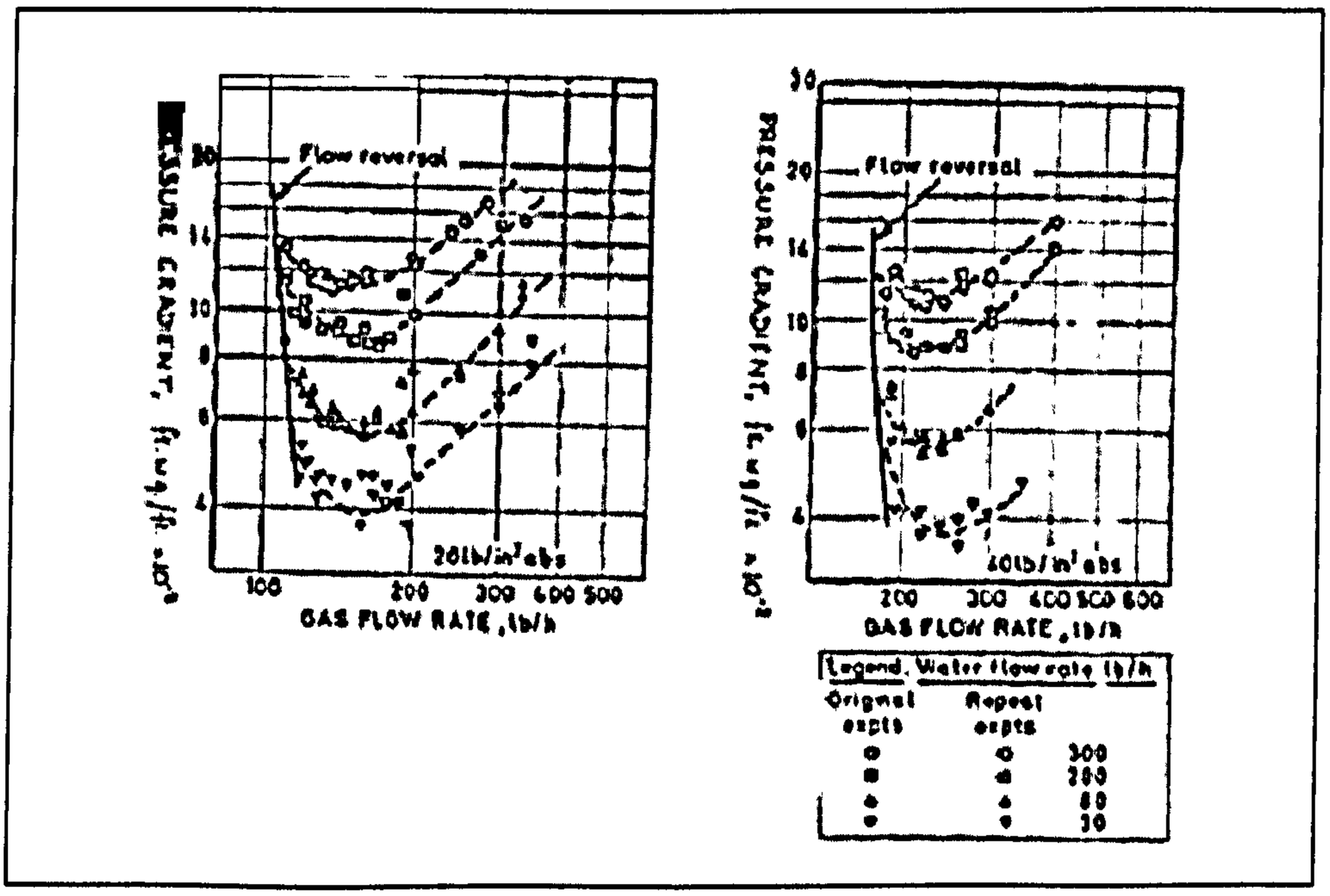

Figure 2.3 Pressure drop data showing the minimum (Hewitt et al. 1965)

2.1.2 Minimum pressure drop and zero wall shear stress

Though pressure drop is one of the most common measurements made in two-phase flow, direct measurements of wall shear stress are more difficult and therefore rarer. For common measurement techniques of wall shear stress in two-phase flow and the difficulties associated with each technique see Chapter 5.

Hewitt et al (1965) who reported the minimum in their experimental data on pressure drop, suggested; that this minimum against gas flow rate corresponded closely to the point at which the wall shear stress becomes zero. According to Hewitt and Hall Taylor (1970) the effect of gravitational force in annular type flow is such that the shear stress in the film decreases from the interface to the wall. So, as the gas velocity reduces, the interfacial shear stress will decrease leading to a lower shear stress on the pipe wall, and with further reduction in the gas velocity, the wall shear stress falls to zero. Any further reduction in the gas flow rate beyond the zero wall shear stress point will lead to a negative value of wall shear stress, i.e., a downward movement of the liquid phase adjacent to the wall. Govan (1990) who calculated the mean wall shear stress from the measured pressure drop and the liquid holdup in the region close to churn flow has also reported similar relationship between the minimum pressure drop and zero wall shear stress. However, the condition at which the zero wall shear stress occurred was at a lower gas velocity than the minimum pressure gradient.

According to the laminar flow model the pressure drop at minimum point and zero wall shear stress can be expressed in terms of dimensionless parameters

and as following (Hewitt and Hall Taylor, 1970):

$$(\Delta p^*)_{\tau=0} = \frac{\rho^*}{1-\rho^*} r_i^{*2} + \frac{1}{(1-\rho^*)}(1-r_i^{*2}) \tag{2.3}$$

$$(\Delta p^*)_{\min} = \left(\frac{2-\rho^*}{1-\rho^*}\right) + \left(\frac{r_i^{*2}}{1-r_i^{*2}}\right) \ln r_i^* \tag{2.4}$$

$$\text{Where } \Delta p^* = \left(-\frac{dp}{dz}\right) \frac{1}{\rho_L g(1-\rho^*)} \tag{2.5}$$

and r_i^* is defined as r_i / r_o and ρ^* as ρ_G / ρ_L.

As reported by Govan (1990); although experimentally obtained points that representing the minimum pressure drop are in reasonable agreement with the laminar flow model, however, the pressure gradients at zero wall shear stress conditions are significantly under predicted. And this explained as due to highly disturbed and turbulent nature of the flow which could hardly to be described by a laminar theory.

2.2 The Liquid Film

In annular gas-liquid two-phase vertical flow the liquid moves partly upwardly as a thin film on the pipe wall. In churn flow although it is less understood than other flow patterns, it is generally agreed the liquid film motion is not unidirectional but it has an oscillatory nature and it is covered with a complicated system of waves. Further, the liquid in slug flow moves as a falling film around the Taylor bubble. Based on these, the liquid film on the pipe wall regardless of its thickness, direction and the roughness of its surface is an important feature of most of the flow patterns exist in vertical two phase flow as described in Chapter 1.

2.2.1 The separated flow conservation equations

Considering an element of simplified vertical annular gas-liquid flow in a channel (Figure 2.4) with the liquid phase moving as a film on the wall at an actual mean liquid velocity of, u_L, and gas phase as a core in the center at an actual mean velocity of, u_G. As can be seen, there are several forces acting on the liquid film which are; the shear force at the channel wall, the shear force at the liquid-gas interface, the force due to gravity and the pressure force on bottom and top surface of the element.

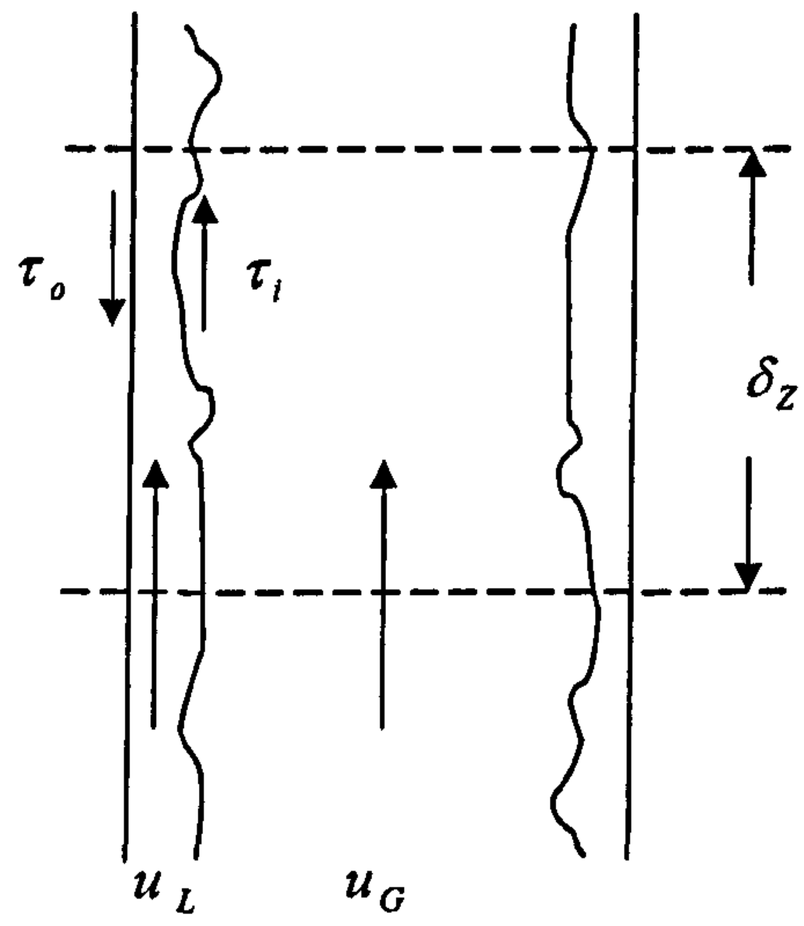

Figure 2.4 Element of channel with separated flow.

Treating each phase as separated flow these forces can be balanced in the momentum equation for the element above as the following (Hewitt and Whalley, 1989):

$$\begin{pmatrix} Rate \\ of \\ creation \\ of \\ momnetum \end{pmatrix} = \begin{pmatrix} momentum \\ out.flow \\ rate \end{pmatrix} - \begin{pmatrix} momentum \\ in.flow \\ rate \end{pmatrix} + \begin{pmatrix} momentum \\ storage \\ rate \end{pmatrix} = \begin{pmatrix} sum\ of \\ forces \\ acting\ on \\ the \\ control \\ volume \end{pmatrix} \quad (2.6)$$

The terms in Equation 2.6 for the liquid phase are given as the flowing:

- The momentum out-flow, in-flow and storage rate:

$$\mathrm{M}_L u_L + \delta_Z \frac{\partial}{\partial z}(\mathrm{M}_L u_L) \qquad -\mathrm{M}_L u_L \qquad +\frac{\partial}{\partial t}[\rho_L u_L (1-\varepsilon_G) A \partial z]$$

Momentum out-flow rate — Momentum in-flow rate — Momentum storage rate

Where; M_L is the mass flow rate of the liquid phase (kg/s), which can be found from:

$$\mathrm{M}_L = \rho_L u_L (1-\varepsilon_G) A \quad (2.7)$$

- The rate of creation of momentum:

$$\delta_Z \{\frac{\partial}{\partial z}[\rho_L u_L^2 (1-\varepsilon_G) A] + \frac{\partial}{\partial t}[\rho_L u_L (1-\varepsilon_G) A]\}$$

- The sum of forces acting on the control volume of liquid:

$$p(1-\varepsilon_G)A \qquad -\{p(1-\varepsilon_G)A + \delta_Z \frac{\partial}{\partial z}[p(1-\varepsilon_G)A]\} \qquad -\{-p\delta_Z \frac{\partial}{\partial z}[(1-\varepsilon_G)A]\}$$

Pressure force on bottom surface of element — Pressure force on top surface of element — Pressure force on sloping surface of the element due to change in the cross sectional area of the liquid

$-\rho_L g(1-\varepsilon_G)A\delta_z$	$-\tau_o P\delta_z$	$-\tau_i P_i \delta_z$
Force due to gravity	Shear force on the outer surface of the element (at the channel wall)	Shear force on the inner surface of the element (at the liquid-gas interface)

Where
p = pressure (N/m^2)
g = acceleration due to gravity (m/s^2)
τ_o = wall shear stress (N/m^2)
τ_i = interfacial shear stress (N/m^2)
P = periphery of the channel (m)
P_i = periphery of the interface (m)

Balancing the rate of creation of momentum against the sum of the forces acting on the control volume of liquid at steady state flow ($\partial/\partial t = 0$) and in a duct of constant cross sectional area leads to:

$$-(1-\varepsilon_G)\frac{dp}{dz}-\rho_L g(1-\varepsilon_G)-\frac{\tau_o P}{A}+\frac{\tau_i P_i}{A}=\frac{d}{dz}[\rho_L u_L^2(1-\varepsilon_G)] \qquad (2.8)$$

Similar equation can be derived for the gas phase:

$$-\varepsilon_G\frac{dp}{dz}-\rho_G g\varepsilon_G-\frac{\tau_i P_i}{A}=\frac{d}{dz}[\rho_G u_G^2\varepsilon_G] \qquad (2.9)$$

Where:

ε_G = fraction of the cross sectional area occupied by the gas phase.

$1-\varepsilon_G$ = the fraction of the cross sectional area occupied by the liquid.

Both u_L and u_G can be expressed as the following:

$$u_L=\frac{m(1-x)}{\rho_L(1-\varepsilon_G)} \qquad (2.10)$$

$$u_G=\frac{mx}{\rho_G\varepsilon_G} \qquad (2.11)$$

Where m is the total mass flux (kg/m^{2}s) and is given by:

$$m = \rho_L u_L (1-\varepsilon_G) + \rho_G u_G \varepsilon_G \qquad (2.12)$$

x = quality or fraction of the total flow which is in the form of gas.

For circular tube with diameter of d_o, the periphery P, is given as:

$$P = \pi d_o \qquad (2.13)$$

and the cross sectional area of the tube A, is given by:

$$A = \frac{\pi d_o^{\,2}}{4} \qquad (2.14)$$

By adding Equations 2.5-2.11, the separated momentum equation for steady state gas-liquid flow in vertical circular tube can be written as:

$$-\frac{dp}{dz} = \frac{4\tau_o}{d_o} + m^2 \frac{d}{dz}\left[\frac{(1-x)^2}{\rho_L(1-\varepsilon_G)} + \frac{x^2}{\rho_G \varepsilon_G}\right] + \rho_{TP} g \qquad (2.15)$$

Total Pressure = gradient	Frictional Pressure Gradient	+	Acceleration Pressure Gradient	+	Gravitational Pressure Gradient

Equation 2.15 is perhaps the most popular equation used for two phase flow predictions. As from the right hand side of this equation, the total pressure gradient Consists of three components which are; frictional, gravitational and acceleration pressure drop. The frictional term of pressure gradient is represented by the shear stress and the gravitational term by the density of two-phase mixture, bearing in mind that the density of the liquid phase is significantly higher than the density of the gas phase. Therefore, the liquid holdup which the liquid film represents a considerable part of it in annular or semi annular type flow may represent a major part of this component. Lastly

the acceleration pressure drop is the third component and it is normally very small in vertical pipes therefore its effect on total pressure drop is negligible. Based on what have been mentioned the total pressure drop is related strongly to the liquid film properties such as the shear stress on the pipe wall and in the interface between the gas and the liquid phase this is in addition to the thickness of the film.

Many empirical correlations have been developed in the past from the experimental data for predicting two-phase pressure gradient which differ in the manner used to calculate these three components above of the total pressure drop (Hewitt, 1982a, Brill and Beggs, 1991 and Azzopardi, 2006). It is worth mentioning that even with many empirical correlations and models that available in the literature they are not appear to be valid over a very wide range of gas and liquid flow rates, physical properties and pipe diameters therefore researchers normally test the performance of these methods of prediction with the experimental data they are obtaining.

Due to the lack of experimental data in large diameter pipes it is not surprising if there is no specific correlation derived based on experimental data in such pipe sizes. This being the case, in Chapter 4 some of the commonly used correlations and models are examined against the experimental data on total pressure drop that obtained during this study.

2.2.2 The Triangular Relationship

This relationship is so called because it relates three dependent variables in annular two-phase flow which are: film thickness, film flow rate and wall shear stress or pressure drop. It is described in detail by Hewitt and Hall-Taylor (1970) and Hewitt and Whalley (1989) and summarized by Govan (1990) in four steps as following:

- The momentum balance equation on the liquid film element, i.e., Equation 2.5 for a circular tube (Figure 2.5) and assuming negligible acceleration can be written as:

$$\tau(r) = \tau_i \frac{r_i}{r} - \frac{1}{2}\left(\rho_L g + \frac{dp}{dz}\right)\frac{r^2 - r_i^2}{r} \qquad (2.16)$$

- The momentum balance equation on the gas core element (Equation 2.6) with same assumption above is given as:

$$\tau_i = -\frac{r_i}{2}(\rho_c g + \frac{dp}{dz}) \qquad (2.17)$$

Where ρ_c is the homogenous gas/droplets core density.

- The velocity distribution in the film is obtained by following expressions:

$$\tau = \mu_L \frac{du}{dy} \qquad \text{for laminar flow} \qquad (2.18)$$

$$\tau = \mu_E \frac{du}{dy} \qquad \text{for turbulent flow} \qquad (2.19)$$

Where y = distance form the wall (m) and given as:

$$y = r_o - r \qquad (2.20)$$

u = local velocity with the film(m/s)

μ_L = liquid viscosity (Ns/m^2)

μ_E = the effective liquid viscosity for turbulent flow (Ns/m^2)

- The velocity profile obtained above can be integrated to give the film flowrate.

$$M_{LF} = \int_0^{\delta} 2\pi r u \rho_L dy \qquad (2.21)$$

In practice the shear stress within the liquid film may vary greatly particularly in the region approaching the transition to churn flow when the film is relatively thick (Hewitt and Whalley, 1989). The distribution of shear stress in the film can be calculated from Equation 2.16.

If the variation of shear stress within the film and the actual curvature of the film is taken into account, and appropriate expressions for turbulent viscosity introduced, then the solution of the equations above requires a numerical integration (see Hewitt, 1961). However and according to the thin film approximation for the triangular relationship, the solution can be greatly simplified based on the following assumptions (Hewitt and Whalley, 1989):

(i) The film thickness is very small compared to the tube radius.

(ii) Acceleration and gravitational effects are very small and can be ignored.

(iii) The effect of curvature in the film is small.

(iv) The wall and interfacial shear stress are approximately equal.

And the resultant solution can be expressed as:

$$M_{LF} = 2\pi r_o \delta \left[\frac{2\tau_o \rho_L}{f_{LF}}\right]^{1/2} \qquad (2.22)$$

Where

$$f_{LF} = \frac{\tau_o}{\frac{1}{2}\rho_L u_{LF}^2} \qquad (2.23)$$

and u_{LF} = the mean velocity in the liquid film (m/s) which is given:

$$u_{LF} = \frac{M_{LF}}{2\pi r_o \delta \rho_L} \qquad (2.24)$$

The f_{LF} for laminar and turbulent flow as shown in Figure 2.6 can be calculated from the single phase relationship (Hewitt and Taylor, 1970):

$$f_{LF} = 16/\mathrm{Re}_{LF} \qquad \text{for laminar flow} \qquad (2.25)$$

$$f_{LF} = 0.079/\mathrm{Re}_{LF}^{0.25} \qquad \text{for turbulent flow} \qquad (2.26)$$

$$\text{Where } \mathrm{Re}_{LF} = \frac{m_{LF} d}{\eta_L} \qquad (2.27)$$

However at transitional region between laminar and turbulent flow ($200 < \mathrm{Re}_{LF} < 8000$) another relationship is required which may be approximated by the following equation: (Govan, 1990):

$$f_{LF} = 0.00106 + 143.38(\log \mathrm{Re}_{LF})^{-4.5} \qquad (2.28)$$

Based on what has been presented in this chapter; parameters such as: pressure drop, wall shear stress and liquid film thickness are of great importance in vertical two-phase flow and a simultaneous measurements of theses parameters can provide very useful information on the flow behavior. In addition to the works presented previously a number of studies for small pipes can be found in the literature that provide a simultaneously measured data on the above parameters in vertical gas-liquid flow , e.g., Martin (1983), Zabaras et al (1986) and Wolf (1995).

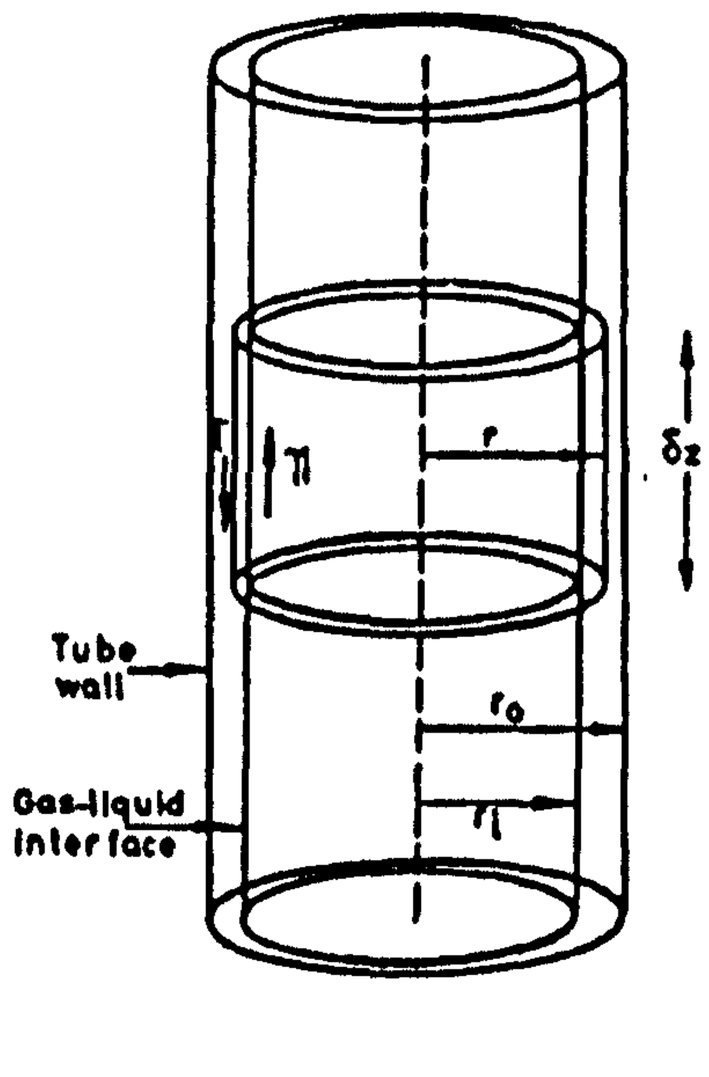

Figure 2.5 Element of film for force balance (Hewitt and Whalley, 1989)

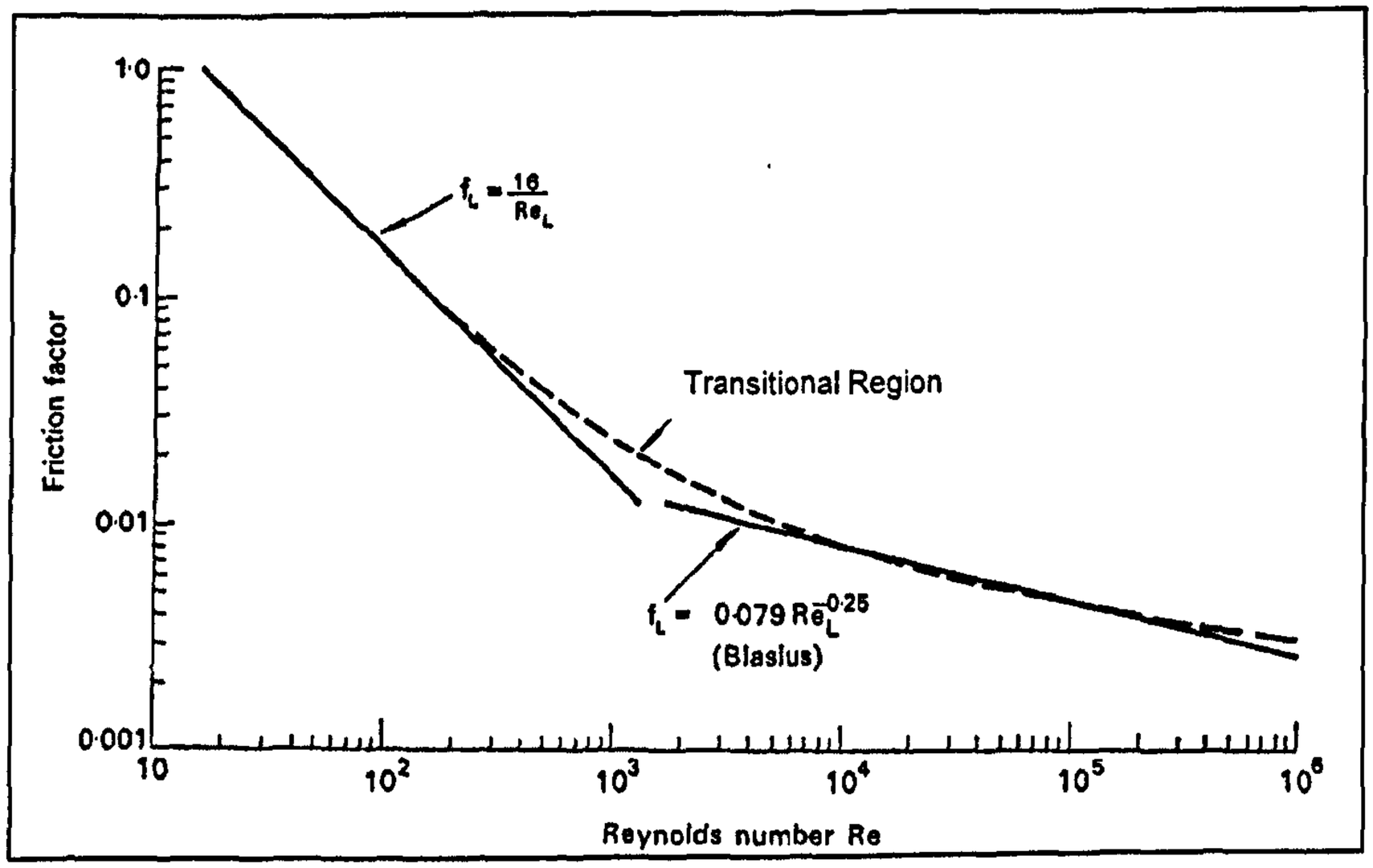

Figure 2.6 Relationship between f_{LF} and Re_{LF} for thin film approximation

(Hewitt and Hall-Taylor, 1970)

Chapter 3

Experimental Arrangement

The main objective of the current study as presented in Chapter 1 is to obtain experimental data for parameters necessary for design such as pressure drop and liquid film properties in two phase flow for vertical pipes with inner diameters similar or close to those typical of oil field applications. Therefore, the two phase flow experiments in this work were carried out on the large scale closed loop facility in the Department of Chemical and Environmental Engineering at Nottingham University. A number of experimental campaigns were performed in this study to measure total pressure drop, liquid film thickness and wall shear stress simultaneously using different measurement techniques. This is in addition to a visualization campaign using a high speed video camera. The results of each campaign are presented in the following chapters. In all the experimental runs air and water were used as the test fluids at ambient temperature and a pressure of 3 bara. During the selection of the gas and liquid superficial velocity ranges the attention has been paid to the erosion velocities those for oil and gas production applications as discussed in Chapter 1. The conditions of the present experiments are given at the end of this chapter and listed in Appendix A. In this chapter, namely in Section 3.1

the major components of the large scaled two phase flow closed loop test facility are outlined, followed by the Sections 3.2-3.4 which describe the measurement techniques employed in the present study. The flow rate measurements are presented in Section 3.5 and the details of the data acquisition software and instrumentation given in Section 3.6 followed by visualization study arrangement and experimental conditions in Sections 3.7 and 3.8 respectively.

3.1 Large Scale Two-phase Flow Closed Loop

The large scale closed loop test facility was used previously by Omebere-Iyari (2006) in part of his work. A data schematic flow diagram of the rig is shown in Figure 3.1 and the major components of the test facility are illustrated in Figure 3.2.

The test facility consists of a 11 m riser with 127 mm inner diameter. The water stored in the bottom of the separator is used as the liquid phase and was delivered to the riser base by a centrifugal pump (ABB IEC 60034-1) with a volumetric flow rate up to 68 m^3/hr. The separator is a cylindrical stainless steel vessel of 1 m in diameter and 4 m height with a capacity of 1600 liters. The separator is the source of the liquid phase to the system. Therefore, it must be filled partially with water before the start of the experiments. Air was used as the gas phase. The fluid properties used are as shown in Table 3.1. Two liquid ring pumps with 55 kw motors were employed to compress and deliver the air to the riser base. The gas flow rate was regulated by varying the speed of the motors (up to 1500 rpm) and by operating valves VF1a and VF3a. The

gas and liquid phases come together in the mixing unit at the riser base. The mixing device consisted of 105 mm diameter tube placed at the centre of the test section (127 mm). The gas passed up this tube and the liquid phase entered in the annular space between this tube and the test section wall (Figure 3.2e).

Downstream of the mixer; the gas and the liquid both travel together through the riser to the measurement section. The measurement devices used were ring conductance probes, pressure tappings and directional shear stress probes. The latter were each surrounded by 4 flush mounted pin probes for local film thickness measurement. The locations of these techniques are given below:

Three identical conductance ring probes (for time-varying, averaged liquid film thickness measurement) are placed at 8, 8.1 and 8.3 m above the mixer. This corresponds to 62.7, 63.8 and 65.5 pipe diameters respectively. Two pressure tapping holes were drilled in the test section at 6.69 m and 8.33 m from the mixer (i.e., 52.7 and 65.6 pipe diameters respectively) for measurement of time-varying, pressure difference over 1.64 m. The shear stress probes (and their associated flush mounted pin conductance probes) were placed at 8.05 m (i.e. between the first and second ring probes). Part of the test section was also enclosed in a transparent box which was filled with water to reduce the refraction during the visualization study. The box placed at 7.7 m from the mixer (60.2 pipe diameters). The locations of the items are shown in Figure 3.3

Beyond the riser the two phase flow travels along 2.34 m of horizontal pipe and then 9.6 m downward in a vertical pipe before the flow is directed horizontally for 1.47 m to the separator, where the gas and the liquid separated

and directed back to the compressors and the pump respectively, so creating the closed loop.

Air from the main supply is used to pressurize the system before the start of the experiments. For the present work the system pressure set at 3 bara. Several valves were used to regulate the flow of the gas and the liquid, namely valves VF1a and VF3a for the gas and VF2a and VF4a for the liquid. The liquid and the gas flow rates were monitored using calibrated vortex and turbine meters respectively. The temperature and the pressure of the system were monitored, close to the liquid and the gas flow meters and at the riser base. Before using this facility the operator was made familiar with all the safety features and the operating instructions as summarized in Appendix B.

Table 3.1 Properties of the fluids used for the present experiments at 25 C and 3 bara.

Fluid	Density (kg/m^3)	Viscosity (kg/ms)	Surface tension (N/m)
Air	3.55	0.000018	
Water	997.05	0.00089	0.072

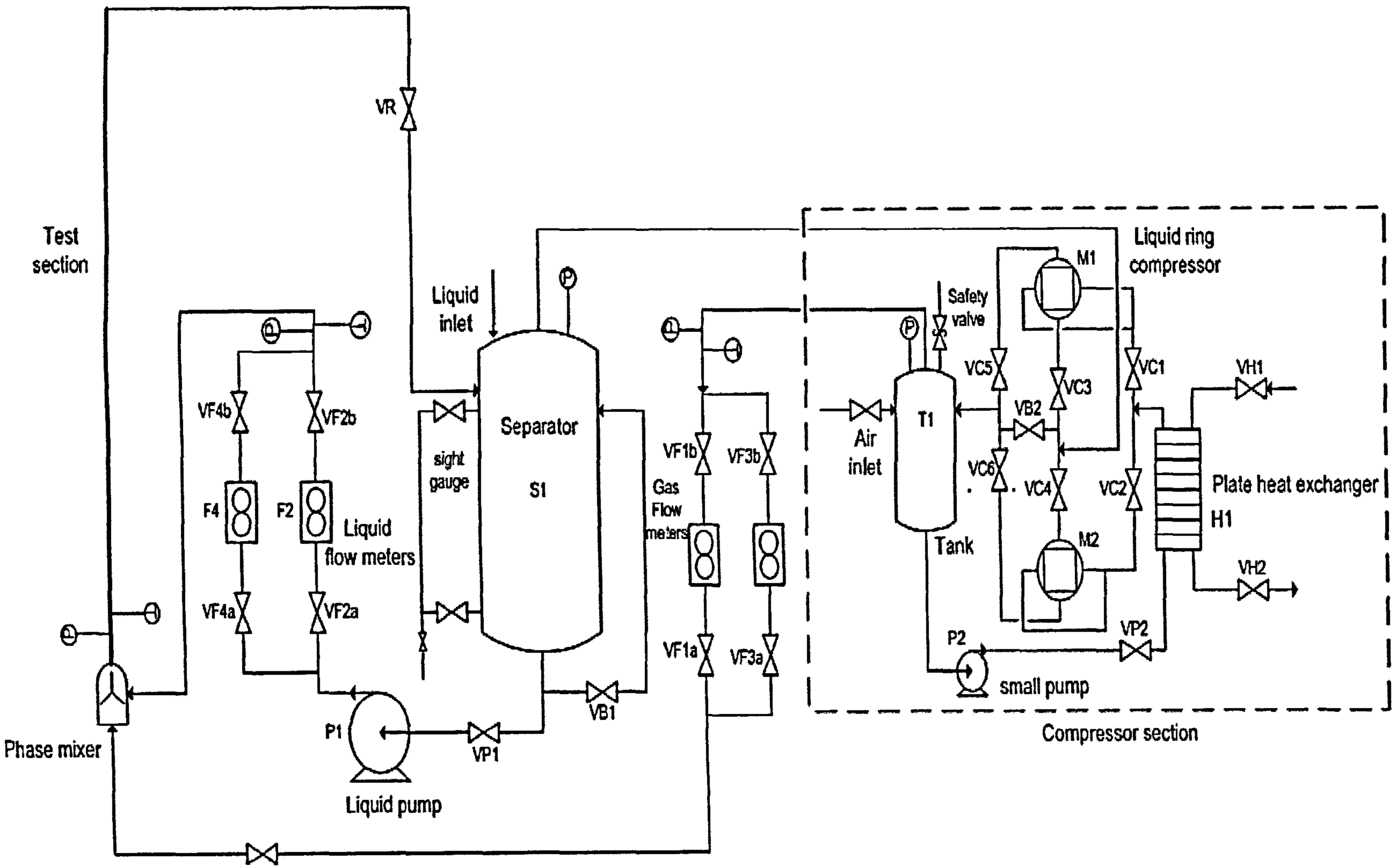

Figure 3.1 Flow sheet of the large scale closed loop facility (127 mm) in the Department of Chemical and Environmental Engineering/Nottingham University

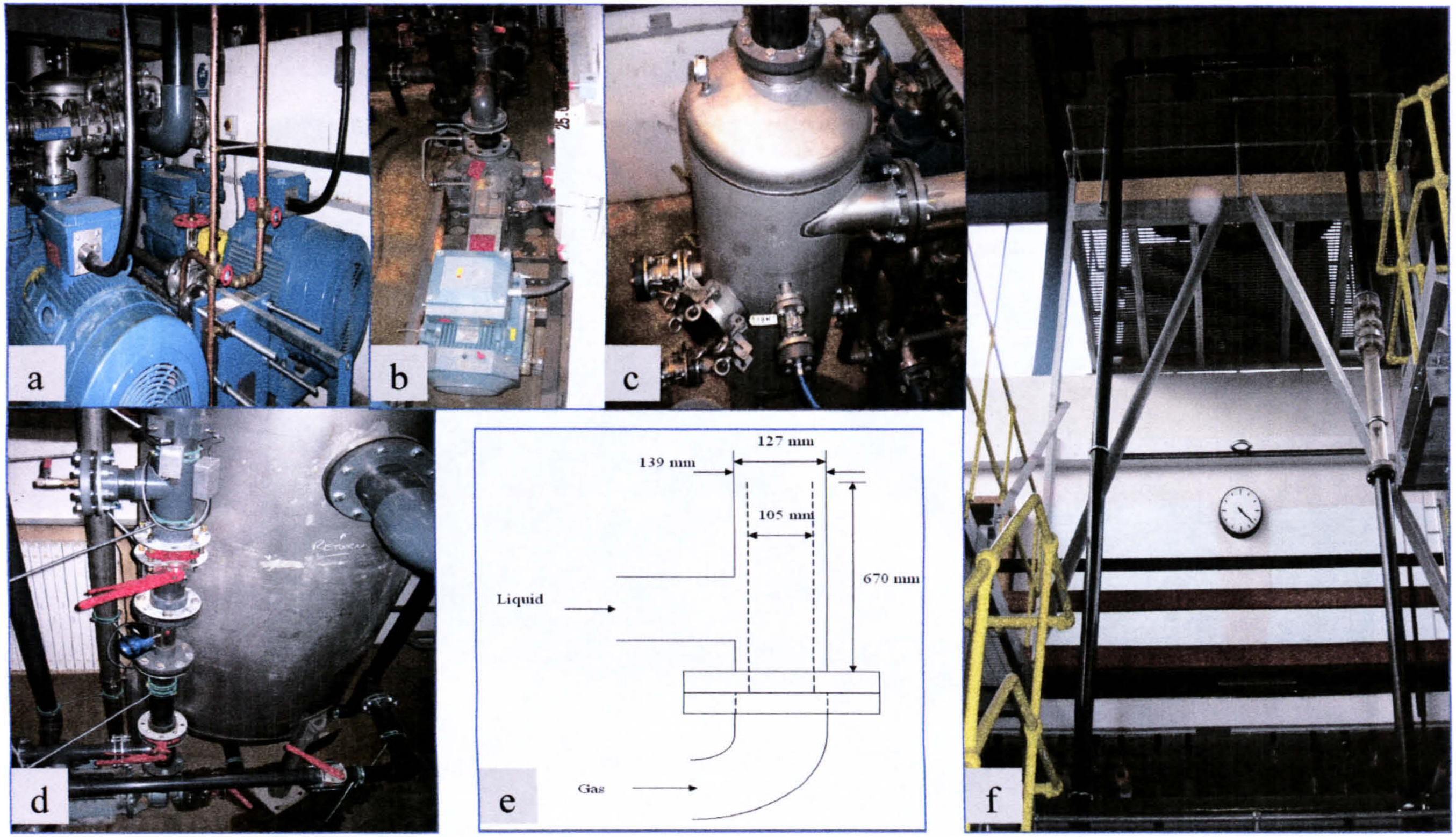

Figure 3.2 The major components of the rig : a) The liquid vacuum pumps b) The liquid centrifugal pump c) The pressure tank d) The separator e) The diagram of the mixing unit and f) The riser.

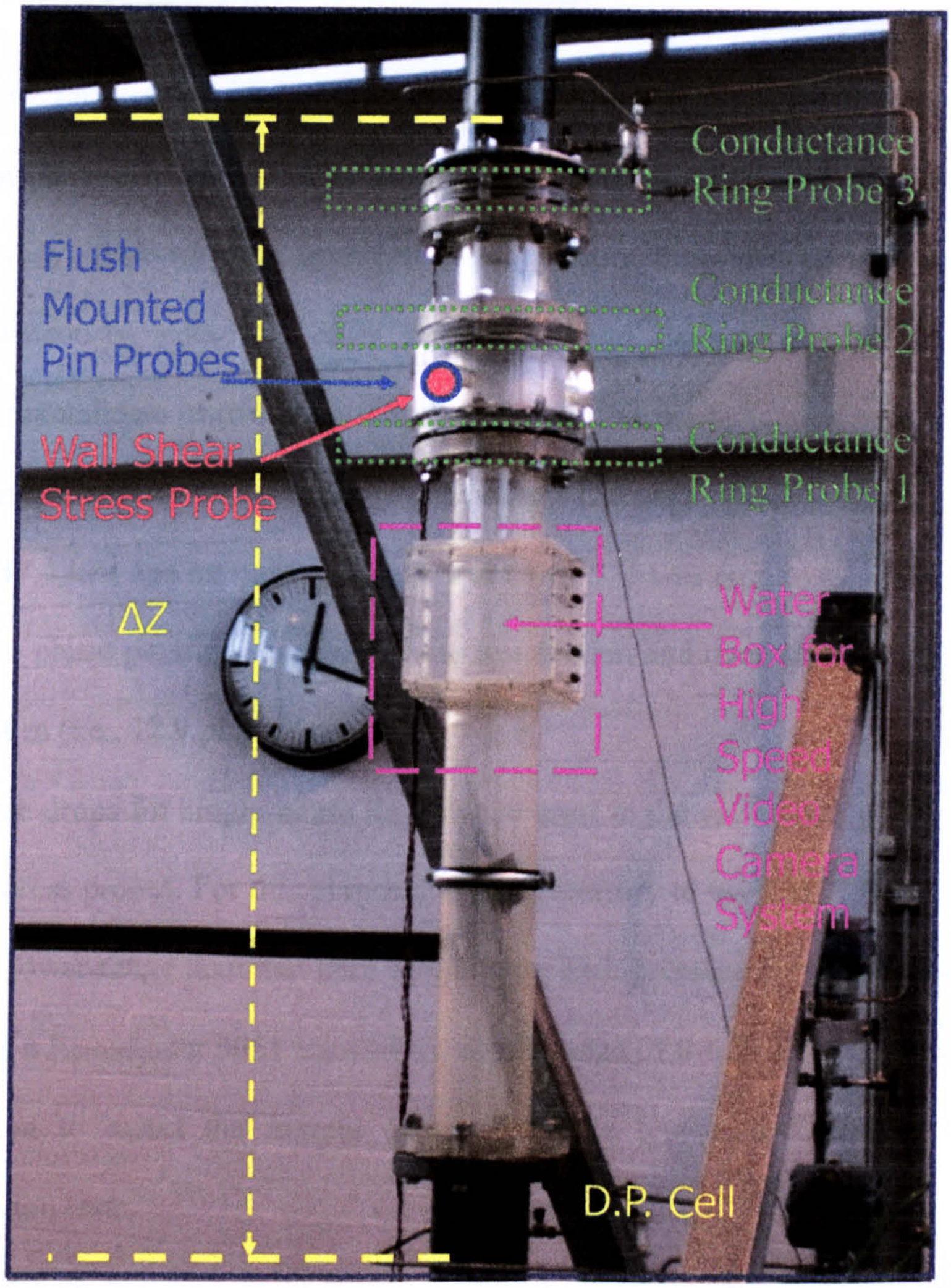

Figure 3.3 The locations of the measurement techniques on the transparent test section of the riser.

3.2 Pressure Drop Measurement

Pressure drop is the driving force for the flow and is therefore an important design parameter. In all the two phase experimental campaigns presented in this study, time-varying, averaged total pressure drop has been measured simultaneously with the other parameters and as a result a bank of experimental data of two phase pressure gradient were obtained. An electronic differential pressure transmitter (Rosemount 1151 smart model) with a range of 0- 37.4 kPa and an output voltage from 1 to 5 V was employed to measure the two phase pressure drop across the test section and over an axial distance of 1.64 m (i.e., 12.9 pipe diameters).

Pressure drops for single phase liquid were used in the calibration of the wall shear stress probes. For this purpose, it was necessary to use a D.P. transmitter with a lower range than that used in the two-phase pressure drop experiments, namely a Rosemount 3051 transmitter with a range of 0-6.23 kPa. Care had to be taken to avoid the ingress of gas into the test section during these calibration tests.

To eliminate any sources of the error during the measurement of two phase flow pressure drop in the present study, close attention was paid to the following steps:

3.2.1 The Efficiency of the Liquid Purging System

The pressure tapping holes across the test section must be made carefully so that their edges are clean; the tubing lines that connect the DP transmitters and

the tapping holes must be tested very carefully against any leak before any real measurement of pressure drop. This has been done in the present study by using a special leak detector spray. Finally the pressure tapping lines must be filled with liquid followed by an efficient purging procedure. The main purpose of the purging is to keep the density constant along the pressure tapping lines, i.e., to prevent any air to be trapped into the tapping lines. As this assured in this work by an efficient purging procedure as the following:

Before running the rig and pressurizing the system, the liquid purging system were activated by filling the pressure tapping lines with water through opening valves made specifically for regulating the purging liquid. A schematic diagram of present pressure drop measurement and the liquid purging system shown in Figure 3.4 and the DP transmitters on the test section are pictured in Figure 3.5. The liquid purging was set at a high rate first. This is to push out any bubbles of air presented in the tapping lines into the main system. The venting valves on DP transmitters were also used by opening them half-way for enough time and then closed, the reason for that is to get rid of any bubbles of air in the tapping lines that might be directed toward the DP transmitter instead of returning back to the main system.

During the time required for preparation of the rig for experimental work, the purging liquid in the purging line left open to flow continuously through the pressure tapping lines to the main system; the liquid rate is reduced significantly when the two phase pressure drop measurement is being made.

The efficiency of the current purging procedure was tested by repeating the measurement of two phase pressure drop for the same condition over time. As it can be seen clearly from the result (Figure 3.6), that the mean value of total

pressure drop were stayed almost constant over that period of time when the measurement taken place. Based on that, there are no noticeable traces of density changes for the liquid in the pressure tapping lines. Moreover every time the rig was started the pressure drop system was purged following the same procedure as stated previously and after each set of experiments, the two phase pressure drop measurement of one of the conditions has been repeated and compared this is as an extra checking.

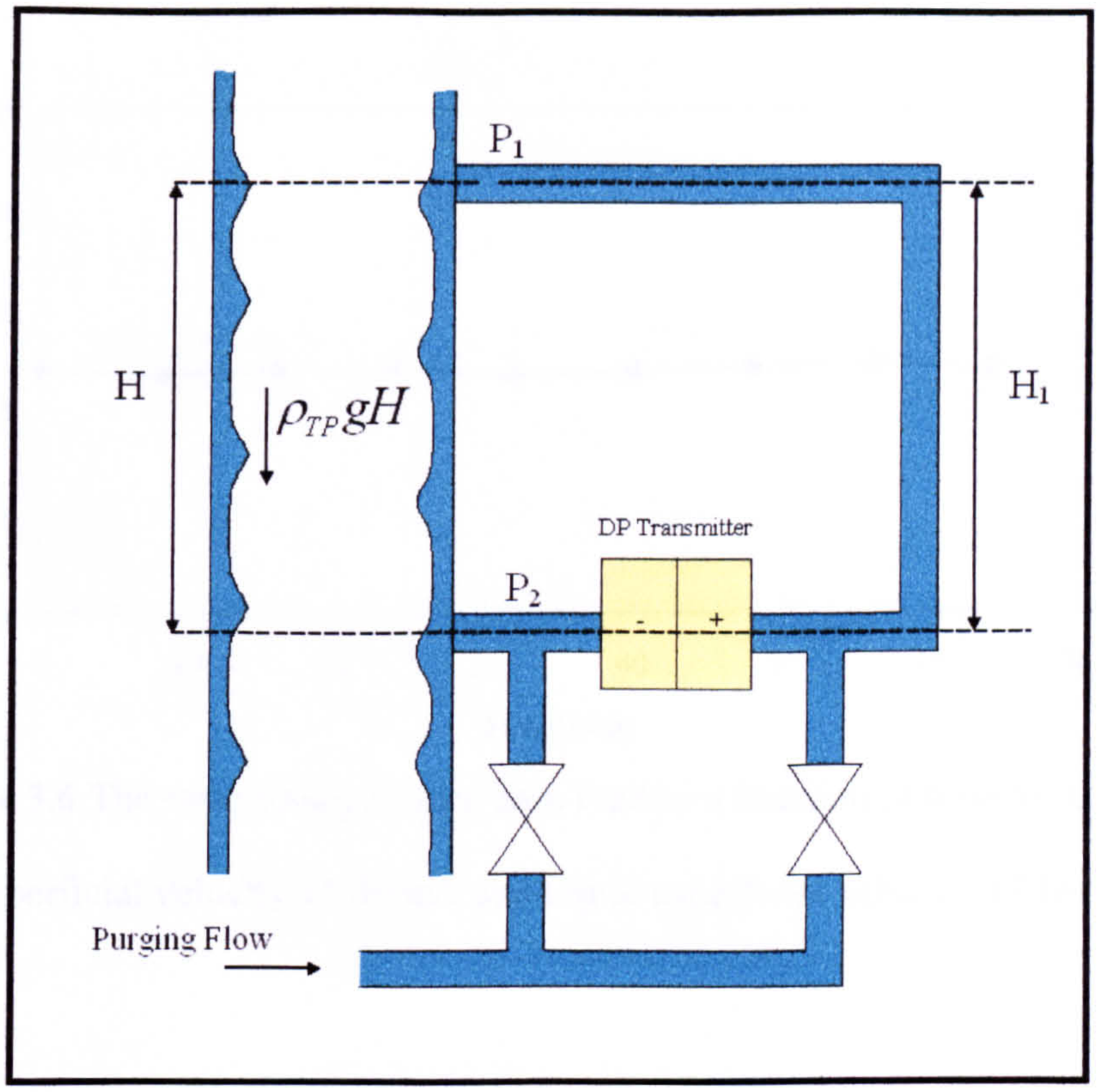

Figure 3.4 The geometry of pressure drop and liquid purging system

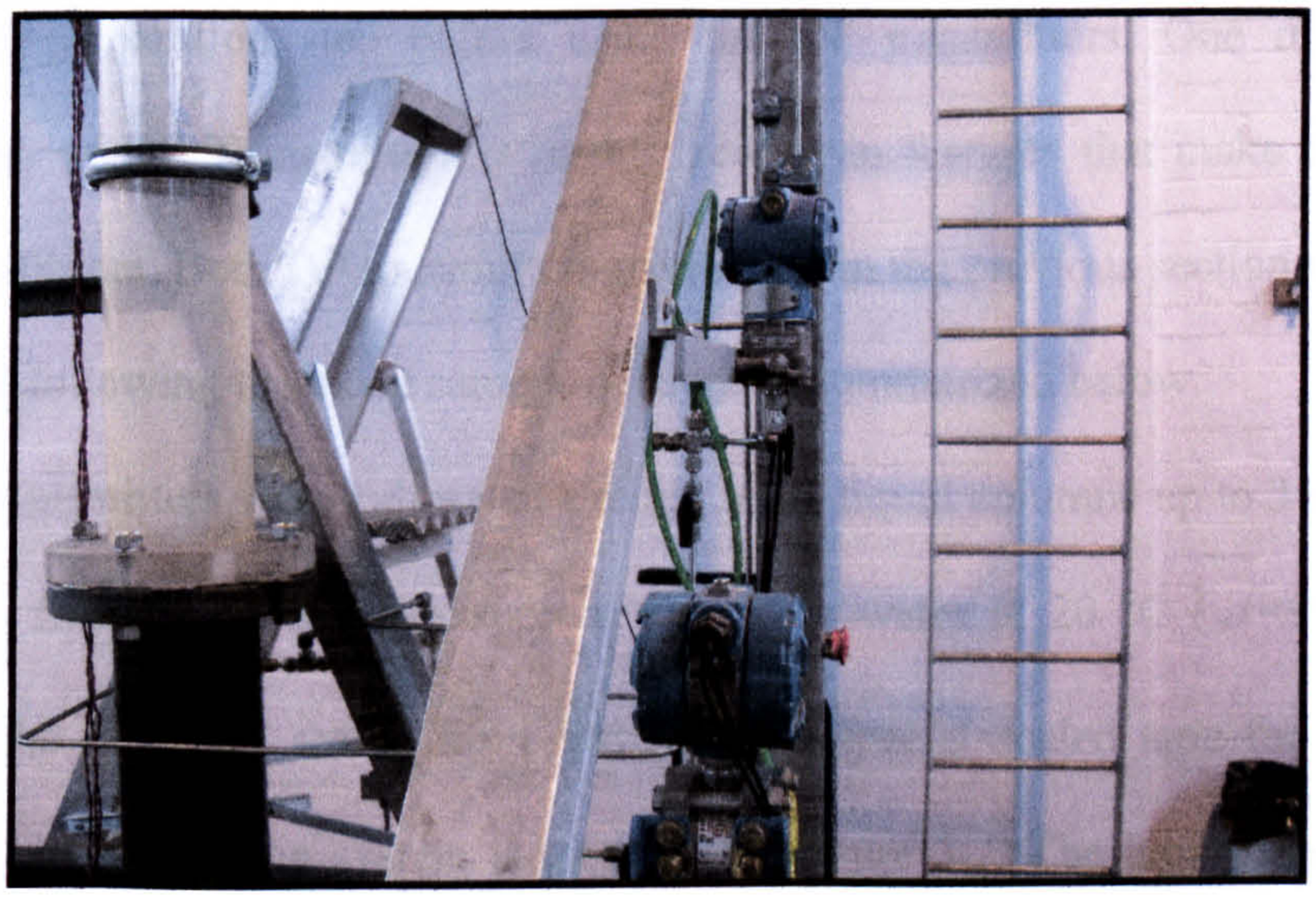

Figure 3.5 The DP Transmitters on the test facility.

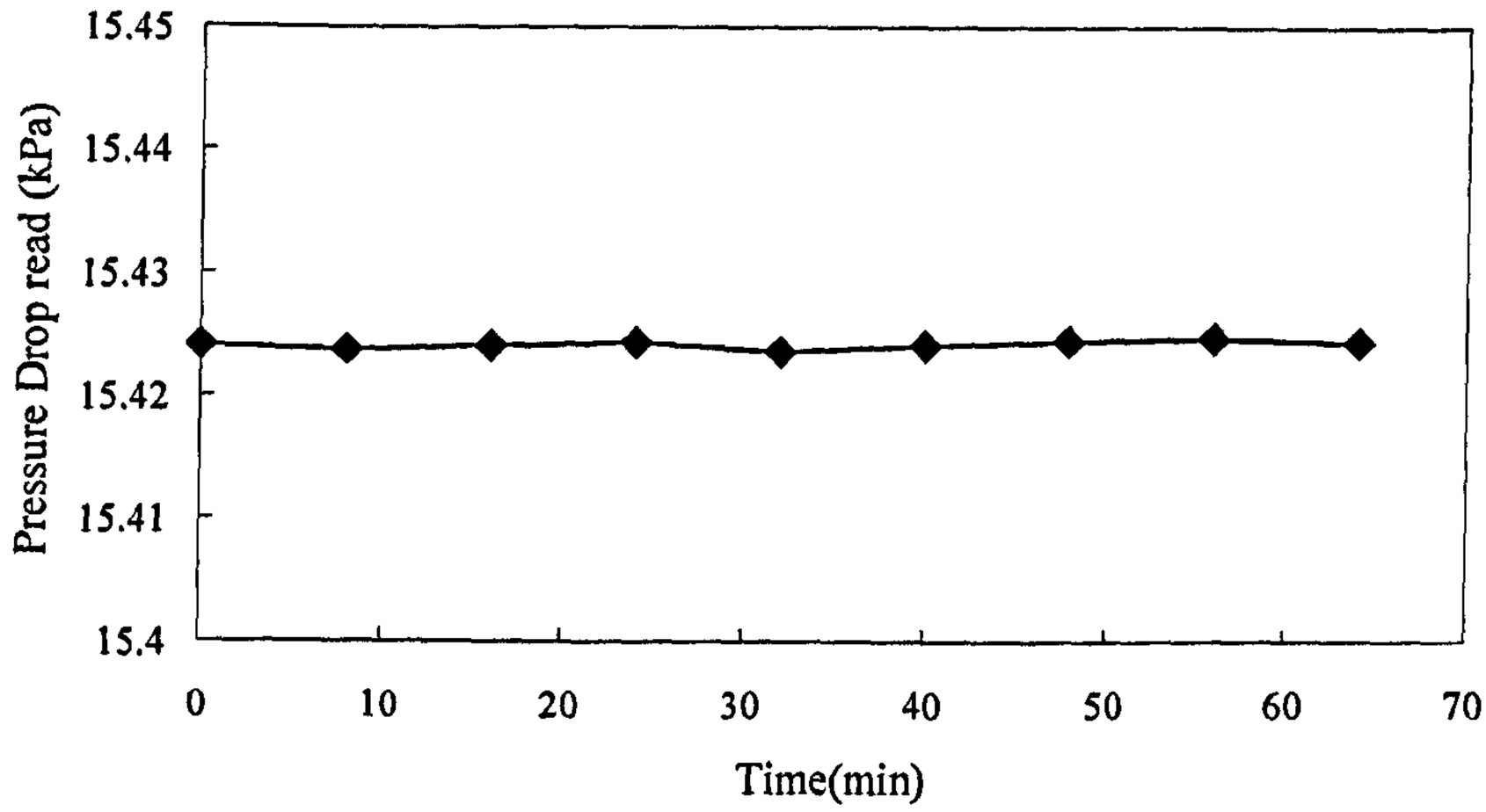

Figure 3.6 The two phase pressure drop read as a function of time for the gas superficial velocity 11.46 m/s and liquid superficial velocity 0.04m/s

3.2.2 The Calibration of DP Transmitters

As for any other measurement techniques, calibration is an essential and important preparation step before using the DP transmitters. One of the advantages of DP Transmitters is having zero span features that make them easy to calibrate. Both DP transmitters mentioned in the previous section were calibrated following the exact same procedure as summarized below:

The DP transmitters were calibrated against static liquid columns up to 3 m in length by filling a vertical transparent tube with water at 20 °C (ρ=998.2 kg/m^3). The tube was scaled from zero using a special scaled tape for that purpose. The calibration system is pictured in Figure 3.7. The high pressure inlet port (HP) of the differential pressure transmitter connected to the water column, while the low pressure inlet port (LP) just left free to the atmosphere. Before starting any reading, care has been taken to purge the system by using

the venting valves, this is to make sure that there is no air bubbles are trapped. The output voltage from the D.P. transmitter was recorded using a digital multi meter (MASTECH M-830BZ).

The calibration started by zeroing the D. P. transmitter at the lowest level of the water in the water column, the output voltage recorded was 1V at that point. Then the height of the water increased gradually by adding small amount of water to the column from the top, and with every changes of the water level the output voltage has been recorded until it reached the highest level, i.e., output voltage of 5 V. The change of the output voltage is plotted against increasing the water static head to obtain the calibration curve for each D. P. transmitter. The calibration curves are shown in Figures 3.8a and b.

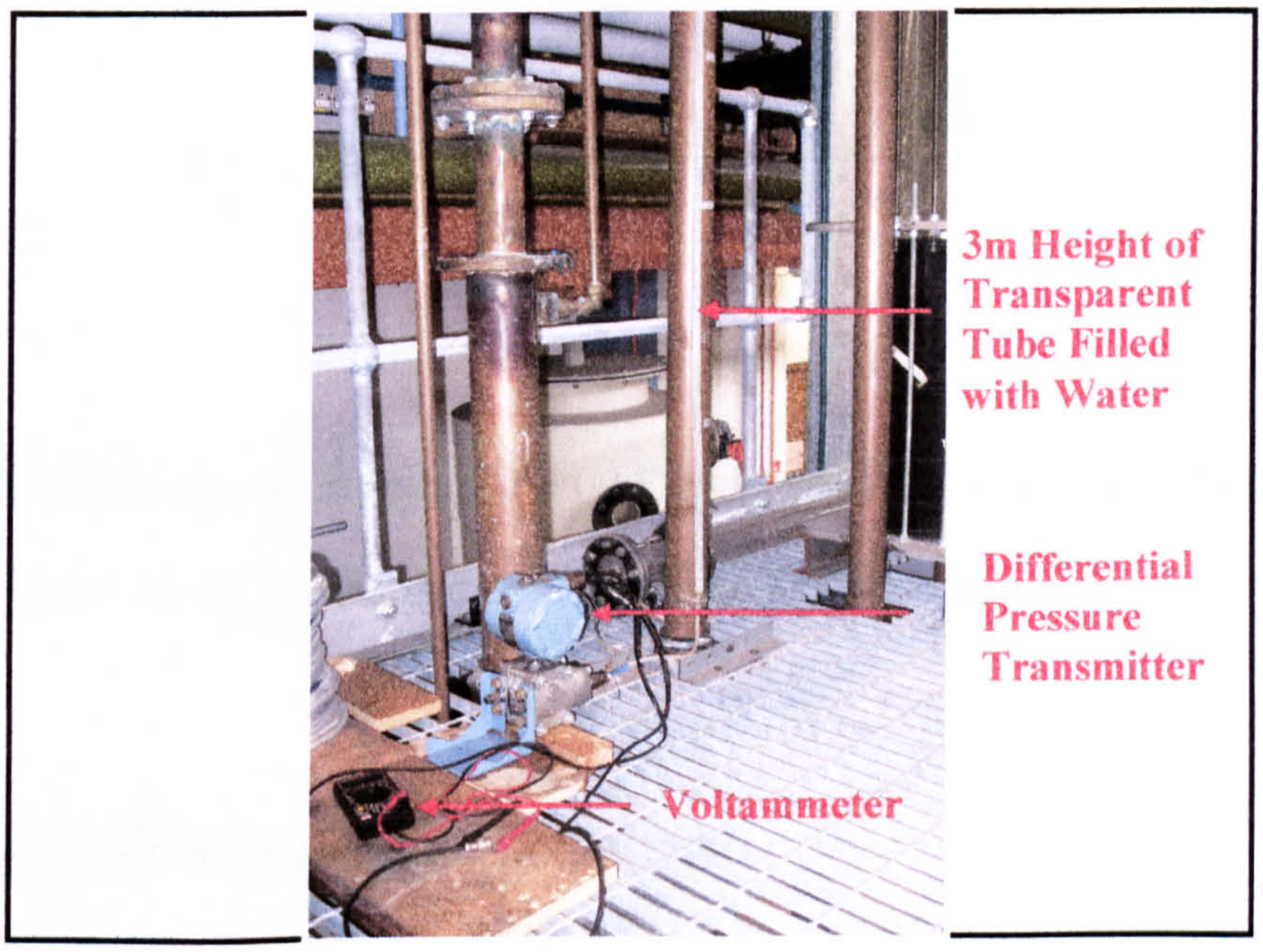

Figure 3.7 Calibration arrangements for pressure differential transmitter.

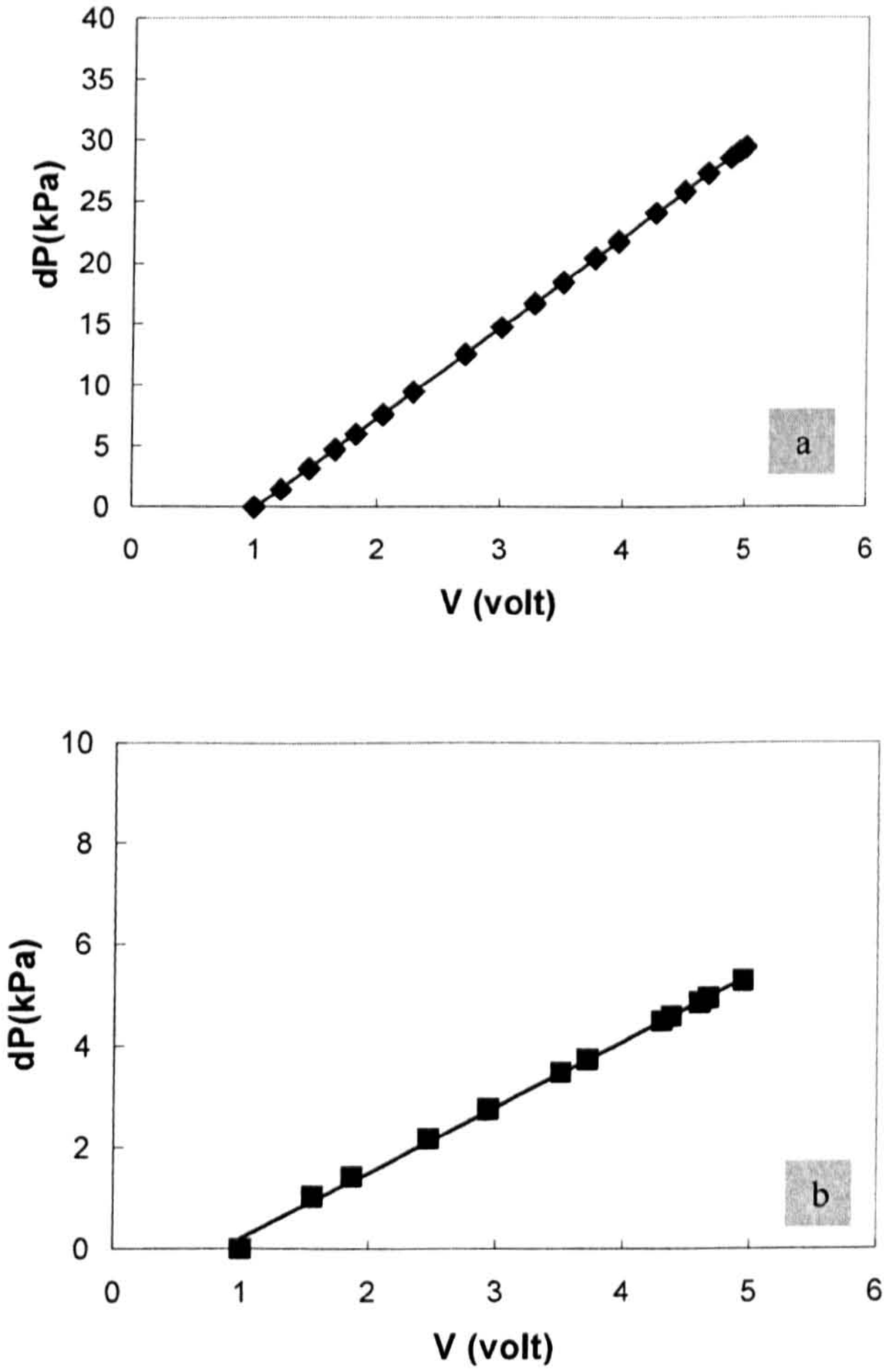

Figure 3.8 Calibration relationships for (a) Rosemount 1151 smart model D.P. transmitter (b) Rosemount 3051 smart model D.P. transmitter.

3.3 Film Thickness Measurement

In gas-liquid annular flow in pipes with a liquid that is electrically conducting, the conductance measurements are the most widely used technique to measure the liquid film thickness. The technique based on measurements of the electrical conductance between two electrodes in contact with the liquid film. Different types of electrodes such as needle probes, wire probes and flush

mounted conductance probes have been reported by the researchers over the last decades, e.g., Sekoguchi et al (1985), Koskie et al (1989), Fossa (1998), Conte et al (2003) and Belt (2007).

The non-intrusive feature of flush-mounted conductance probes was among the reasons that made this type of technique more attractive to the researchers. In addition, its ability to pick a small impedance and low mechanical difficulty during the construction in comparison with any other types of probes, make it a more practical and cost effective technique.

In the present study, the flush mounted conductance ring and pin probes were employed for the measurement of liquid film thickness. Both techniques are non- intrusive, so the flow is not to be disturbed. The flush mounted pin probes were used to measure the local thicknesses of liquid films on the pipe wall. Besides, the conductance ring probes were employed to measure the time varying liquid hold-up over the cross sectional area of the pipe and as a result the average liquid film thickness for annular-type flow can be obtained from the following relationship (Kaji and Azzopardi, 2010):

$$\delta = \frac{D}{2}(1 - \sqrt{\varepsilon_G}) \tag{3.1}$$

Where D is the diameter of the pipe and ε_G is the gas void fraction.

3.3.1 Flush Mounted Parallel-Conductance Ring Probes and their Calibration

In the present study three parallel conductance ring probes were employed and they were located at three different heights on the riser from the mixing unit as stated in the beginning of this chapter. The probes are the same as described by Omebere-Iyari (2006). They were identical in the shape and the size. Each probe consists of a pair of stainless steel electrodes of 3 mm thickness (s) and spacing (D_e) of 25 mm (Figure 3.9); this gives an electrode width to pipe diameter ratio (s/D) of 0.024 and the electrode spacing to pipe diameter ratio (D_e/D) of 0.2. The electrodes were insulated using non- conducting acrylic resin. The probes were flush mounted with the pipe wall and they were designed to have the exact diameter as the test section.

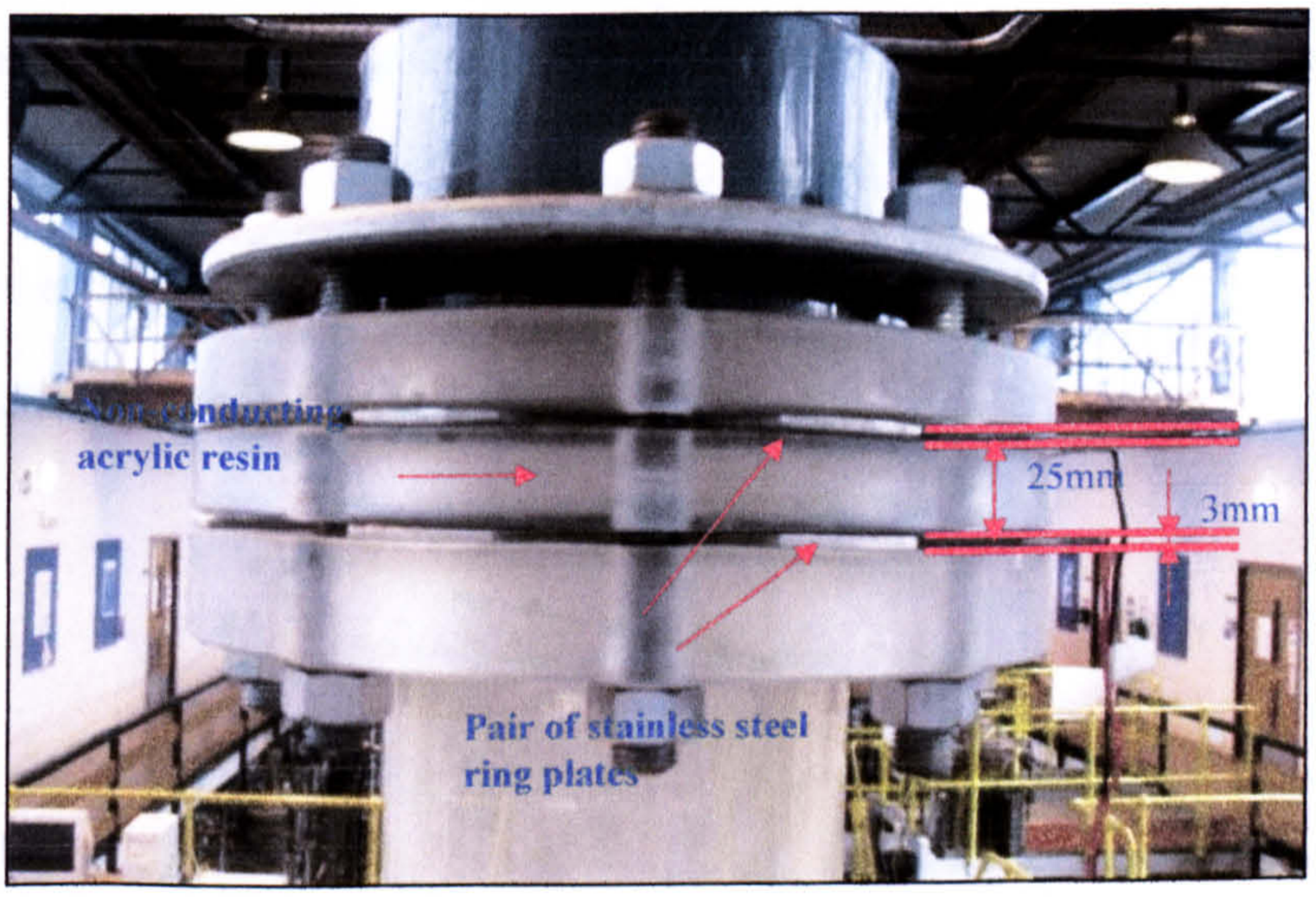

Figure 3.9 the parallel conductance ring probe

To assure better accuracy, the probe must be calibrated before the measurement as recommended by other researchers, e.g., Fossa (1998). The parallel conductance ring probes employed in the present study were calibrated by Omebere-Iyari (2006) for both bubble and annular flow regimes. The latter type of flow is simulated by placing a non-conducting cylindrical plastic rod with a known diameter inside the pipe and filling the annulus between the rod and pipe wall with a conductive liquid. By repeating this procedure with plastic rods of different diameters, void fraction/ dimensionless conductance relationship were obtained. Following the same procedure the probes were re-calibrated by Van der Meulen et al (2009). However, in the latter approach the effect of gas bubbles in the liquid film was taken into consideration. The gas bubbles in the liquid film were simulated by adding a known volume of spherical glass beads with different diameter ranging from 3 to 6 mm to the annulus between the non-conducting rod and the pipe wall (for further detail on the role of the glass beads during the calibration see Van der Meulen et al, 2009). The calibration curves for annular type flow for both approaches shown in Figure 3.10.

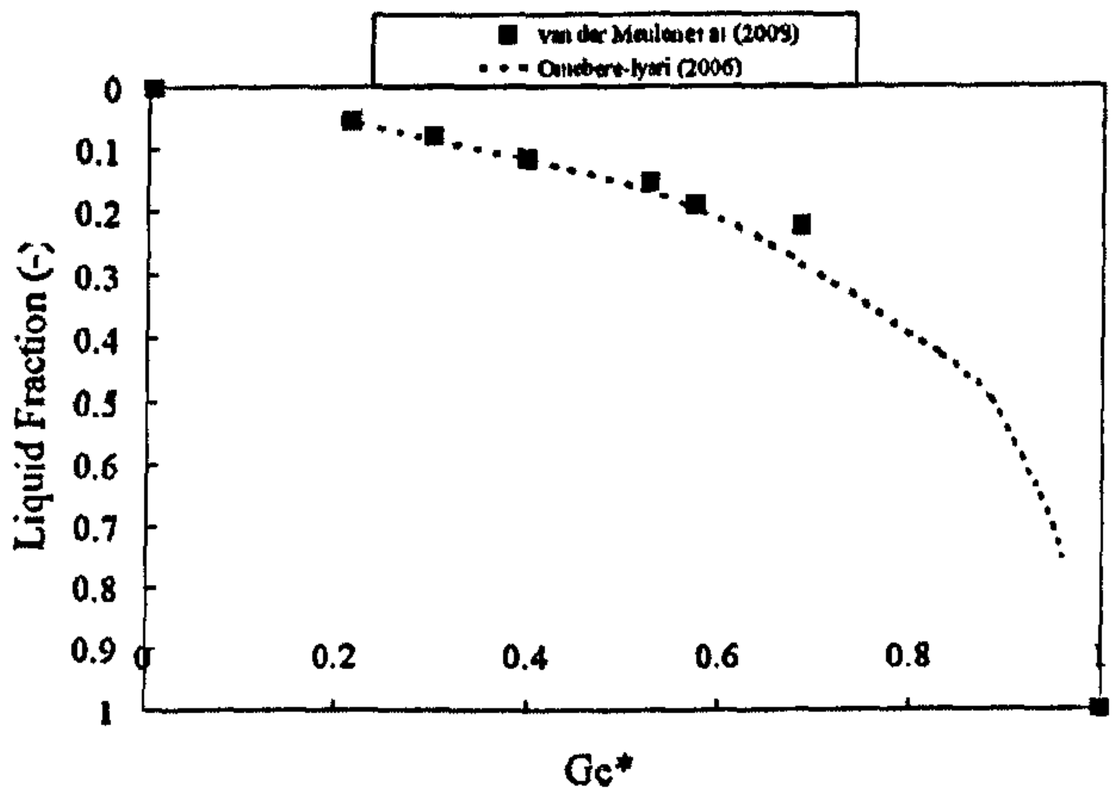

Figure 3.10 calibration relationships of conductance ring probes for annular type flow.

3.3.2 Flush Mounted Pins Probe and their Calibration

In annular type flow it is important to measure the liquid film thickness and wall shear stress simultaneously as they are related to each other and to the liquid film flow rate through the triangular relationship described in Chapter 2. Such measurements of liquid film thicknesses in small diameter pipes has been reported by researchers, e.g., Martin (1983) and Wolf (1995), using conductance measurement technique at different positions of the test section. In the present study, 4 pairs of flush mounted pins probe were employed on each side of the test section (Figures 3.11 a and b and 3.12 a and b) to locally measure the liquid film thickness on the pipe wall without disturbing the flow and at four different positions around the wall shear stress probe, i.e., close to the bottom, top, right and left of the wall shear stress probe. In spite of the fact that these probes have the same principle as described by Martin (1983), Wolf (1995), Conte (2000) and Belt (2006), however this arrangement can be considered as unique in terms of the selected locations of the probes to the wall shear stress sensor. Govan et al (1990) and Martin (1983), have reported a significant effect of disturbance waves on wall shear stress when they pass moving upward in vertical annular flow, that being the case, the current arrangement of liquid film thickness measurement can be more reliable specially for the large diameter pipes as the waves are circumferentially localized according to Azzopardi et al (1983) instead of being coherent as been observed by Hewitt and Lovegrove (1969) for smaller diameter pipes.

Each of the current probes consists of a pair of stainless rod of 1.5 mm

diameter with a spacing distance of 4.5 mm as shown in Figure 3.11a. The spacing distance between two electrodes, i.e., the transmitter and the receiver, is based on the principle that the measurement accuracy of the probes is a function of the distance between the electrodes (Coney, 1973). Higher spacing between the electrodes leads to lower resolution and accuracy of the liquid film thickness measurement. The probes were positioned onto the test section by inserting each pair of the electrodes through a cylindrical Perspex rod of 10 mm diameter to assure an accurate location of the probes without causing any damage to the test section. For the probes to be perfectly flush with the inner diameter of the test section they were machined very carefully taking different hardness of the steel and the Perspex into consideration. On each side of the test section, 4 pairs of electrodes were located as shown in Figures 3.12a and b. The signals from 4 probes on each side of the test section were obtained simultaneously. The voltage was applied by an electronic box designed and previously used by Conte (2000); the probes were driven by 10 kHz current. The flow of electrical current from a transmitter in one probe to the neighbor receivers and transmitters (cross–talk) will decrease the spatial resolution of the sensor and increase the measurement errors of the liquid film thickness (Belt 2006). For the probes employed in the present study, each probe has an average distance from another probes of 12 times the distance between the transmitters and the receivers in one probe this is in addition that all the probes are located in the body of the test section which is made from acrylic resin (i.e., they were insulated from each other by non conductive material). Moreover all the probes were calibrated simultaneously in the same position as they were located in the test section and with the same signal acquisition

arrangement as been used during the experiments (Figures 3.13 a and b).

During the calibration of the local film pins probe, a high level of care has been taken as dealing with a thin film of liquid. The conductance pins probes were calibrated simultaneously as they were employed during the measurements of liquid film thickness in vertical two-phase flow. The calibration procedure consists of using a non-conducting solid rod (PVC) with the same diameter as the test section. The rod was machined very carefully to reduce its diameter by 0.5 mm each time until 3.5 mm thickness achieved (i.e., 7 mm total diameter reduction). This is done to produce a static film of liquid on the wall of the test section by filling the annulus between the PVC rod and the pipe wall with a conductive liquid (water). The diameter of the rod was measured with an accuracy of better than 10 μm. The rod was centred correctly at the bottom and the top of the test section using a plastic insert made specifically for that purpose. The calibration repeated several times and with different rotations as an extra check. The probes were calibrated with three different conductivities (589, 498 and 235 μS/cm). The conductivity of the liquid was kept constant during the calibration over temperature changes of less than 0.5 °C. The output voltage as a function of liquid film thickness was recorded and as a result the calibration curve for each probe was obtained. The calibration curve of probes 3 and 4 are shown in Figure 3.14.

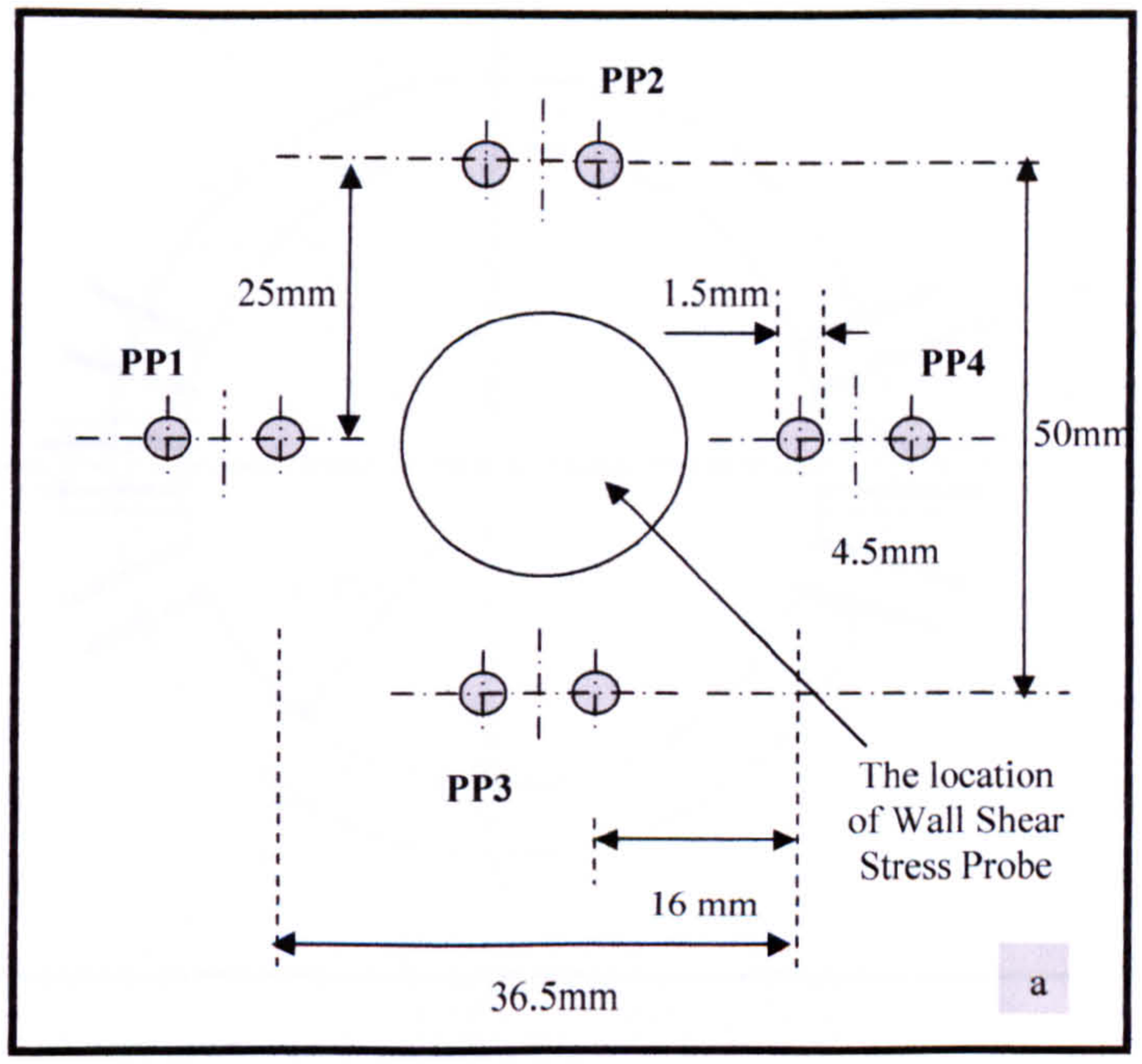

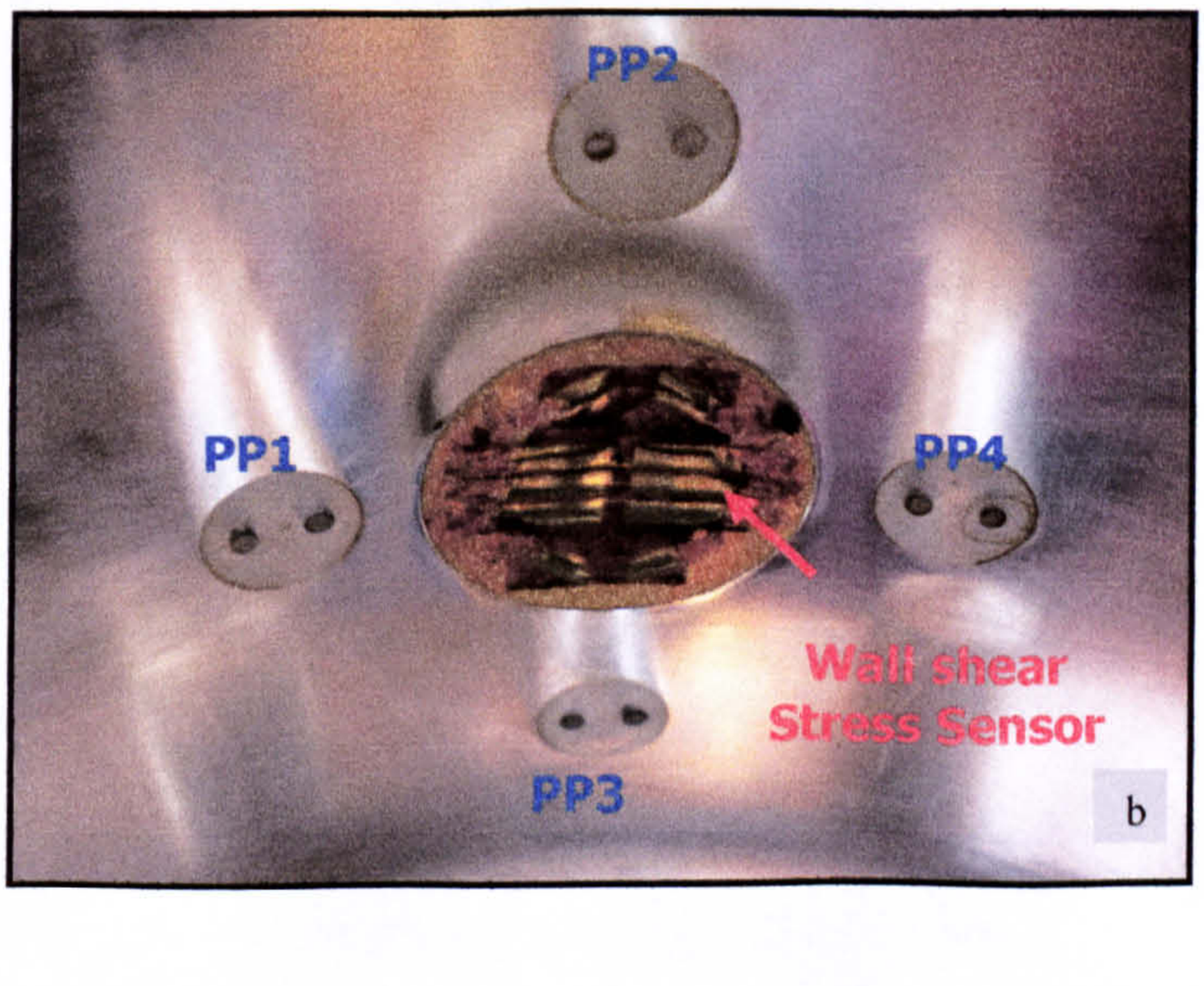

Figure 3.11 a) the diagram of the flush mounted pins probe b) the pins probe as mounted flush inside the test section.

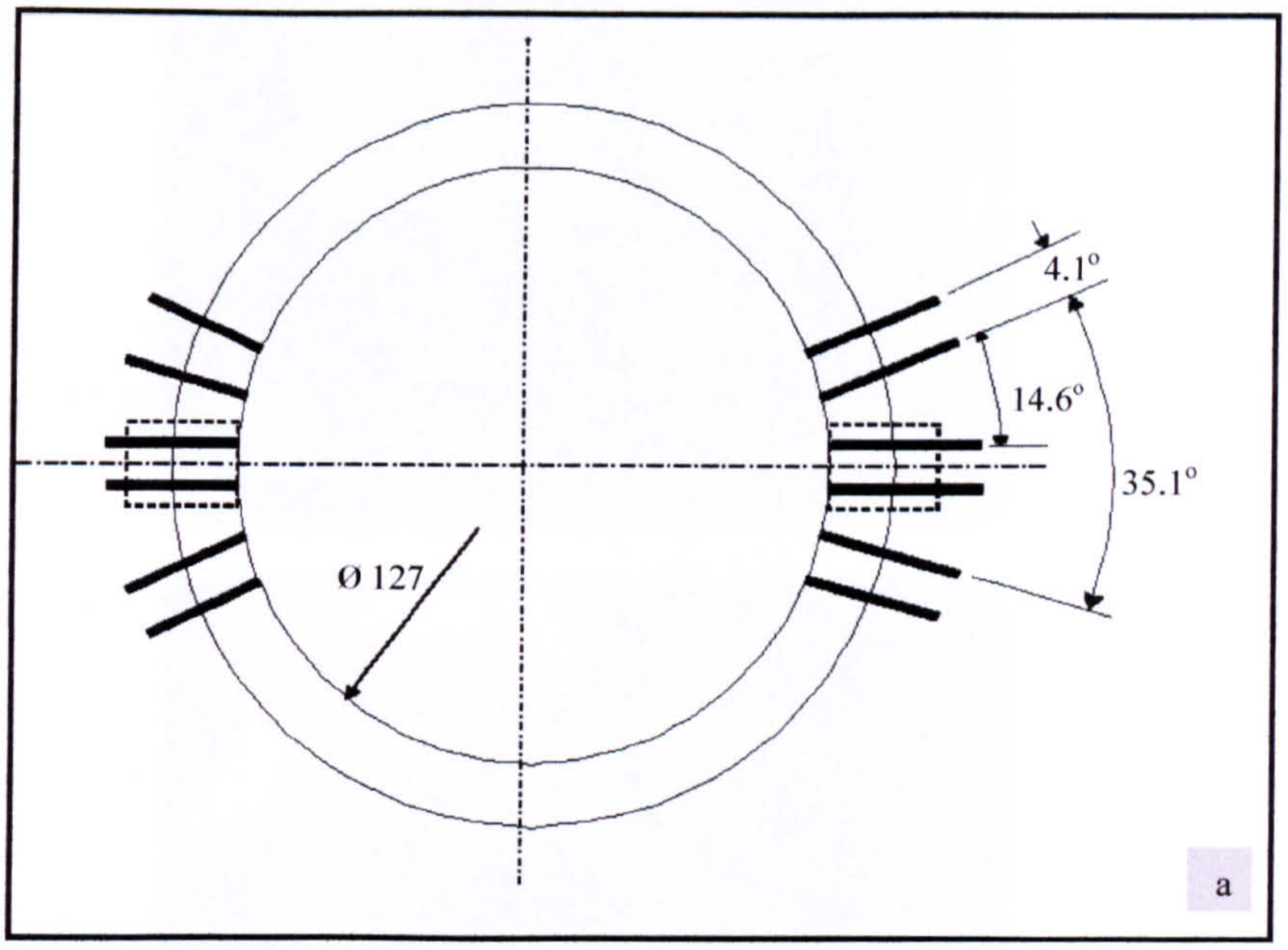

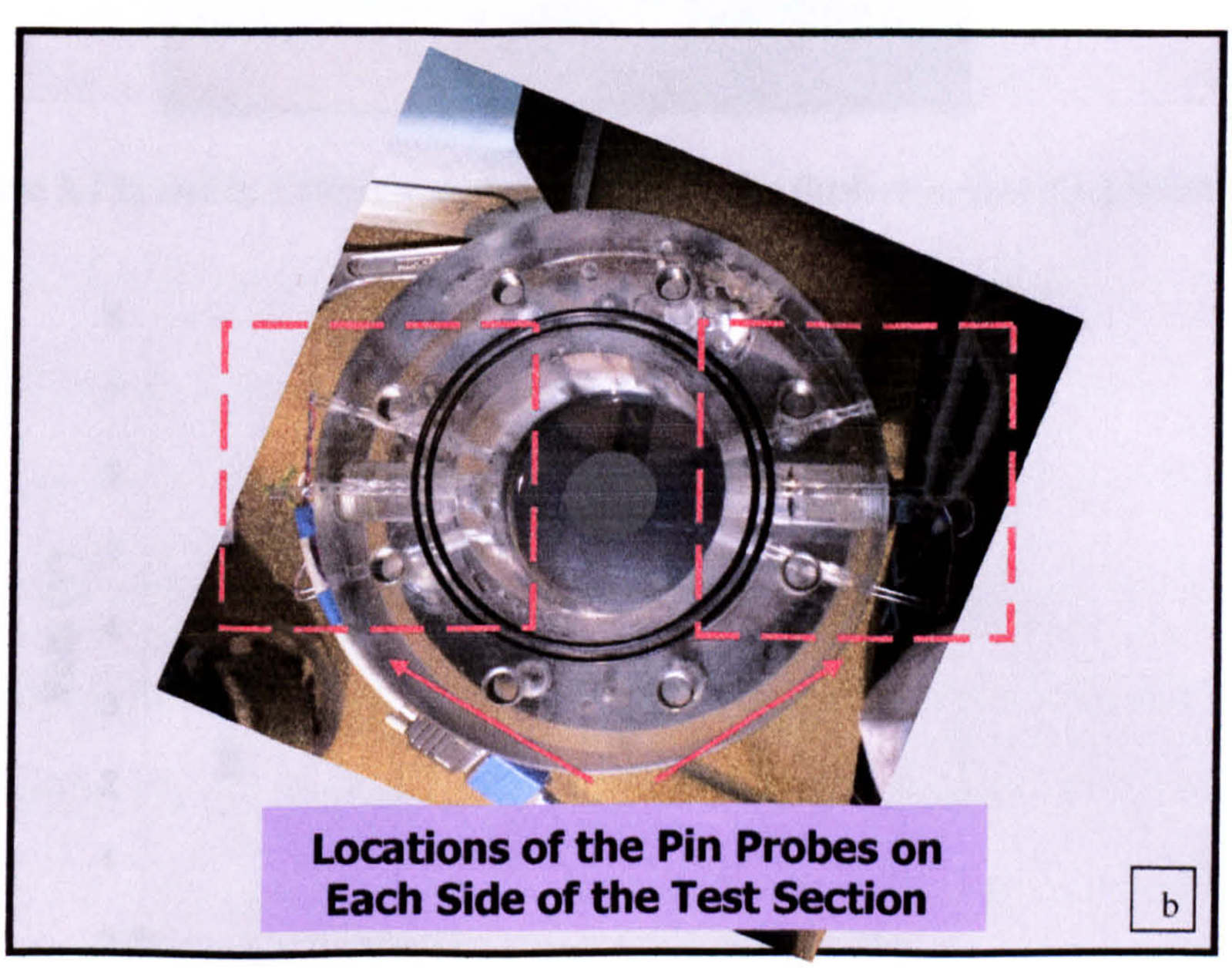

Figure 3.12a and b: Cross section view of the test section with the flush mounted pins probe

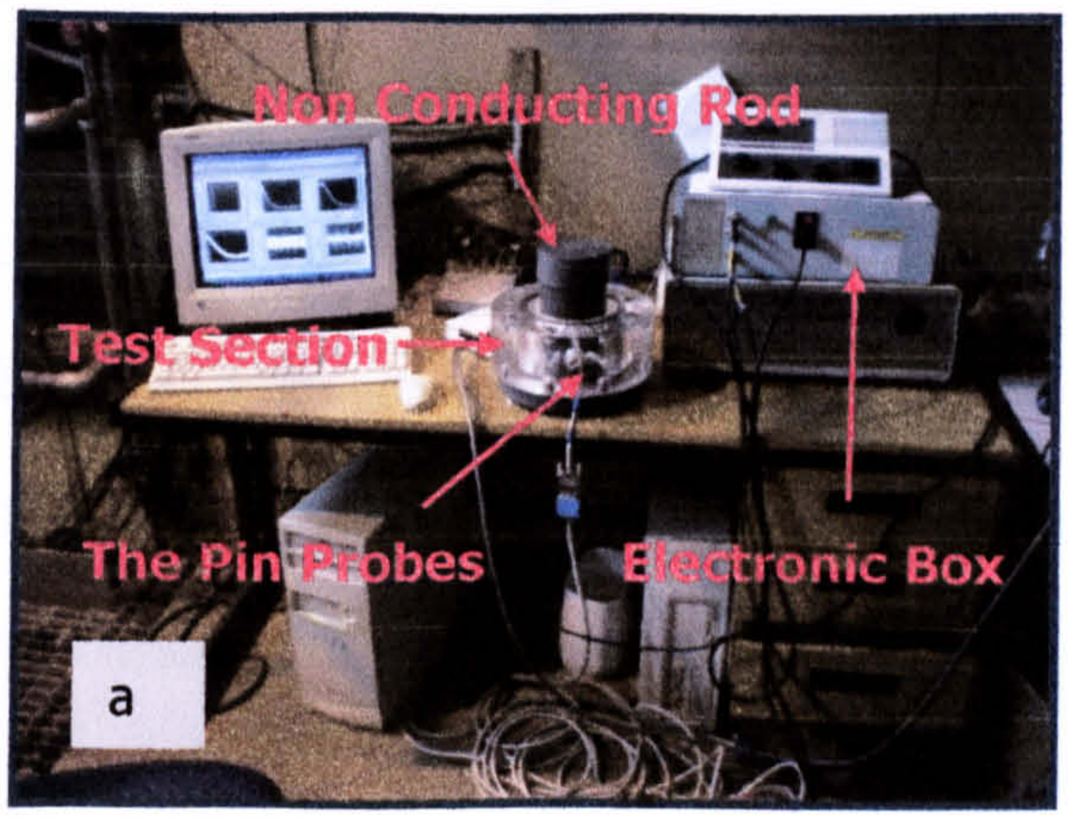

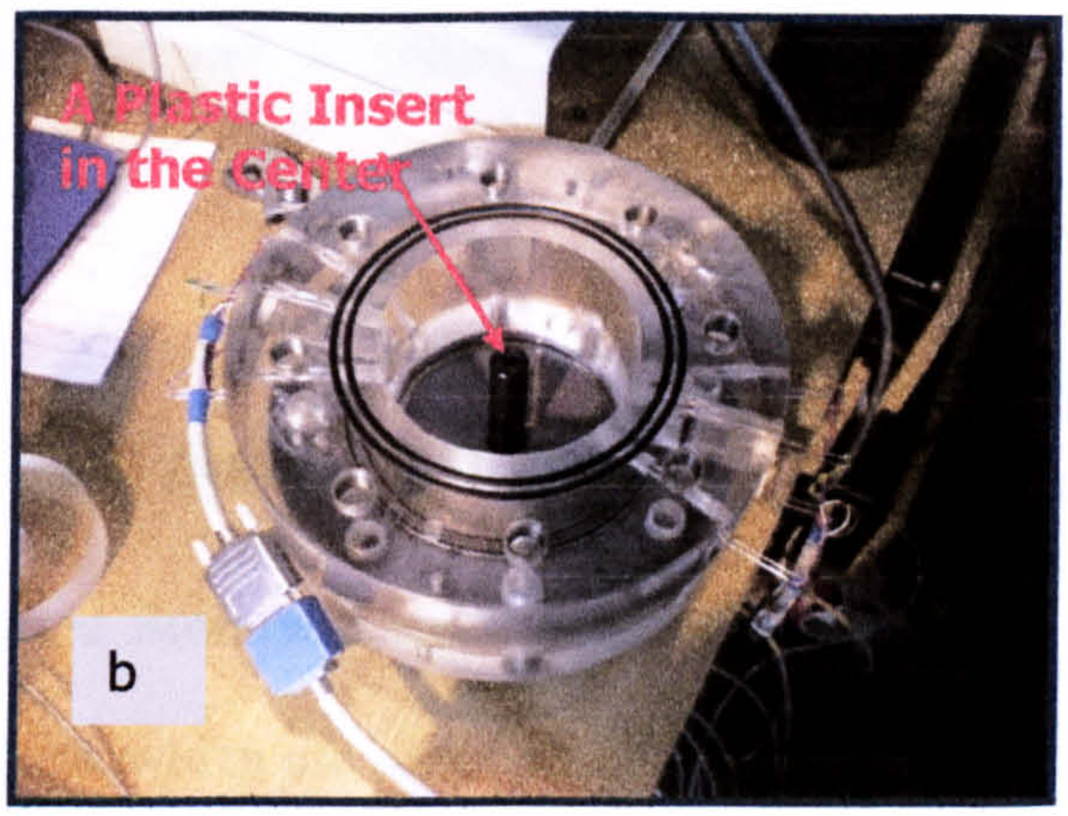

Figure 3.13a and b: Calibration arrangement of the flush mounted pin probes

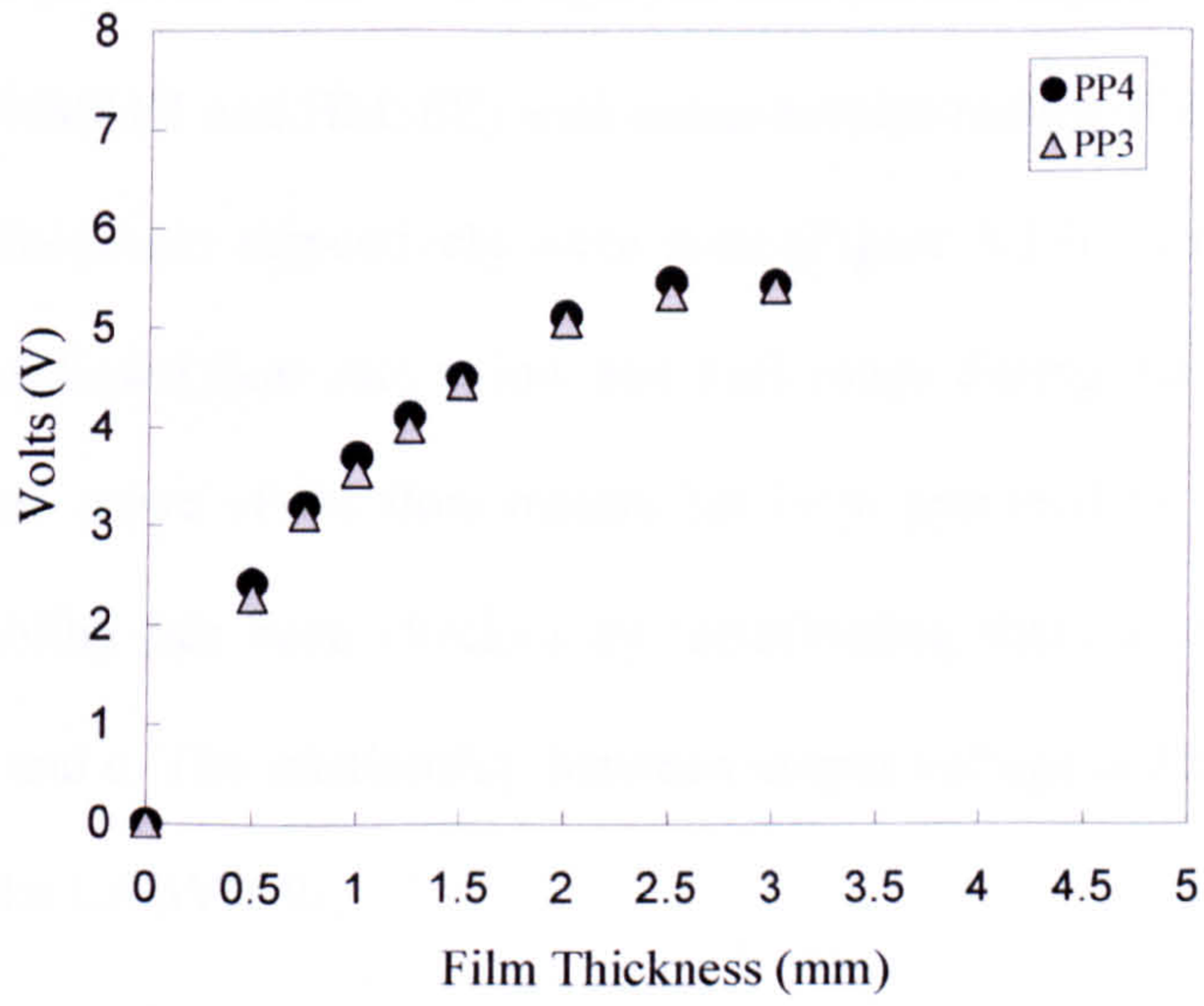

Figure 3.14 Calibration curves of pin probes 3 and 4.

3.4 Wall shear stress measurement

During the current study data on wall shear stress in large diameter riser has been obtained using a commercial hot film probe marketed by DISA Electronics (DANTEC 55R47) and directional wall shear stress which is manufactured at Nottingham University. A trial using Micro Pillar Sensor (MPS) were also carried out. The principles, the construction, the methodology of use and all others details of the techniques are given in Chapter 5.

3.5 Flow rate measurement

The gas and liquid flow rates were measured using vortex and turbine flow meters respectively which are supplied by Kuppers Elektro Mekanic (KEM)-GmbH. For the gas flow rate a flow meter (KVM 080) with a measurement range of 35-1030 m^3/hr was employed and for the liquid flow rate two flow meters (HM11R and HM36E) with measurement ranges of 6-60 liters/min and 40-500 liters/min respectively were used (Figure 3.15). This is done to keep control of liquid flow rate at low and high range during the experiments. The calibration curve of the flow meters has been provided by manufacturer and their stability has been checked by recalibrating them as shown in Figures 3.16a, b and c. The relationship between output voltage and the flow rate were used in the LABVIEW.

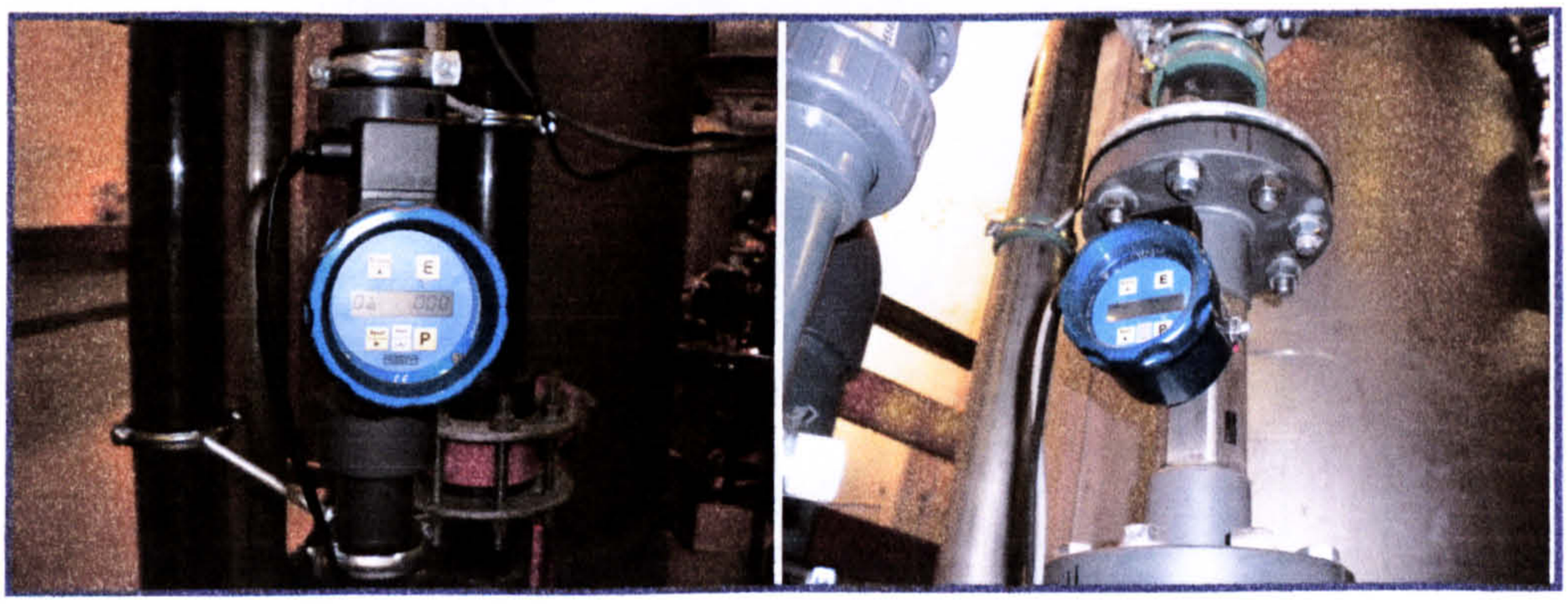

Figure 3.15 Turbine flow meters on the test facility.

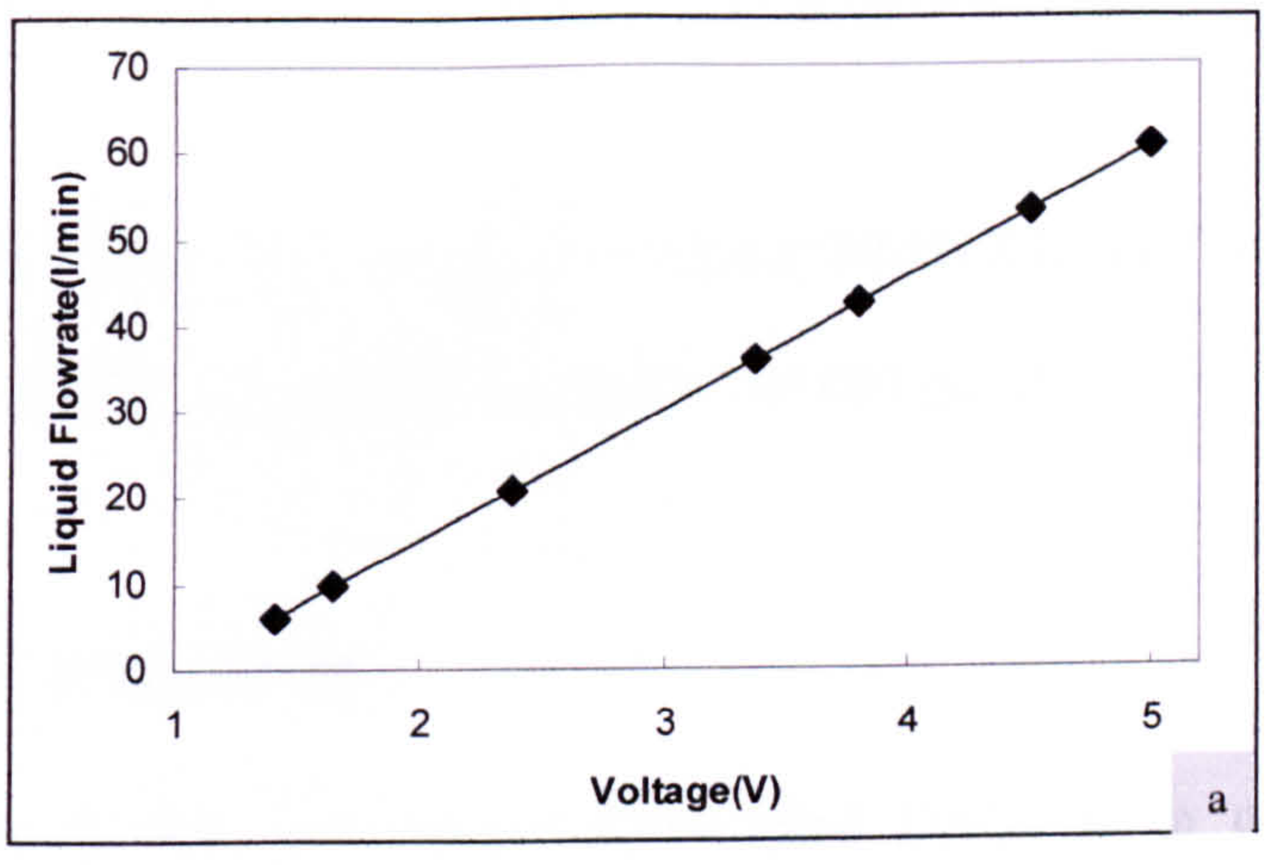

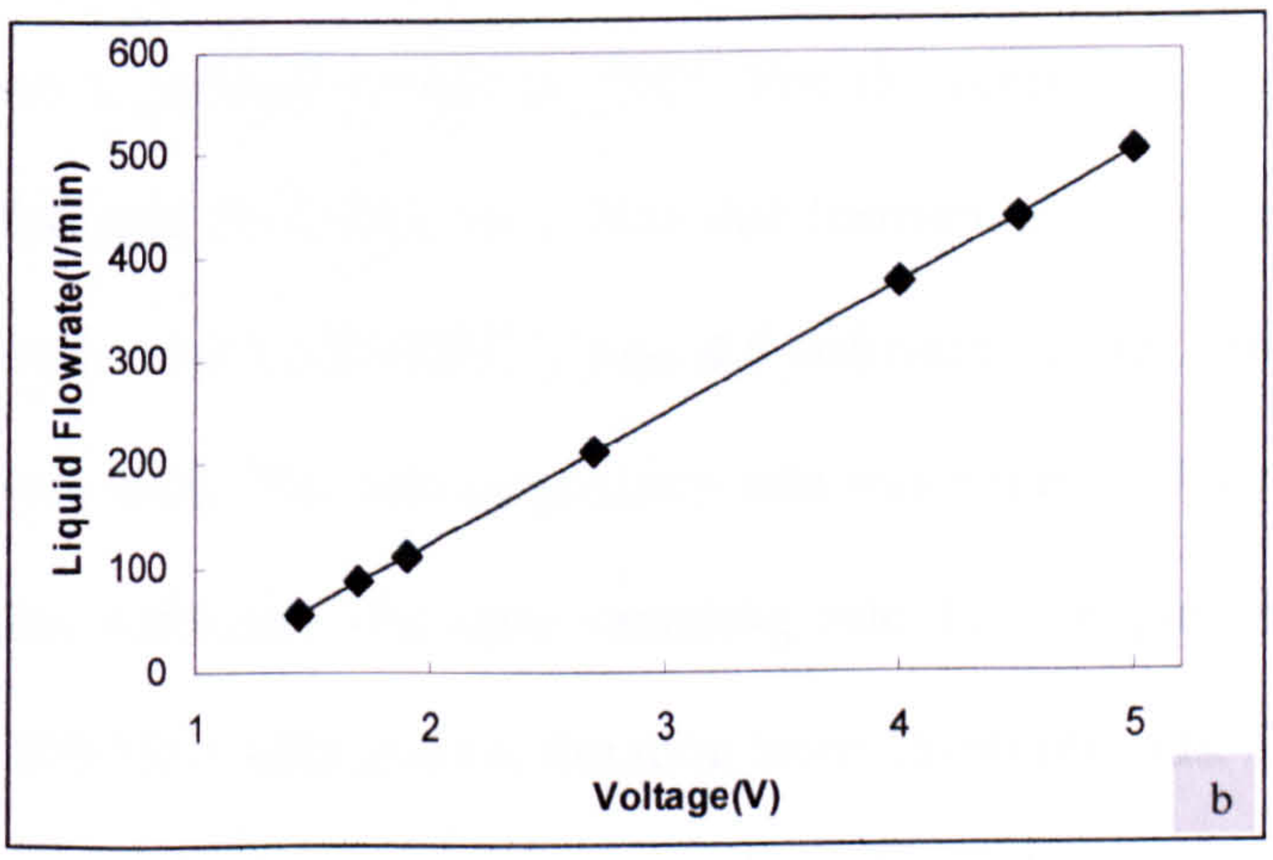

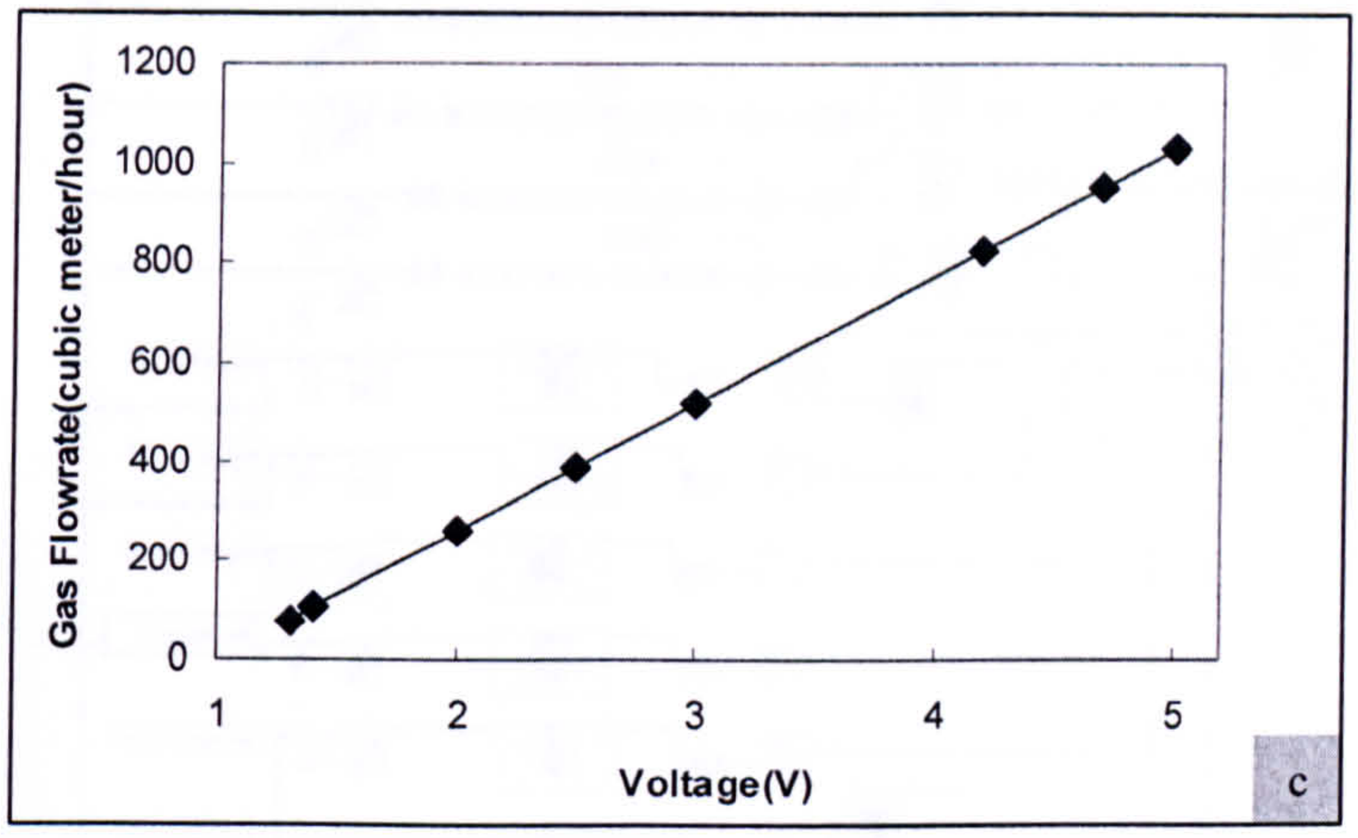

Figure 3.16 voltage/flow rate relationships a) HM11R liquid flow meter. b) HM36E liquid flow meter c) KVM 080 gas flow meter.

3.6 Data acquisition

The objective of data acquisition (abbreviated DAQ) is to convert the electrical signals from the sensors to the digital numeric values that can be manipulated on a personal computer (PC). For the present data acquisition system a 32 channels DAQ card from National Instruments were employed as a DAQ hardware, and LABVIEW 7 and 8.6 software, again form National Instruments were used. The data acquisition rate was controlled using built-in functions in the software. The data sampling rate for the present study is ranging from 200 Hz-1 kHz and for duration from 15-60 seconds. The signals from the sensors were obtained simultaneously and saved on a PC as EXCEL files. The block diagram that the current data acquisition was carried out on is shown in Figure 3.17.

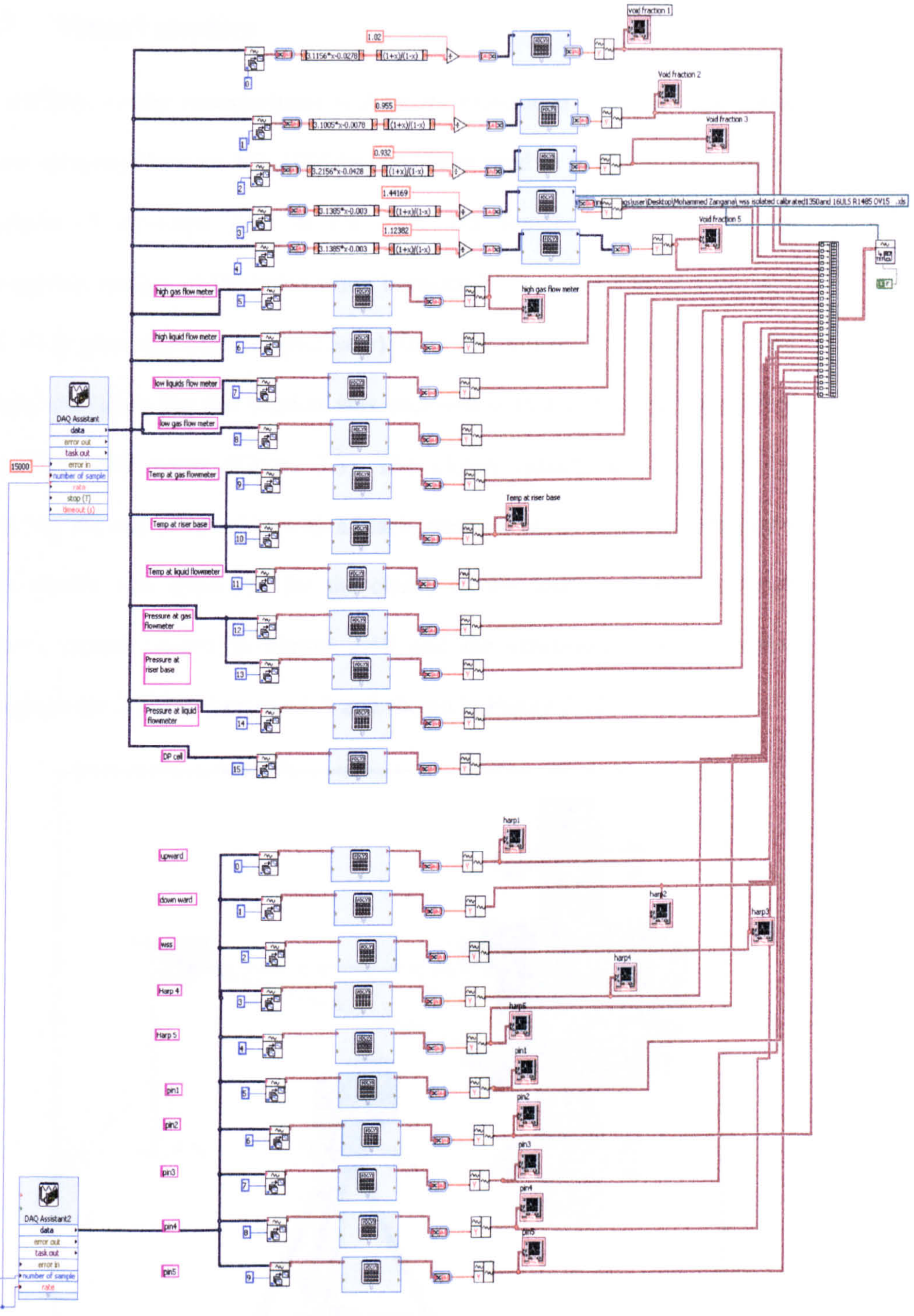

Figure 3.17 Block diagram of the Labview program for data acquisition

3.7 Visual studies

In addition to the measurement techniques mentioned above a high speed video camera (Phantom V7, 1000fps) has been used to visualise the complex structure of air-water flow in the riser. The images were taken in the transparent section of the test section between 7.65 m and 7.85 m (i.e., 60.2 and 61.8 pipe diameters respectively) from the mixer. To reduce the pipe optical curvature the test section was enclosed with a cubic and transparent box filled with water (Figure 3.3). The picture quality was improved by covering the rear of the pipe with a black plastic sheet as a background and a light source was employed for the clarity of the images. The high speed camera system shown in Figure 3.18 and the conditions studied in this campaign are listed in Appendix A and shown in Figure 3.22.

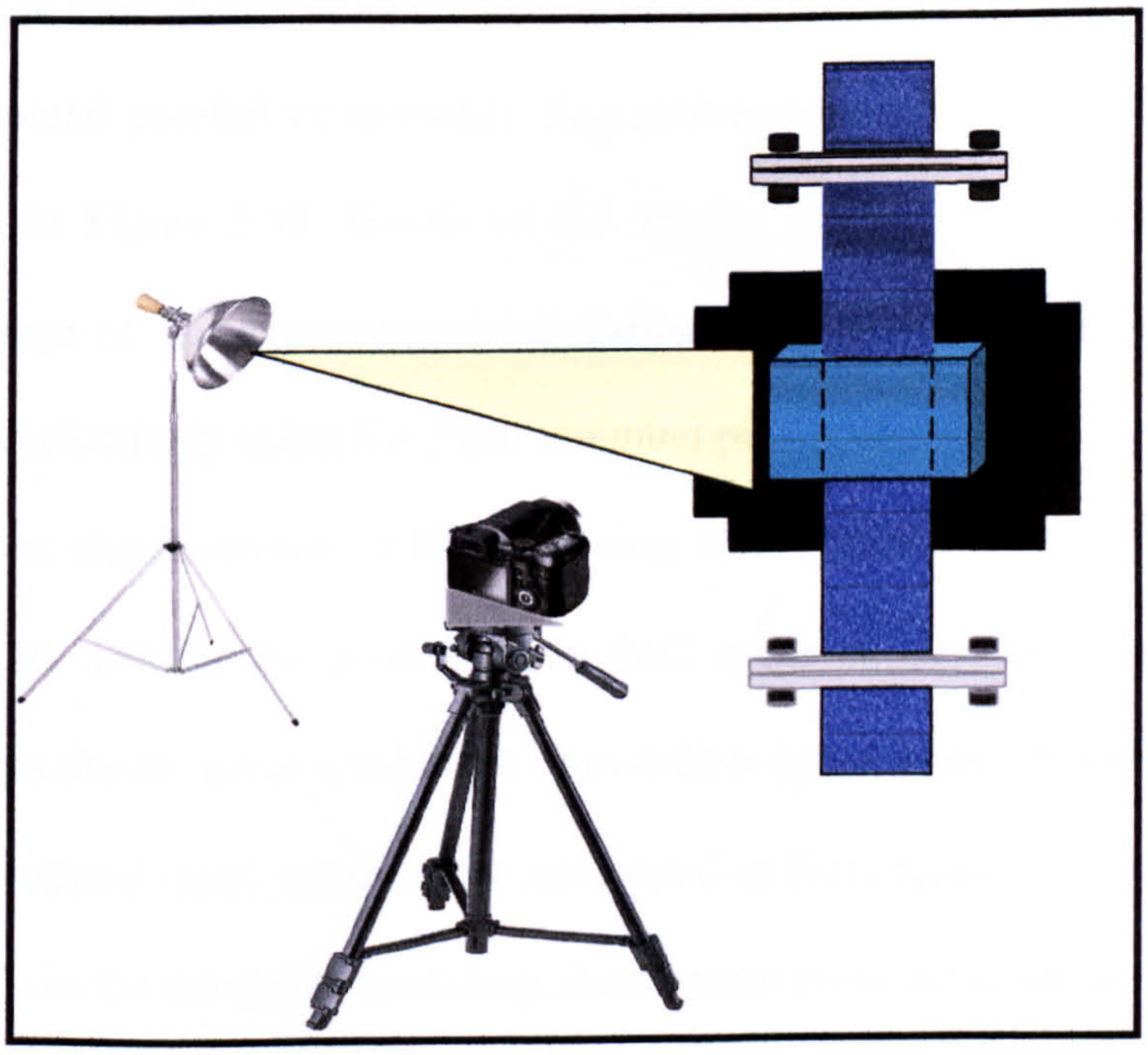

Figure 3.18 High speed video camera systems.

3.8 Experimental conditions

All the experiments presented in this study were performed on the large diameter vertical pipe at various gas and liquid superficial velocities ranging from 2.5-16.5 m/s and 0.008-0.7 m/s respectively. The conditions are listed in Appendix A and the ranges of the gas and liquid superficial velocities studied in various experimental campaigns are also shown in Figures 3.19, 3.20, 3.21 and 3.22. Experimental data on total pressure drop, liquid film thickness and wall shear stress were obtained in systematically planned campaigns which are summarised below:

In the first stage a total of 600 runs were performed to measure simultaneously the total time-varying and averaged pressure drop and the averaged liquid film thickness at three different heights along the riser using a D.P. transmitter and flush mounted parallel conductance ring probes respectively. Conditions are indicated in Figure 3.19. Based on the results from the first stage, in the second stage of the experimental campaigns the liquid film thickness were measured selectively using the flush mounted pins probe and the conductance ring probes simultaneously with measuring total pressure drop as shown in Figure 3.20. During the present study wall shear stress was measured for selected conditions using a commercial non-directional sensor (Dantec 55R47) and a directional shear stress probe developed at Nottingham University (see Chapter 5).in the campaign including shear stress measurements, the ring and pin conductance film thickness probes were also used and the pressure drop was measured. The conditions for this campaign are summarised in Figure 3.21.The experimental campaigns performed in this work also included a

visualization study of the flow using a high speed video camera for the conditions shown in Figure 3.22.

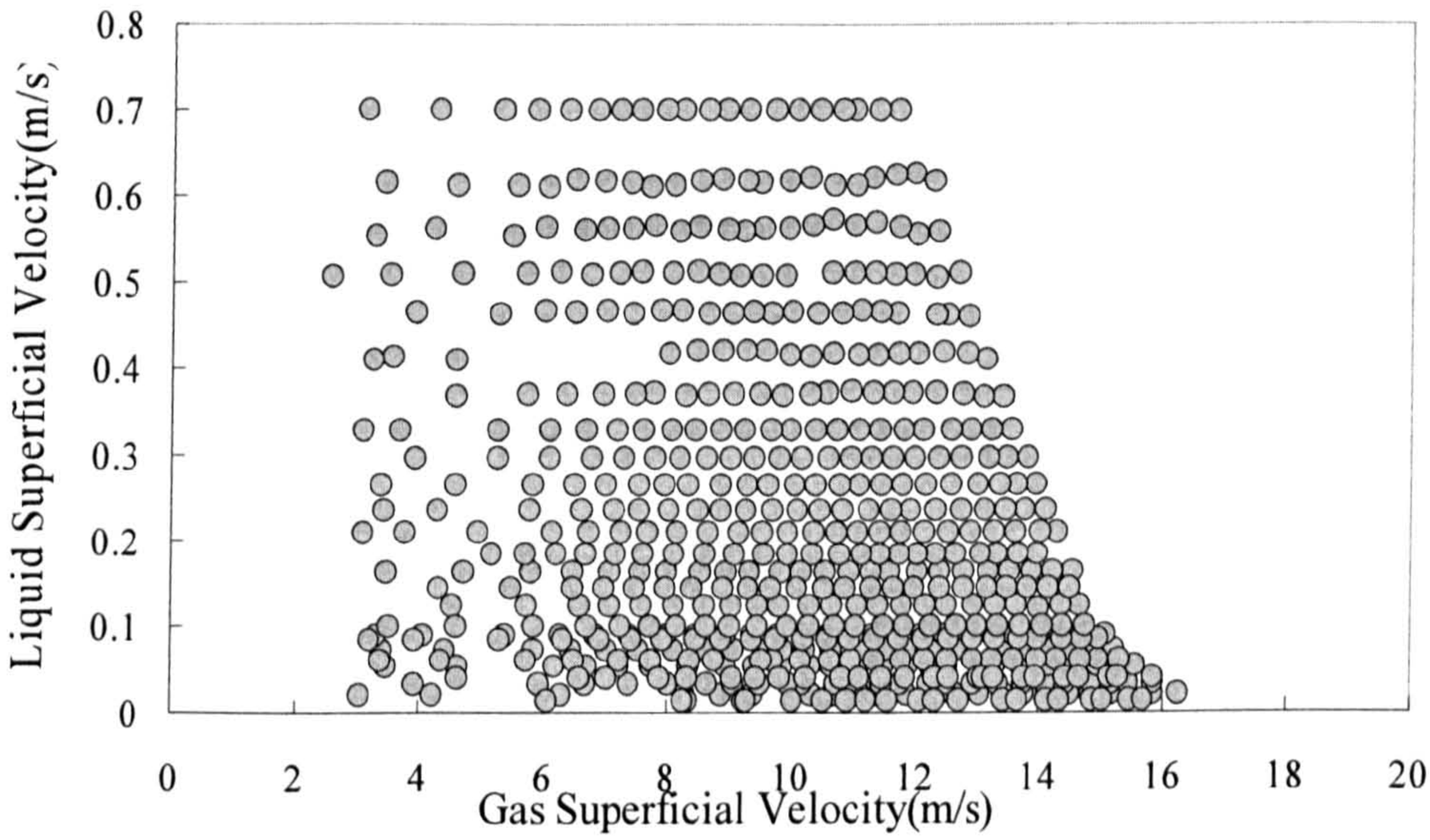

Figure 3.19 Conditions studied during the simultaneous measurement campaign of total pressure drop and liquid film thickness using the conductance ring probes.

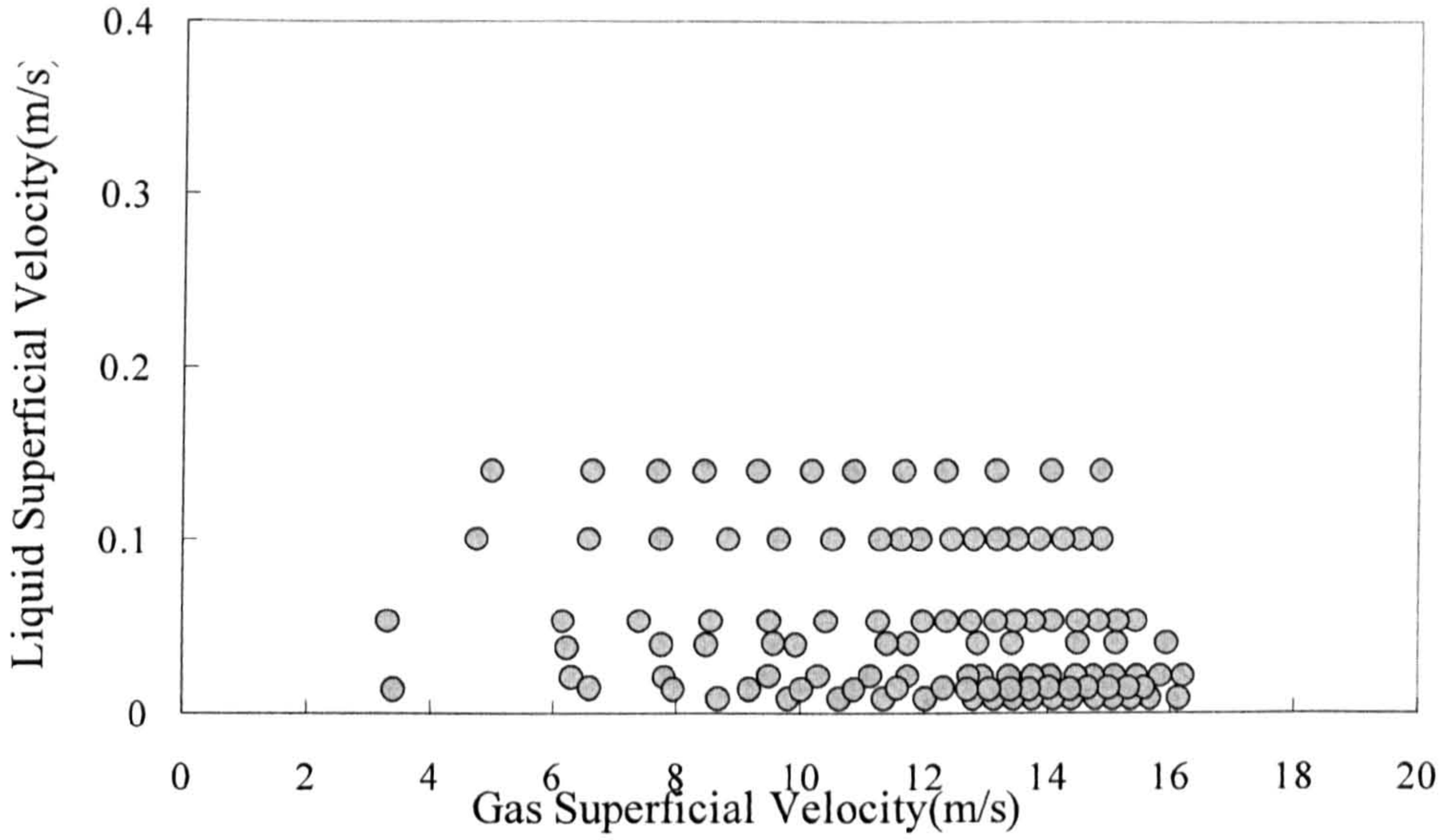

Figure 3.20 Conditions studied during the simultaneous measurement campaign of total pressure drop and liquid film thickness using both conductance pins and ring probes.

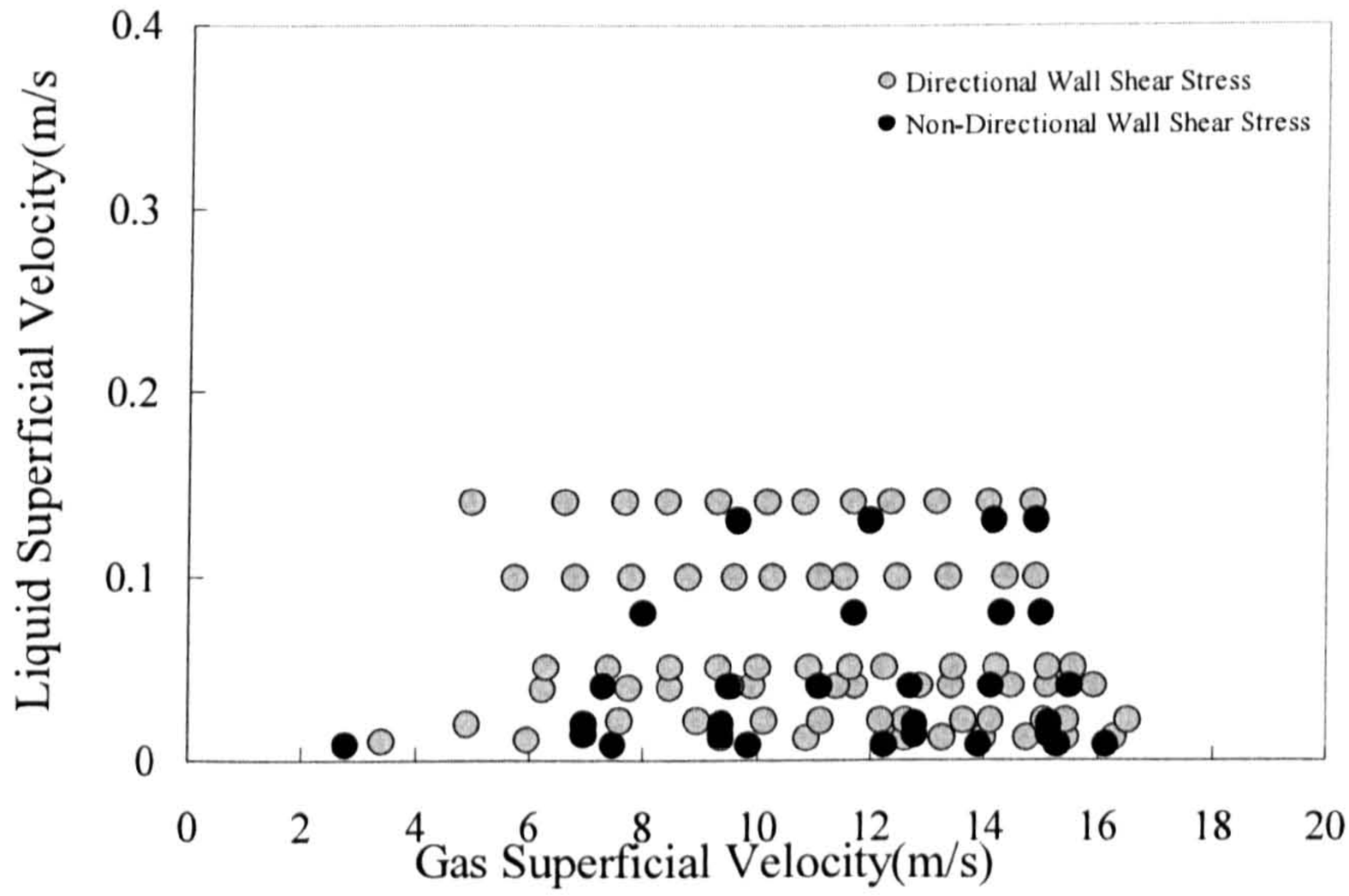

Figure 3.21 Conditions studied during the simultaneous measurement campaign of total pressure drop, liquid film thickness and wall shear stress.

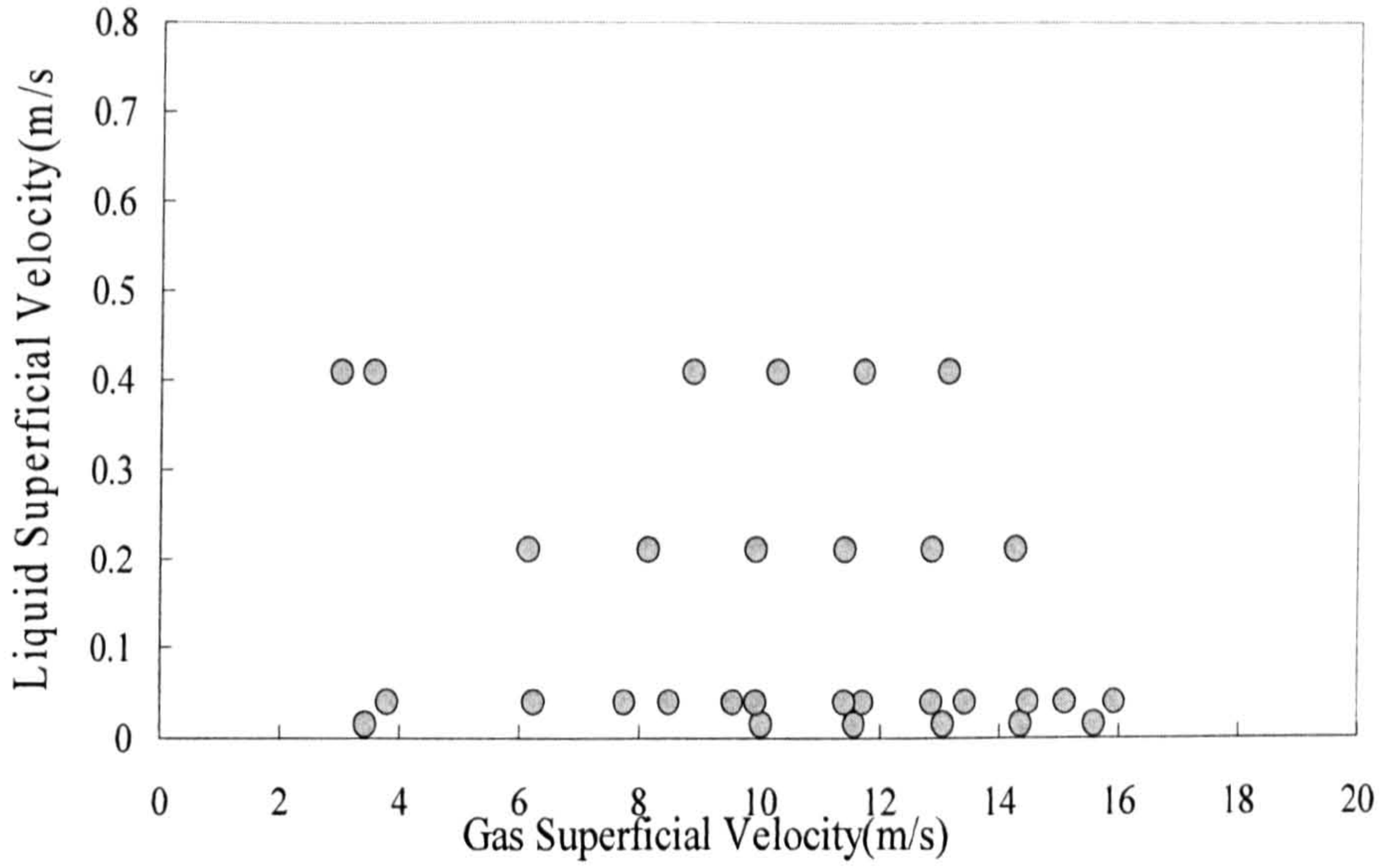

Figure 3.22 Conditions studied during the visualization campaign

Chapter 4

Two-Phase Pressure Drop in the 127mm Vertical Pipe

Although pressure drop measurements are very common in two-phase flow due to its importance, there is still a clear lack of experimental data on this parameter in large diameter vertical pipes as described in previous chapters. In the present study an experimental data bank of 600 runs on time-varying and averaged total pressure drop in a 127 mm diameter vertical pipe were obtained. The data were analyzed in different ways and the results are presented and discussed in this chapter.

4.1 Time-averaged pressure drop

Time-averaged total pressure drop for the ranges 0.01-0.7 m/s of liquid superficial velocity and 2.5-16.2 m/s of gas superficial velocity are presented in the subsequent sections. Firstly, the effect of liquid and gas superficial velocity on time-averaged total pressure drop for the present work are discussed. Secondly, the present data are compared with experimental data of different pipe diameters discussing the minima and maxima in the pressure drop profiles, the flow regime transition regions based on the variation of

time-averaged total pressure drop with gas flow rate, and the effect of pipe diameter on the mean value of total pressure drop.

4.1.1 The effect of liquid and gas superficial velocity

The effect of liquid flow rate variations on time-averaged total pressure drop is shown in Figure 4.1. The general trend of the graph is that the time-averaged total pressure drop increases systematically as the liquid flow rate increases. The increase in total pressure drop as the effect of liquid superficial velocity might be explained based on the fact that as the liquid flow increases the liquid film thickness on the pipe wall becomes thicker and the interfacial roughness between the liquid film and the gas core increases leading to the higher pressure drop. However, the pressure gradient changes sharply with liquid flow rate only at liquid superficial velocities lower than 0.1 m/s especially for the range of gas superficial velocities of 6-12 m/s. The best explanation for that is might be the one that given by Holt (1996), that most of the liquid flow rate is in the form of entrained droplets; hence any further increase in liquid flow rate only serves to increase in the entrained liquid flow rate. As a result the film flow rate and the film thickness will not change significantly and hence the limited influence of the liquid flow rate on the two-phase total pressure drop.

With the liquid superficial velocity as the parameter the total pressure drop of the present work is shown in Figure 4.2 as a function of gas superficial velocity and both Kutateladze number and dimensionless gas velocity. It can be seen that over the range of the gas superficial velocities studied, three major

regions of total pressure drop can be identified as the result of liquid flow rate variations; the first area being at low liquid velocities (0.014, 0.02, 0.03 and 0.04 m/s), where the total pressure rapidly drops as the gas superficial velocity increases from 3 m/s to 8.2, 8.8, 10.2 and 10.3 m/s respectively before the trend is changed to a gradual decrease in the total pressure drop at higher gas superficial velocities. It is suggested that the change of the slope linked to a transition of flow regime from churn to annular flow. However, there is no clear minimum pressure drop over the range of the conditions studied in the present work in contrast to what has been reported for the smaller pipes (Hewitt et al, 1985).

The second area can be identified by two particular conditions, namely liquid superficial velocities of 0.053 and 0.06 m/s. In this area the slope of the graph for two phase total pressure drop do not follow the trends that seen in the low liquid velocity data, the trend has a smoother nature rather than exponential.

The trend becomes more complicated with increasing the liquid superficial velocity further (in the range of 0.07 to 0.7 m/s). In this third region there is no visible change in slope.

From the above it can be concluded that the liquid and gas superficial velocity variations have a significant effect on the total pressure gradient profile for the present data especially for the range of liquid superficial velocities less than 0.1m/s.

The effect of liquid and gas flow rate on total pressure drop can also be presented by plotting the total pressure drop as function of mixture velocities $(u_l + u_g)$ or gas mass flux $(\rho_g u_g)$. Similar forms are reported by researchers,

e.g., Kaji et al (2007), Kaji and Azzopardi (2010), Sawai et al (2004), Holt (1996), Govan (1990). However the differences in the graphs for the present work will not change significantly from what have been discussed above and this can be accounted to the fact that $u_l << u_g$ and ρ_g remained almost constant for the data presented. Therefore using mixture velocity or gas mass flux terms instead of gas superficial velocity will not change the trend of the graph significantly. However they can remain as a very useful alternative form to present such experimental data.

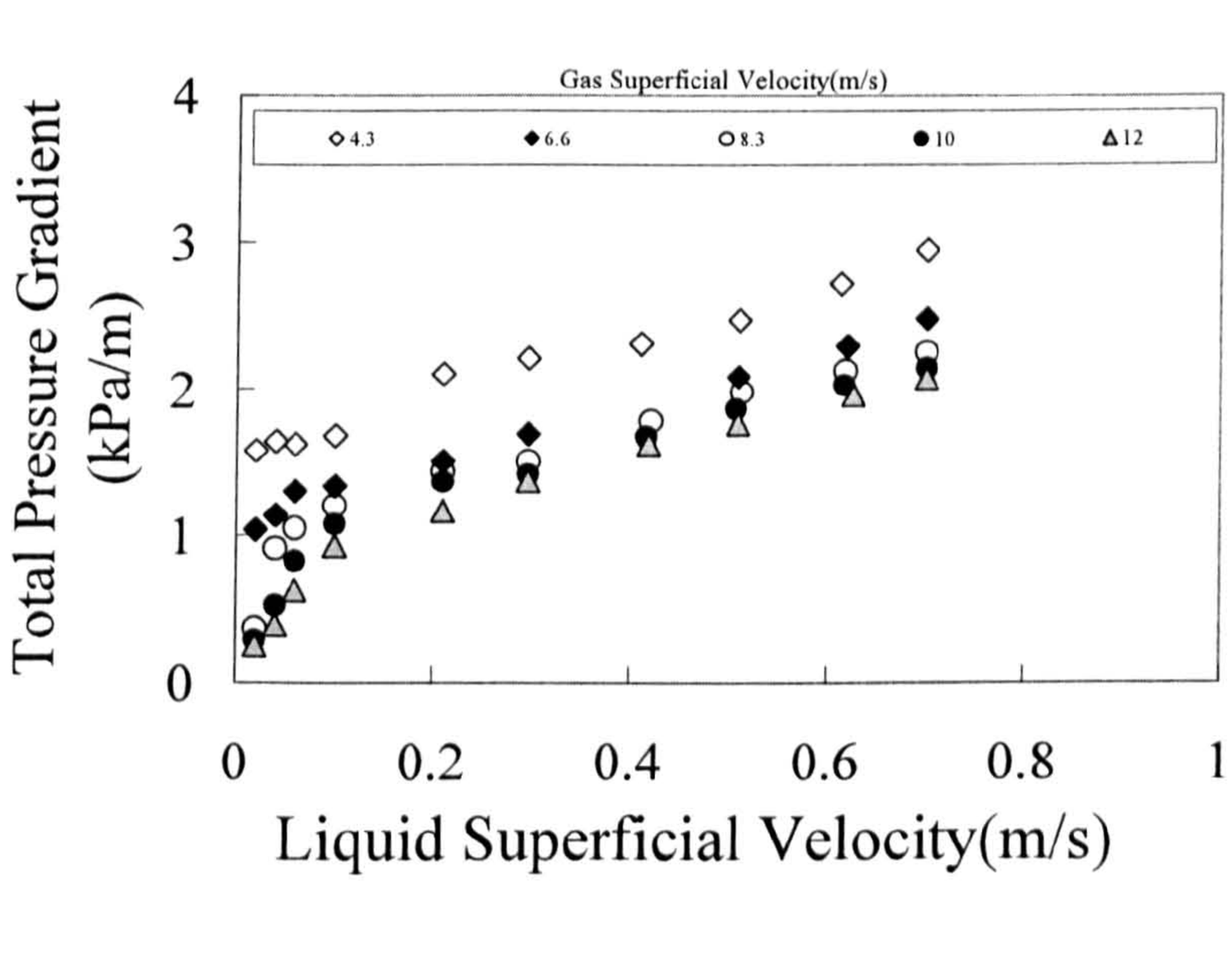

Figure 4.1 Total pressure drop as a function of liquid superficial velocity

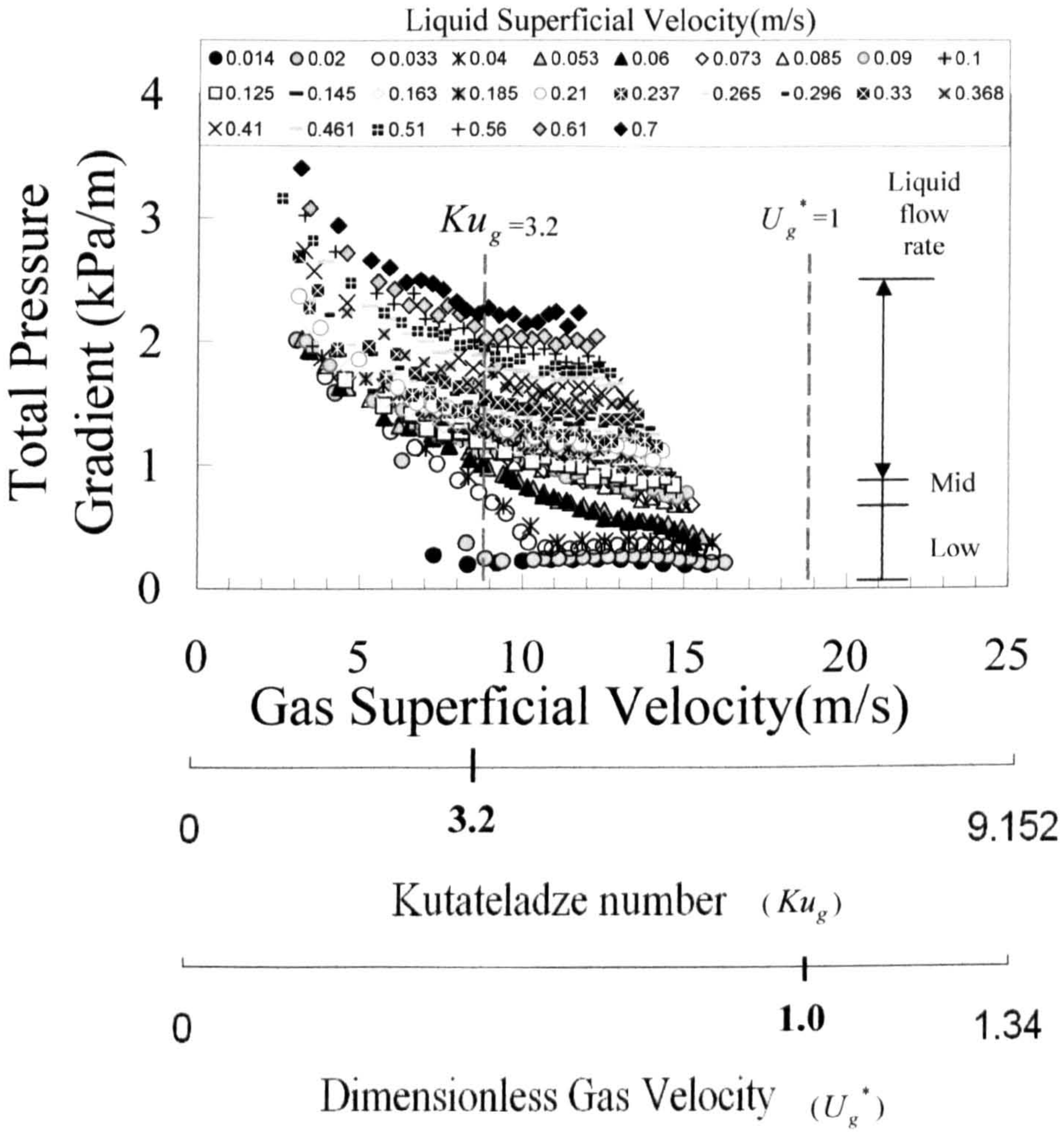

Figure 4.2 Total pressure drop as a function of, U_{gs}, Ku_g and U_g^*

4.1.2 The effect of pipe diameter

Experimental data on two phase pressure drop in vertical pipes with diameters larger than 100 mm is scarce, since the majority of the studies in this area are for smaller diameter pipes. Lists of the known works on the topic can be found in the literature, e.g., Spedding et al (1998), Kaji and Azzopardi (2010), who reported a noticeable effect of pipe diameter on two-phase pressure drop in the range of small diameter pipes, i.e., up to 50 mm. This being the case comparison between present work and the data from different sources in literature and for different diameter pipes can provide very useful information on the flow behavior as the effect of such diameter pipes.

Although presenting experimental data based on the variation of the liquid and gas superficial velocity is very common in the two phase flow subject, However it can be difficult to compare the data from two different measurements directly as a function of gas and liquid superficial velocity especially if the data were taken at different operation conditions, e.g., the system pressure, as the physical properties particularly of the gas phase can be affected significantly. Another way to present such data as described previously is as a function of gas and liquid mass flux where the density of the fluids to be taken into account.

As discussed in Chapter 2, the data on total pressure drop in small diameter (i.e. <100 mm) vertical pipes in the literature are available at different ranges of liquid and gas mass fluxes. Some researchers (e.g. Owen, 1986) studied the full range of flow patterns in vertical pipe and some only covered a certain flow pattern (e.g. Sawai et al, 2004). For comparison with present

experimental data the two-phase total pressure drop data in vertical up-flow pipes from various sources and for different diameter pipes are gathered as listed in Table 4.1.

The total pressure drop data of Holt (1996), Kaji (2008), Sawai et al (2004), Martin (1983) and the present data for diameters of 10, 19, 25.8, 32, 58 and 127 mm respectively are plotted in Figures 4.3 and 4.4 over a various gas mass flux and at liquid mass fluxes of 20-30 and 100 kg/m^2s.

As the data from each source subjected to their availability in a certain ranges of the liquid and gas mass fluxes, therefore they are also compared with the present data independently as shown in Figures 4.5-4.9.

As over all trends, a systematic decrease in total pressure drop can be seen clearly in Figures 4.3-4.9 as the pipe diameter increases; a similar observation has been reported by other researchers, e.g., Kaji and Azzopardi (2010). However, there are deviations from the trend at lower gas mass fluxes. For example, at gas mass fluxes less than 4 kg/m^2s, the pressure drop is higher in a pipe of 25.8 mm than it is in a pipe of 19 mm. Also, the pressure drop in the 127 mm is higher than that in smaller diameter pipes in the gas mass flux range 10-20 kg/m^2s. It can be concluded that the effect of pipe diameter starts to appear for each pipe at certain gas mass flux depending on the pipe size and the liquid flow rate as that value of gas flow rate increases as the pipe diameter increases or the liquid flow rate decreases. This might be explained by the frictional pressure component in the total pressure drop being the most affected by pipe diameter changes. The effect of pipe diameter on total pressure drop can be expected to appear when the frictional pressure becomes dominant. To capture accurately the effect of pipe diameter on time-averaged

total pressure drop, the liquid and gas flow rates and physical properties of the fluids must be taken into account. Therefore, employing larger diameter pipe will not necessarily lead to lower pressure drop over the whole range of the gas and liquid mass fluxes.

From Figures 4.3-4.9 it can also be observed that in certain gas mass fluxes two or more pipes can have the same value of total pressure drop in spite of having different diameters. They cross over at a certain point and this can be related to the fluctuation nature of the total pressure drop profile (i.e., minima and maxima characteristic) as a function of gas flow rate. Spedding et al (1998) described the general trend of the total pressure drop in a 26 mm diameter pipe as a maximum value set between two minima situated at medium and low gas flow rates. Kaji and Azzopardi (2010) also reported the maxima and minima for their data in 19 mm diameter pipe at liquid flow rates less than 0.25 m/s. Sawai et al (2004) classified the variations of time-averaged pressure drop in 25.8 mm diameter pipe with the gas flow rates at relatively low liquid flow rate into four regions; two negative and two positive slope regions. Holt (1996), who focused on pipes with diameters of 10 and 5 mm, observed the minimum and maximum for helium-water fluid pairing in 10 mm diameter and only minima were observed by him for air-water, however no minima or maxima were observed in the case of 5 mm diameter pipes for any of the fluid pairings. Owen (1986), who measured the total pressure drop in 32 mm diameter vertical pipe over the full range of the flow patterns, clearly showed that the minima and the maxima in his pressure drop profile were clearly related to the bubble/slug, slug/churn and churn/annular transitions. The total pressure drop for the present work, i.e., in 127 mm

diameter pipe as shown in Figure 4.2 and as discussed in Section 4.1.1, no clear minimum or maximum pressure drop has been observed in spite of the noticeable change in the trend of the total pressure drop profile with the variation of the gas flow rate specially when the liquid flow rates are relatively low (0.01-0.04 m/s). This is also the case for the pressure drop data by Omebere-Iyari (2006) for 189 mm vertical pipe as will be discussed later. According to the information above the pipes can be classified into three ranges based on the minima and maxima characteristic of their total pressure drop profile as: small diameters (D_t <10 mm) with no minima or maxima, intermediate diameters (10=< D_t < 100 mm) with a maximum value set between two minima, and large pipe diameters (Dt >100 mm) with no clear minima or maxima. Although the medium range of the pipe diameters can be reduced further as no sufficient studies in pipe diameters larger than 70 mm are known so far. The above leads to a very important conclusion that for pipes smaller than 10 mm the pressure gradient is expected to increase as the gas flow rate increases, in contrast, to pipes larger than 100 mm as the pressure gradient decrease with increase of gas flow rate over a wide range. However for the intermediate range of pipe diameter both increase and decrease are expected with increasing gas flow rate. And this can be linked to the flow patterns that exist in each range of pipe diameters above as will be discussed subsequently.

Table 4.1 Two-phase pressure drop data of various diameter pipes in vertical up flow.

Source	Pipe Diameter (mm)	Pressure (bara)	Liquid Mass Flux (kg/m^2s)	Range of Gas Mass Flux (kg/m^2s)
Holt (1996)	5	1.5	40,80	6.5-120
	10	1.5	20,60,100,140	6.5-120
Kaji (2008)	19	1.5	30,100,250,400	1.5-61
Sawai et al (2004)	25.8	1	20,100,200,400	0.2-26
Owen (1986)	32	2.4	5.3,111.8	4-90
Martin (1983)	32	1.5	20,40,60,80	20-100
	58	1.5	20,30,40,60	20-80
Omebere-Iyari (2006)	189	20	7, 35, 70	2.2-350
Present	127	3	14,20,33,40,60,80 100,144,209,264 366,414	9.1-57.7

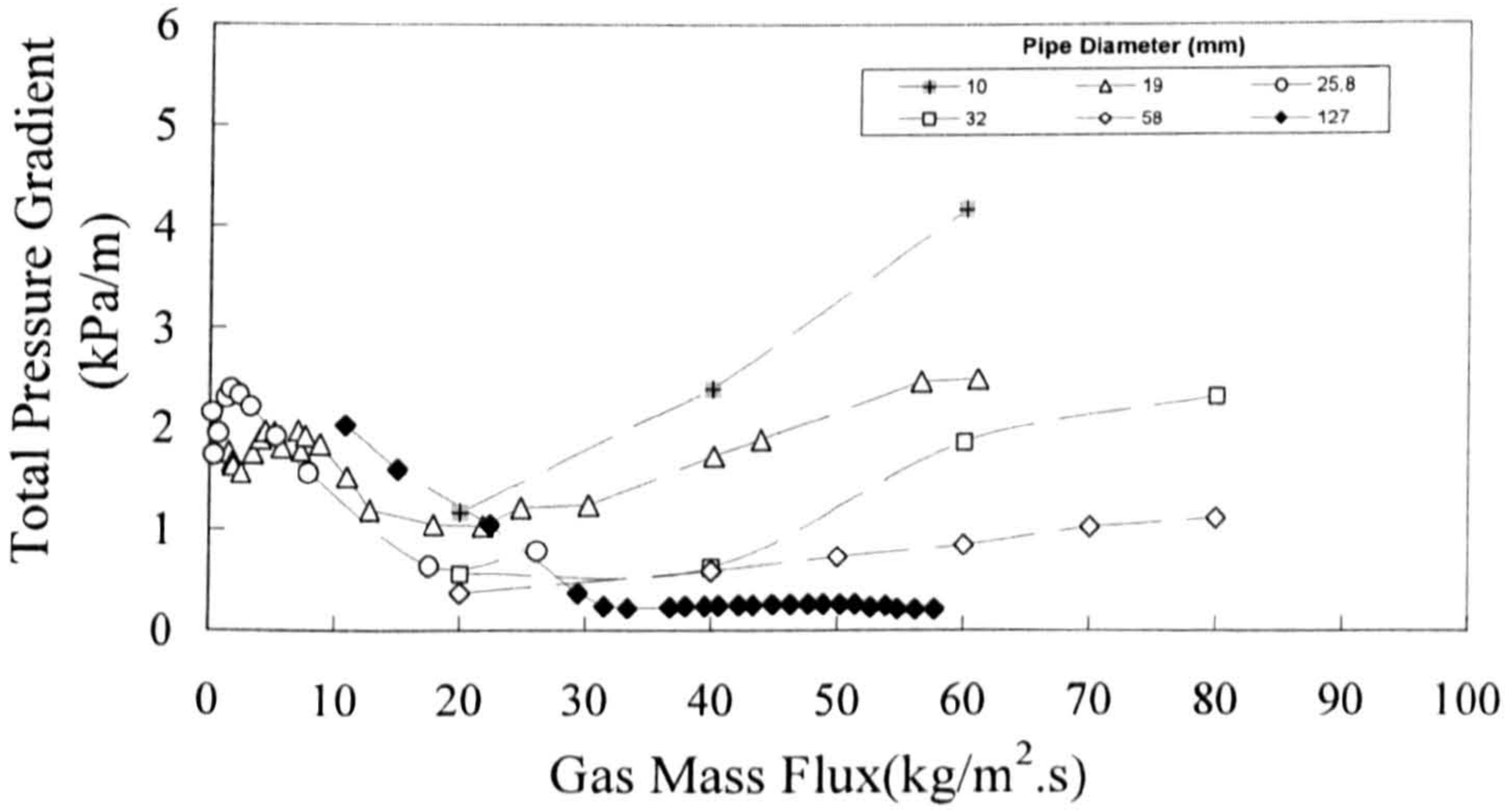

Figure 4.3 Total two-phase pressure drop as a function of gas mass flux for various diameter pipes (liquid mass flux of 20-30 kg/m^2s).

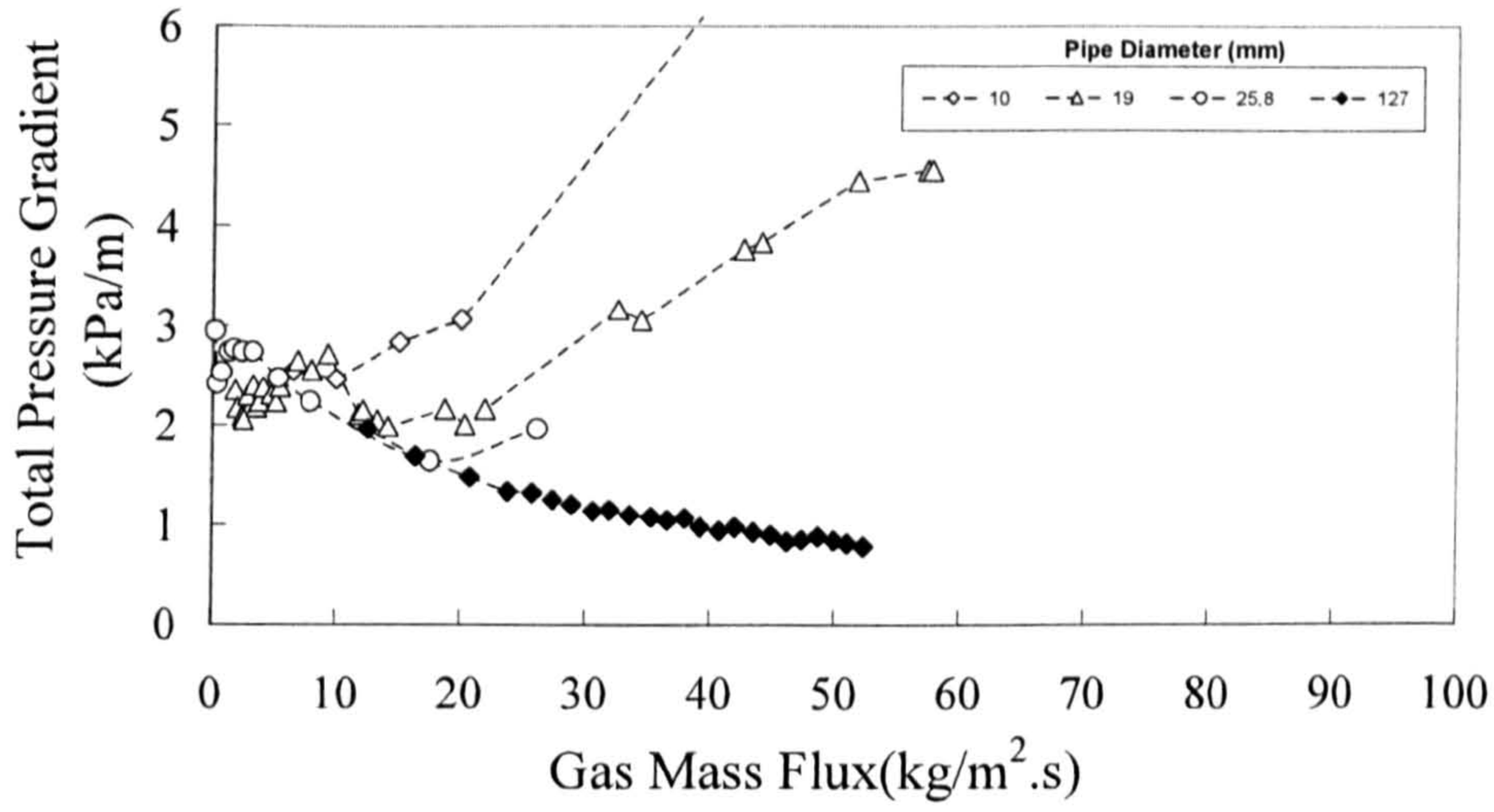

Figure 4.4 Total two-phase pressure drop as a function of gas mass flux for various diameter pipes (liquid mass flux of 100 kg/m^{2}s).

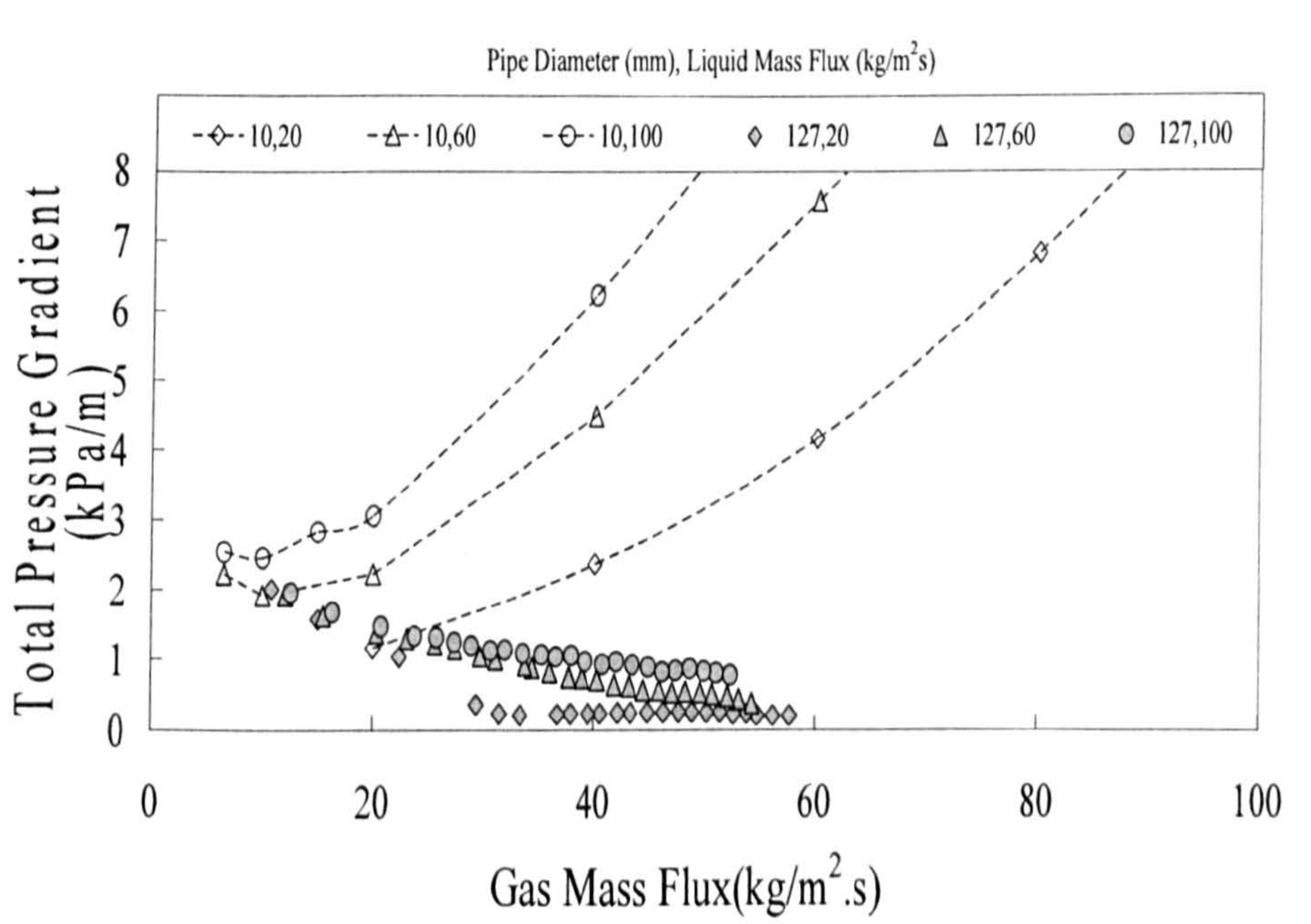

Figure 4.5 Total two-phase pressure drop data from 127 mm diameter vertical pipe compared with data from 10 mm diameter pipe (Holt, 1996).

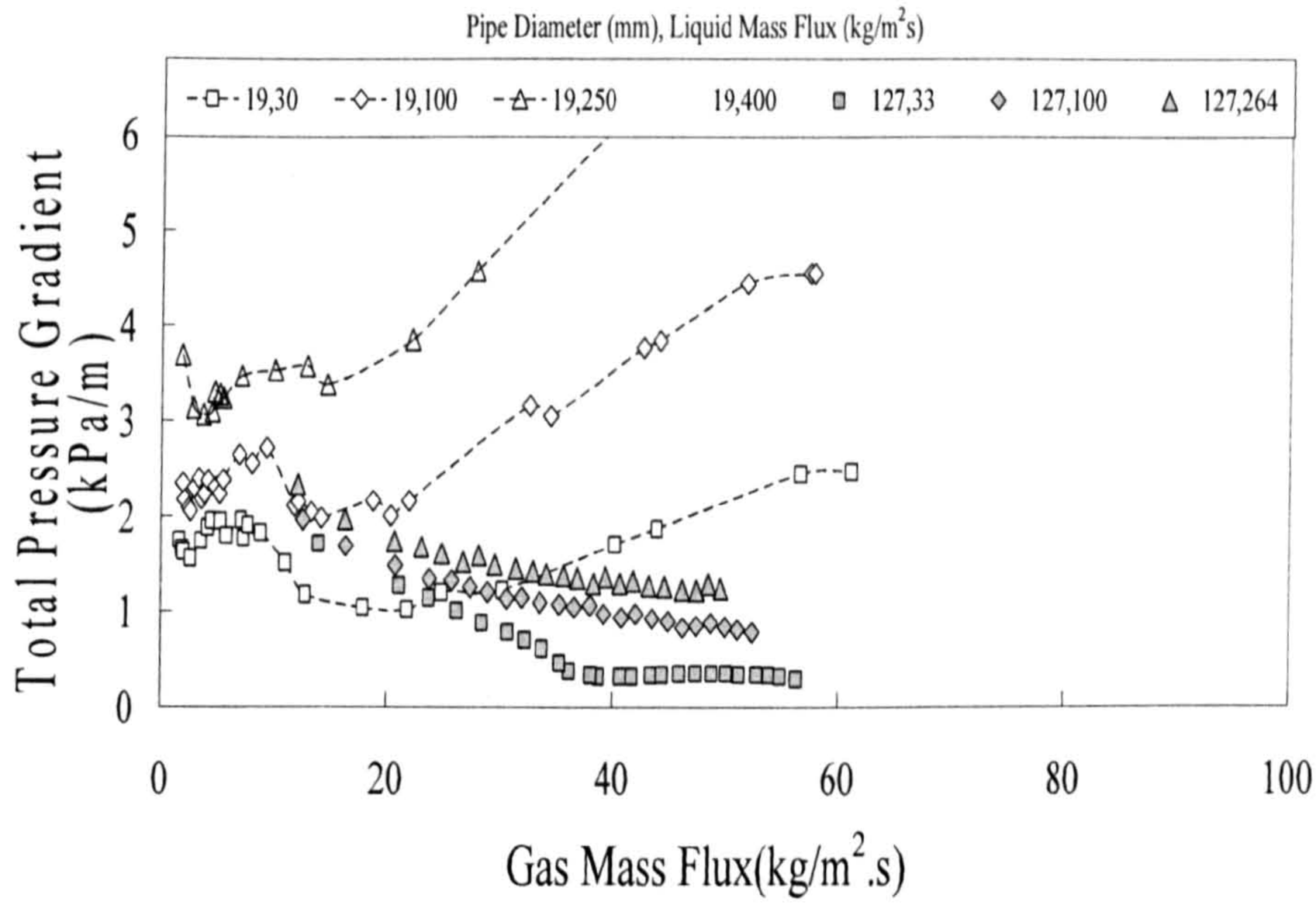

Figure 4.6 Total two-phase pressure drop data from 127 mm diameter vertical pipe compared with data from 19 mm diameter pipe (Kaji, 2008).

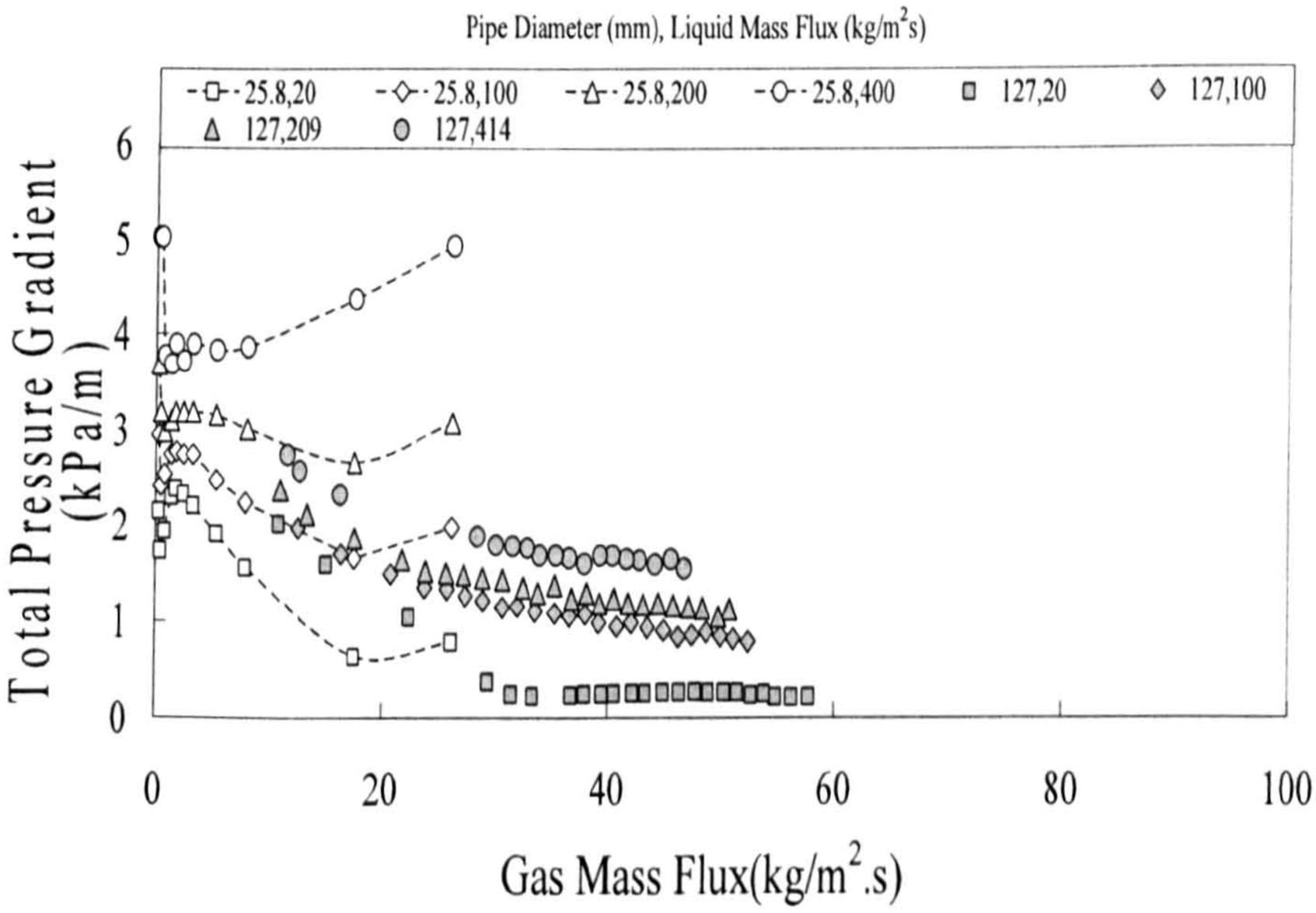

Figure 4.7 Total two-phase pressure drop data from 127 mm diameter vertical pipe compared with data from 25.8 mm diameter pipe (Sawai et al, 2004).

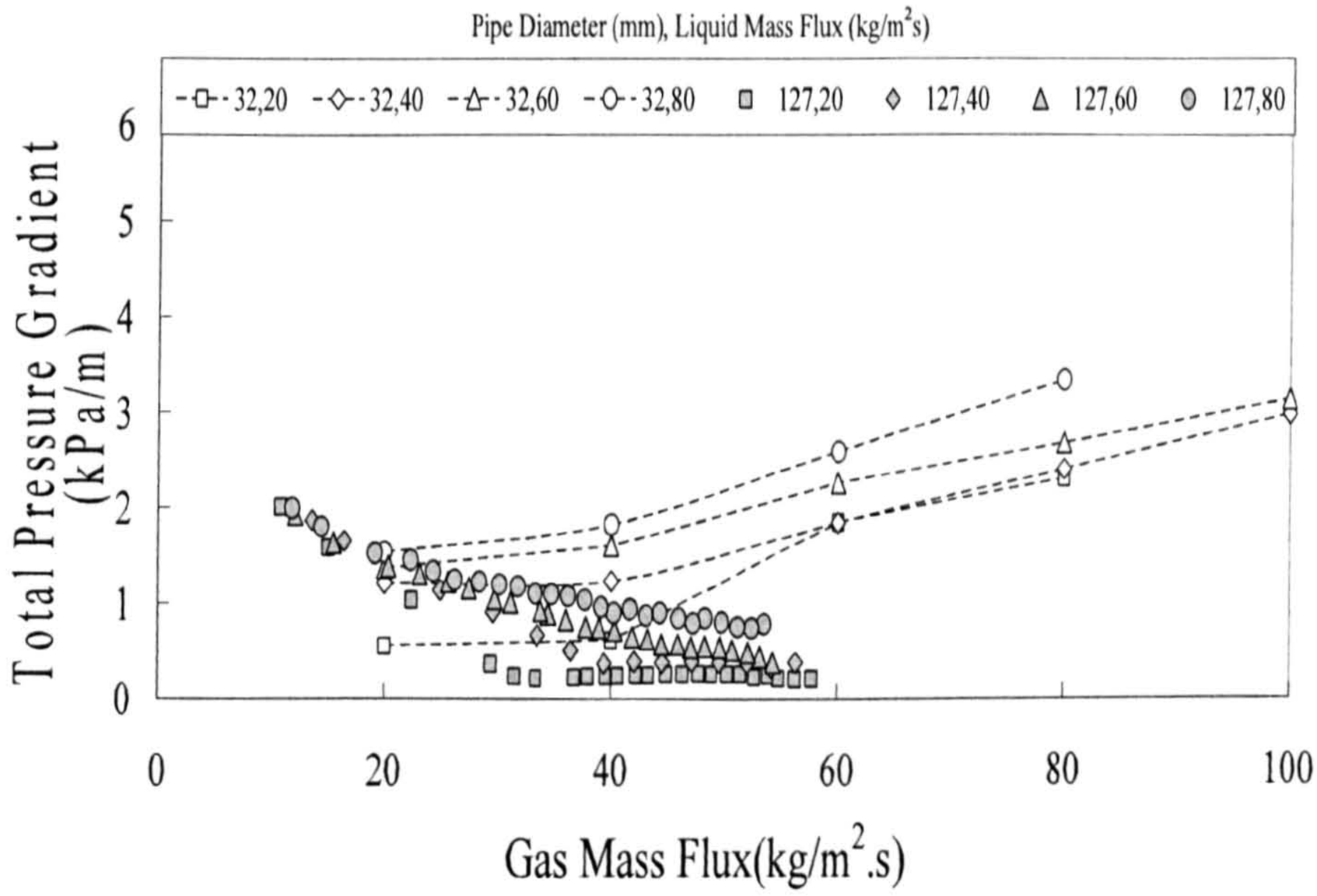

Figure 4.8 Total two-phase pressure drop data from 127 mm diameter vertical pipe compared with data from 32 mm diameter pipe (Martin, 1983)

Figure 4.9 Total two-phase pressure drop data from 127 mm diameter vertical pipe compared with data from 58 mm diameter pipe (Martin, 1983).

Due to the different behavior of each flow pattern from another, the total pressure gradient profile in vertical pipes and its variations with the gas and the liquid flow rates can be used as another method for identification those flow patterns and the expected transition regions between them (see Chapter 2). From that perspective the present data which is for 127 mm vertical pipe and data by Omebere-Iyari (2006) for 189 mm diameter that fall in the range of large diameter pipes are compared with the data from Owen (1986) and Holt (1996) which are for 32 and 5 mm diameters respectively and in the ranges of intermediate and small pipes as discussed early in this section.

The total pressure drop as a function of dimensionless gas velocity (see Section 2.1.1) for the current work at liquid mass fluxes of 20 and 100 kg/m^{2}s, i.e., at low and relatively high liquid flow rates are presented in Figures 4.10 and 4.11 together with the experimental results of Omebere-Iyari (2006), Owen (1986) and Holt (1996) at liquid mass fluxes of 7, 70, 5.3, 111.8 and 40, 80 kg/m^{2}s respectively.

The two-phase pressure drop data by Omebere-Iyari (2006) in 189 mm vertical pipe has shown a very good agreement with the trend of present work which is for 127 mm diameter. That data has a limited number of data points in the churn and churn-annular regions. However, that region has been studied in better detail in the present study. Together, the Omebere-Iyari (2006) data and the present data represent a very important data resource for large diameter pipes, covering a wide range of gas and liquid flow rates. The data for large diameter pipes clearly have different trends to those found in data for smaller diameter pipes and these trends appear not to have been reported so far in the literature.

Based on the results of Owen (1986) of flow regime transitions in 32 mm vertical upward air-water flow, Figures 4.10 and 4.11 were marked with number of regions, i.e., bubble, slug, and churn, churn-annular and annular flow. The range of gas flow rates over which the flow regime transitions occur according to Owen (1986) at liquid mass fluxes 5.3 and 111.8 kg/m^2 are shown in Figures 2.1 and 2.2 respectively. These data are re-plotted in Figures 4.10 and 4.11. In the results of Owen (1986) two clear minima can be seen, the first at the bubble-slug and slug churn transition regions and the second at region of churn/annular flow. For first one the total pressure drop falls dramatically at the transition region from the bubble to slug flow regime and this might be resulted from a rapid increase of void fraction at, U_g^*, of 0.19 causing a dramatic decrease in the two phase density hence the gravitational component of the two-phase pressure drop (which is dominant). Then followed by a large and sudden increase in total pressure drop at the transition region from slug to churn, leading to the first minimum in the pressure drops profile. According to Jayanti and Hewitt (1992) who compared various mechanisms of slug to churn flow transition against the data of Owen (1986), the flooding of the liquid film in the Taylor-bubble is the most likely cause for this transition. Kaji (2008) has shown that around this transition there are waves moving upwards and waves moving downwards in the film around Taylor bubbles.

The clear minima that situated between bubble-slug and slug-churn transition regions in the pressure gradient profile by Owen (1986) is not observed for the pipe diameters 127 and 189 mm diameter pipes as illustrated in Figures 4.10

and 4.11. Although the bubble flow was not the focus of the present study however the lowest values in the range of gas flow rates studied were just before the bubbles to appear in the test section in another word just before the bubble flow to be reached. This is also supported strongly by data of Omebere-Iyari (2006) as no minima in that range of gas flow rate was observed. For the 5 mm diameter pipe the data of Holt (1996) was limited for a higher gas flow rates therefore the first minima can not be confirmed. This being the case the absence of first minima in the large pipes that resulted from bubble-slug and slug-churn transition regions lead to the conclusion that the slug flow does not occur clearly in such pipes. Instead, the bubble-churn transition can be expected and this has been supported strongly by the available phase distribution studies in the large diameter pipes, e.g., Ohnuki et al (1995), Cheng et al (1998) and Omebere-Iyari et al (2008) as described in Chapter 1.

The second minima in the Owen (1986) data can be seen at, U_g^*, close to 1 in the churn/annular region which spread over a broad range of gas flow rates. Besides it can be seen in that region the trend of the pressure drop profile for the present work are changing visibly as the total pressure drop moving from dramatic to the gradual change for the liquid mass flux of 20 kg/m^{2}s with no clear minima however no sensible movement can be seen in the case of 100 kg/m^{2}s. The data of Omebere-Iyari (2006) although has a limited number of data point in the churn and churn / annular region however no clear minima also can be seen up to, U_g^*=1.6. This non clear minima in the pressure drop in large diameter pipes can be accounted to the fact that the pressure drop as a

function of gas flow rate decreases with increasing pipe diameter in the churn-annular transition region (at relatively higher gas flow rates) as it is clear for example in Figure 4.3. No clear minimum in the churn/annular region also reported by Holt (1996) for 5 mm diameter pipes that accounted by him to the fact that the transition from slug to annular flow is much smoother in small diameter channels and as a consequence the region of churn flow in small diameter channels maybe somewhat smaller than that observed in larger channels and in addition to which Mishima et al (1995) observed an absence of churn flow in small rectangular channels and this also stated by Taitel et al (1980) for small pipes without indicating the pipe diameter range. Based on the above the transition from churn to annular is very gradual in the large diameter pipe which can not be sensed from the pressure drop profile. However in 5 mm diameter pipes a transition from slug to annular can be expected rather than churn to annular.

Linking the flow patterns in vertical pipes to the pressure drop profile bubble, slug, churn and annular flow can observed for 32 mm diameter pipe, however, churn and slug flow regime are missing in 5 and 127 mm diameter pipes respectively.

As described in Chapter 2 the transition to annular flow is normally associated with two phenomena; the first one as suggested by Taitel et al (1980) that the annular flow cannot exist unless the gas velocity in the gas core is sufficient to lift the entrained droplets and the minimum gas velocity required to suspend that droplets is determined by what is recognized as Kutateladze number (Equation 2.1) at values higher than 3.2. The second phenomenon is associated with the gas velocity at which a flow reversal takes place and can be expressed

by, U_g^*, which is used in Figures 4.10 and 4.11. Taking these two parameters into consideration the churn-annular transition for the present data can be further discussed. The time-averaged total pressure drop for the current work as a function of Kutateladze number (Ku_g) and dimensionless gas velocity (U_g^*) over the whole range of the liquid flow rates studied are presented in Figure 4.2. It can be seen that at Kutateladze number ≥ 3.2 the trend of the pressure gradient profile especially for the low liquid flow rates, i.e., 0.01-0.02 m/s starts to transform to the gradual decrease, in another word, Kutateladze number indicates the change in the movement of the pressure drop profile and this can be linked to the transition from the churn to the annular flow regime, It is also worth mentioning that Vijayan et al (2001) who reported a different mechanism of flooding for pipes of 67 and 99 mm from that of 25 mm agrees with the thoughts of Richter (1981) and Jayanti et al. (1996) that the Wallis-type correlation would work well in small diameter tubes and Kutateladze-type in large diameter tubes. However as described previously no clear minimum pressure drop similar to the one reported by Hewitt et al (1965) was observed in the range of the conditions studied. In addition the flow reversal point not expected to be reached as we will see in the next chapters that the direction of the flow observed to be fluctuating between upward and downward over the conditions studied. The zero wall shear stress point not reached either.

In conclusion, Kutateladze number indicated the change in the trend of the pressure drop profile for the present work especially for the low liquid flow rates however the reversal flow point not reached according to the flow

reversal phenomenon. Bearing in mind that in the calculation of former parameter the effect of diameter pipe not taken into account however that effect has been considered in the dimensionless gas velocity (U_g^*). So there is a question rising about whether that transition is from churn to annular or from turbulent-churn to semi-annular (see Chapter 1), and the answer will be the later transition if annular flow in large diameter pipes also described in the same way as the typical definition of annular flow in vertical pipe by researchers, e.g., Azzopardi (2006), and Hewitt and Taylor (1970), i.e., the liquid film to flow in a unidirectional manner upward on the pipe wall.

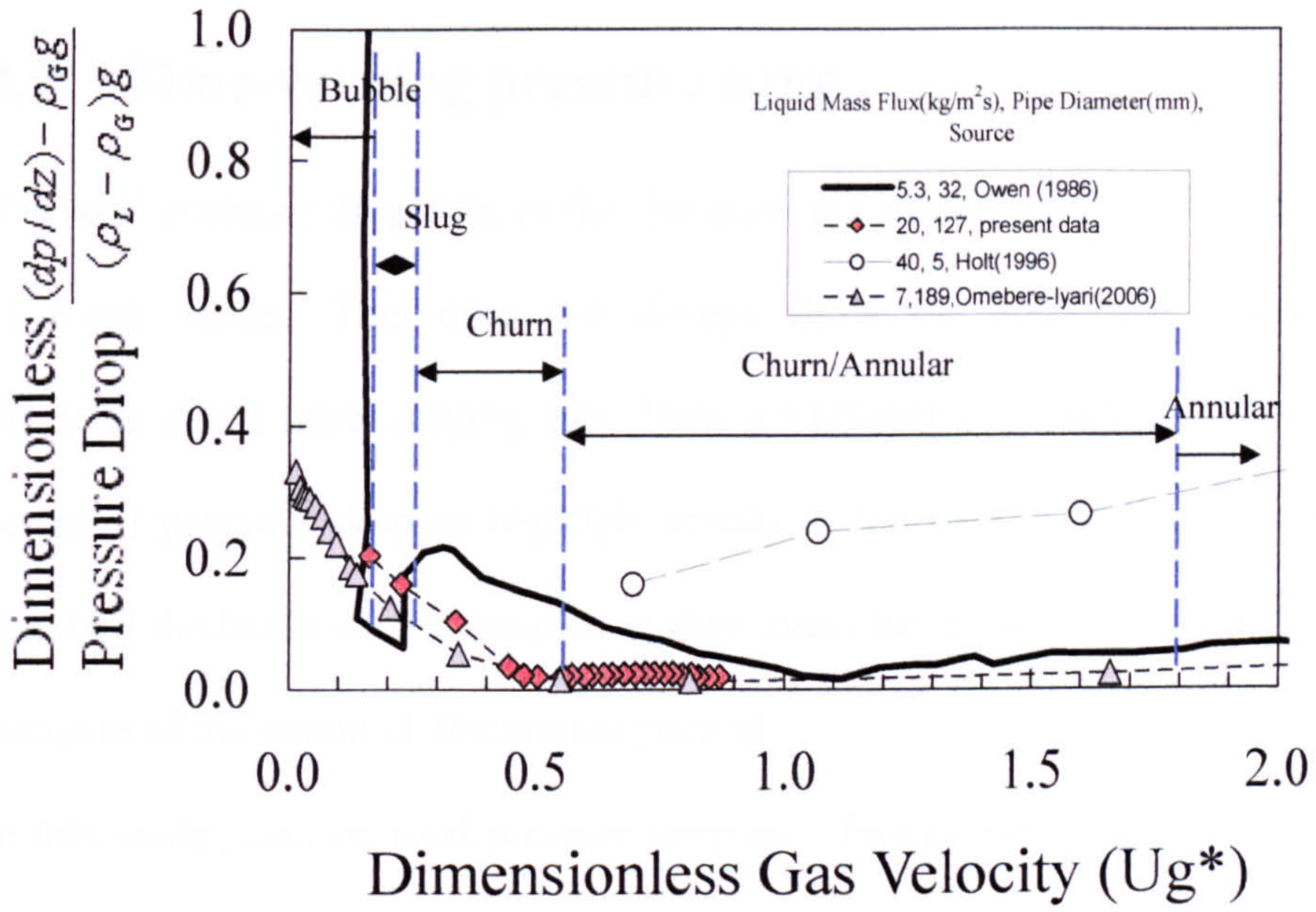

Figure 4.10 Dimensionless pressure drop as a function of U_g^* for present study, Owen (1986), Holt (1996) and Omebere-Iyari (2006) at low liquid flow rate

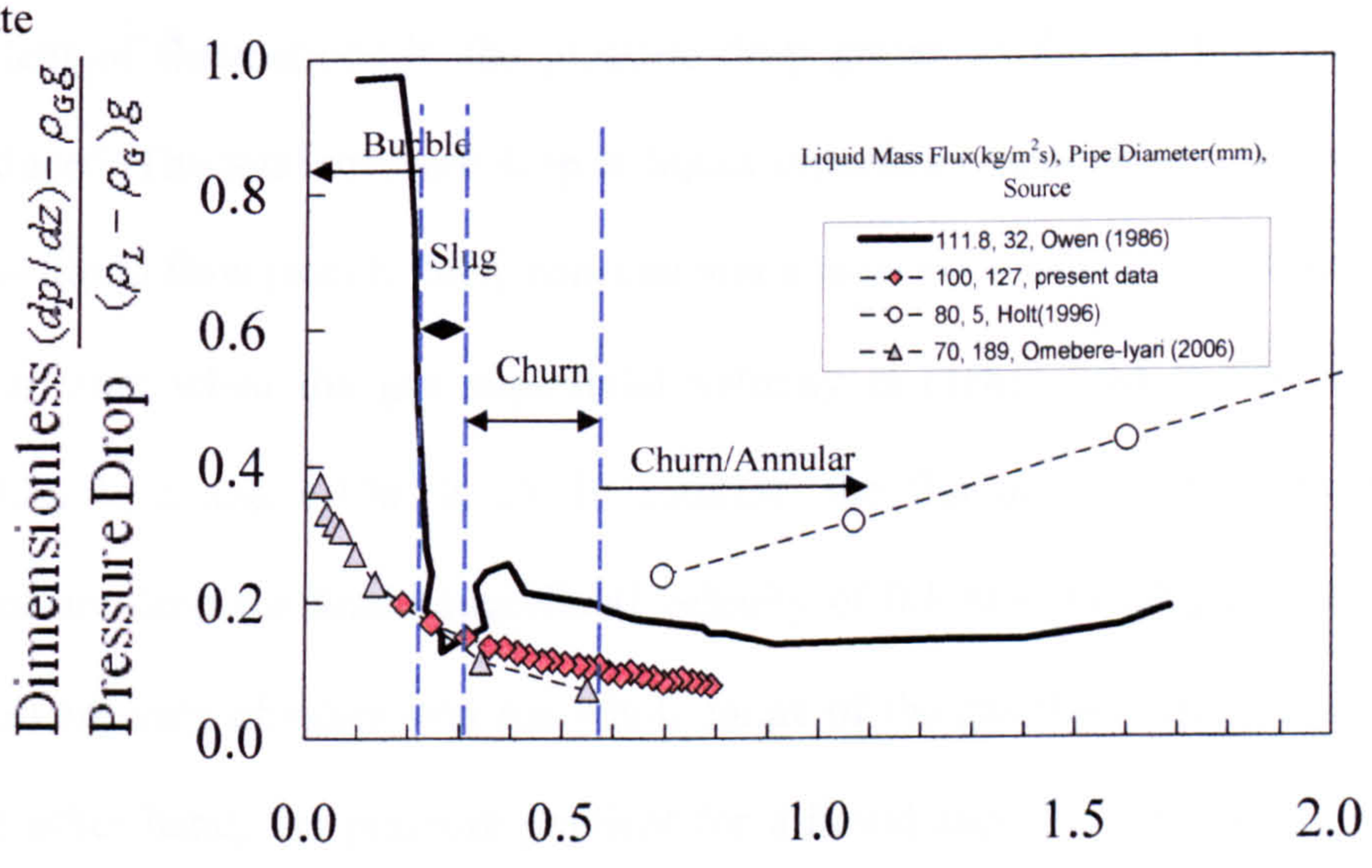

Figure 4.11 Dimensionless pressure drop as a function of U_g^* for present study, Owen (1986), Holt (1996) and Omebere-Iyari (2006) at high liquid flow rate.

4.2 Time-varying pressure drop

The total pressure drop data in the literature are mainly presented in the form of mean values. This does not always show the additional information available in the time–varying data. Here we present some representative time series of pressure drop to highlight trends in the data. The behavior of the standard deviation of the samples is then considered, as this is the first level measure of the extent of fluctuation present.

In this study, data on total pressure drop as a function of time were obtained directly from the D. P. transmitters. Results for low, intermediate and high liquid flow rates, i.e., 0.02, 0.06 and 0.1 m/s are presented in Figures 4.12-4.14 over a various gas superficial velocities. In all graphs it can be seen that the extent of fluctuations in the pressure drop grows as the gas flow rates are reduced. The total pressure drop at liquid superficial velocity of 0.02 m/s (i.e., low liquid flow rate) is fairly constant and almost without any clear fluctuation over time when the gas superficial velocity is higher than 8 m/s (Figures 4.12a, b, c and 4.13a, b, c). In contrast, the fluctuations of time-varying pressure drop for liquid superficial velocity of 0.1 m/s (i.e., high liquid flow rate) are very obvious over the whole range of the gas flow rates studied. On the other hand, the pressure gradient for a liquid superficial velocity of 0.06 m/s (i.e., intermediate liquid flow rate) starts to fluctuate at gas superficial velocity $\leq$ 12 m/s, and as the gas flow rate getting lower the height of the peaks and the frequency of the variations become larger as this is also correct for the other two liquid flow rates, i.e., 0.02 and 0.1 m/s until the fluctuation in their time series become very obvious with almost similar frequencies and

peak heights as the gas superficial velocity approaching 3 m/s (Figure 4.14c). This also can be observed from the standard deviation obtained from the time-varying total pressure drop for the liquid superficial velocities stated above, i.e., 0.02, 0.06 and 0.1 m/s and at various gas superficial velocity as presented in Figure 4.15 which shows an increase in the standard deviation as the liquid flow rate increases in another word the higher the liquid flow rate the bigger the size of the fluctuation, in contrast the standard deviation decrease as the gas velocity increases and the trend at low liquid flow rate namely at 0.02 m/s consists of a sharp decrease in standard deviation before starting change gradually at gas velocity higher than 8 m/s.

This fluctuation nature in the time series of total pressure drop has been linked to the characteristic of flow patterns by some researchers, for instance Hernandez-Perez (2007) has attributed that to the occurrence of slugs. From similar perspective the fluctuation observed in the time series of total pressure drop in the present study especially for low liquid flow rate can be linked to the transition from churn to churn-annular or annular flow regime as the variation of total pressure drop with time becomes less disturbed as the gas velocity rises above 8 m/s.

According to Hernandez-Perez et al (2010) The unsteady character in the time varying total pressure drop can lead to the conclusion that the average value of pressure drop might not be accurate enough for the design purposes as the critical pressure drop can get bigger than that and instead the standard deviation in the relative form can be used which is taking the size of the fluctuations into account with respect to the mean value of the pressure drop. The relative standard deviation of total pressure drop for the present study as a

function of gas superficial velocity is introduced in Figure 4.16. It can be observed that this parameter is getting lower as the gas superficial velocity getting higher in the range of lower and intermediate liquid velocity, i.e., 0.02-0.06 m/s however the movement of the graph changes to the increase in the relative standard deviation as the gas velocity increases for the high liquid flow rate. The fluctuation size in the time-varying total pressure drop will increase significantly and lead to a noticeable difference between the time-varying and the mean of total pressure drop. Based on that, it might be more reliable to consider the relative form of standard deviation for the design purposes as recommended by Hernandez-Perez et al (2010).

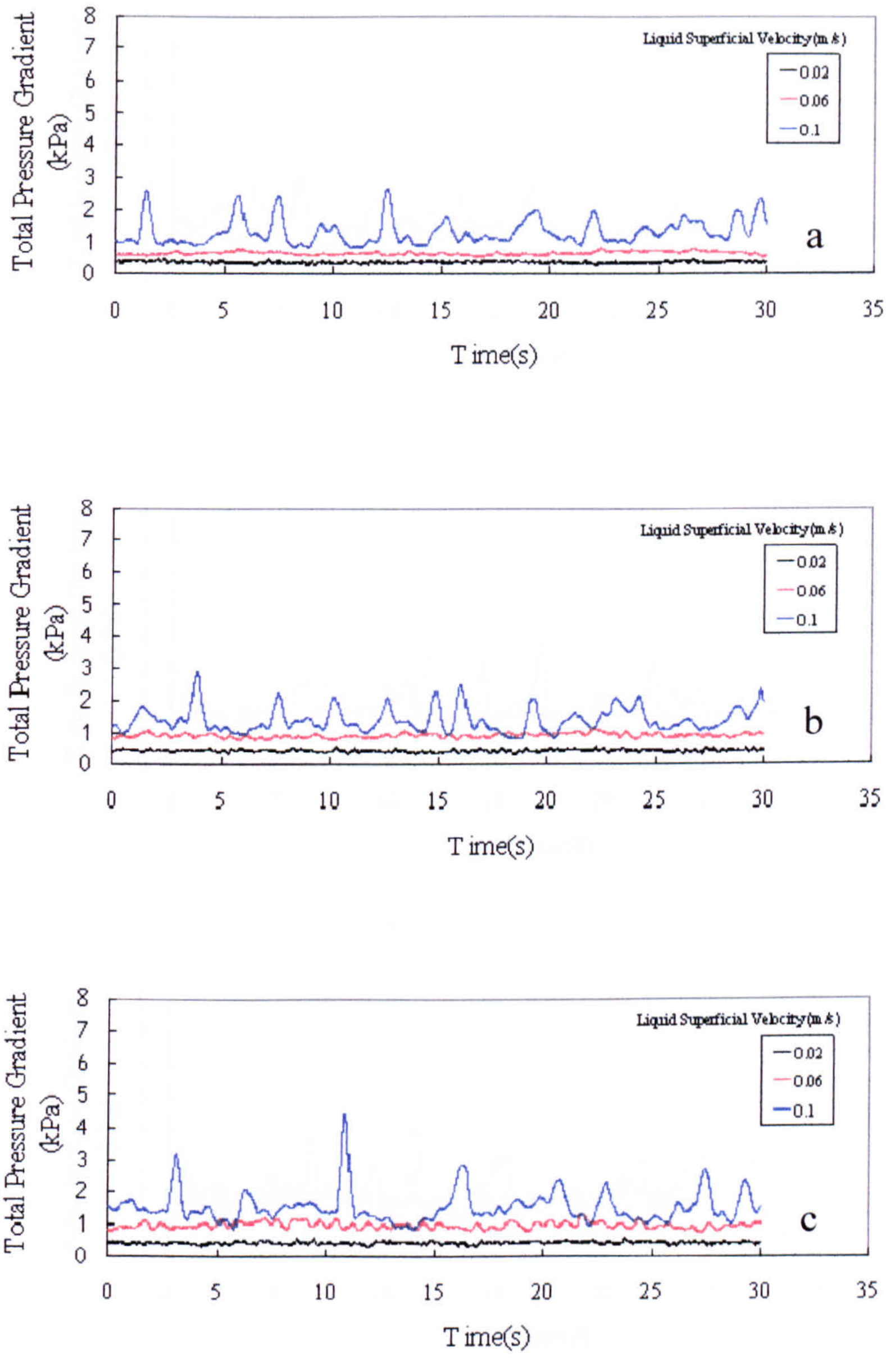

Figure 4.12 Time series of total pressure drop at liquid superficial velocities of 0.02, 0.06 and 0.1 m/s and gas superficial velocity (m/s): a) 15.4 b) 14.1 and c) 12.6.

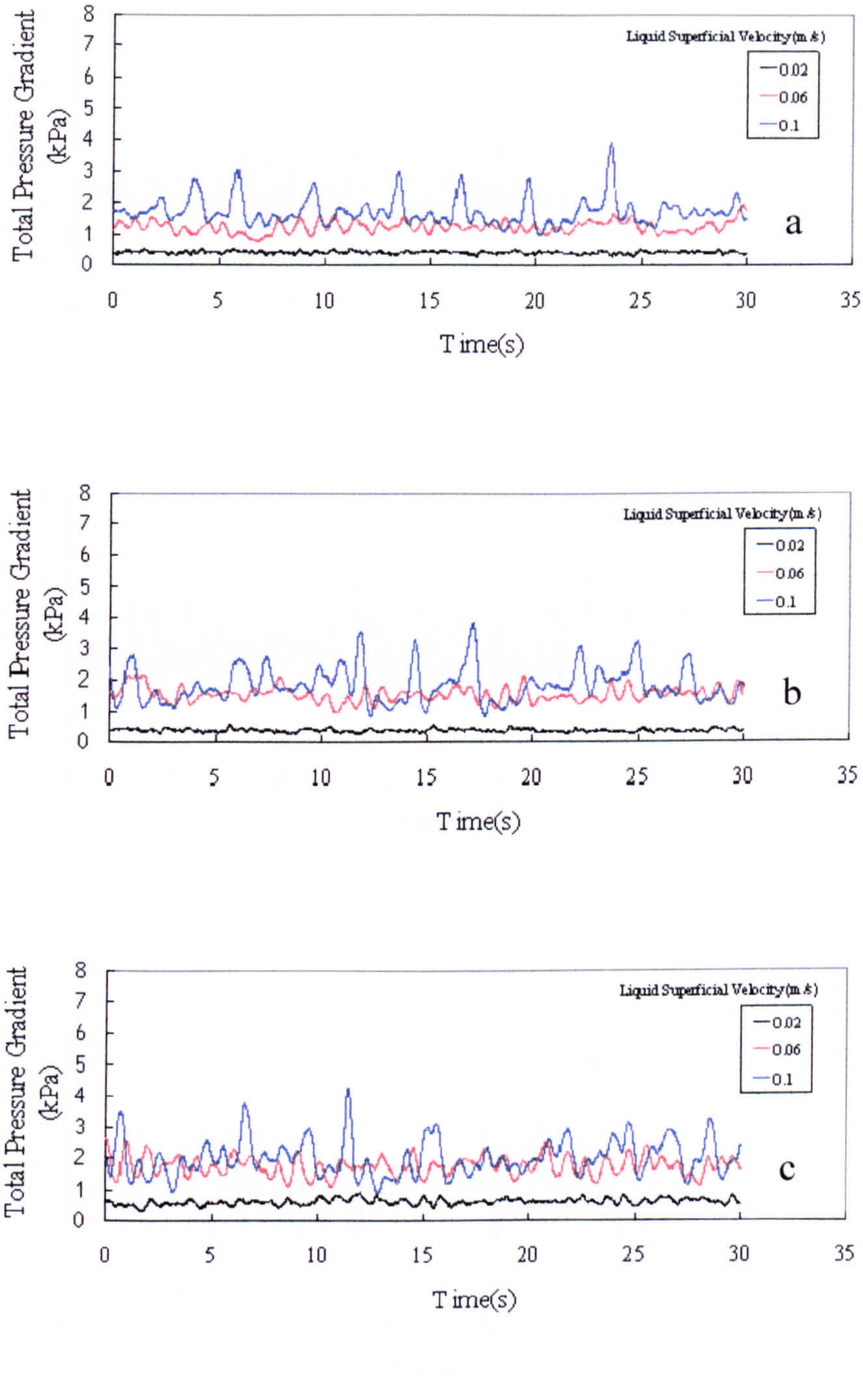

Figure 4.13 Time series of total pressure drop at liquid superficial velocities of 0.02, 0.06 and 0.1 m/s and gas superficial velocity (m/s): a) 11.1 b) 9.3 and c) 8.2.

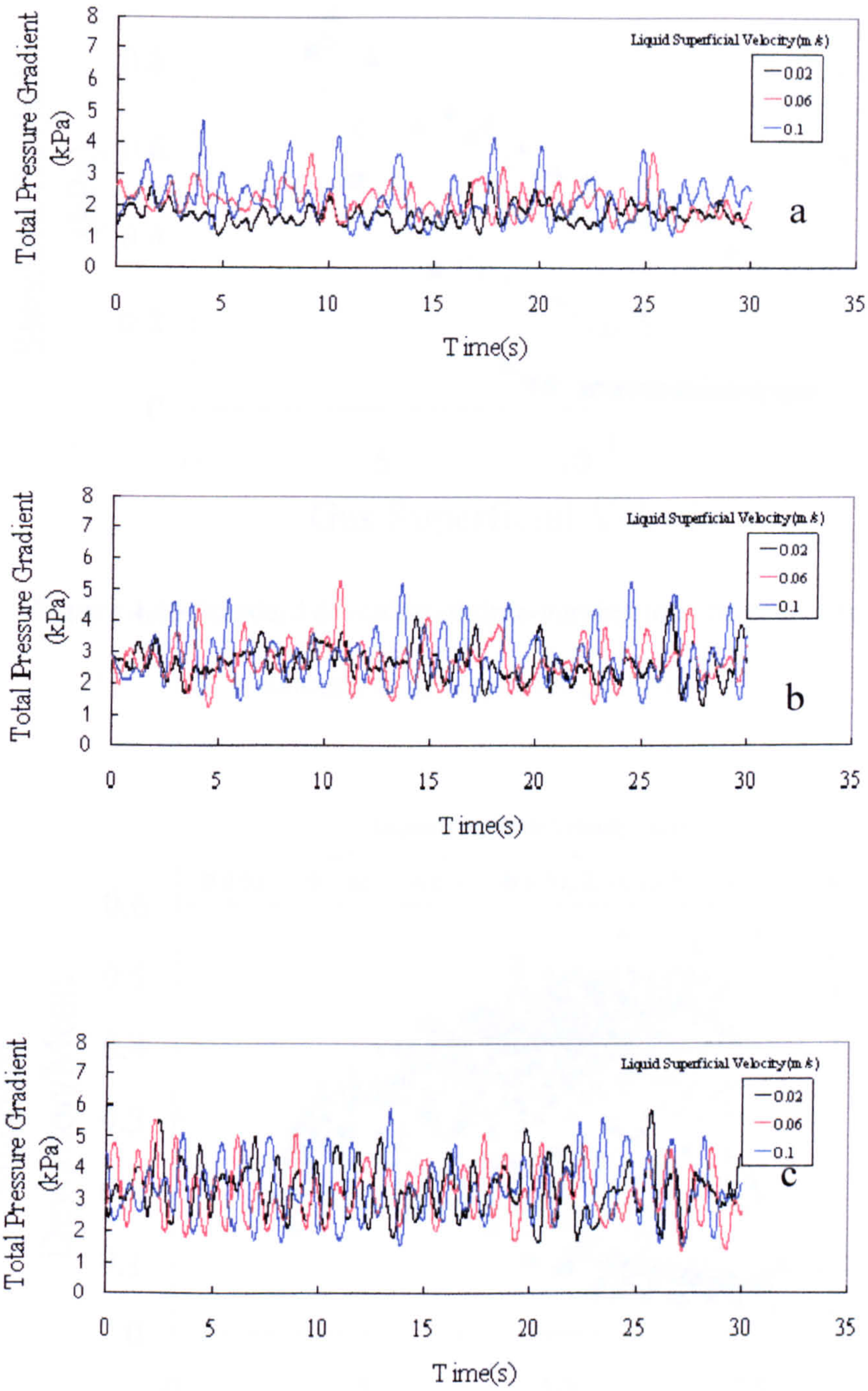

Figure 4.14 Time series of total pressure drop at liquid superficial velocities of 0.02, 0.06 and 0.1 m/s and gas superficial velocity (m/s): a) 6.3 b) 4.2 and c) 3.

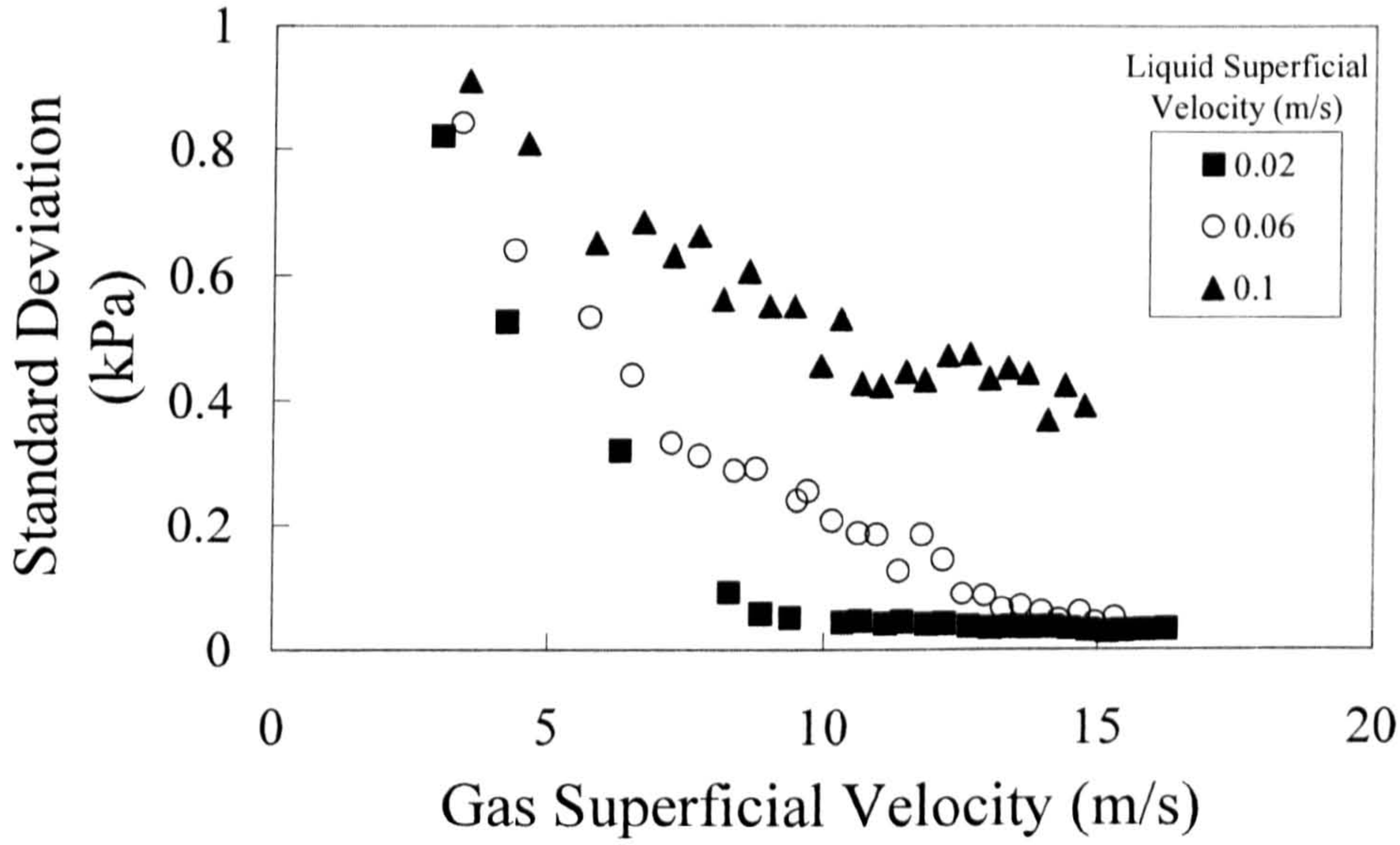

Figure 4.15 Standard deviation of time-varying total pressure drop as a function of gas superficial velocity.

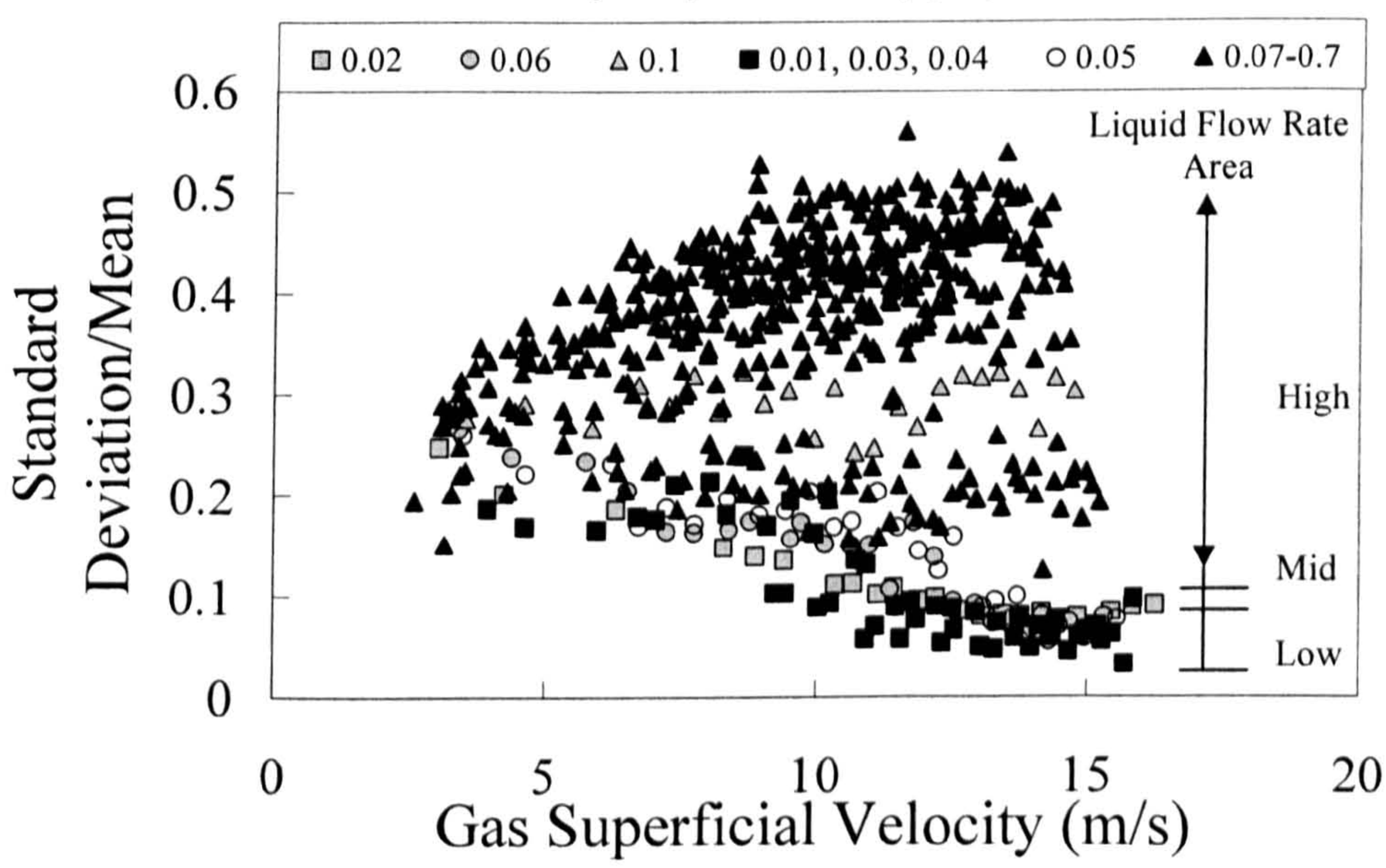

Figure 4.16 Relative standard deviation of pressure drop for a 127 mm vertical pipe as a function of gas superficial velocity at liquid superficial velocities 0.01-0.7 m/s.

4.3 Predicted total pressure drops in large diameter vertical pipe

There are very few experimental data on pressure drop in large diameter vertical pipes. Therefore it is not surprising if there is no a specific model or correlation derived for this geometry. The published correlations can be classified as *homogenous* and *separated* flow models. All the models require a correlation for wall friction but the separated flow models also require a correlation for void fraction.

A comparison of the present experimental data with the homogenous model (Cicchitti et al., 1960) is presented in Figure 4.17a. It can be seen, that the performance of this model is very poor with a large under prediction of the data. The reason for this might simply be that the two phase flow over the ranges of the conditions studied can not be treated as a single phase hence the velocity of the gas and the liquid can not be assumed the same in the pipe. According to Whalley (1987) the homogenous model can give reasonable predictions if the gas mass flux > 2000 kg/m^{2}s and similar judgment on the accuracy of homogenous model has been made by Azzopardi (2006); when the mass fluxes are high enough for the phases to be mixed well, the model may give reasonable predictions.

In contrast to the homogenous model, it is appear that treating the liquid and the gas as a separate phases and flowing at different velocities the present data will be better predicted as can be observed in Figure 4.17b which introduces the separated flow approach using the Chisholm (1967) algebraic correlations against the present experimental data. The Friedel (1979) correlation gives a

consistent under-prediction of the data (see Figure 4.17c). This is surprising since this correlation has been widely recommended; for instance Azzopardi (2006) reported it as probably the best correlation in the open literature.

The present data were also compared with predictions from Beggs and Brill's (1973) correlations (which combine predictions of void fraction and frictional pressure drop). This is one of the few (if not the only) popular correlation derived from data base of inclined pipes including 90°. As it can be seen in Figure 4.17d, that the Beggs and Bill (1973) correlation gives a significant over-prediction of pressure drop compared to the present data. This might be accounted to the fact that they developed their correlation based on the data gathered using 25 and 38 mm. Therefore it is not surprising if looses its accuracy as the pipe diameter 3-5 times larger.

From what have been discussed, the separated flow model based on Chisholm (1967) algebraic correlations was the best among other correlations that tested against current data. The Beggs and Brill (1973) correlation gives a significant over-prediction of pressure drop compared to the present data whereas the homogeneous model and the correlation of Friedel (1979) gave a significant under-prediction.

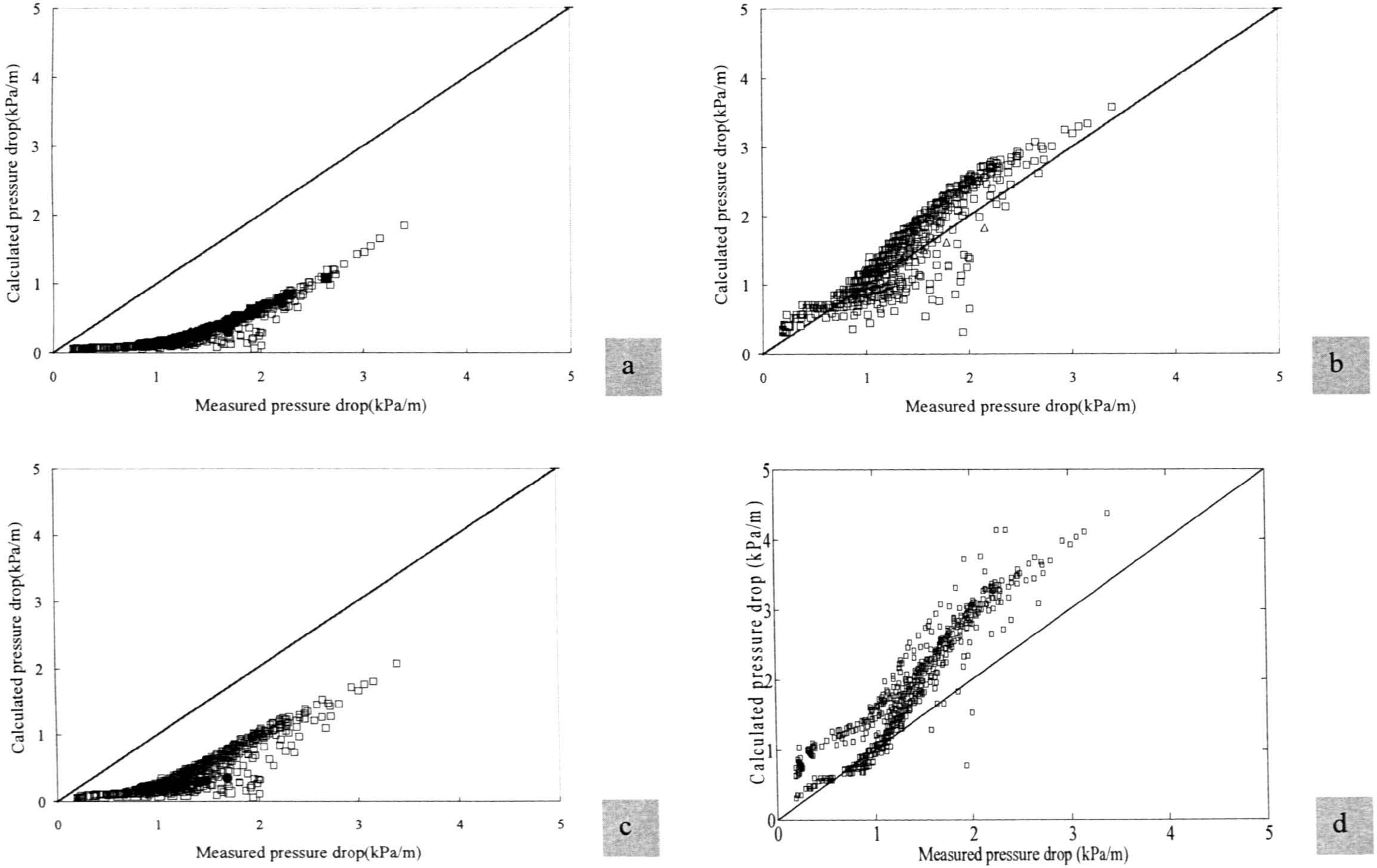

Figure 4.17 Comparison of the experimental pressure drop data with: (a) Homogenous flow model, (b) Chisholm (1967) algebraic correlations (separated flow model), (c) Friedel (1979) correlation, (d) Beggs and Brill (1973) correlation.

Chapter 5

The Wall Shear Stress Measurement

Wall shear stress is an important parameter in two phase flow and it can provide very useful information about pressure drop and velocity profile characteristics. In annular two phase flow liquid film thickness and film flow rate are related to wall shear stress according to the Triangular Relationship as described in Chapter 2. In addition simultaneous measurements of wall shear stress and liquid film thickness can lead to a better understanding of the nature of the waves in the interface between the gas and the liquid film which have a considerable effect on total pressure drop (Martin and Whalley, 1983).

Wall shear stress is known to be a difficult parameter to measure especially in two phase flow which is more complicated than single phase flow. In this chapter the methods of wall shear stress measurement in two phase flow are presented and particularly the hot film technique: the principles of operation and the calibration procedure of both the glue on probe (Dantec 55R47) and the directional hot film probes are presented; the construction of directional wall shear stress probe outlined and the necessary precautions needed to be taken during the measurement are highlighted; this is followed by results from

directional and non directional hot film probes and comparison between the magnitude and the directional wall shear stress. In addition, at the end of this chapter the principle of the micro-pillar sensor are discussed and the necessary developments suggested for the sensor to be employed in the two phase flow area.

5.1 Methods of wall shear stress measurement

Wall shear stress can be measured by variety of techniques and based on their principles they can be classified into two major categories namely direct and non-direct measurement techniques (see the diagram in Figure 5.1). Winter (1977) reviewed the available measurement techniques up to 1977. Hanratty and Campbell (1996) discussed experimental issues associated with using the various shear stress sensors. Fernholtz et al (1996) investigated the range of applicability of different techniques and compared them with each other and recently researchers, e.g., Sheplak et al (2004) and Etebari (2008) reviewed the existing Micro Electro Mechanical Sensors (MEMS) which have been emerged as a new class of shear stress sensors.

Due to the large number of the available techniques, attention in this study was focused on those techniques that been known by their applicability in two phase flow area as presented in the subsequent sections:

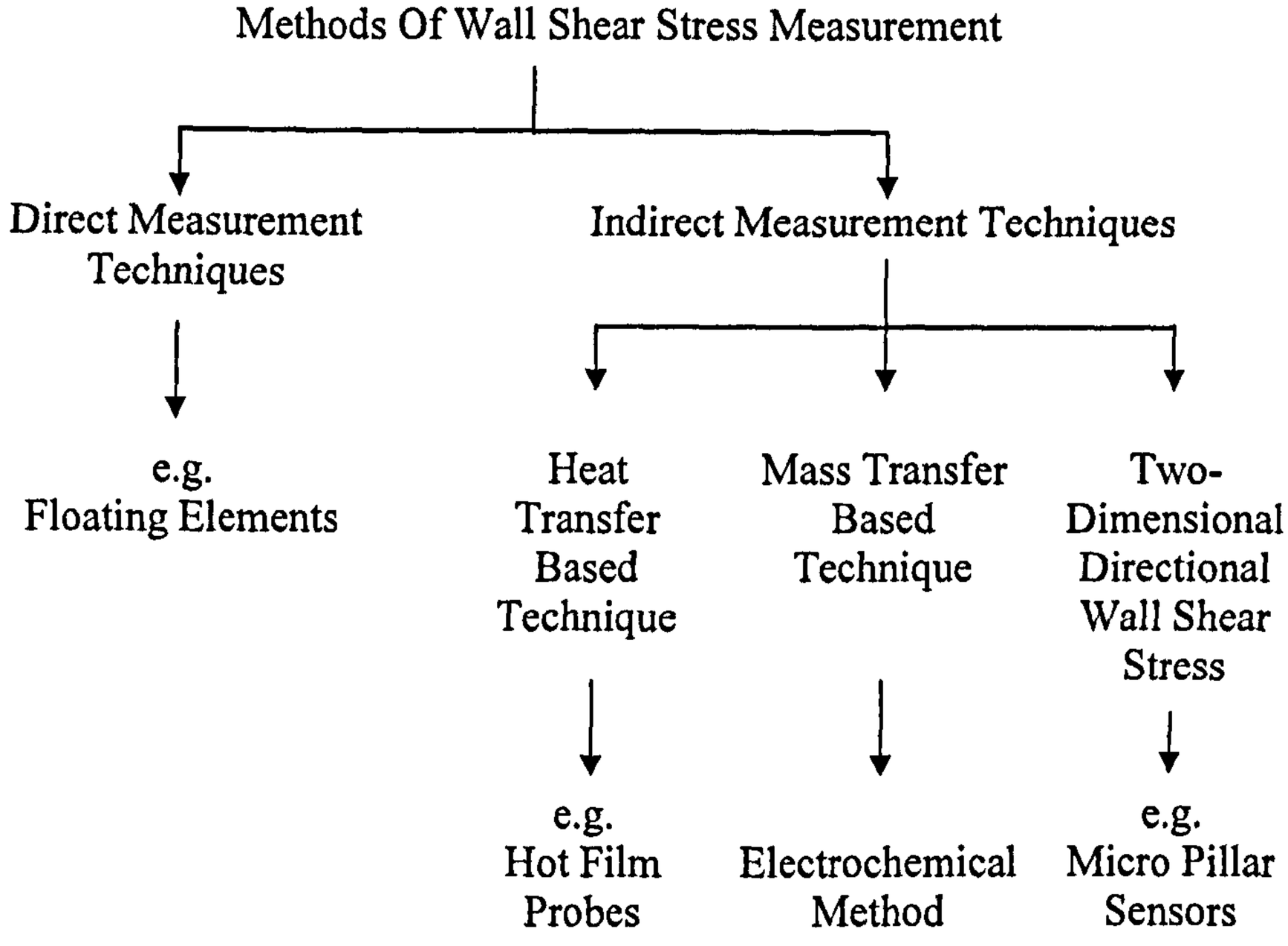

Figure 5.1 Summary of wall shear stress measurement methods

5.1.1 Direct shear stress measurement techniques:

The conventional method of measuring wall shear stress directly is to arrange for a section of the pipe wall to be free to move in the direction of the flow. As the result of wall shear stress action, the force on the section is balanced by measured external force, and then the mean wall shear stress will be calculated over the floating section. This method has been discussed in detail by Winter (1977). Due to the mechanical difficulties associated with manufacturing this kind of the technique it has only been used by a small number of the researchers in two phase flow, e.g., Cravarolo et al (1964) and Kirillov et al (1978). Note that this technique can only give time averaged values. In

addition, there are worries of the device disturbing the flow. The floating element sensor works on the same principle as above. It has been introduced recently under the MEMS family can provide a direct wall shear stress measurement, however this is also subject to mechanical fouling according to Etebari (2008). Therefore the direct method of wall shear stress measurement is less attractive than the indirect method, especially for two phase flow.

5.1.2 Indirect Shear Stress Measurement Techniques:

The mechanical difficulties and the errors that associated with the direct methods has led to development of indirect wall shear stress measurement techniques which require an empirical or theoretical relation between the wall-shear stress and the output of the sensor. Most researchers in two phase flow have used the indirect methods based on the analogy between mass or heat transfer and momentum transfer as discussed below:

5.1.2.1 Mass transfer based technique:

Those mass transfer based techniques known as Electrochemical, Polarography or Electrodiffusion methods consist of the basic electric circuit (Anode and Cathode) and electrolytic solution, e.g., Potassium Ferricyanide and Ferrocyanide as a Redox system. The experimental procedure of this technique has been given in detail by Hanratty and Campbell (1996). The technique has been employed in two phase flow by a number of researchers over the last four decades, e.g., Kutateladze et al (1969), Cognet et al (1984), Zabaras et al (1986) and recently, e.g., Kashinsky et al (2006). Although the

electrochemical method has the advantages that it can be used in a wide variety of flows and offers the possibility of measuring time-varying flow contrast to other methods, calibration is not necessary. However, the heat transfer based technique still the most preferred technique by the researchers especially for the air-water systems as explained by Martin (1983) as the following:

1- Light and oxygen will influence the mass transfer measurement; therefore this method is not suitable with the test facilities that use Perspex as the test section for visual observation purposes.

2- The use of an electrochemical reaction in the system would make the using of conductivity methods for the liquid film thickness and void fraction measurements difficult.

3- According to Fortuana and Hanratty (1971) the frequency response for a hot film probe is greater than for a mass transfer probe; in another word the use of heat transfer based technique for the wall shear stress measurement is the most convenient method for air-water system when a high frequency response is needed, so as to study the effect of waves.

5.1.2.2 Heat transfer based technique:

Thermal anemometry is one of the most widely used methods for the study of turbulent flow. The measurement using this technique is based on the analogy between heat transfer and momentum transfer. Hot wire probes are mainly used in the gas flows due to their small size and well defined calibration characteristics as described by Bruun (1996). However, they are thin and very

fragile in comparison with hot film probes. Therefore the later is more suitable for the measurement in the liquid. In the case of two phase flow, the hot film probes are the most used for the measurement of wall shear stress because the liquid in the most flow regimes is on the pipe wall. Hot film probes can have different design configurations as presented by for example Bruun (1995). Among those, the flush mounted or so called glue-on-probes are the most preferred technique in two-phase flow as they are non-intrusive and do not disturb the flow. A number of researchers have used similar probes in two phase flow in both vertical and horizontal pipes, e.g., Martin (1983), McQuillan (1985), Kowalski (1987), Govan et al (1989), Wolf (1995), Shaha (1999), Badie (2000) and Descamps et al (2008). In the present study both commercial glue on hot film probes from Dantec dynamics (DANTEC 55R47) and the directional flush mounted wall shear stress probe which is manufactured at Nottingham University have been employed for the measurement of shear stress near the pipe wall. The principle of operation, the construction and the calibration of the probes are presented in the subsequent sections of this chapter. The precautions needed in the operation of these probes are discussed and comparisons between the results obtained with different forms of probe are presented.

5.1.2.2.1 Principle of operation of hot film probes

To measure wall shear stress in pipes using these probes a thin film of metal (nickel or platinum) is heated by electrical current and mounted flush with the inner diameter of the pipe. The probe to remain at constant temperature it is

necessary to be connected to a constant temperature anemometer (CTA). The main component of the anemometer circuit is a Wheatstone bridge. The probe is connected to one of its arms (Figure 5.2). The other part of the circuit is the servo amplifier which keeps the bridge in balance (Equation 5.1) by controlling the current to the sensor hence its resistance:

$$\frac{R_{\text{var}}}{R_1} = \frac{R_c + R_{ps} + R}{R_{\text{int}}} \qquad (5.1)$$

Where; R_c is the resistance of the cable to the hot film probes, R_{ps} is the resistance of the probe support, R_1 and R_{int} are the internal resistances in the anemometer bridge, R_{var} is the variable resistance in the bridge and R or as known R_W is the resistance of the probe at its operating temperature.

The resistance of the probe is proportional to its temperature. Therefore maintaining a constant resistance of the probe means its temperature is also kept constant which must be higher than the fluid temperature near the probe. That pre-selected excess temperature is defined by so called overheating ratio, a which can be expressed as the following (Jorgensen, 2002):

$$a = \frac{R_W - R_0}{R_0} \qquad (5.2)$$

Where; R_W is the sensor resistance at operating temperature T_W and R_0 is its resistance at ambient (reference) temperature T_0. The over temperature $T_W - T_0$ can be calculated as:

$$T_W - T_0 = \frac{a}{\alpha_0} \qquad (5.3)$$

Where; α_0 is the sensor temperature coefficient of resistance at T_0. Usually the

manufacturer for commercial probes supply the values of R_0 and α_0 at T_0=20 ^{0}C.

From above when the liquid is flowing over the probe it will be cooled and its resistance drops causing the bridge to be imbalanced. To rebalance the bridge the amplifier will signal the current source to increase its output (the bridge voltage) and reheat the probe which occurs almost instantaneously (Hanratty and Campbell, 1996).Thus, the faster the flow, the higher the output voltage, i.e., the higher the wall shear stress.

In the present work a DISA constant temperature anemometer (CTA) type 55M system with 55M10 CTA standard bridges were employed, the operating instructions are given in Appendix C.

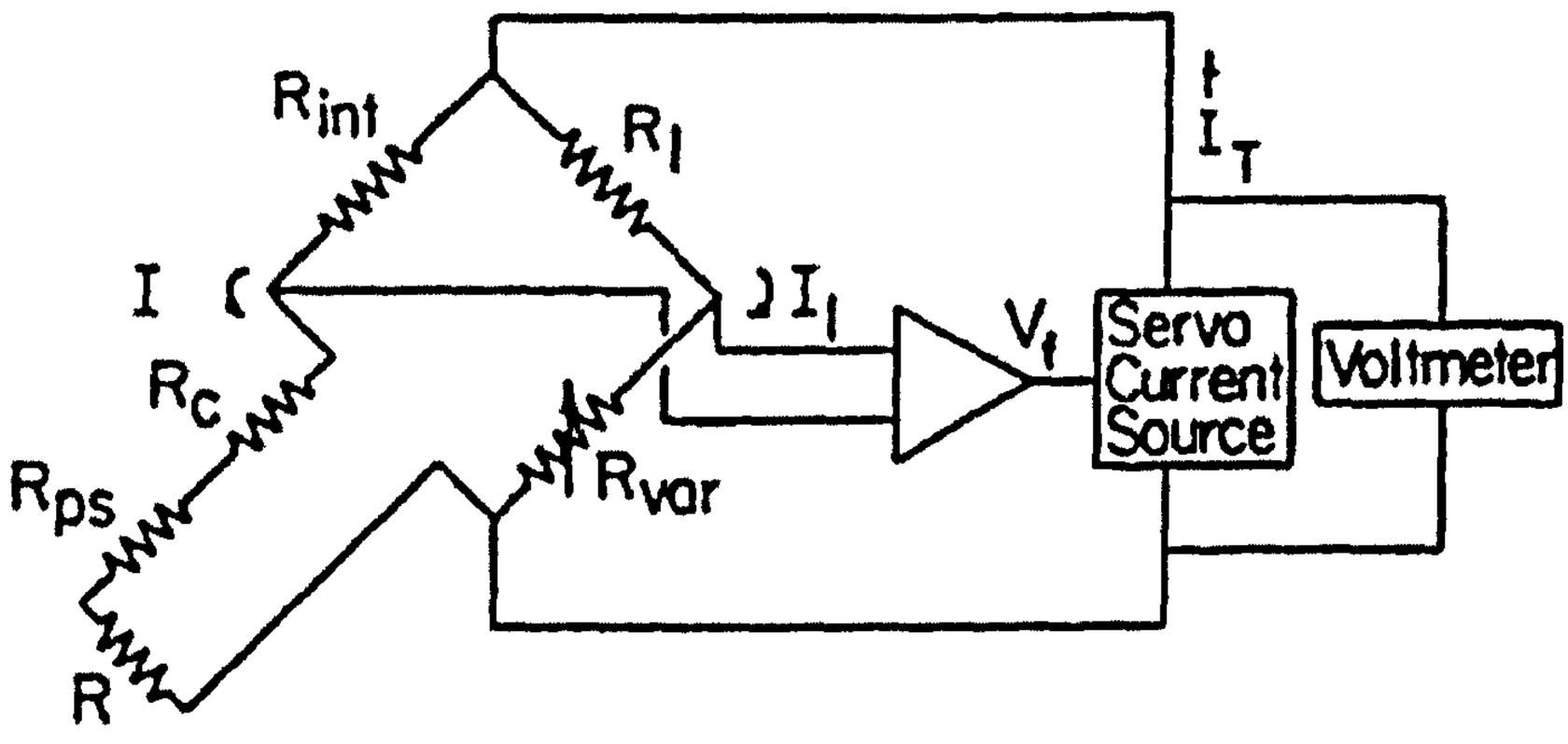

Figure 5.2 The simplified electronic circuit of constant temperature anemometer (CTA) bridge (Hanratty and Campbell, 1996).

Researchers, e.g., Martin (1983), McQuillan (1985), Kowalski (1987), Govan et al (1989) and Wolf (1995) who measured wall shear stress in two phase

flow employing the flush mounted hot film probes have used the following relationship between the output voltage V from the anemometer and the wall shear stress τ_W :

$$V^2 = A + B\,\tau_w^{1/3} \qquad (5.4)$$

As described by Martin (1983) and Boyer et al (2002) Constants A and B in the Equation 5.4 are related to the physical properties of the fluid near the probe and the geometry of the probe and it is not possible to calculate their values therefore the probe calibration is essential.

Researchers agree that the Equation 5.4 is valid only when the thermal boundary layer of the film probe is within the viscous sub-layer of the turbulent boundary layer, i.e., thinner than the laminar sub-layer of the momentum boundary layer where the velocity profile is linear. However employing such probe in two phase flow facing further restriction as the thermal boundary layer as well must not exceed the thickness of the liquid film on the pipe wall.

The thickness of thermal boundary layer, δ_T, of the flush mounted hot film probes is expressed as the following (Martin, 1983):

$$\delta_T = \frac{k}{h} = 1.86\left(\frac{\mu\alpha x}{\tau_w}\right)^{1/3} \qquad (5.5)$$

Where;

k is the thermal conductivity of the liquid (w/m k).

h is the heat transfer coefficient from heated wall to the fluid (w/m^2 k).

μ is the liquid viscosity (Ns/m^2).

α is the thermal diffusivity of the liquid (m^2/s).

x is the width of the probe (m).

τ_w is wall shear stress (N/m^2).

And the momentum boundary laminar sub-layer can be calculated as the following:

$$y = \frac{\mu u^+}{\rho u^*} \quad \text{at} \quad y^+ < 5 \qquad (5.6)$$

Where;

y is the momentum boundary laminar sub-layer.

y^+ is the dimensionless distance from the wall of the pipe.

μ and ρ is the liquid viscosity and density respectively.

And;

$$u^* = \sqrt{\frac{\tau_w}{\rho}} \qquad (5.7)$$

$$u^+ = \frac{u}{u^*} \qquad (5.8)$$

For the present study and based on the operating conditions and the results from the local film thickness probes and the conductance ring probes, the thermal boundary layer, δ_T, of the hot film probes employed is kept smaller than the momentum boundary laminar sub-layer, y, and the liquid film thickness, δ, during the measurement of the wall shear stress as shown in Figure 5.3.

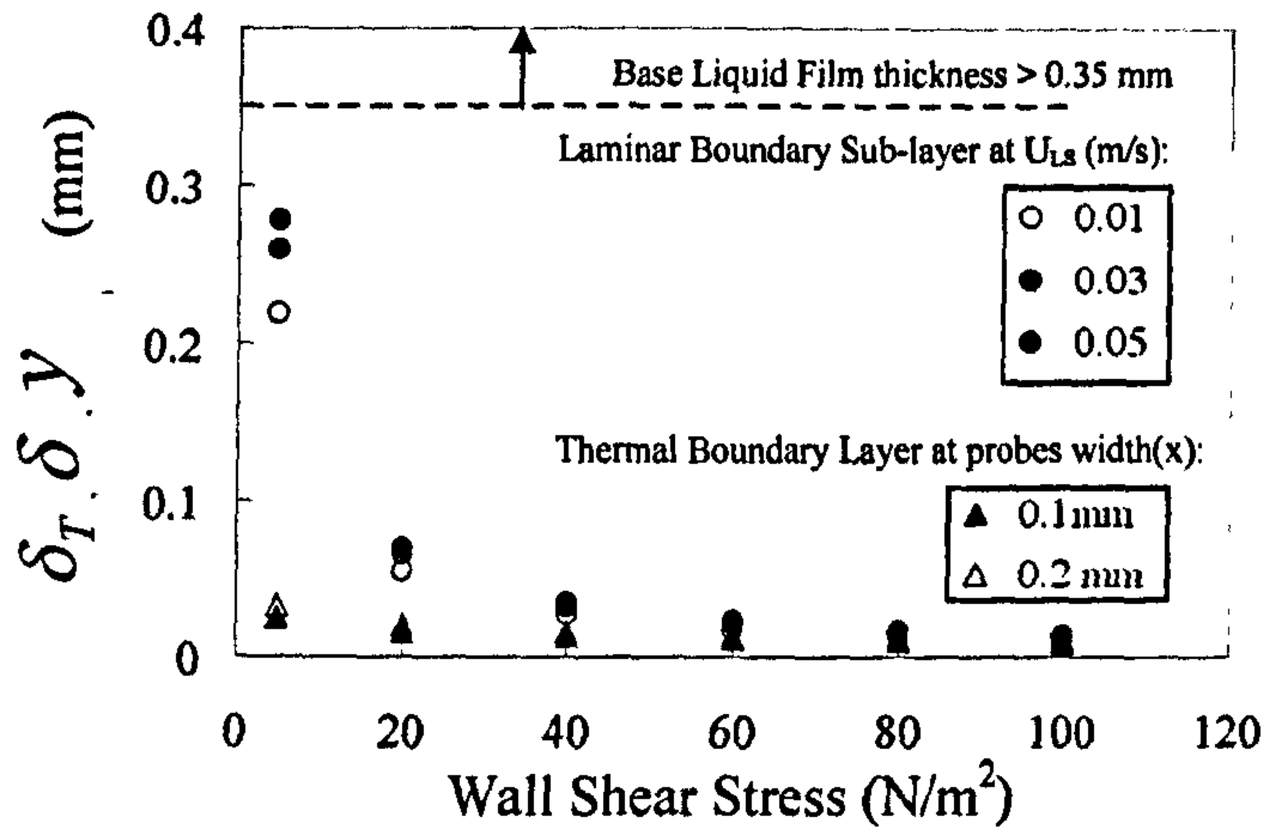

Figure 5.3 Thermal boundary layer and momentum laminar sub-layer as a function of wall shear stress and the minimum values of the liquid film thickness

5.1.2.2.2 Calibration of the hot film wall shear stress probes

Calibration of the hot film probes is essential to find the constants in the relationship between the output voltage from the anemometer and the wall shear stress (Equation 5.4). It is desirable that the calibration to be performed in the same position in which the measurements are to be taken because of the probes sensitivity to changes in position (Miller, 1980 and Bruun, 1995).

Different calibration techniques of the hot film probes have been reported over the last decades; Bruun (1995) has summarized the most commonly used. For applications in two-phase flow, the calibration involves the measurement of pressure drop either in single phase or in two phase flow. Researchers, e.g., Martin (1983), McQuillan (1985), Kowalski (1987), Shaha (1999), Badie (2000) and Descamps et al (2008) have used a single phase calibration

method; however the two phase calibration method were used by Govan et al (1989) and Wolf (1995). The single phase calibration method necessitates a high flow rate of liquid because the wall shear stress in two phase flow is relatively higher than single phase flow. For the present study the single phase calibration method was preferred mainly because: on the one hand, in the range of the two phase flow conditions that investigated in this work a change in the flow direction are expected which can result in errors in the measured mean wall shear stress; on the another hand sufficiently high liquid flow rate can be achieved with the current test facility, as the liquid pump employed can drive upto 68 m^3/hr of liquid to the riser as described in Chapter 3. So the hot film probes used in the present study, i.e., the glue on probes (Dantec 55R47) and the directional wall shear stress probes, were calibrated in situ using the single phase liquid flow. The calibration procedure can be summarized as the following:

The frictional pressure drop in the single phase flow (water) was measured using the electronic D.P. Transmitters as described in Chapter 3. From the measured frictional pressure drop the values of wall shear stress were calculated according to the following relationship:

$$\tau_w = \frac{\Delta P_f d}{4l} \tag{5.9}$$

Where; ΔP_f, is the frictional Pressure drop, d, is the diameter of the pipe and, l, is the distance between the pressure drop tapping holes.

By repeating procedure above over different liquid flow rates the calibration curve were obtained and the values of constants A and B in the Equation (5.4) were found; from the calculated wall shear stress and the output voltage

signals from the anemometer. The calibration curve of the probe shown is in Figure 5.4.

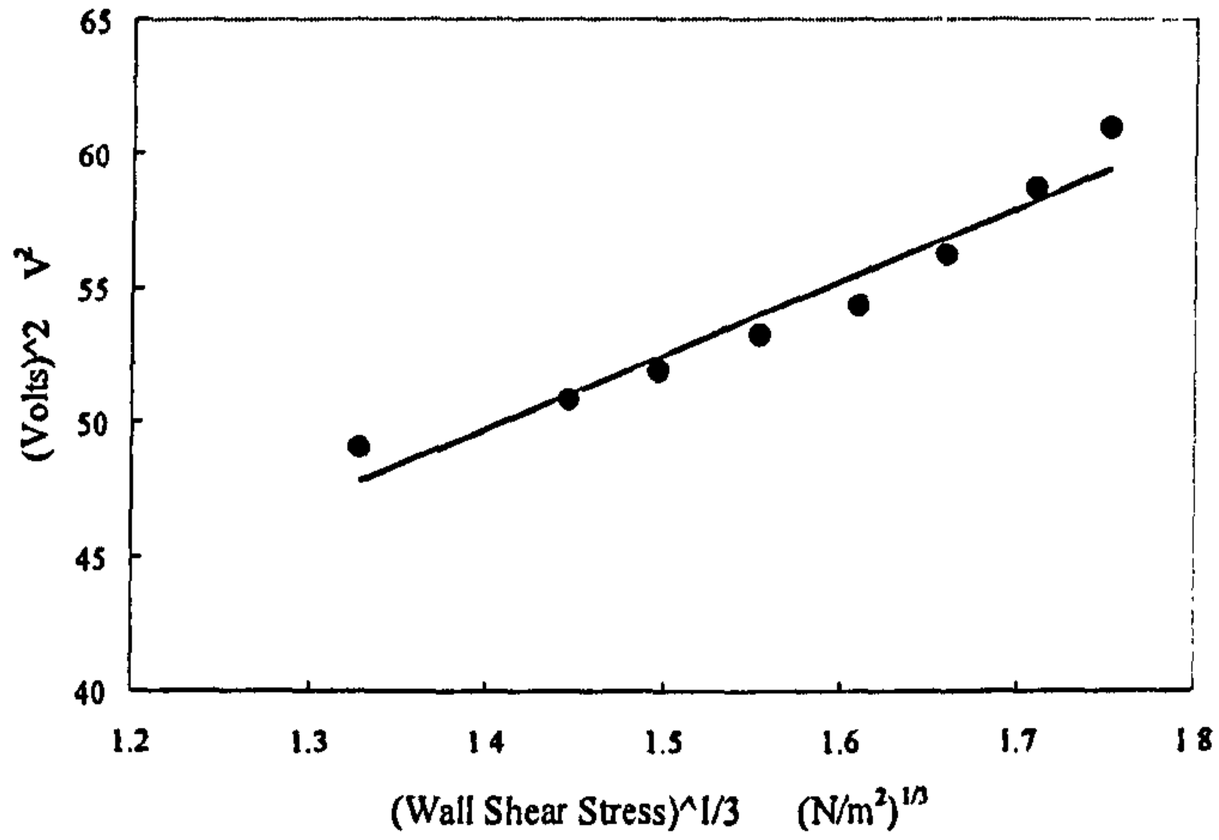

Figure 5.4 Calibration curve of the directional wall shear stress hot film probe.

5.1.2.2.3 Glue-on hot film probe (Dantec 55R47)

During the first campaign measuring wall shear stress commercial glue on hot film probe (Dantec 55R47) was employed. The probe consists of a thin film of nickel (0.1x 0.9 mm) deposited on a thin foil of polyamide (0.05 mm) and coated with 0.5 μm of quartz to protect it from any electrolytic attacks (Figure 5.5a). The electrical connections to the sensor are made through the gold plated lead areas onto which copper wires are soldered; this is to connect the probe to the leading cables to the anemometer. The advantage of using this sensor is: It can be glued directly in the points of interest on the surface wall and it is flexible enough to take the shape of the curved surfaces. For the present work the probe were glued on a curved surface of Perspex rod which had been machined very carefully to have the same shape as the inner

diameter of the pipe (Figure 5.5b). The Perspex plug with the probe on it is inserted into the test section through a specially made guide. The main objective of the guide was to keep the probe completely mounted flush and perpendicular to the direction of the flow. Small holes along the plug were drilled for the electrical wires to connect the cables that led to the anemometer. Water leakage from the holes or around the plug may lead to a significant errors as a result of lost currents in the circuit due to the conductivity therefore it is not tolerated, i.e., the water leakage was stopped completely using non-conducting adhesives and rubber O-rings. The hot films probe (Dantec 55R47), as flush mounted inside the pipe and on the test section are illustrated in Figures 5.5 c and d.

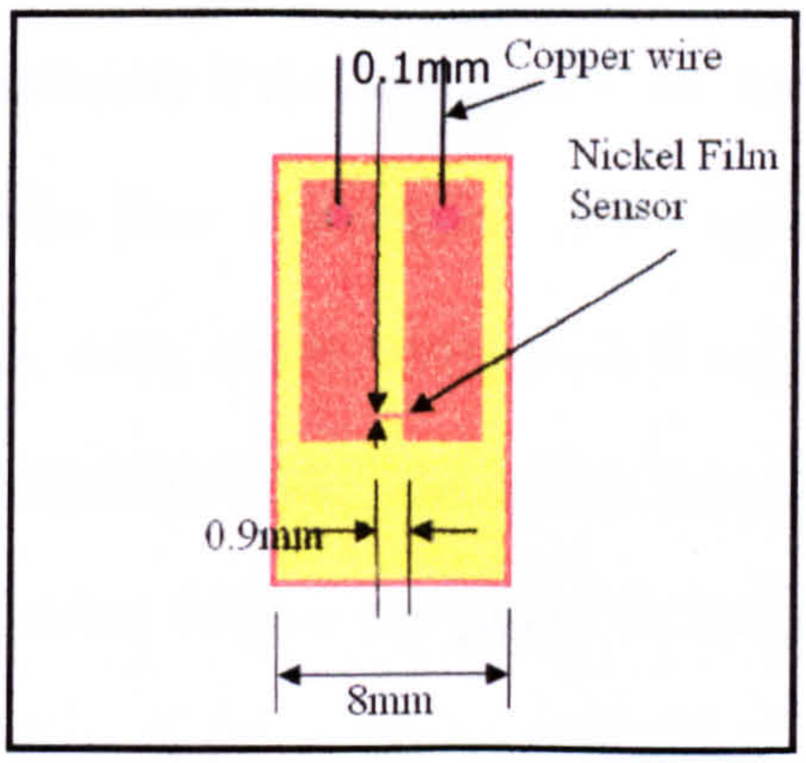

a

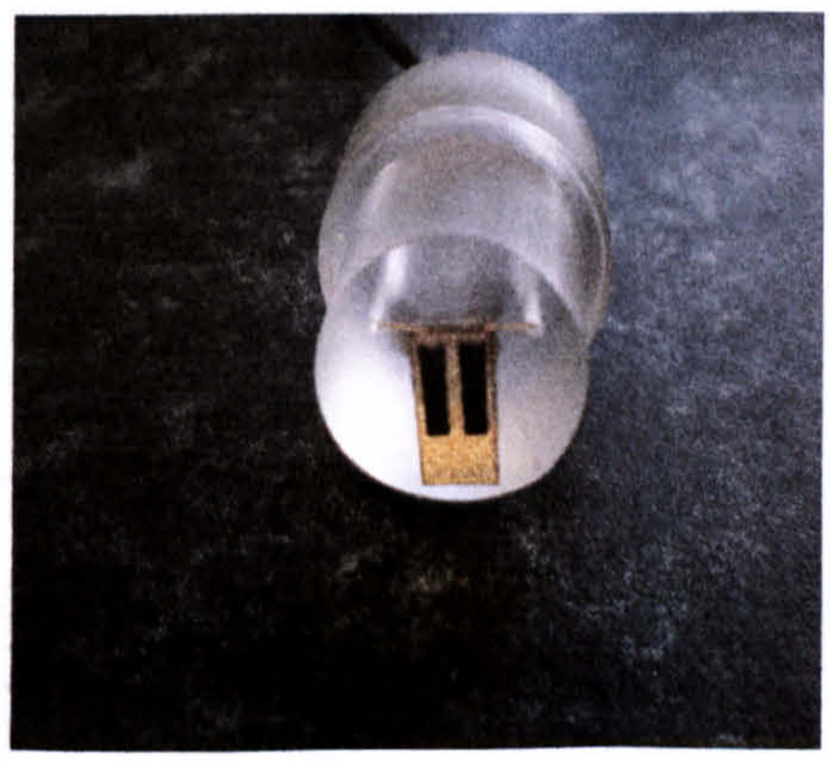

b

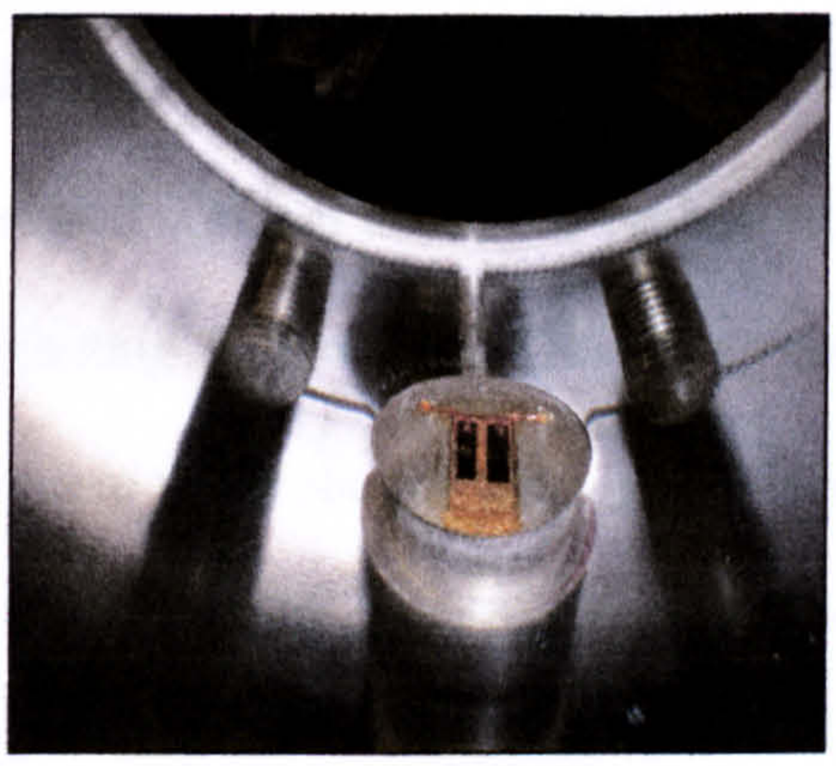

c

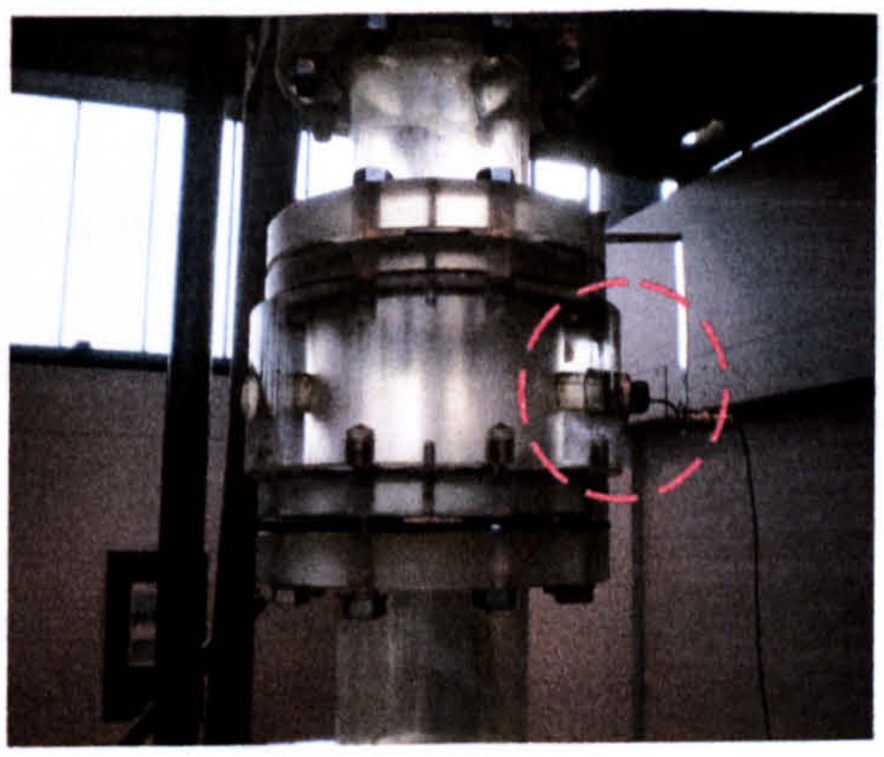

d

Figure 5.5 Glue on hot film probe (Dantec 55R47): a) the layout of the probe b) glued on the Perspex plug c) flush mounted inside the pipe d) installed on the test section.

5.1.2.2.4 Directional hot film wall shear stress probe

The glue-on probe type hot films are not able to detect the direction of the flow. Therefore it can lead to erroneous values of the mean shear stress, especially if they are used when the oscillatory flow occurring as in two-phase churn flow. The Dantec 55R47 type glue-on probe has further limitations as it has been coated with a thin layer of quartz (0.5 μm) and according to McQuillan (1985) the quartz coat is prone to cracking when the probe is bent in order to glue the probe on the mounting rods. This is less likely for the present work as the pipe diameter that used in the current study is 4 times larger than that employed by McQuillan (1985). However, coating the probe with polyamide still a good alternative and can provide more reliable insulation. Other researchers, e.g., Wicaksanaa et al (2009), have also expressed concern about the probes when it is utilized in a liquid medium as the coating is too thin. Therefore, they have added an extra thin layer of lacquer to the probe for extra protection. Moreover, it has been argued that the fact that the electrical wires were soldiered onto the front face of the probe can cause a noticeable roughness on the surface and consequently might disturb the flow.

Because of the above and to overcome the limitations of the commercial glue-on probe hot films when applied to the two-phase flow, it was decided to use a locally constructed multiple hot film probe (the directional wall shear stress probe) in the present study. Originally such probes were developed by a team at the UKAEA, Harwell laboratory and used by Whalley and McQuillan (1985), Govan et al (1989) and Wolf (1995). Although the dimensions and the

construction materials of the probe were provided in those papers, the manufacturing details of the probe are not available in the literature. Therefore effort has been put to manufacture probes at Nottingham University. A design detail of the probe was prepared, a number of trial masks have been used and different methods for depositing the nickel films were tried. The probe configuration and the final procedure of making the probe are summarized as the following:

Probe design: The Directional wall shear stress sensor consists of 5 individual probes which are thin films of nickel, (0.2x 3 mm) for probes 1, 3 and 5 and (0.1x 3 mm) for probes 2 and 4 deposited onto a thin sheet of Kapton and coated with 1-1.5 μm of polyamide to protect them from any electrolytic attacks (Figure 5.6.a). The probe dimensions were chosen to ensure that the thermal boundary layer was smaller than both the momentum boundary laminar sub-layer and the liquid film thickness for the range of the conditions studied in the present work. Probe 3 (the central probe) was used to measure the wall shear stress on the same way as described previously for the commercial glue-on hot film probe (Dantec 55R47). It is connected to the DISA anemometer (CTA). The electronic requirements for the directional wall shear stress are shown in Figure 5.7. Probes 2 and 4 were used to detect the direction of the flow by detecting the direction of motion of the liquid heated by the wall shear stress probe (probe 3). The outer probes (probe 1 and 5) are designed to provide the temperature compensation by using one of them to sense the bulk temperature and a second overheated probe to serve as the heat source however this set-up was found by Wolf (1995) to be inferior for the application as it is tended to burn out the probes very quickly. The electrical

connections to the probes were made through stainless pins inserted to the body of the acrylic resin rod that the probes were glued to. The connections were made through the polyamide substrate which gives significantly less disturbance to the flow, Figure 5.6b. The probe were inserted into the test section and mounted completely flush with inner diameter of the pipe in similar way as described for the commercial glue-on hot film probe (Figures 5.6c and d).

Probe construction: Several process steps were used to manufacture the directional wall shear stress which can summarized as; After a thin sheet of Kapton had been cut to size and cleaned, a dual layer photolithography step was employed to transfer the sensor pattern from a mask onto the Kapton sheet. Once the pattern had been developed onto the Kapton, this was then placed in a high vacuum thin film evaporator which allowed deposition of 200 nm of high purity nickel. Next di-electric coatings of 1 to 1.5 μm thick were applied over the whole of the sensor. This was achieved using a spin-on polyimide, basically the same material that as Kapton. The polyimide requires curing at 360°C in nitrogen atmosphere for 60 minutes. After initial trials a further process step using photolithography was added just prior to the final curing. This was to open up 'windows' in the polyimide film over the sensor contact pads to overcome the problem of making electrical connectivity to the sensor.

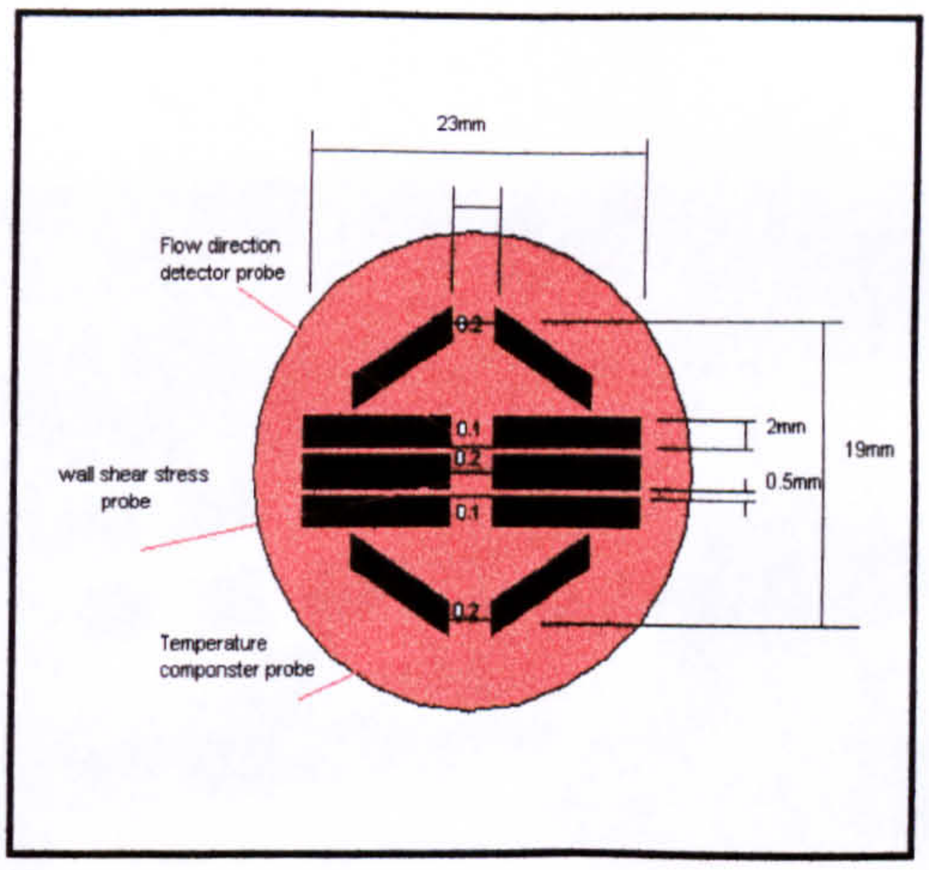

a

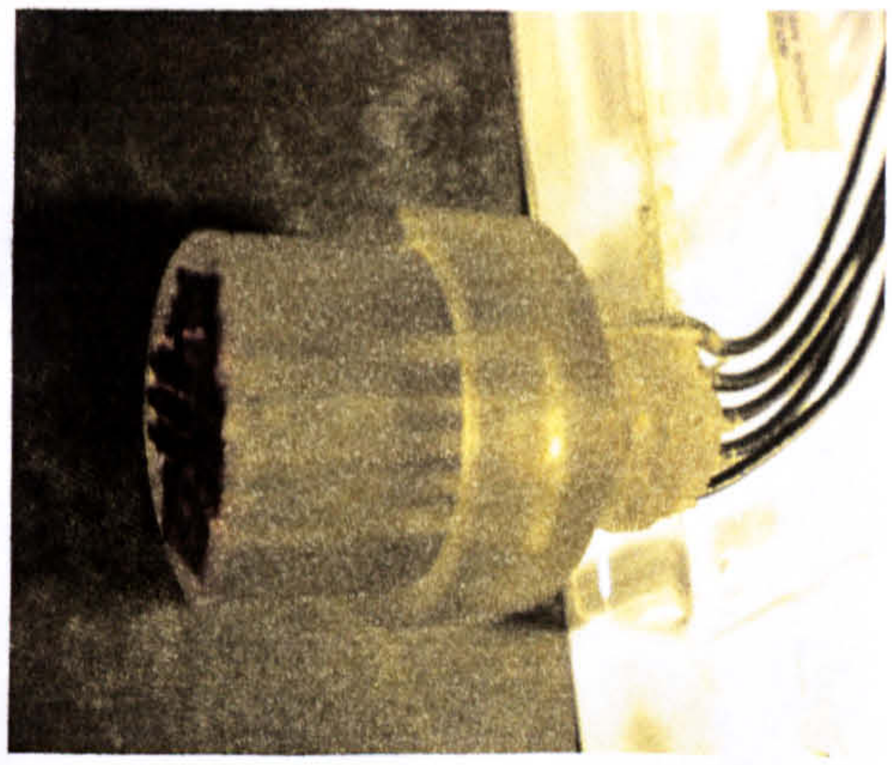

b

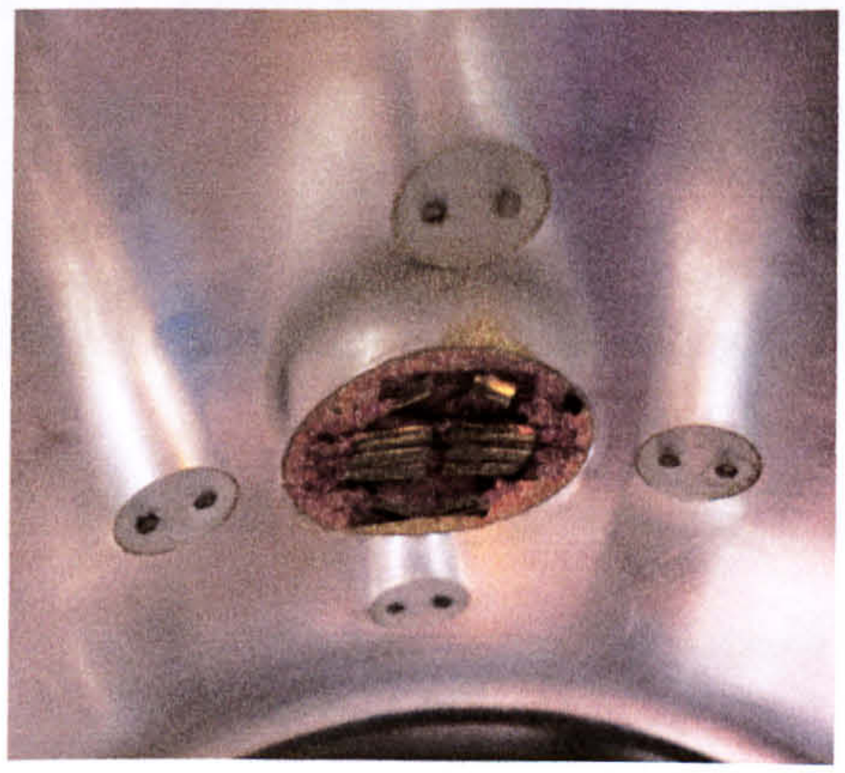

c

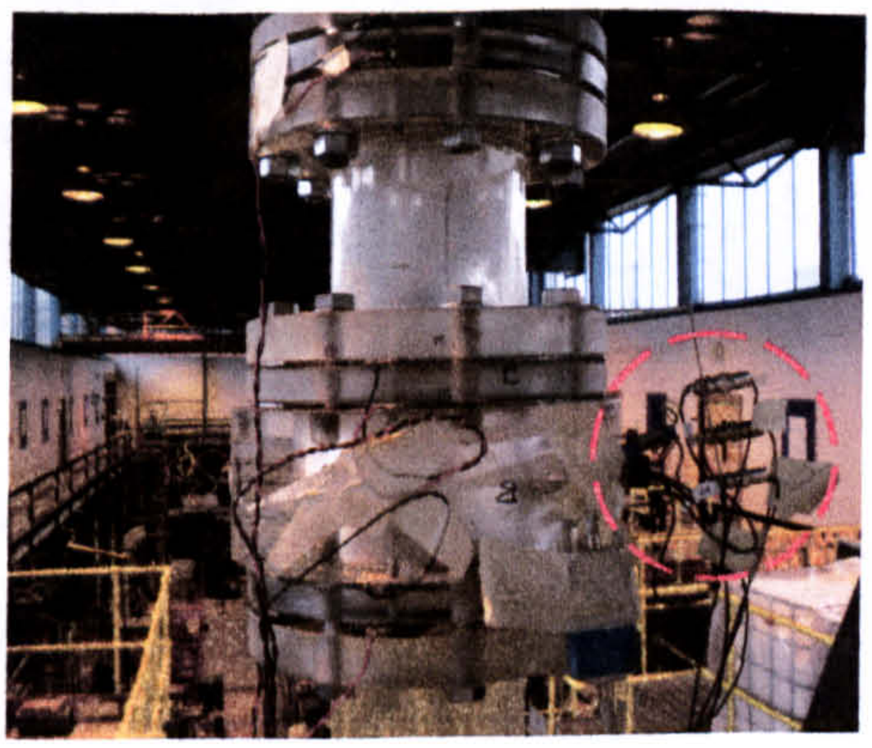

d

Figure 5.6 Directional hot film wall shear stress probe: a) the layout of the probe b) glued on the Perspex plug c) flush mounted inside the pipe d) installed on the test section.

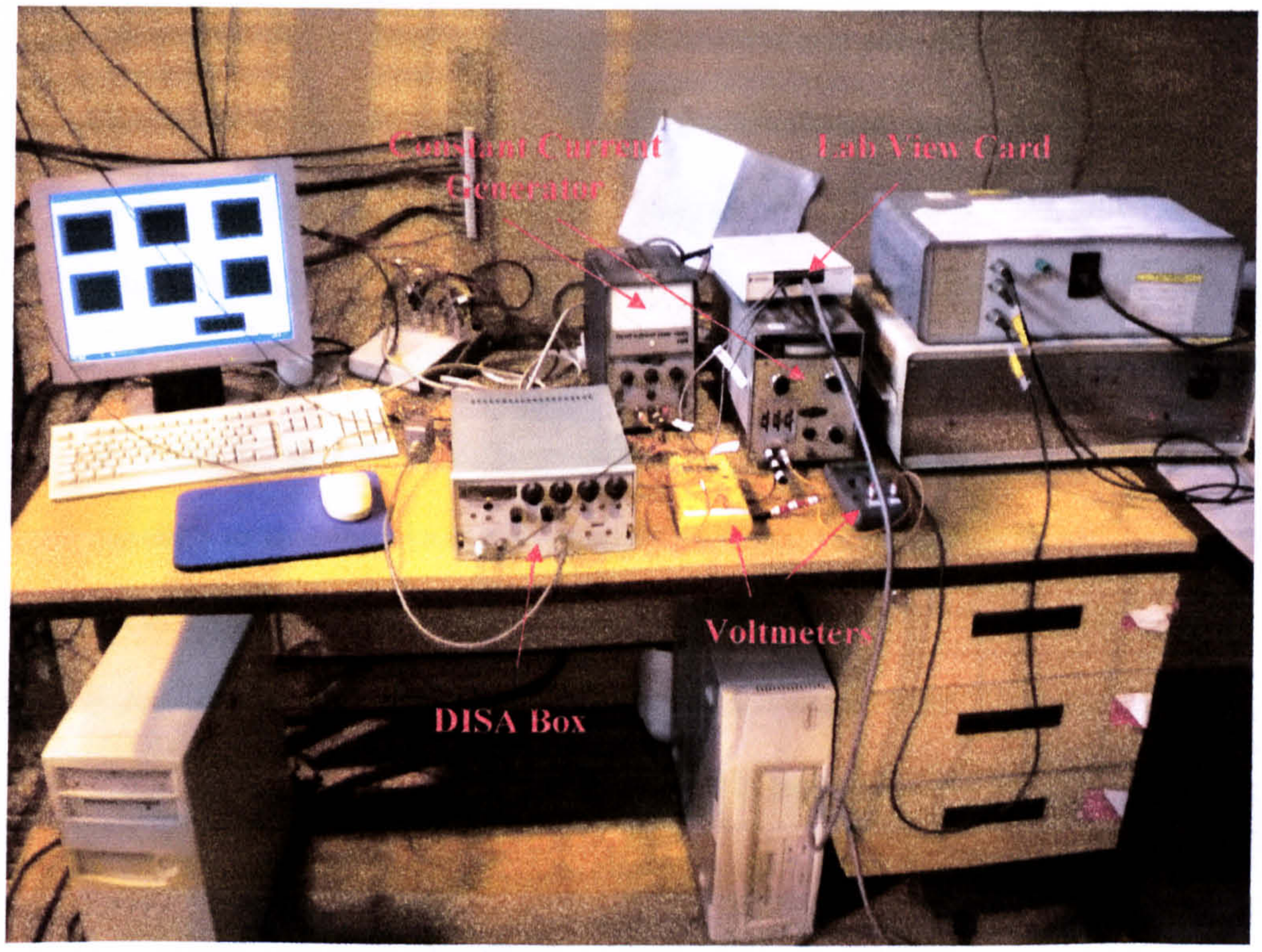

Figure 5.7 Electronic equipments deployed with the directional hot film wall shear stress probe

5.1.2.2.5 Necessary Precautions: Using Hot Film Probes

Previous researchers, e.g., Martin (1983), Boyer et al (2002), Hanratty and Campbell (1996) and Bruun (1996) have outlined the common problems associated with the hot film anemometer when it is used in the liquid flow. They reported that the measurement errors are arise from: flow disturbance due to probe, electrolysis, calibration curve uncertainty, bubble formation on the probe, and temperature non-uniformity. During present study special

precautions have been taken to overcome the sources of errors as summarised below:

Flow disturbance due to the probe: To avoid any disturbance to the liquid film on the pipe wall; in this study both the commercial glue-on hot film probe (Dantec 55R47) and the directional wall shear stress probe were glued on a curved surface of Perspex rod which machined very carefully to have the same shape as the inner diameter of the pipe and a high level of care has been taken to assure the probes were completely mounted flush inside the test section. In addition to that the electrical connections to the directional wall shear stress probes were made through the body of the Perspex rod that the probes were glued on and through the polyamide substrate from the rear which significantly improved the flatness of the front face surface of the probe.

Calibration of the probe: Hot film probes calibration is essential to find the relationship between the output voltage from the anemometer and the wall shear stress. A frequent check of the calibration curve during the measurement is also necessary to ensure optimal performance of the probe. The hot film probes used in this study were calibrated in situ (i.e., the effect of position changes were avoided and it can be repeated frequently during the measurement). As described previously the calibration relationship (i.e., Equation.5.4) is valid only when the thermal boundary layer of the film probe is within the viscous sub-layer of the turbulent boundary layer and thinner than the liquid film thickness in gas-liquid two phase flow therefore and based on the current probes dimensions the thermal boundary layer was kept thinner than the momentum laminar boundary sub-layer and the liquid film thickness in the range of the conditions studied. In addition the single phase calibration

method was used to avoid any direction change of the flow during the calibration.

Electrolysis: the hot film probes to be used in a conducting medium such as water they must be coated with a thin layer of insulating material to protect them from electrolytic attacks. The commercial glue-on hot film probe (Dantec 55R47) are protected with 0.5 μm of quartz and as described previously for better protection and more reliable insulation the directional wall shear stress probe were coated with1-1.5 μm of polyamide as thicker the insulating layer will prolong probes life and according to Bruun (1996) the use of thin protective layer of 1-2 μm has negligible effect on frequency response. Holes in the coating layer cause electrolytic attack to occur locally and also effect the measurement. For the present study the probe coating has examined by frequently calibration check and the resistance measurement of the probes to check the cross talk when it is exposed to the water.

Bubble formation on the probe: generation of gas bubbles on the heated surface of the probe during the measurement can lead to significant calibration shifts due to its effect on the heat transfer rate from the probe. According to Martin (1983) the best method to eliminate the bubbles problem in two-phase flow is by using low over heat ratio. In the literature the range 0.5 -5% of over heat ratio can be found for the application of hot film probes in the liquid medium. The over heat ratio selection must be based on the fact that the high over heat ratio lead to bubble formation and reduce the life time of the probe whilst, on the other hand, a very low overheat ratio will make the measurement much more sensitive to small changes in the liquid temperature. Therefore it is necessary to maintain an acceptable over heat ratio. Bruun

(1996) has recommended the range of 1.05-1.1 however this depend on the temperature coefficient of resistance of the sensor. So for the present work the temperature difference $T_W - T_0$ in Equation (5.3) were kept small by selecting over heat ratio of 1% and 2% for the Dantec 55R47 and the directional wall shear stress probes respectively.

Effect of temperature changes: Hot film probes are a heat transfer based techniques which are based on the analogy between heat transfer and momentum transfer. Therefore, changes in the bulk temperature during the experimental work have a significant effect on the output reading from the anemometer. For instance when the temperature of the liquid increases the anemometer circuit believes that the fluid slowed down since less heat can be transferred, Therefore a great deal of care has been taken during this work to keep the temperature changes within the satisfactory range by :

1 Temporal variation of temperature has been monitored for both single and two phase flow (an example of experimentally obtained rig temperature is shown in Figure 5.8).

2 The data were taken at the same over heat ratio that the probe were calibrated and at the same temperature and the measurement started before and ended after reached that temperature. During the experiments the temperature in the riser was monitored and recorded continuously as described in Chapter 3. The only data accepted were those for which the rig temperature was within ±0.1°C of the reference temperature.

Probe contamination: probe fouling can be a major problem due to the

gradual buildup of scale, algae and minerals on the probe causing a shift in the calibration and loss of sensitivity (Bruun, 1996). To over come this problem several suggestions can be found in the literature. In this work the effect of probes contamination were dealt with as; (i) Apart of the preparation procedure for the test facility is to discharge, flush and refill the storage tanks with a clean water a number of times before any campaign of the experimental work. (ii) Keep eye on the performance of the probe during the measurement by frequent check of the calibration curve (iii) as described previously the Perspex rod that the probe were glued on provided with a special guide that helped to take off the probe and put it back to the test section completely flush mounted without dismantling the test section and by this way it was possible to check the front face of the film under a microscope for any particles deposited or any damage to the coating layer.

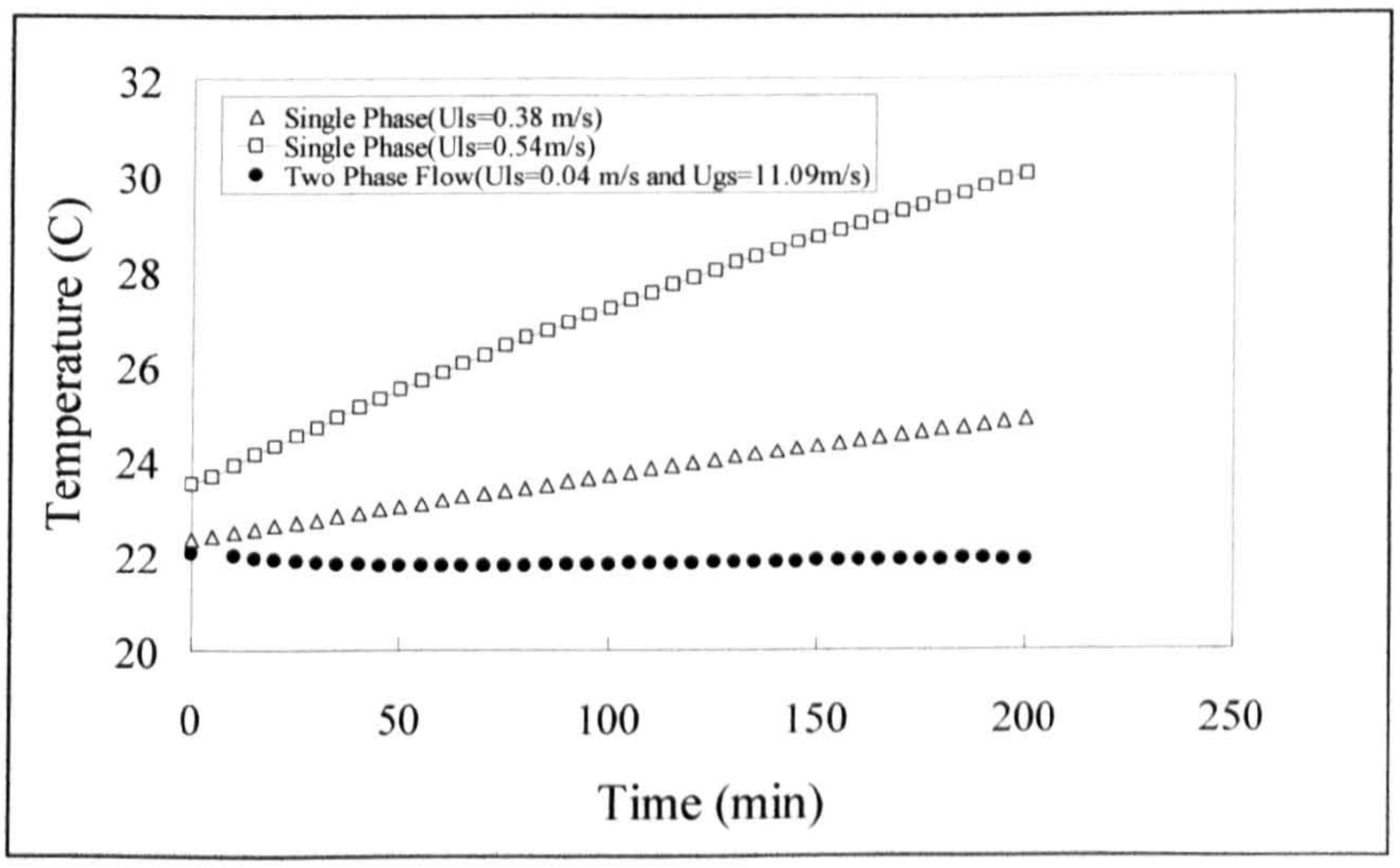

Figure 5.8 The temperature profile in the riser for single and two phase flow.

5.1.2.2.6 Magnitude and directional wall shear stress

The magnitude values of wall shear stress from the directional hot film probe were obtained from probe 3 which is located between the flow direction detector probes, i.e., probes 2 and 4 however the commercial glue-on hot film probe (Dantec 55R47) is a single probe and can measure only the magnitude wall shear stress. Figure 5.9 presenting the time-averaged magnitude wall shear stress from both probes, i.e., Dantec 55R47 and the directional hot film probe and as it can be seen there are acceptable agreement between them over the range of the liquid and gas superficial velocities presented in the graph.

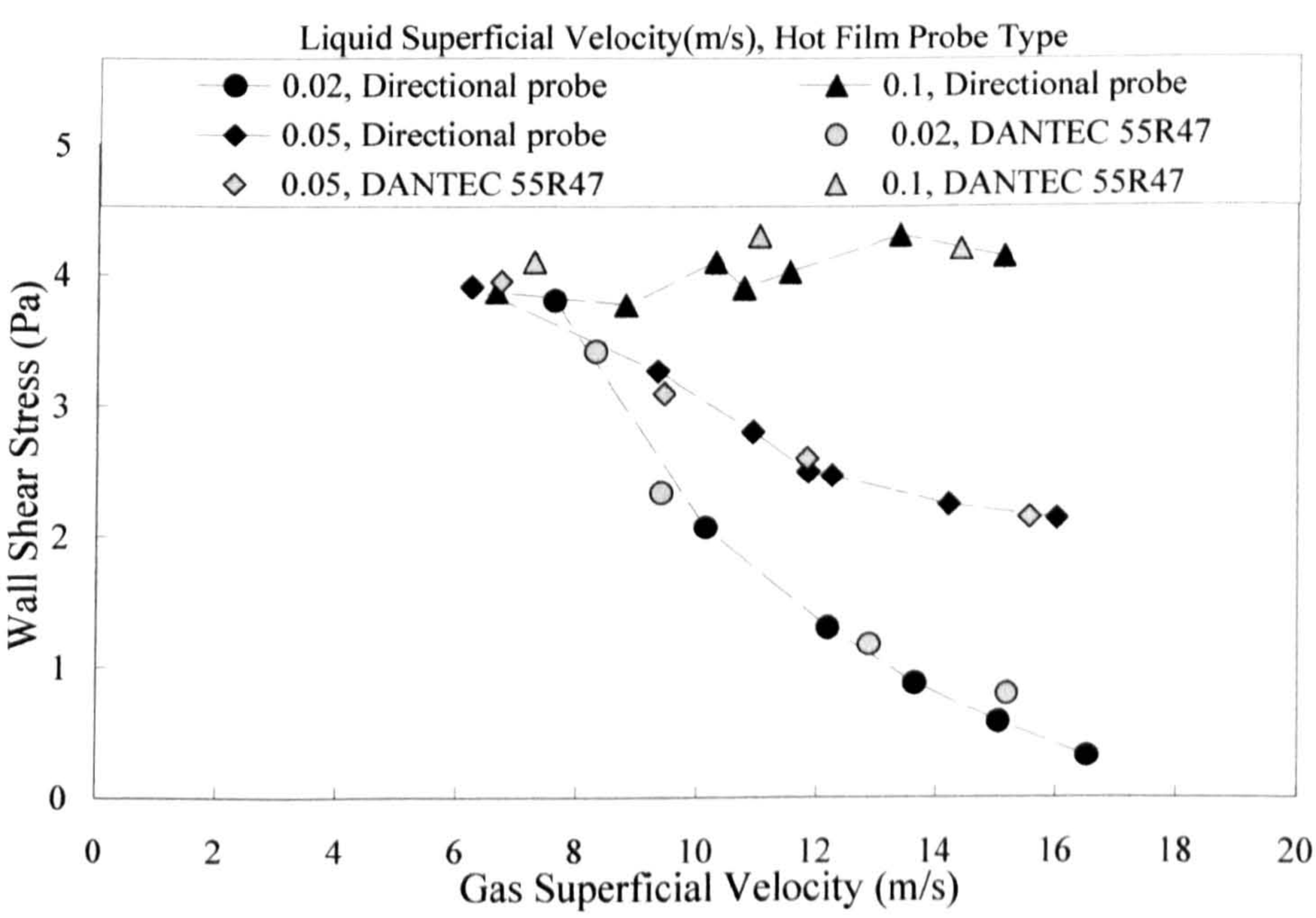

Figure 5.9 The magnitude values of time-averaged wall shear stress from the directional hot film probes and the commercial glue on hot film probes (Dantec 55R47).

To obtain directional values of wall shear stress from the directional hot film probe; the magnitude values of wall shear stress from probe 3 must be multiplied by ± 1 according to the positive and negative signals which are obtained from the out put voltages of probes 2 and 4. Before using the directional wall shear stress probe in two phase flow probe 3 must be calibrated as described previously in this chapter and probes 2 and 4, i.e., the flow direction detector probes also must be examined. The ability of the directional probes were tested by McQuillan (1985) using the two-phase plug flow and single liquid phase flow, however and as described in the previous chapters the two phase plug flow does not obviously occur in the present test facility, therefore the single phase liquid flow was employed to test the probe. The change in the liquid flow direction was caused by stopping the pump which had provided the upward flow and then letting gravity cause the liquid to flow downward back to the bottom of the riser. Figure 5.10 and Figure D.1 in Appendix D showing the time-varying wall shear stress for the single phase liquid flow with change in the flow direction and Figures 5.11 and Figure D.2 are for the single phase liquid flowing upward in the riser.

In addition, the time varying values of gas-liquid directional wall shear stress for the liquid superficial velocity of 0.02 m/s and at gas superficial velocities of 16.5 and 7.5 m/s are illustrated in Figures 5.12 and 5.13 respectively. For more conditions see Appendix D. Each figure consists of: time-varying magnitude wall shear stress obtained from probe 3, the output signals from probes 2 and 4 (i.e., the flow direction detector probes), the flow direction in positive and negative signals based on the outputs from probes 2 and 4, and

finally the normalised wall shear stress which is calculated in the similar way as described by McQuillan (1985) using the following relationship:

$$\tau_{wn} = \pm \frac{(v^2 - v_5^2)^3}{(v^2_m - v^2_5)^3} \qquad (5.10)$$

Where v = Anemometer output voltage (V)

v_5 = 5th lowest anemometer output voltage (V)

v_m = Maximum anemometer output voltage (V)

τ_{wn} = Normalized wall shear stress (-)

From the time-varying directional wall shear stress results, i.e., Figures 5.12, 5.13 and D.3-D.9., it is clear that the flow direction of the liquid film is changing and it is oscillating on the pipe wall over the range of the conditions presented. This implies that the typical annular flow as defined by researchers, e.g., Hewitt and Taylor (1970) and Azzopardi (2006) is not reached even with gas superficial velocity as high as 16.5m/s. In addition, the slug or plug flow presented by Whalley and McQuillan (1985) from the output signals of the probes that they used is not detected as clear and as regular over the time as they reported although at low gas velocity it can be seen that the liquid flow downward for longer time but on irregular basis. The fluctuation in the flow direction has a visible effect on time-averaged values of wall shear stress as it can be seen from Figure 5.14 that the magnitude values of wall shear stress are higher than the time averaged directional wall shear stress especially for the high liquid superficial velocity and also for low gas superficial velocity. This might be explained based on the fact that in the calculation of magnitude mean wall shear stress the values are always considered positive regardless of the

flow direction however, the downward flow in the directional wall shear stress values are considered negative which consequently lead to a lower mean values of directional mean wall shear stress in the range of the conditions that the flow is not unidirectional. As the frequency of the fluctuation increases the difference between the magnitude and directional mean wall shear stress might become more visible.

In Chapter 6 the directional and magnitude wall shear stress both the time-varying and mean values are discussed in more detail in relation to the other parameters such as total pressure drop and liquid film thickness.

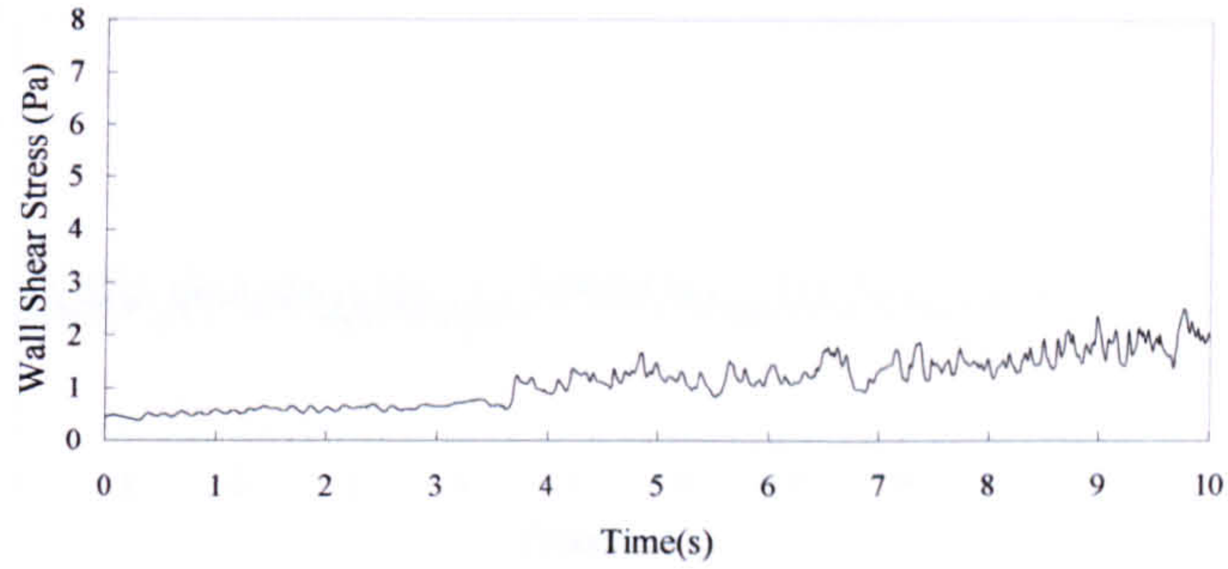

a

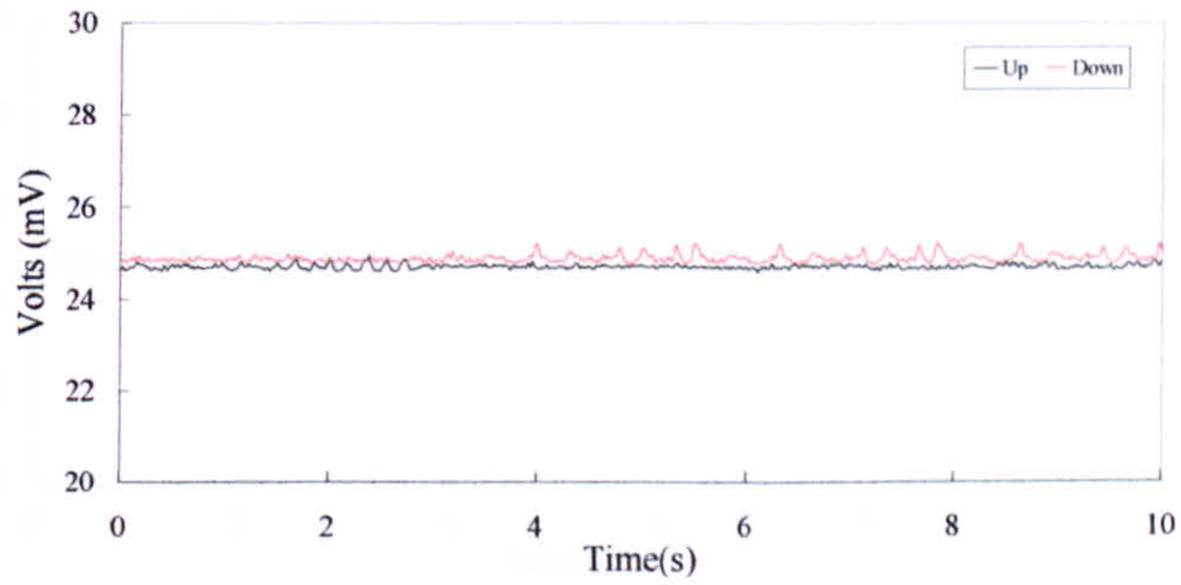

b

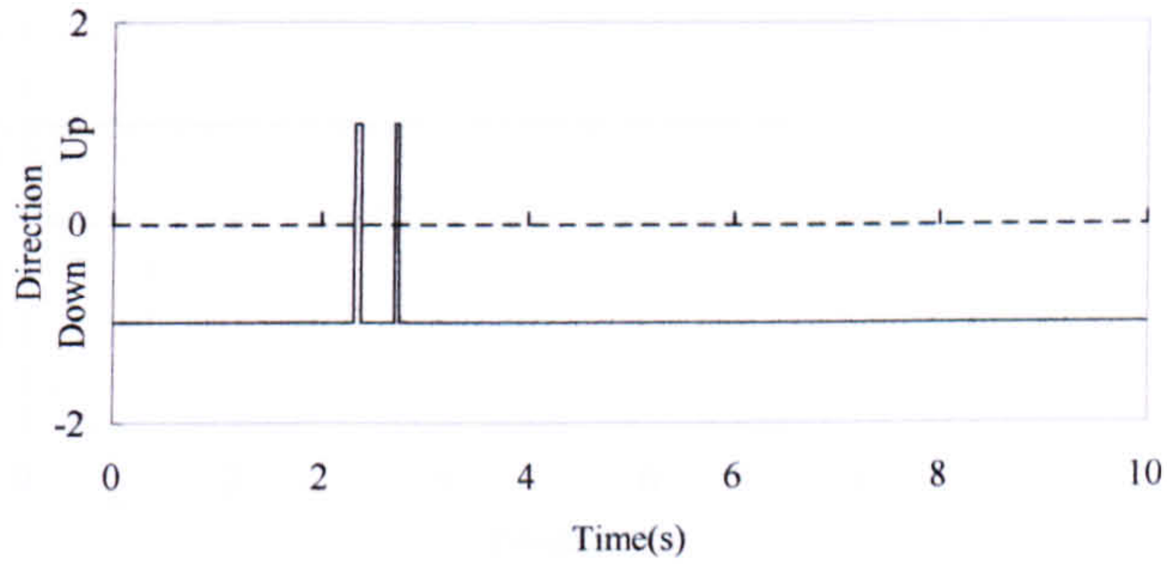

c

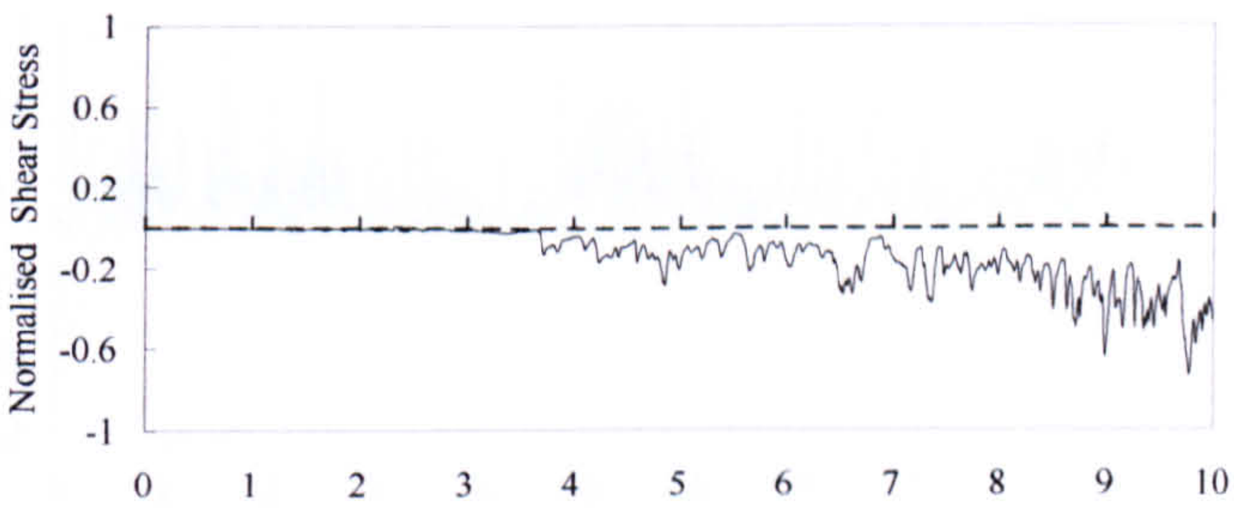

d

Figure 5.10 The magnitude and direction of wall shear stress in single phase flow with change of direction

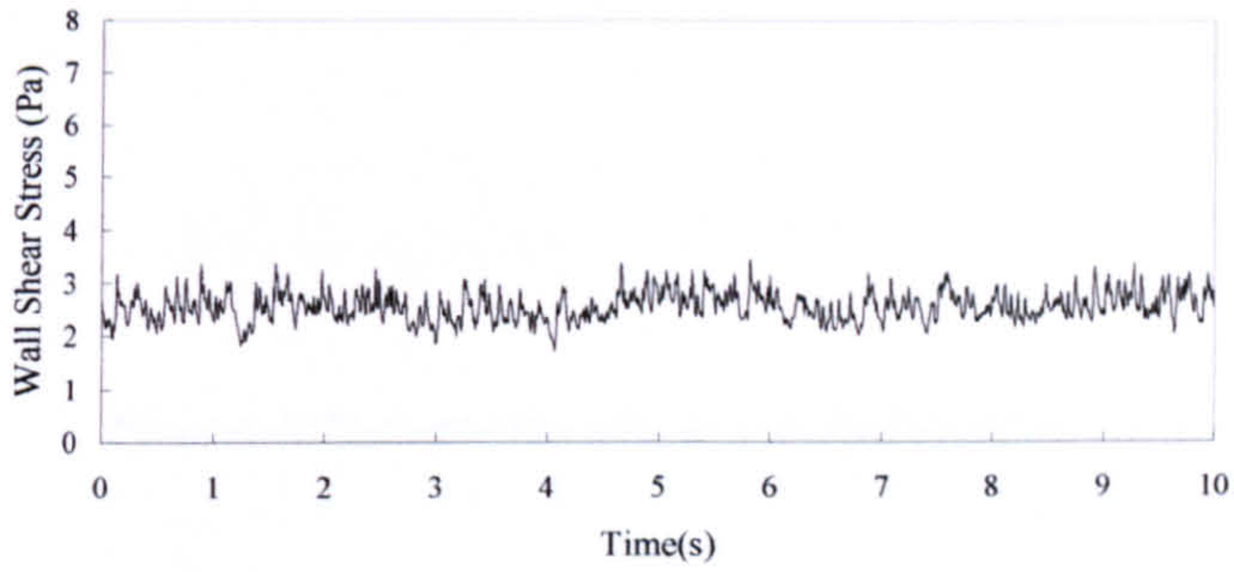

a

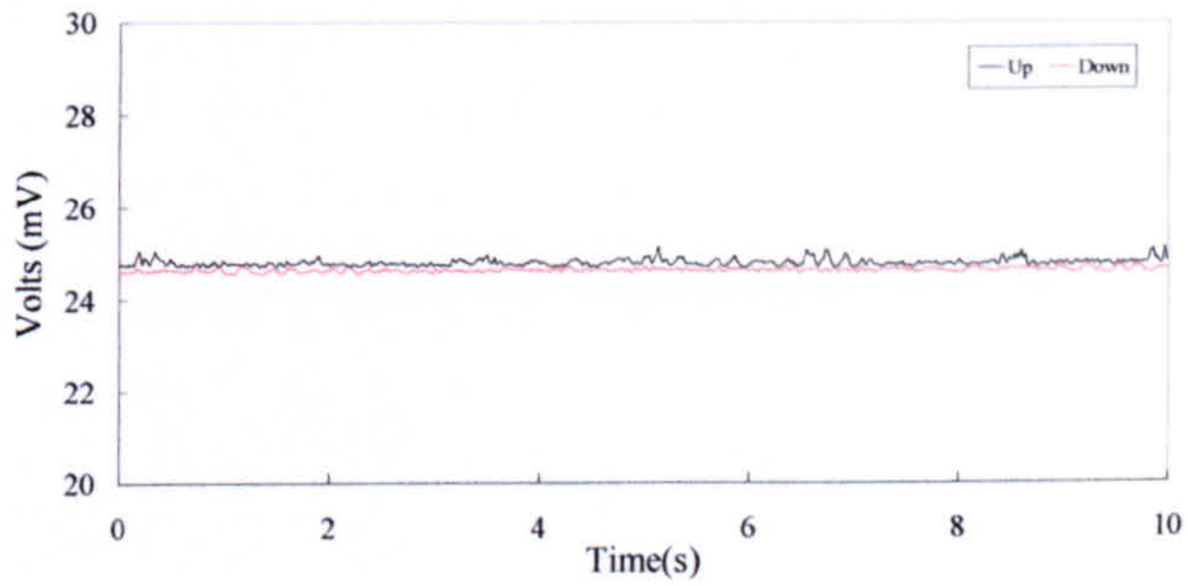

b

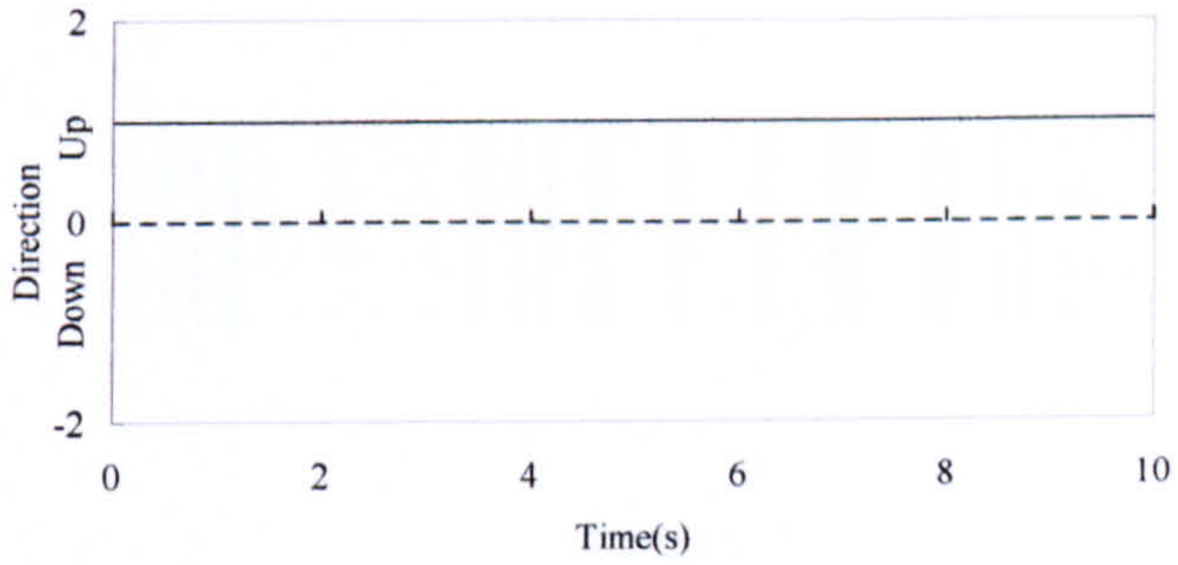

c

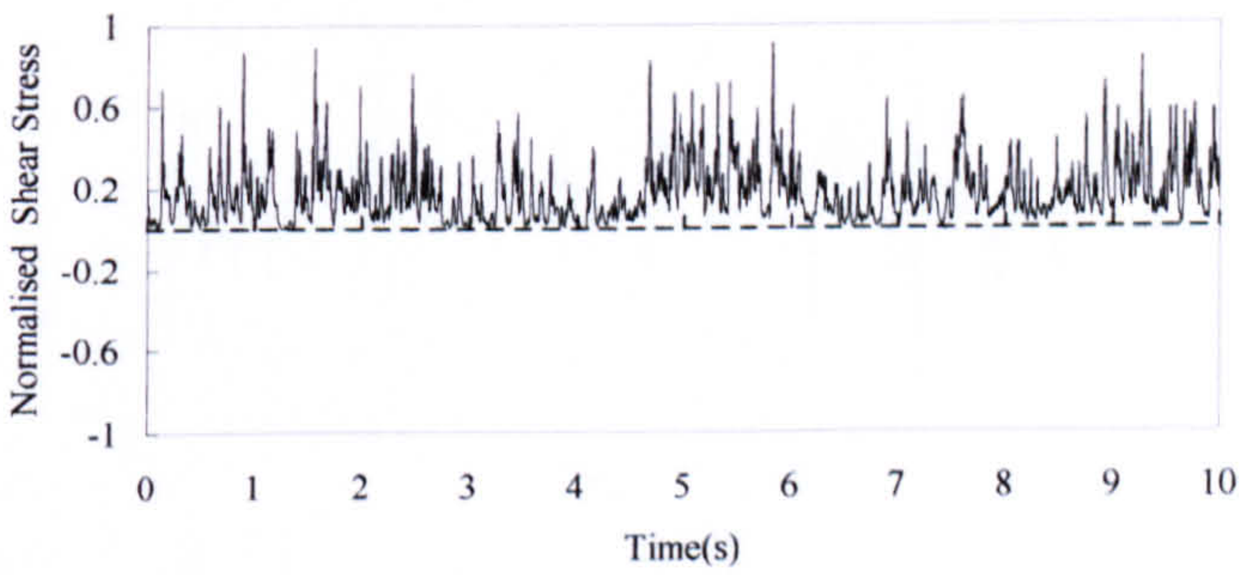

d

Figure 5.11 The magnitude and direction of wall shear stress in single phase upward flow (U_L = 0.83 m/s).

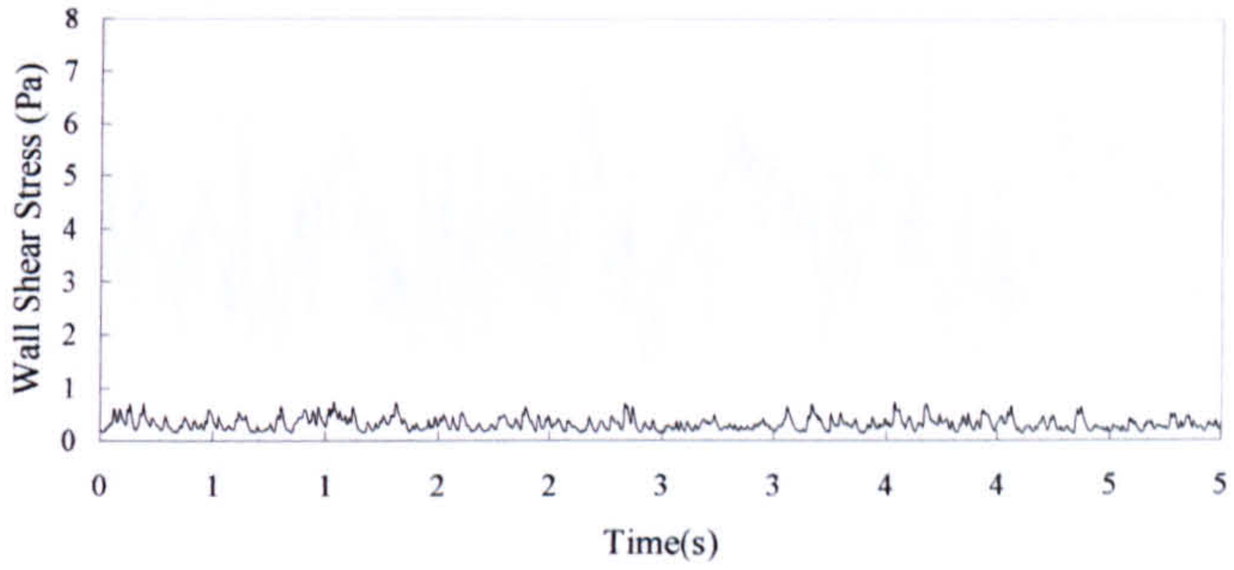

a

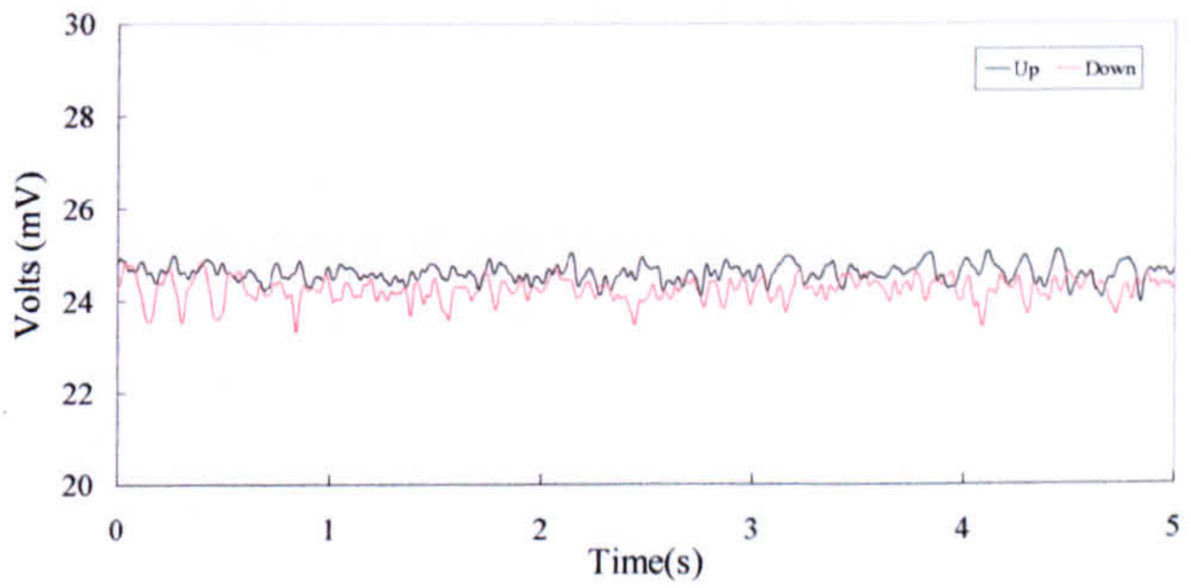

b

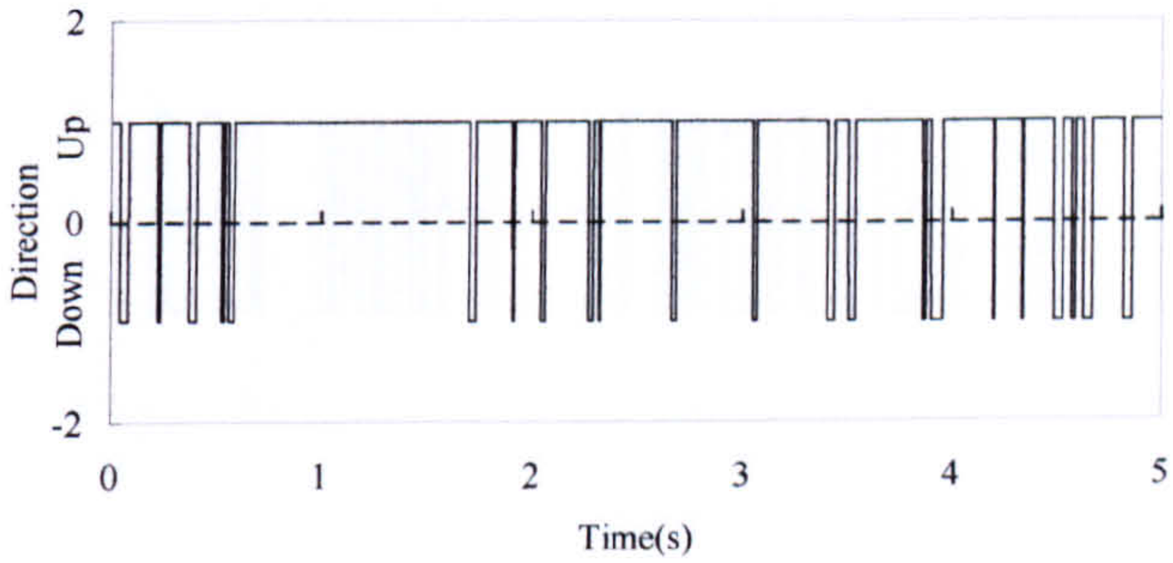

c

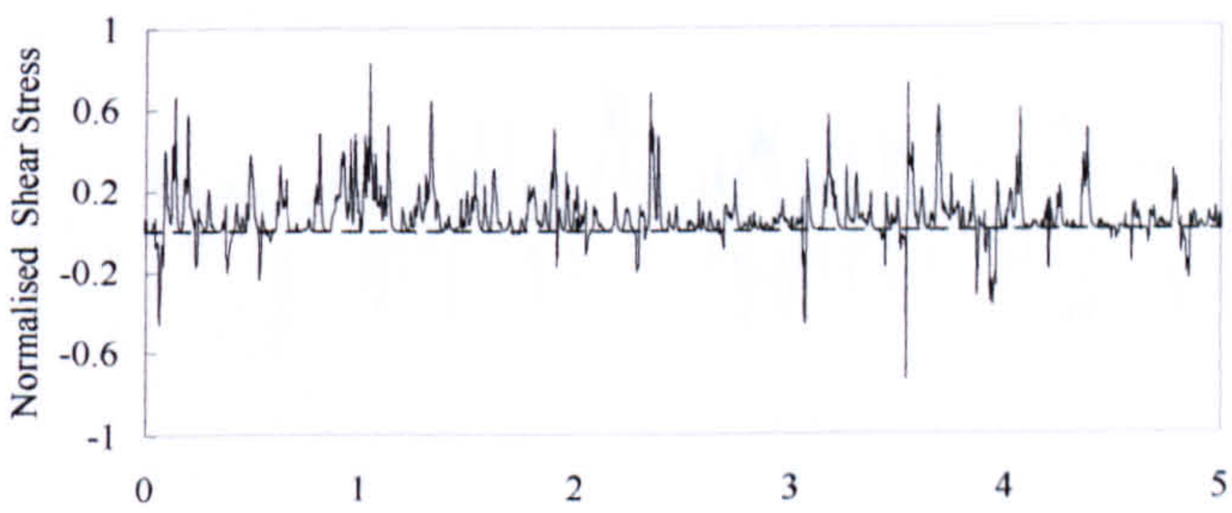

d

Figure 5.12 The magnitude and direction of wall shear stress in two phase flow (U_{GS} = 16.5 m/s and U_{LS} =0.02m/s).

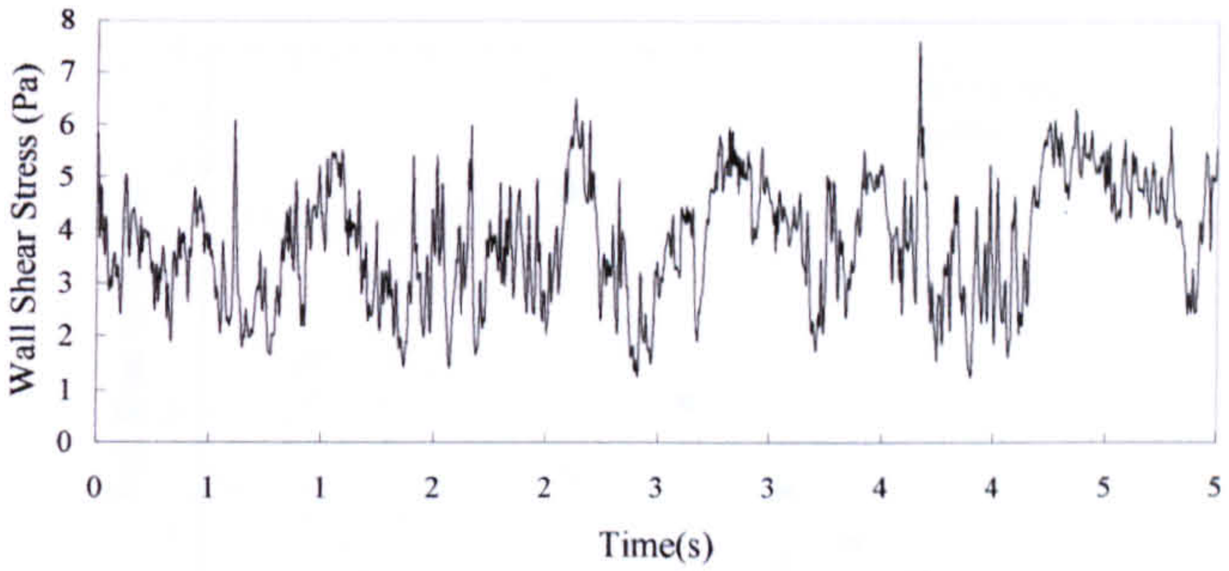

a

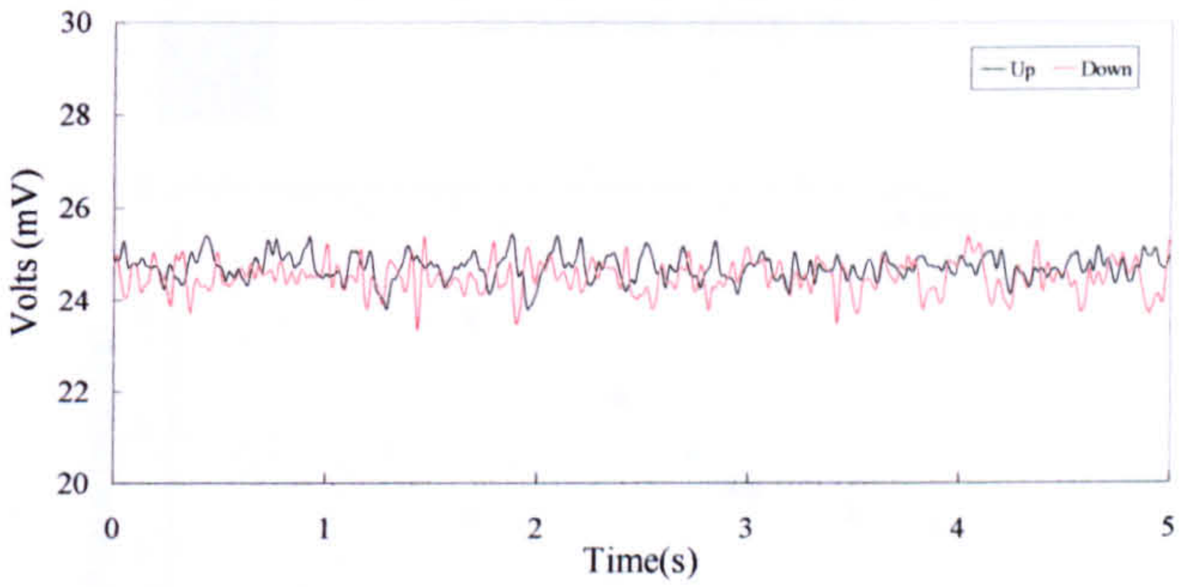

b

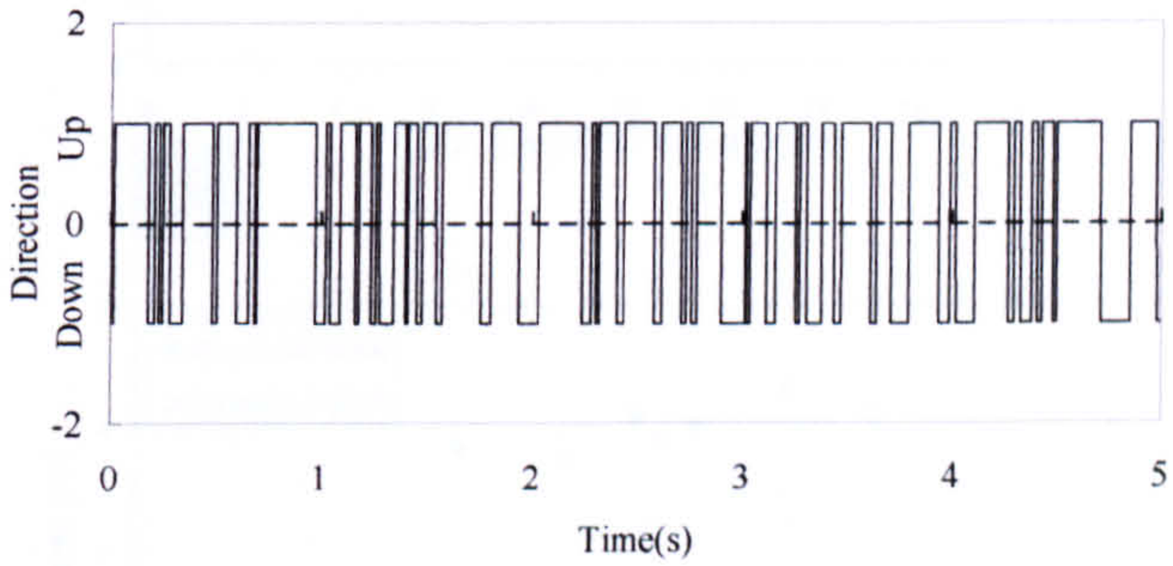

c

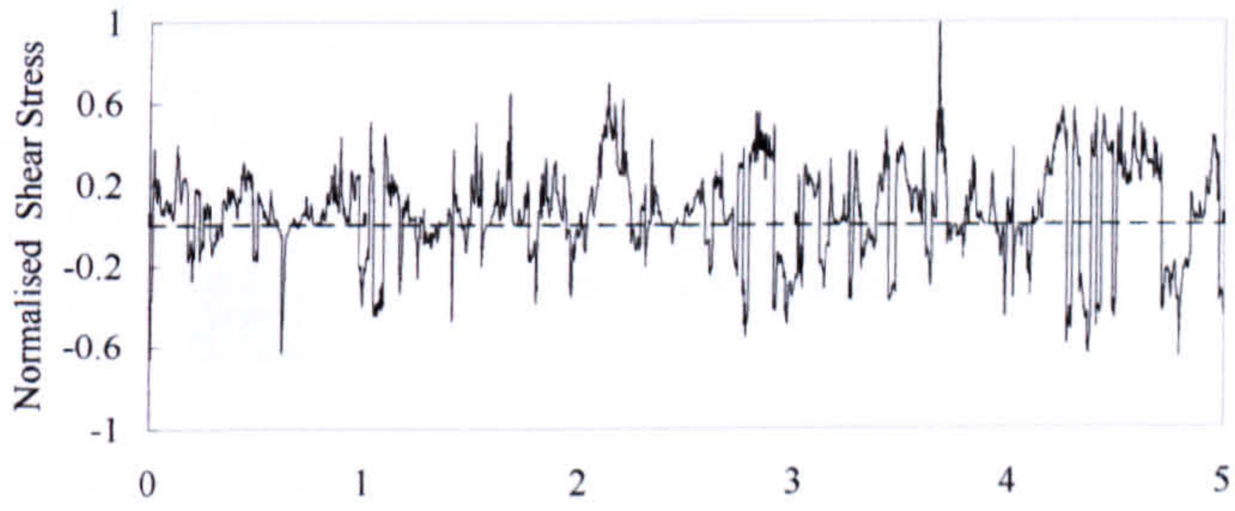

d

Figure 5.13 The magnitude and direction of wall shear stress in two phase flow (U_{GS} = 7.6 m/s and U_{LS} =0.02m/s).

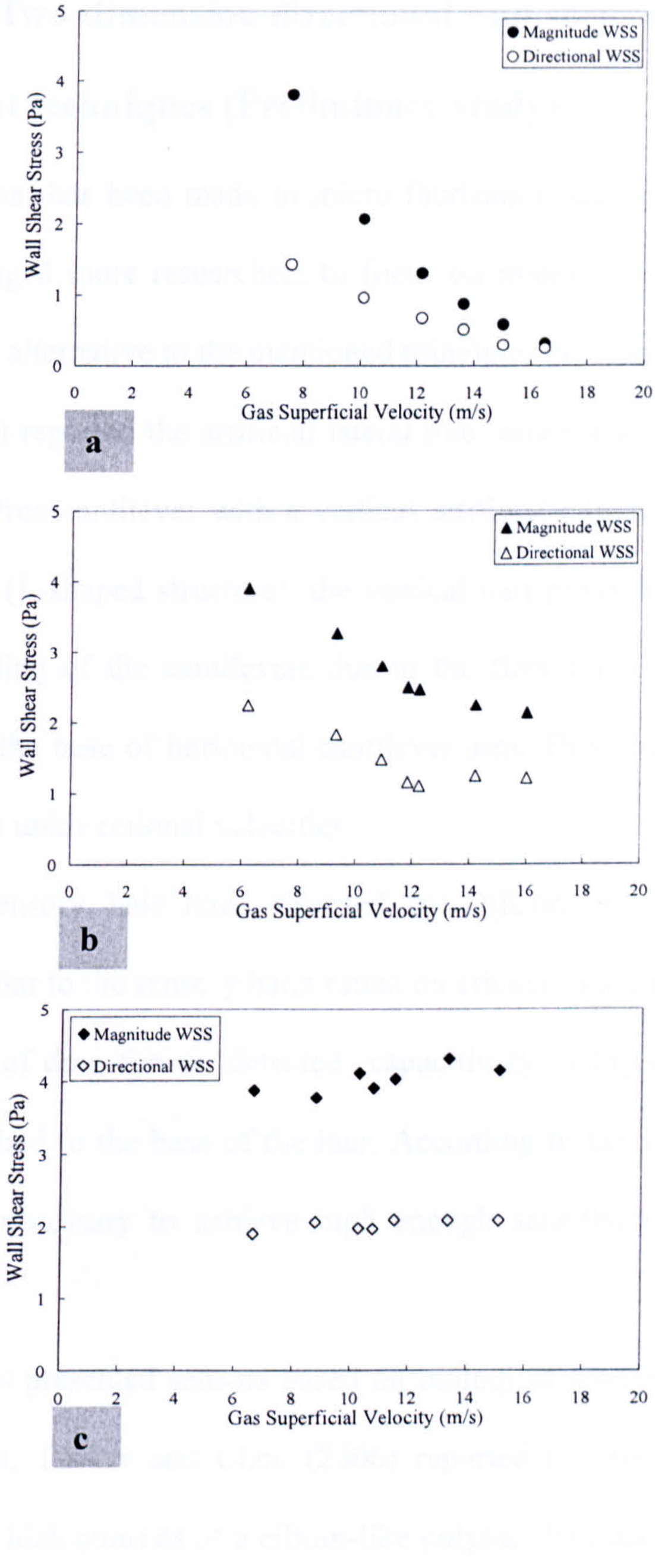

Figure 5.14 Magnitude and directional mean wall shear stress as a function of gas superficial velocity and at liquid superficial velocity of: (a) 0.02m/s, (b) 0.05m/s, (c) 0.1m/s.

5.1.2.3 Two-dimension directional wall shear stress measurement techniques (Preliminary study)

The progress that has been made in micro fabrication technology in the last decade encouraged more researchers to focus on micro fences or wind hair principles as an alternative to the mentioned principles previously.

Fan et al (2002) reported the artificial lateral line sensor which consists of an in-plane fixed free cantilever with a vertical artificial cilium attached at the distal, free end (L-shaped structure), the vertical part protrudes into the flow field. The bending of the cantilevers due to the flow forces is detected by strain gages in the base of horizontal cantilever arm. This kind of the sensor can only detect unidirectional velocities.

An artificial sensory hair have reported by Dijkstra et al (2005) with dimensions similar to the sensory hairs found on crickets, the movement of the hair as a result of drag forces detected capacitively using electrodes on a membrane attached to the base of the hair. According to the authors, up to 1 mm heights is necessary to achieve high enough sensitivity of the sensor structure.

More researchers presented sensors based on biological inspiration of animal hair cell sensors, Tucker and Chen (2006) reported the artificial hair cell sensor (AHC), which consists of a cilium-like polymer hair and the deflection is measured by silicon piezoresistive strain gages in the sensor base, this sensor is able only to detect the deflection in one direction.

To determine the flow in two directions, Engel et al (2006), presented a new AHC sensor which consists of a cylindrical polyurethane hair, and the

deflection of the hair has been detected using carbon-impregnated polyurethane force sensitive resistors (FSRs). According to the authors, for this sensor to be used in a high accuracy commercial application, the design needs to be improved to reduce cross axis coupling.

In a new optical sensor technique called micro pillar sensor (MPS), introduced by Brucker et al. (2005), the sensor device consists of a flexible micro-pillar which extends from the wall into the viscous sublayer. The sensor principle uses the pillar tip deflection in the viscous sublyaer of turbulent boundary layer flows as a measure that is proportional to the wall shear stress. The pillars are cylindrical shape and they are manufactured from the elastomer poly dimethylsiloxane (PDMS). The pillar images are recorded simultaneously using a high speed imaging. A detailed description of the probe has been given by Grobe and Schroder (2008) who have employed the probe to measure the mean and dynamic wall shear stress in turbulent single phase flow in pipe.

The main advantages of the probe are it can measure the two-dimensional wall shear stress and it is possible to detect the planar wall-shear stress distribution by using arrays of micro-pillars sensor or what we so called mini-forest sensor. In addition the micro pillar sensor doesn't require any wiring or complicated electronic circuits for data collection. This kind of the technique unknown to be used in two phase flow, based on its principle and it is potential to detect the flow in more than one direction; it can be very useful to be employed in two phase flow, therefore in the present study we have investigated the possibility of employing this sensor in such flow which is more complicated than single phase. As several trial sensors of this type have been produced during the present study and mounted on a small transparent

rods of Perspex this is for the probe to be located correctly inside the pipe, the sample of the sensor and its arrangement is shown in Figure 5.15 and an example of the pillars deflection shown in Figure 5.16.

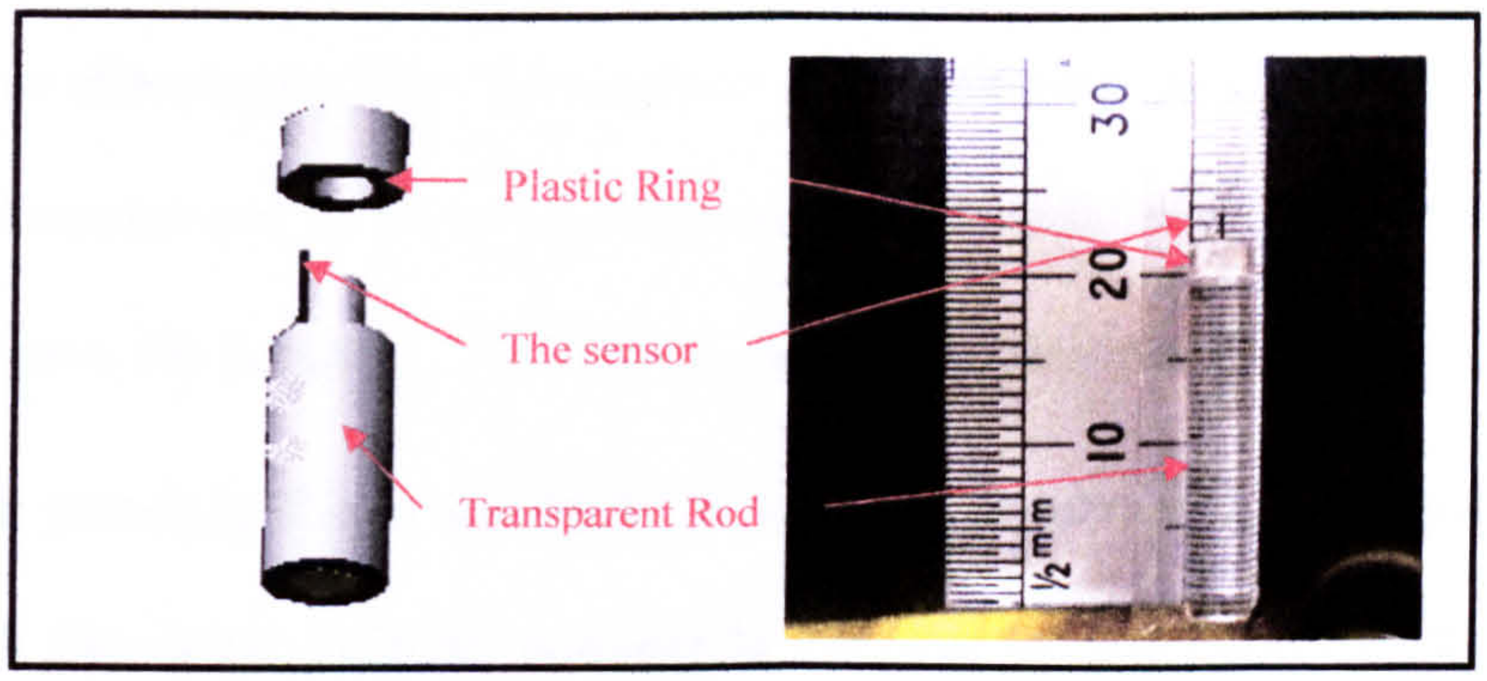

Figure 5.15 a sample of the micro pillar sensor and its transparent support (The dimensions are in mm).

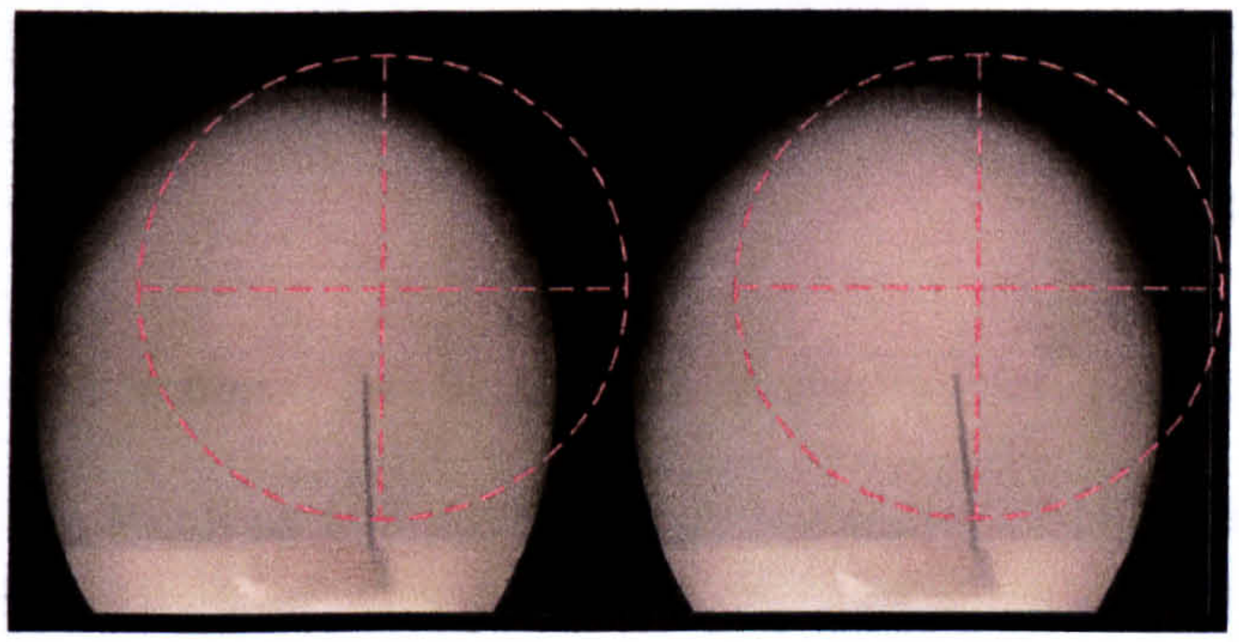

Figure 5.16 Showing the deflection of the pillars tip inside the pipe for single phase flow detected at angle of 90°.

Although the micro pillar sensor is proposed not very long ago and rooms still open to test its limitations, however for the sensor to be applied in gas-liquid

two phase flow and in the range of the conditions of the present study and for the pipe diameters similar to the one employed in this work; the dimensions of the sensor and the detection angles of the pillar-tip deflection must be modified as summarized below:

Sensor dimension: The micro-pillars used by Grobe and Schroder (2008) for the measurement of mean and dynamics wall shear in turbulent single phase flow have the height, L_p, of 350 μm and mean diameter, D_p, of 45 μm. Based on its principle the probe needs to be fully immersed in the flow field for which the linear velocity gradient is guaranteed (the height of the pillar is limited by the height of the viscous sub-layer). In addition to that in gas-liquid flow its height is also restricted by the thickness of the liquid film on the pipe wall. And according to the results shown in Figure 5.2 the height of the pillars, L_p, must kept less than 100μm and the ratio $L_p/D_p \geq 10$ can be selected for the range of the conditions studied in the present work.

Angles of detection: To detect the deflection of flexible pillars with dimensions as small as 100 μm height and diameter of 10μm inside a vertical pipe as large as 127 mm diameter, for gas-liquid two phase flow, obviously require a special arrangement. The deflection of the sensor can be detected from four angles in another word four different positions where the lenses and high speed camera can be located which are; 0°, 90°, 180° and 270° (Figure 5.17). The detection angle of 180° which has been used by Grobe and Schroder (2008) for the detection of the pillar tips deflection in the single phase flow can not be considered in gas-liquid two phase flow this is as well

as both the detection angles of 90° and 270° because of being two different fluids inside the pipe having two different physical properties and in another word two different refraction indices which consequently have a significant effect on the images taken for these angles. In addition the pipe diameter employed in the current is obviously out of focus for most available microscopes. There fore the 0° detection angle (monitoring the deflection of the probe from the rear) is might be the only and the best way to monitor the deflection of the pillars as this method of detection will provide accurate information related to the direction of the flow in two dimensions.

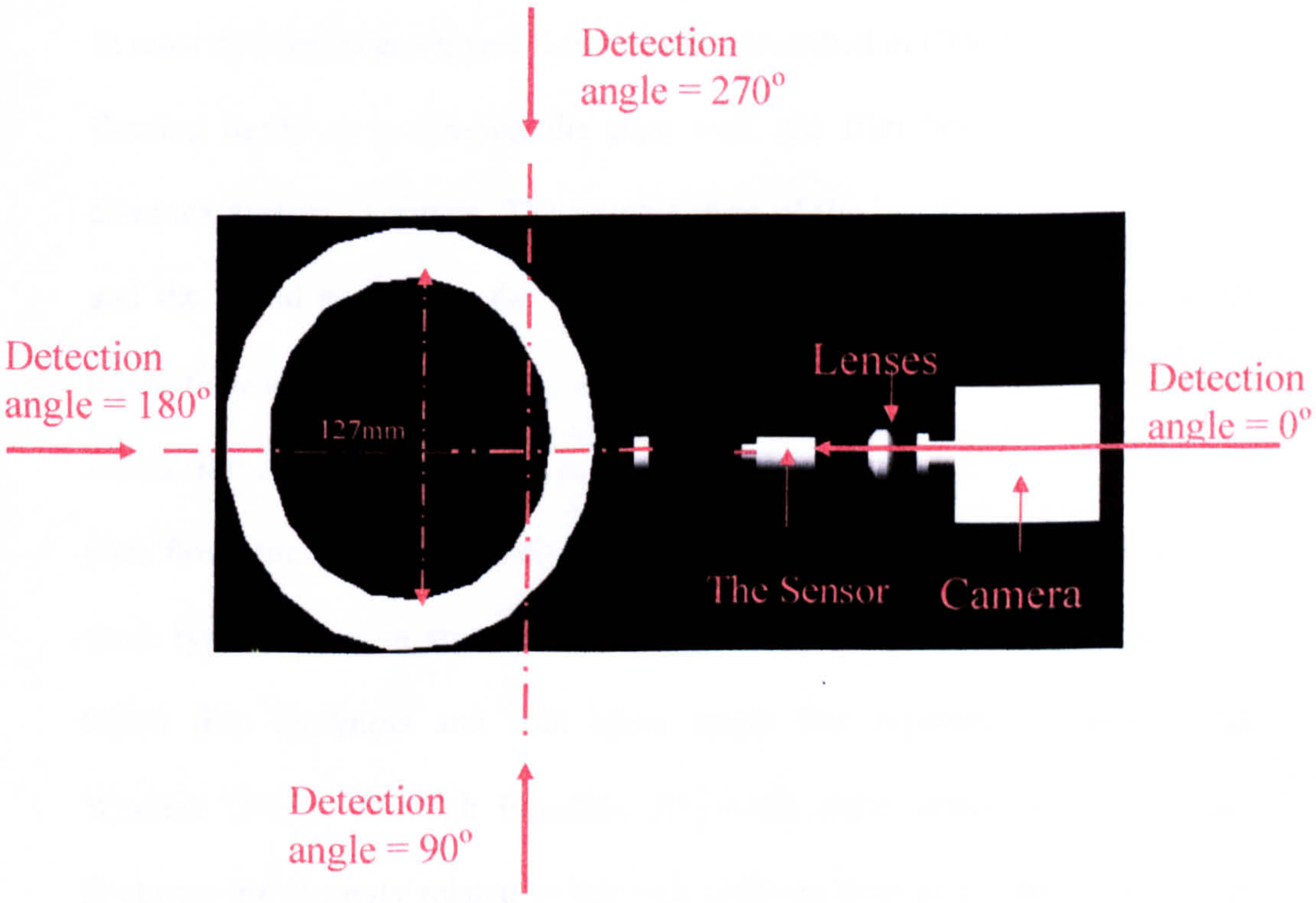

Figure 5.17 Possible angles of detection of the pillars deflection.

Chapter 6

Liquid Film Properties of Gas-Liquid Flow in 127mm Diameter Vertical Pipe

In most of vertical gas-liquid flow regimes described in Chapter 1, the liquid is flowing partly as a film on the pipe wall, the film being covered with a complex system of waves. The rough nature of the interface between the gas and the liquid and hence the interfacial shear stress will vary with gas and liquid flow rates in a complex way. As described in Chapter 2 the thickness of liquid film on the pipe wall in annular-type flows is related to both the liquid film flow rate and wall shear according to the Triangular relationship. For same type of flow in small diameter pipes a close relationship between the liquid film thickness and wall shear stress was reported by Martin and Whalley (1983). Through Equation 2.15 both shear stress and liquid film thickness are strongly related to the total pressure drop as the later consists of three components which are frictional, gravitational and acceleration pressure drop. The frictional term of pressure drop is represented by shear stress and the gravitational term by the density of two-phase mixture (the liquid holdup

of which the liquid film thickness represents a considerable part of it in annular type flow). The acceleration component of total pressure drop is normally negligible in adiabatic flows. So the total pressure drop is significantly affected by the liquid film property such as the thickness of the film, the interfacial roughness of the surface of the film and the shear stress on the pipe wall. Therefore the measurements of such parameters, i.e., liquid film thickness and wall shear stress simultaneously with total pressure drop can provide very useful information on the liquid film behavior which affects the overall behavior of the flow. In spite of its great importance such measurements in two-phase vertical flow for large diameter pipes have not; to the author's knowledge, have not been performed prior to the present study. This being the case, total pressure drop, liquid film thickness and wall shear stress were measured selectively and simultaneously during this study as described in Chapter 3.

In this chapter the results of two experimental campaigns are presented; the **first campaign** is the simultaneous measurement of liquid film thickness, using the conductance ring probes and local film pin probes, and total pressure drop for the conditions described in Chapter 3. The main objective of this campaign is the comparison of the results from two techniques for the measurement of film thickness. The **second campaign** is a simultaneous measurement of total pressure drop, liquid film thickness and wall shear stress. The time-averaged and time-varying total pressure drop, liquid film thickness and wall shear stress are presented in Section 6.2, followed by a comparison of the obtained wall shear stress results with available data in the literature. Besides in this chapter the direction of the flow of waves on the film extracted

from high speed video images and the time-varying data of locally measured liquid film thicknesses.

6.1 The liquid film thickness measurement

The total pressure drop data that were presented in Chapter 4 were measured simultaneously with the liquid film thickness using three flush mounted conductance ring probes at three different positions in the test section (the probes detail is given in Chapter 3). This technique has been widely used by researchers in two phase gas-liquid flow for the measurement of void fraction in bubble and annular-type flow in conducting mediums such as water after an appropriate calibration for each type of the flow. For annular-type flows Equation 3.1 can be used to calculate the liquid film thickness from the measured liquid holdup (e.g., Kaji and Azzopardi, 2010). The mean values of liquid film thickness data that obtained simultaneously with the data presented in Chapter 4 using the conductance ring probes are illustrated in Figure 6.1. It can be seen that the graph has a similar trend as the variation of total pressure drop with the liquid and gas flow rates (Figure 4.2) and as described in Chapter 4, i.e., three major area of liquid superficial velocity can be identified over the range of gas velocity studied which are the low (0.014, 0.02, 0.03 and 0.04 m/s), intermediate (0.053 and 0.06 m/s) and high liquid velocity (0.07-0.7 m/s). So in overall both pressure drop and film thickness are showing similar trends and the variation of the liquid film thickness can be also classified into that three major areas above of liquid flow rates.

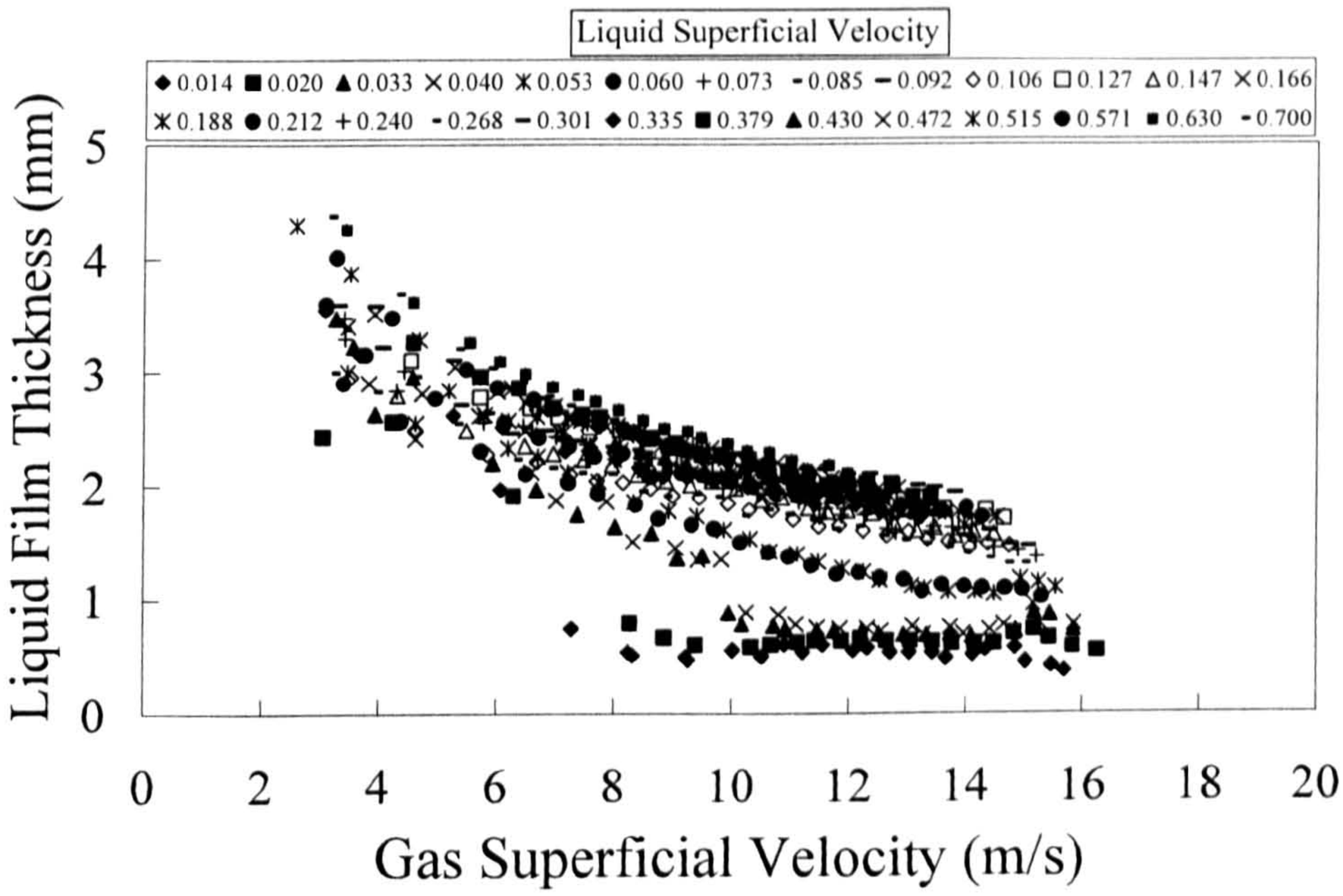

Figure 6.1 liquid film thicknesses obtained from the conductance ring probes.

6.1.1 The difference between ring and local liquid film thickness

Obtaining liquid film thickness from the conductance ring probes is based on the assumption of ideal annular type flow in which the liquid flows as a smooth thin film on the pipe wall with the gas in the center. However in practice this is an over simplification as the liquid film is not smooth but it is covered by a complex system of waves. Which these waves are very important as sources of the droplets that entrained to the gas core (Hewitt and Whalley, 1989 and Azzopardi and Whalley, 1980). In addition the waves in large diameter pipes are circumferentially localized (Azzopardi et al, 1983) instead of being coherent around the circumference as observed by Hewitt and

Lovegrove (1969) in smaller pipes. Based on this it might expected that the thickness of the liquid film is not uniform neither circumferentially nor in axial direction on the pipe wall. The film interface can expected to be three dimensional. In addition, it might be expected that more liquid is atomized to drops than in smaller diameter pipes. Not surprisingly, the averaging effect of the conductance ring probes can result in differences in the time-varying data as some details of the roughness of the film surface are obscured and the height of the film base can be affected. In addition, a close relationship between wall shear stress and the waves in the gas-liquid interface in small diameter pipes has been reported by Martin and Whalley (1983) and Martin (1984). Besides the wall shear measurements have made locally as described in Chapter 5. Therefore the time varying results from the conductance ring probes might not represent accurately the roughness of the film that actually passes the wall shear stress probe and in the right time. This led to 4 pairs of conductance pin probes were mounted on each side of the test section to measure the local values of liquid film thickness. The dimensions of pin probes are small, so they can be located in a cruciform geometry tightly around the wall shear stress probes (their dimensions and exact location are given in Chapter 3).

To compare the results from both film thickness measurement techniques an experimental campaign was performed to measure the liquid film thicknesses using both the flush mounted parallel conductance ring probes and the local film pin probes over the range of the conditions shown in Figure 3.21 and listed in Appendix A. These measurements were carried out simultaneously. Based on the results of total pressure drop data and liquid film thickness which

were presented in Figures 4.2 and 6.1 respectively, the work has concentrated on liquid superficial velocities of 0.02, 0.05 and 0.1 m/s, identified in Figures 4.2 and 6.1 as being in the low, intermediate and high liquid velocities respectively. The time-averaged liquid film thicknesses from each of the techniques are illustrated in Figures 6.2-6.4 as a function of gas superficial velocity. From Figure 6.2, i.e., at low liquid superficial velocity (0.02 m/s) the time averaged liquid film thickness results from both techniques are very close to each other particularly for gas superficial velocity >8 m/s. In contrast the liquid film thicknesses from the conductance ring probes are much higher than those obtained locally from the pin probes for the high liquid velocity (0.1 m/s) and over the whole range of the gas superficial velocity studied (Figure 6.4). However, the disagreement between the results at intermediate liquid superficial velocity (0.05 m/s) appears at gas superficial velocities <10 m/s (Figure 6.3).

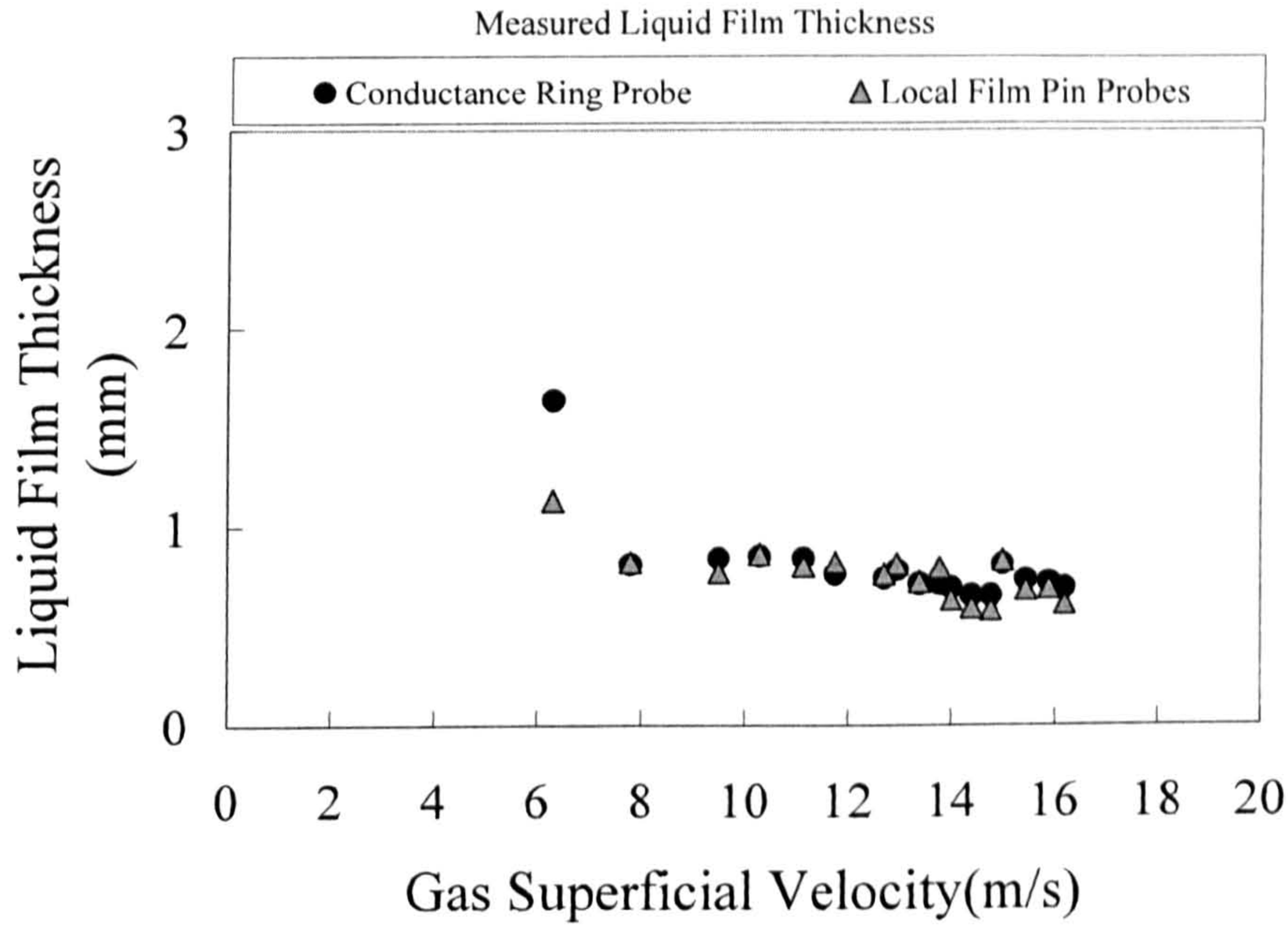

Figure 6.2 Measured liquid film thickness from conductance ring probes and local film pin probes at liquid superficial velocity of 0.02 m/s.

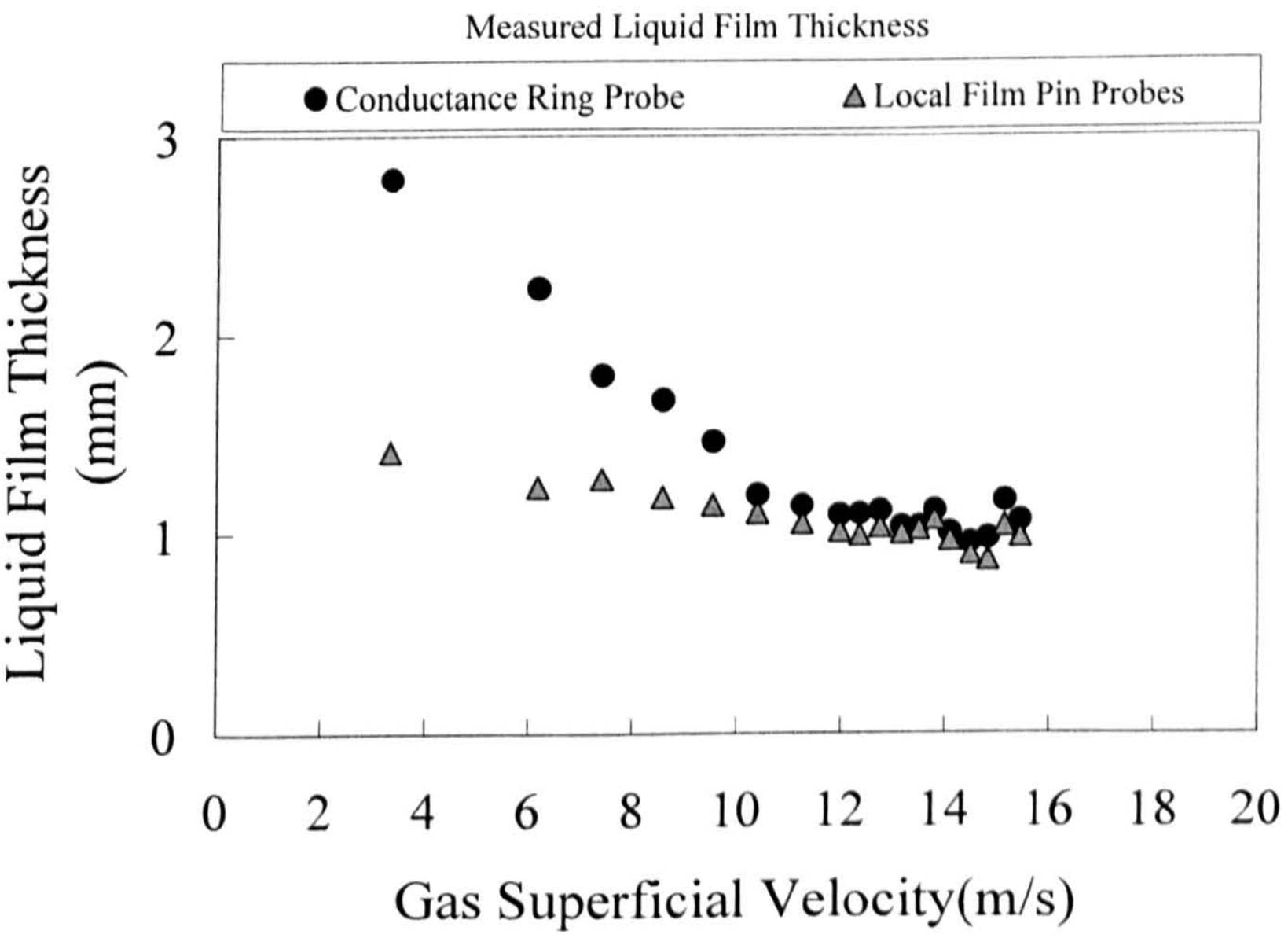

Figure 6.3 Measured liquid film thickness from conductance ring probes and local film pin probes at liquid superficial velocity of 0.05 m/s.

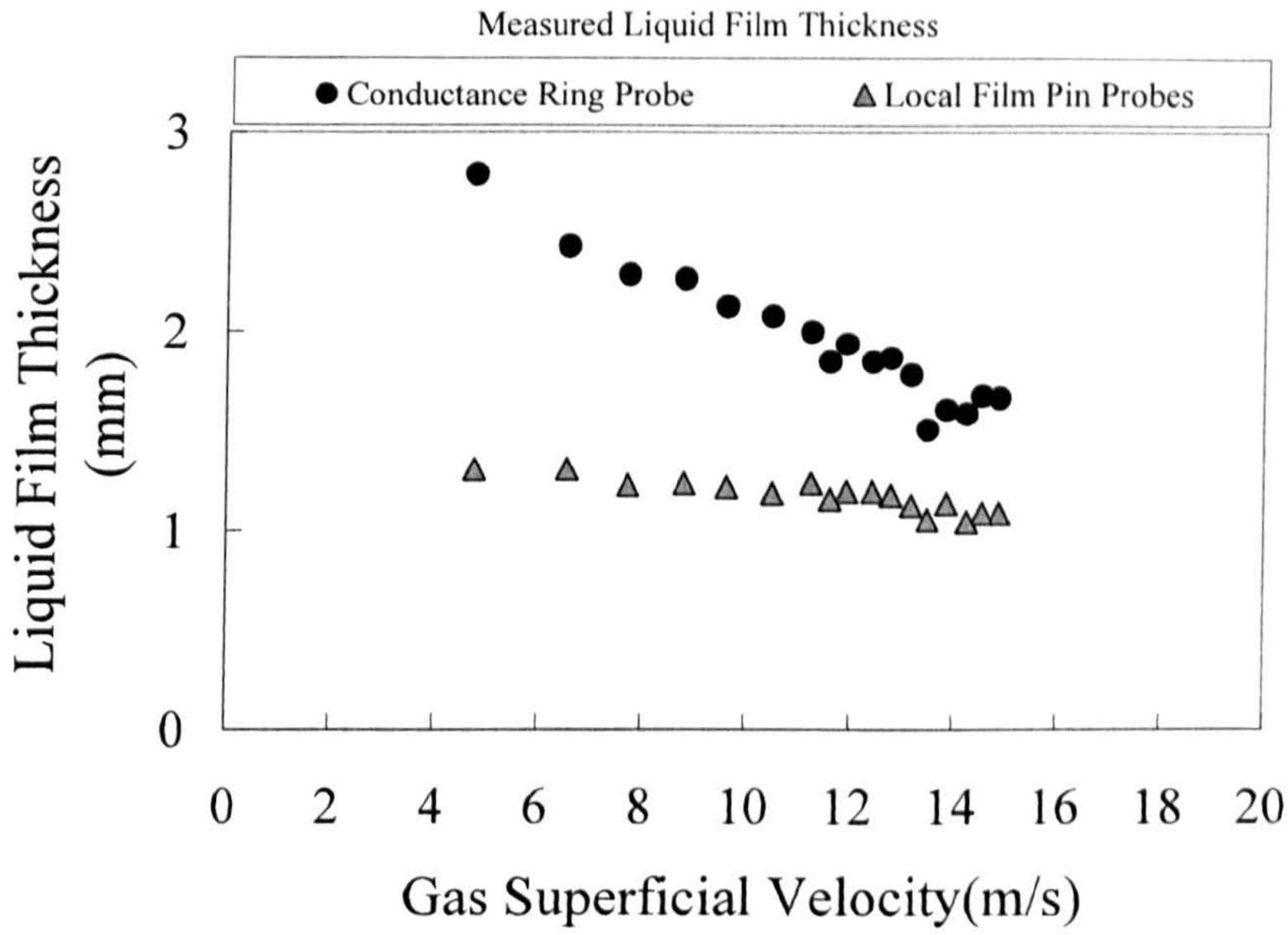

Figure 6.4 Measured liquid film thickness from conductance ring probes and local film pin probes at liquid superficial velocity of 0.1 m/s.

For the difference to become more clear, the time-series data from conductance ring probes and local film pin probes are compared in Figures 6.5-6.7 for the same liquid superficial velocities and for gas superficial velocities of 4.8-16 m/s. Note that the two data sets are transposed in time as they were taken from two axial positions. Over all the figures indicate that both techniques can capture the low frequency structures but only the local data can provide the smaller scale, high frequency data. Some details of the film roughness can be missing in the data by conductance ring probes due to the averaging nature of the technique, for instance, at liquid superficial velocity of 0.02 m/s and gas superficial velocity 11.8 m/s (Figure 6.5 b) several waves with different heights can be seen from the locally measured time-varying data however they are appear much smaller in the data obtained

from the conductance ring probes instead the base film become thicker than the pin probes results. Use of a running average (Equation 6.1) of the same time-series data from the local pin probes for n= 100, 200 and 500 might clarify the effect of the averaging on the time–varying results as shown in Figure 6.8.

$$AM = \frac{1}{n}\sum_{i=1}^{n} a_i \qquad (6.1)$$

Where AM : is the average or the arithmetic mean

a_i : Value of element i

n : Number of values

What is also can be seen from the time-series data of both techniques that the time-varying values from the conductance ring probes are visibly higher at high liquid superficial velocity of 0.1 m/s for the range of the gas superficial velocity presented (Figures 6.7 a, b and c). This is also the case for the gas velocity of 6.2 m/s at liquid superficial velocity of 0.05 m/s. In contrast the time varying data from the pin probes shown acceptable agreement with those obtained from the ring probes at liquid velocity of 0.02 m/s as presented in Figures 6.5a, b and c. Based on what have mentioned the best explanation can be given is; the local film pin probes can measure the film thickness accurately up to 1.5-2 mm according to their calibration curves (Figure 3.14), therefore at high liquid flow rate when the film thickness becomes thicker than the mentioned range, i.e., 2 mm the mean values of liquid film thickness obtained locally are lower than those obtained from the conductance ring probes. In contrast the mean liquid film thickness from each technique is reasonably

agreed at low liquid velocity, i.e., 0.02 m/s.

From the time-varying data presented it can be concluded that arguably the time-varying liquid film thickness results from the local pin probes are better to represent and detect the waves when they pass over the wall shear stress probes even if not accurately determine the heights higher than 2 mm but still can sense those waves and represent the details of the interfacial roughness between the gas and the liquid. However the time-varying data from the conductance ring probes is less reliable due to its averaging nature which leads to hide some details about the roughness of the film surface which also lead to a higher base film. Therefore the mean values of liquid film thickness from the conductance ring probes are more dependable specially for the high liquid velocity, in addition the time-varying results from the local pin probes are arguably more reliable as it can provide more details about the interfacial roughness of the liquid film surface therefore both techniques are necessary for the present work and together can provide very useful information about the mean and time-varying liquid film thickness. In addition they are both sharing the advantage that they are non-intrusive so they are not disturbing the liquid film to compare with other liquid film thickness measurement techniques, e.g., parallel wires.

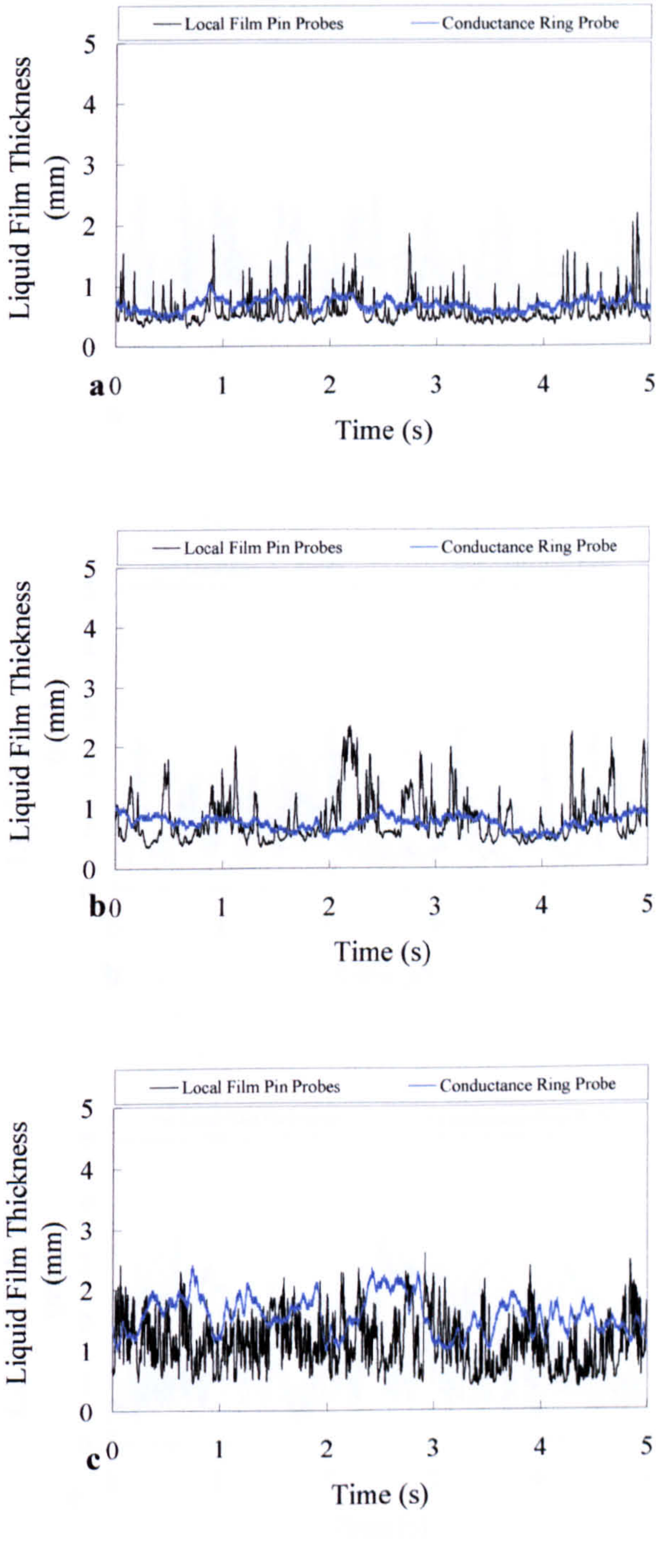

Figure 6.5 Time-varying liquid film thickness from the local pin probes and the conductance ring probes at liquid velocity 0.02 m/s and gas velocity: a) 16.2 m/s b) 11.8 m/s c) 6.3 m/s.

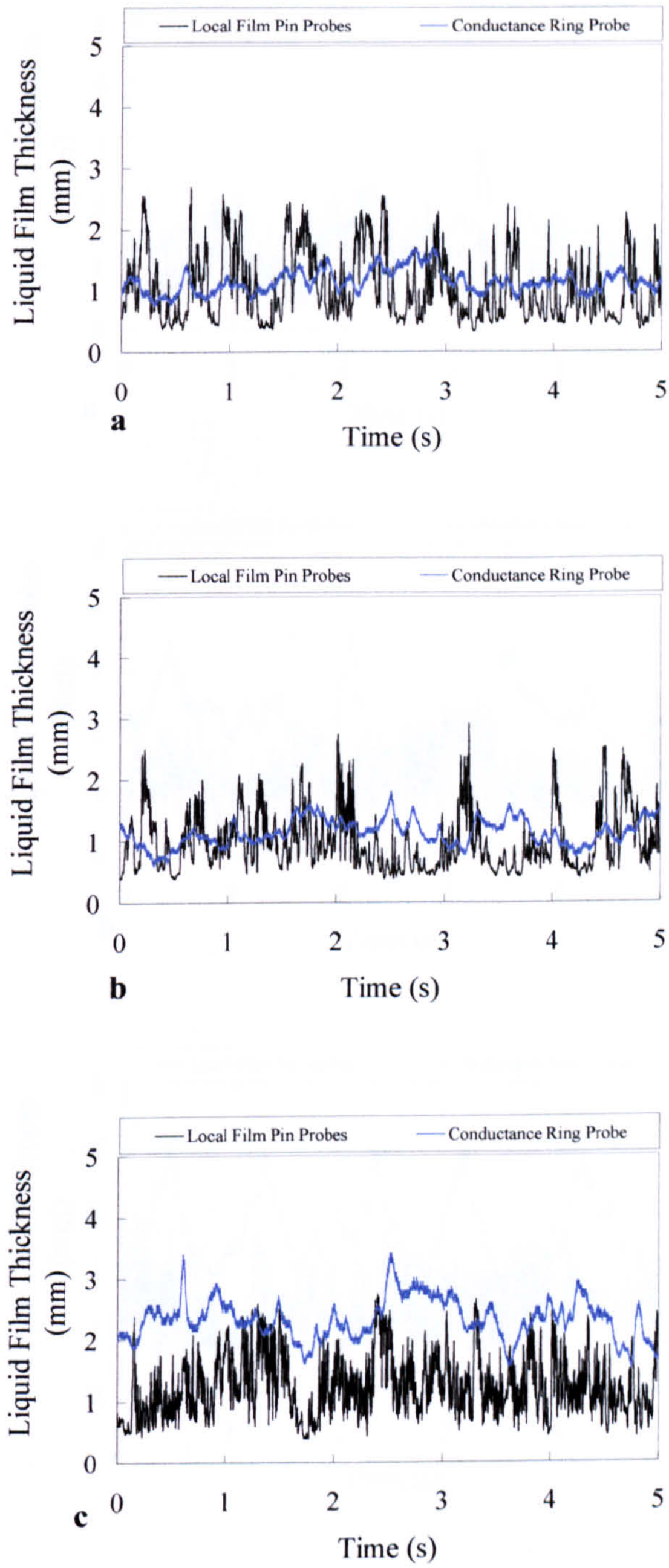

Figure 6.6 Time-varying liquid film thickness from the local pin probes and the conductance ring probes at liquid velocity 0.05 m/s and gas velocity: a) 15.4 m/s b) 11.3 m/s c) 6.2 m/s.

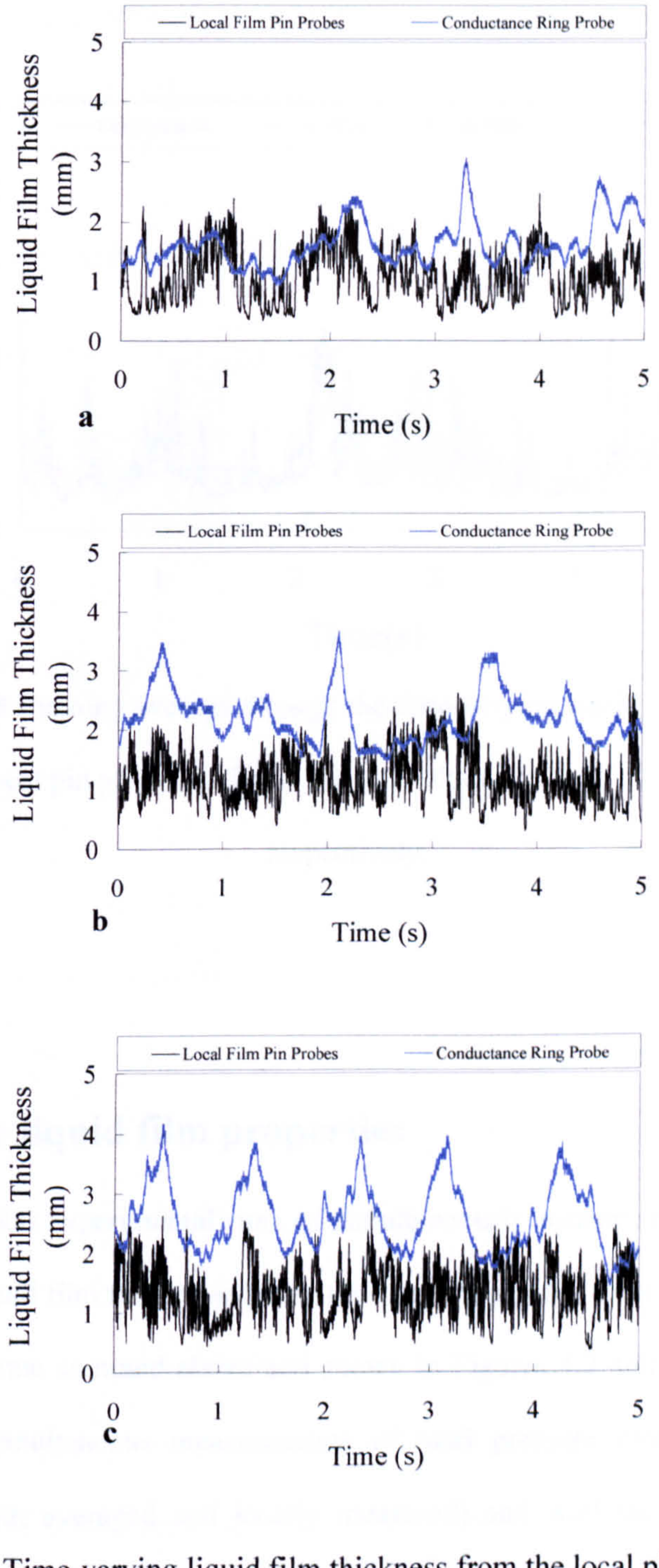

Figure 6.7 Time-varying liquid film thickness from the local pin probes and the conductance ring probes at liquid velocity 0.1 m/s and gas velocity: a) 14.9 m/s b) 10.5 m/s c) 4.8 m/s.

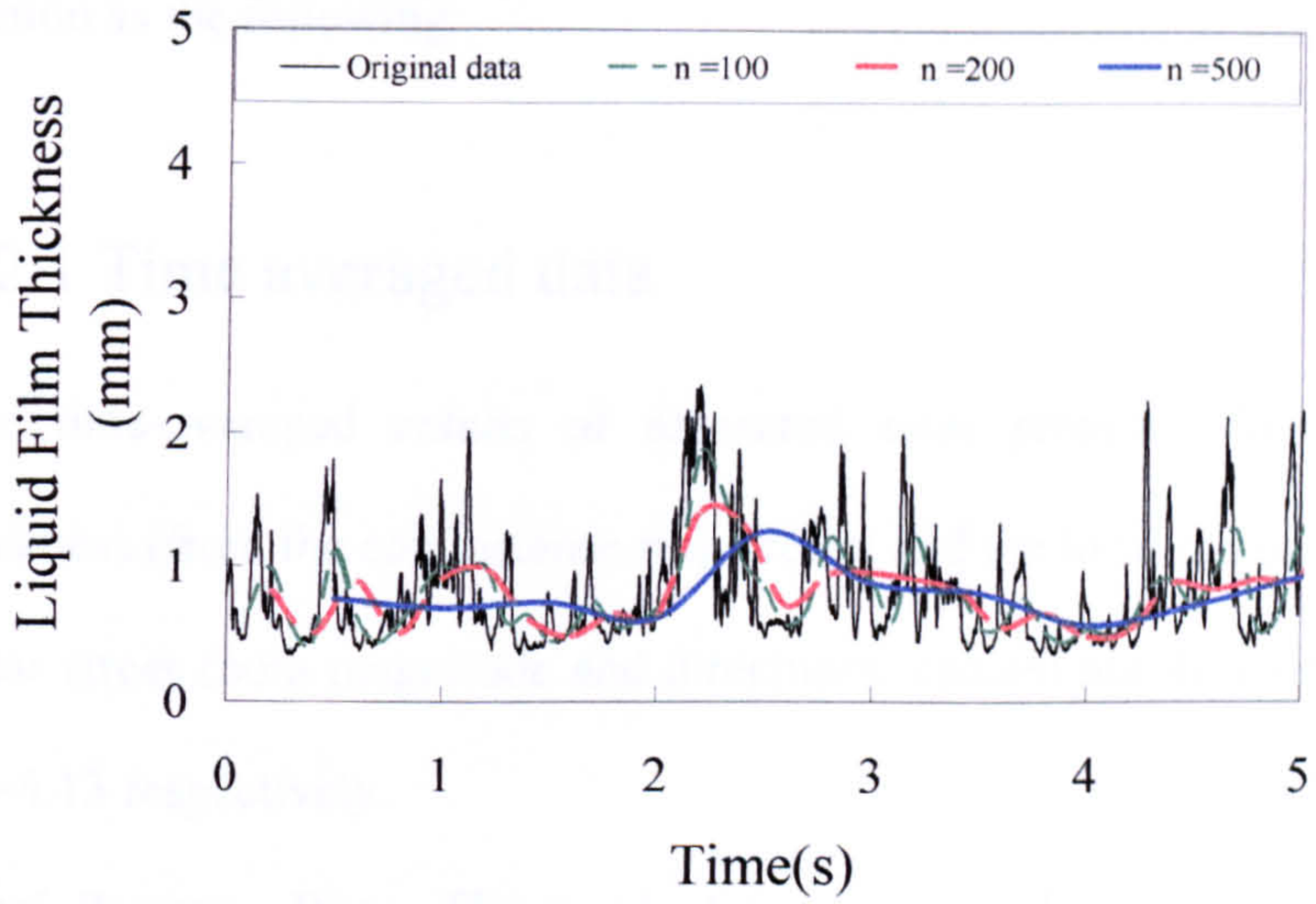

Figure 6.8 Running average through the time-varying liquid film thickness from the local pin probes at liquid and gas velocity of 0.02 m/s and 11.8 m/s respectively.

6.2 The liquid film properties

Results of 600 experimental runs of simultaneously measured total pressure drop and liquid film thickness during this study suggested three major areas of liquid flow rate as noted above and shown in Figures 4.2 and 6.1. Based on those the simultaneous measurements of total pressure drop, liquid film thickness(both averaged and locally measured) and wall shear stress were performed selectively in the range of those three areas of liquid superficial velocity namely 0.02, 0.05 and 0.1 m/s for low, intermediate and high liquid velocity respectively and over different gas velocities. The time-averaged and

time-varying data of measured parameters are presented and discussed in this section as the following:

6.2.1 Time averaged data

The time-averaged results of measured total pressure drop, liquid film thickness (from the conductance ring probes and the local pin probes) and wall shear stress (both magnitude and directional values) are illustrated in Figures 6.9-6.13 respectively.

Total Pressure Drop: The trend of time averaged total pressure drop as a function of gas velocity for liquid superficial velocities of 0.02, 0.05 and 0.1 m/s are described in Chapter 4 which can be summarised as; at low liquid velocity (i.e., 0.02 m/s) the total pressure rapidly drops as the gas superficial velocity increases to $\approx$10 m/s then the change is more gradual at higher gas superficial velocities. It is suggested that the change of the slope linked to a transition of flow regime from churn to annular flow although the lowest pressure drop recorded for this condition was at gas superficial velocity of 15.8 m/s, however the minimum pressure drop that reported for smaller pipes (Hewitt et al, 1985) is not obvious within the conditions studied. In addition, as we will see from the mean wall shear stress data that zero wall shear stress point is not reached either (Hewitt and Hall-Taylor, 1970 and Govan, 1990). The variation of total pressure drop with the gas velocity at the second and third area, i.e., at intermediate (0.05 m/s) and high liquid velocity (0.1 m/s) do not follow the trends that seen in the low liquid velocity as for the intermediate liquid flow rate it has a smoother nature rather than exponential and the trend

becomes more complicated as the liquid velocity increases to 0.1 m/s where the slope change disappear and become less sensible to the gas velocity variation. However the overall trend of the variation of total pressure drop with gas velocity is the total pressure drop decreases with the increase of gas velocity over the liquid velocity range studied. In addition to the effect of liquid and superficial velocity on total pressure drop the results from this study shown that the pipe diameter also has a visible effect on total pressure drop as discussed in Chapter 4.

Liquid Film Thickness: The time-averaged liquid film thickness obtained from the conductance ring probes and the liquid film pin probes are presented in Figures 6.10 and 6.11 respectively. It is apparent that the variation of liquid film thickness with the gas and liquid superficial velocity has a similar trend as the total pressure drop. The effect of liquid velocity on the film thickness might be explained as; the higher the liquid flow rate the more liquid will be add to the film and the higher the thickness of the film will be however Figure 6.1 shown at high liquid superficial velocities, i.e., higher than 0.1 m/s not all the liquid increased will necessarily be added to the film but it might entrained as a droplets to the gas core. For the effect of gas velocity on the liquid film thickness it is clearly related to the roughness of the interface between the gas and the liquid so as the gas velocity increases it leads to a smoother interface and also to a thinner film. However, when the film is smooth enough, increasing the gas velocity does not lead to a significant decrease in film thickness (e.g. when the gas velocity is greater than 10.1 m/s with a liquid velocity of 0.02 m/s). The over all trend of the variation of liquid film thickness with the gas and the liquid velocity (Figures 6.10 and 6.11) is the

liquid film thickness decreases with increasing gas velocity and decreasing liquid velocity.

Wall shear stress: Figure 6.12 shows the average values of the *magnitude* of the shear stress (i.e. irrespective of the direction). Figure 6.13 shows the time average of the shear stress taking account of its *direction*. The trends in the values are quite complex; the average of the magnitude of the shear stress also the average of the directional shear stress generally increase with increasing liquid velocity except at low gas velocity. The average magnitude of the shear stress and the average of the directional shear stress generally decrease with increasing gas velocity, though the influence of gas velocity is small at high liquid velocities (in this case, the shear stress values may increase slightly with gas velocity).

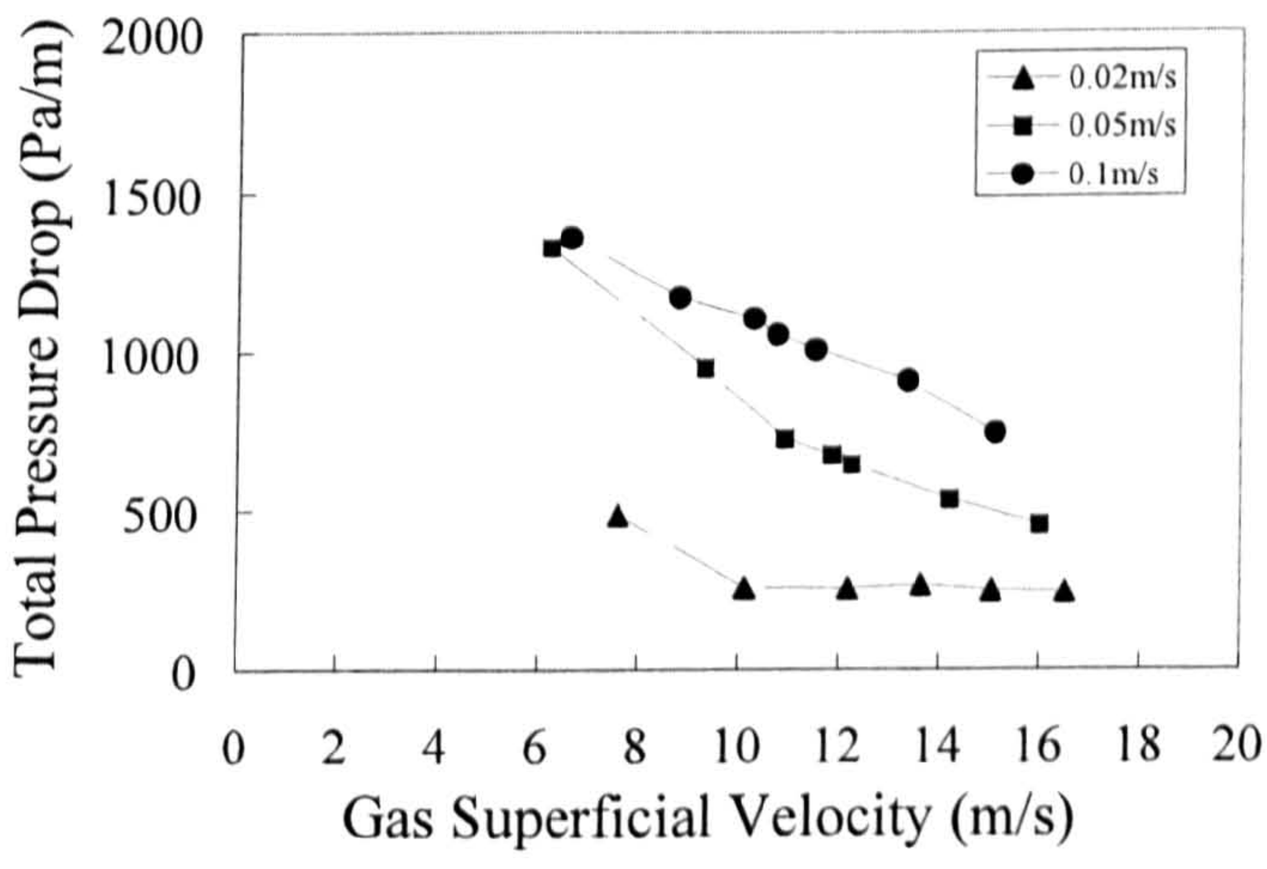

Figure 6.9 Time-averaged total pressure drop as a function of gas superficial velocity

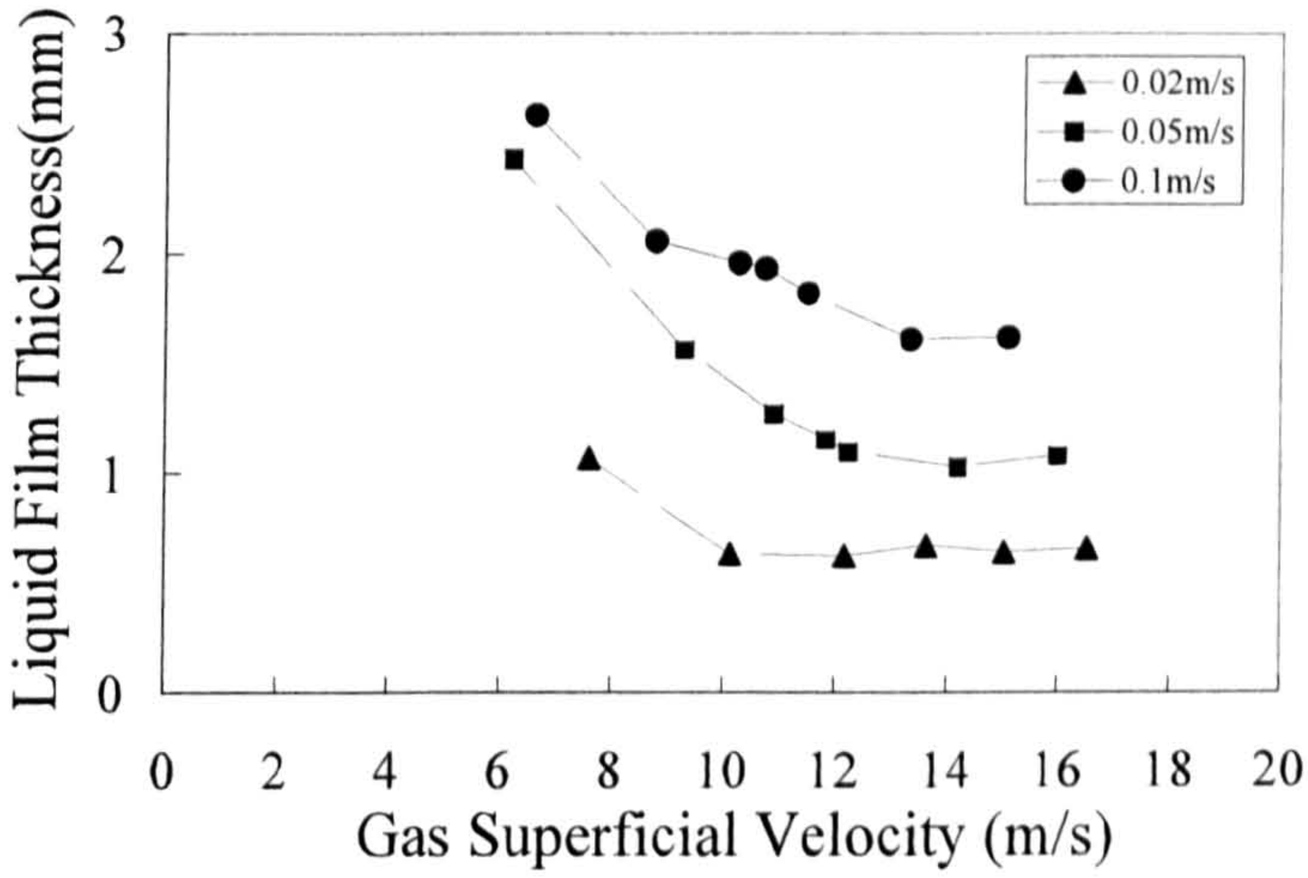

Figure 6.10 Time-averaged liquid film thicknesses from the conductance ring probes.

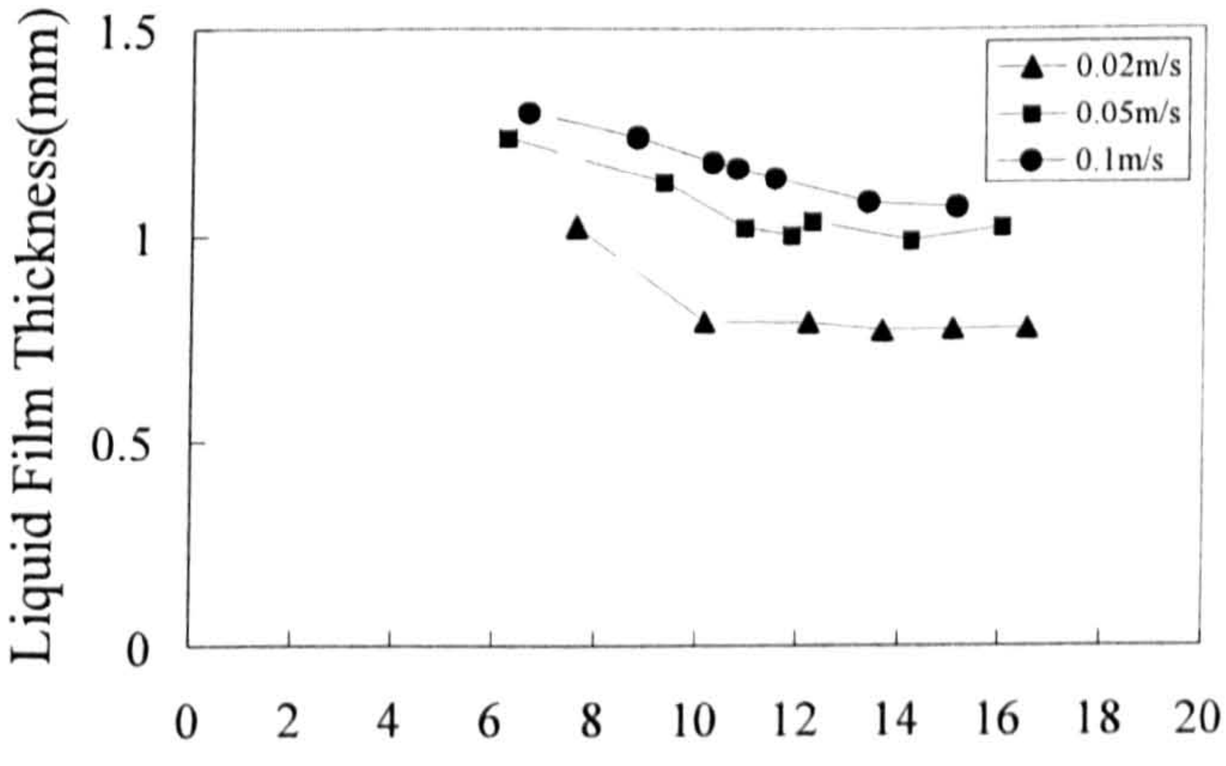

Figure 6.11 Time-averaged liquid film thicknesses from the local film pin probes.

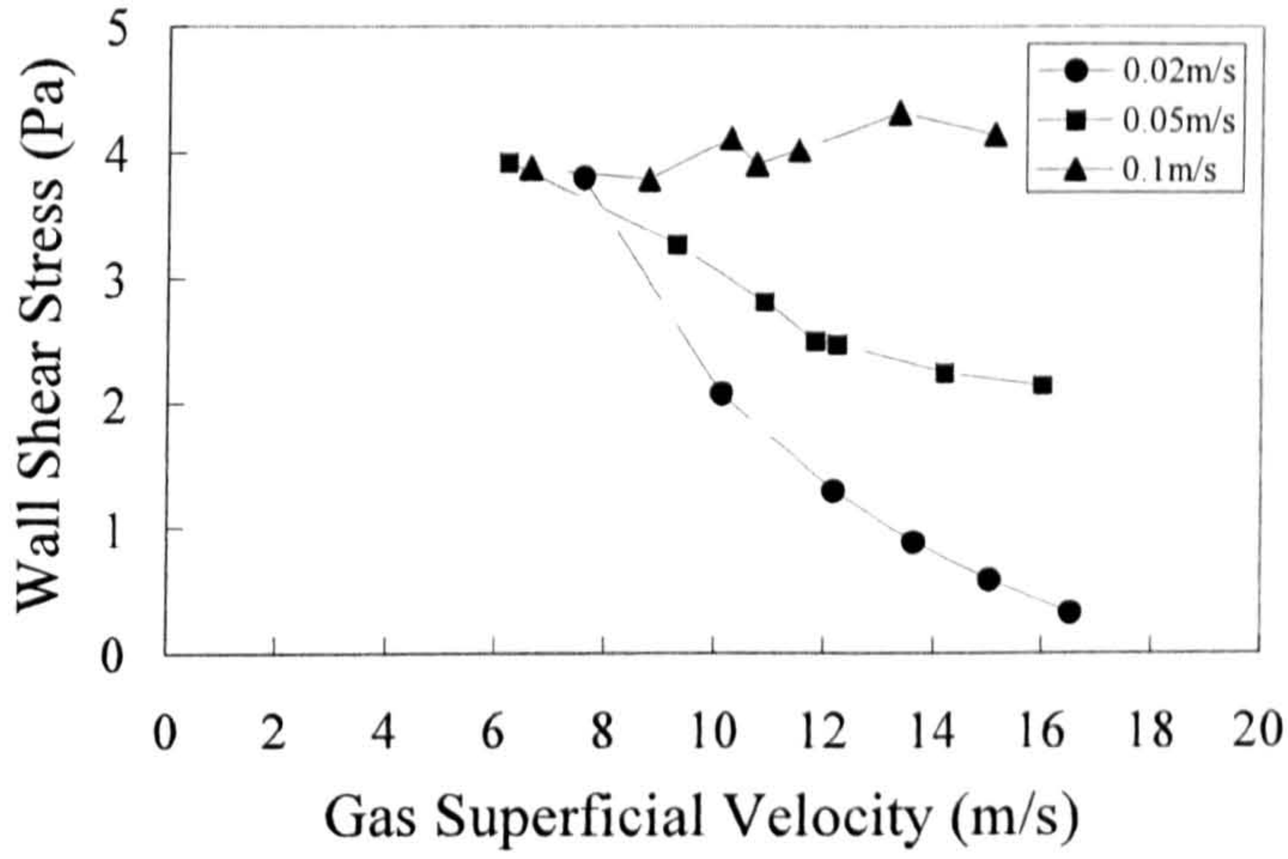

Figure 6.12 Time-averaged magnitude wall shear stress as a function of gas superficial velocity.

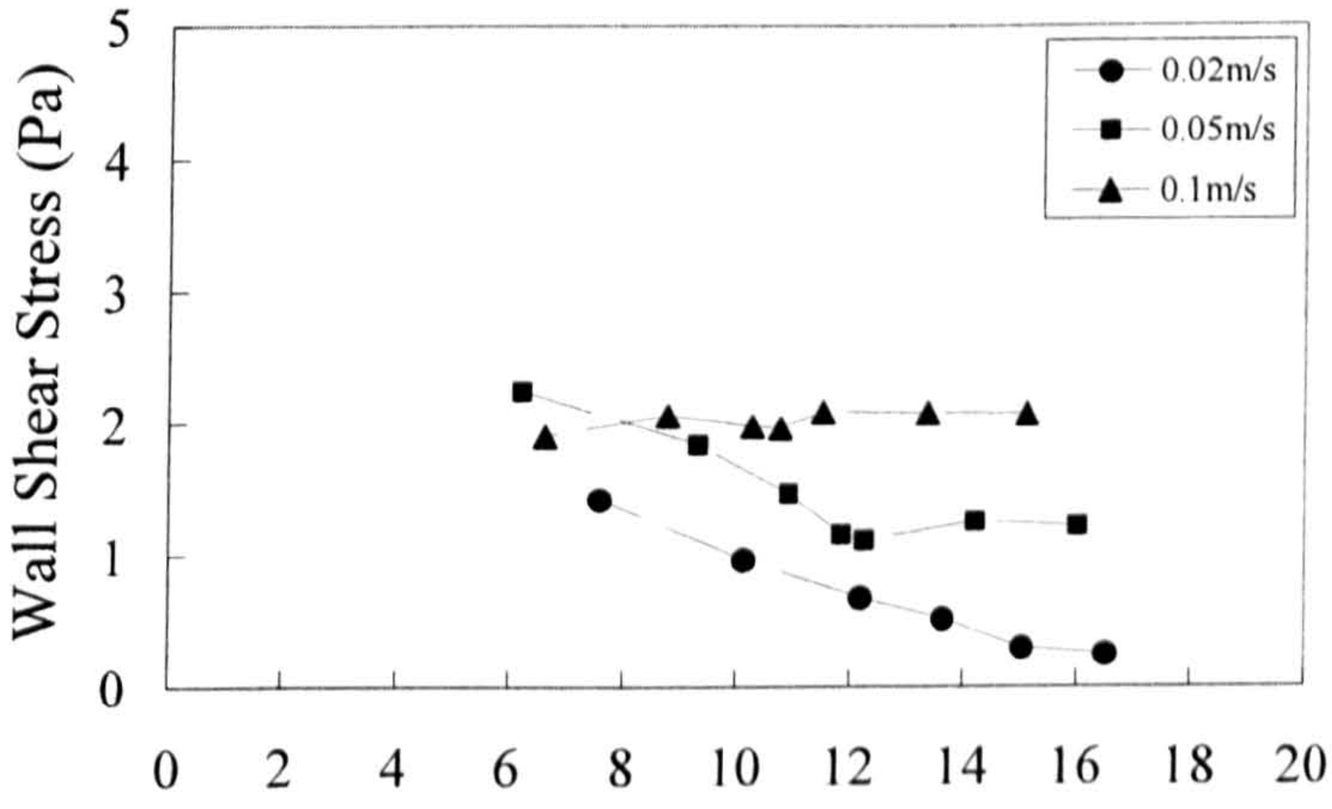

Figure 6.13 Time-averaged directional wall shear stress as a function of gas superficial velocity.

6.2.2 Time-varying data

Total pressure drop in this study were measured over 1.64 m axial distance of the test section as described in Chapter 3 and liquid film thickness measured using both conductance ring probes and local film pin probes this is in addition to the measurement of wall shear stress using the directional hot film probes. The conductance ring probes were located at three different axial heights along the test section between the two tapping holes of the Differential pressure transmitter (their exact locations are given in Chapter 3) and the local film pin probes were surrounded the wall shear probes which they were located between the first and the second conductance ring probes (again the exact locations and dimensions of the probes given in Chapter 3). It is believed that the time-varying of total pressure drop that averaged over that axial distance, i.e., 1.64 m is more reliable to be compared with the time varying data that averaged from the mentioned three conductance ring probes along the test section. In addition the time-varying wall shear stress results to be compared with the time-varying data from the pin probes. Based on the mentioned format the time-varying data of the measured parameters are presented in Figures 6.14, 6.15 and 6.16 for liquid superficial velocities of 0.02, 0.05 and 0.1 m/s respectively. It is apparent that there are a noticeable relationship between the total pressure drop and the liquid film thickness that obtained from the conductance ring probes and a close relationship between the time-varying wall shear stress and the liquid film thickness that obtained locally from the pin probes, here data from pin probe 4 was used which is in the same axial level as the wall shear stress probes (see Chapter 3). As

described in the beginning of this chapter due to the averaging nature of the conductance ring probes some details of the roughness in the interface between the gas and the liquid might hide therefore the time-varying film thickness obtained, i.e., from the pin probes are better related to the wall shear stress results because the later was also measured locally. Although as described previously in this chapter the pin probes can measure the film thickness accurately up to 1.5-2 mm however still can sense the waves when they pass so the variation of locally measured film thickness with time are well related to the variation of wall shear stress with time. The relationship between the total pressure drop, the liquid film thickness and the wall shear stress are very clear in the power spectrum density (PSD) of the mentioned parameters as shown in Figure 6.17 for various gas and liquid superficial velocity. From the time-varying data of measured parameters it can also be seen that the roughness in the interface between the gas and the liquid are affected by the variation of the liquid and gas velocity. As at liquid velocity of 0.02 m/s and gas superficial velocity 16.5 m/s only waves with small amplitude or ripples can be seen and a low wall shear stress so consequently a low pressure drop however at gas velocity of 7.6 m/s the surface of the film become more rough with higher amplitude waves which leads to a higher wall shear stress and higher pressure drop. From the directional wall shear stress time-varying data it can be concluded that the direction of the flow over the conditions studied was always changing and as the gas velocity decreased and liquid velocity increased the flow direction getting more oscillated, in addition and although the downward flow of the film can be seen at liquid and gas velocity of 0.02 m/s and 7.6 m/s respectively which lasts up to 0.14 sec,

however, this is not on regular basis so the variation of directional wall shear stress with time does not show clearly the slug flow as reported by Whalley and McQuillan (1985) which normally consists of downward flow of the liquid film when the Taylor bubble passes and upward when the plug of liquid passes.

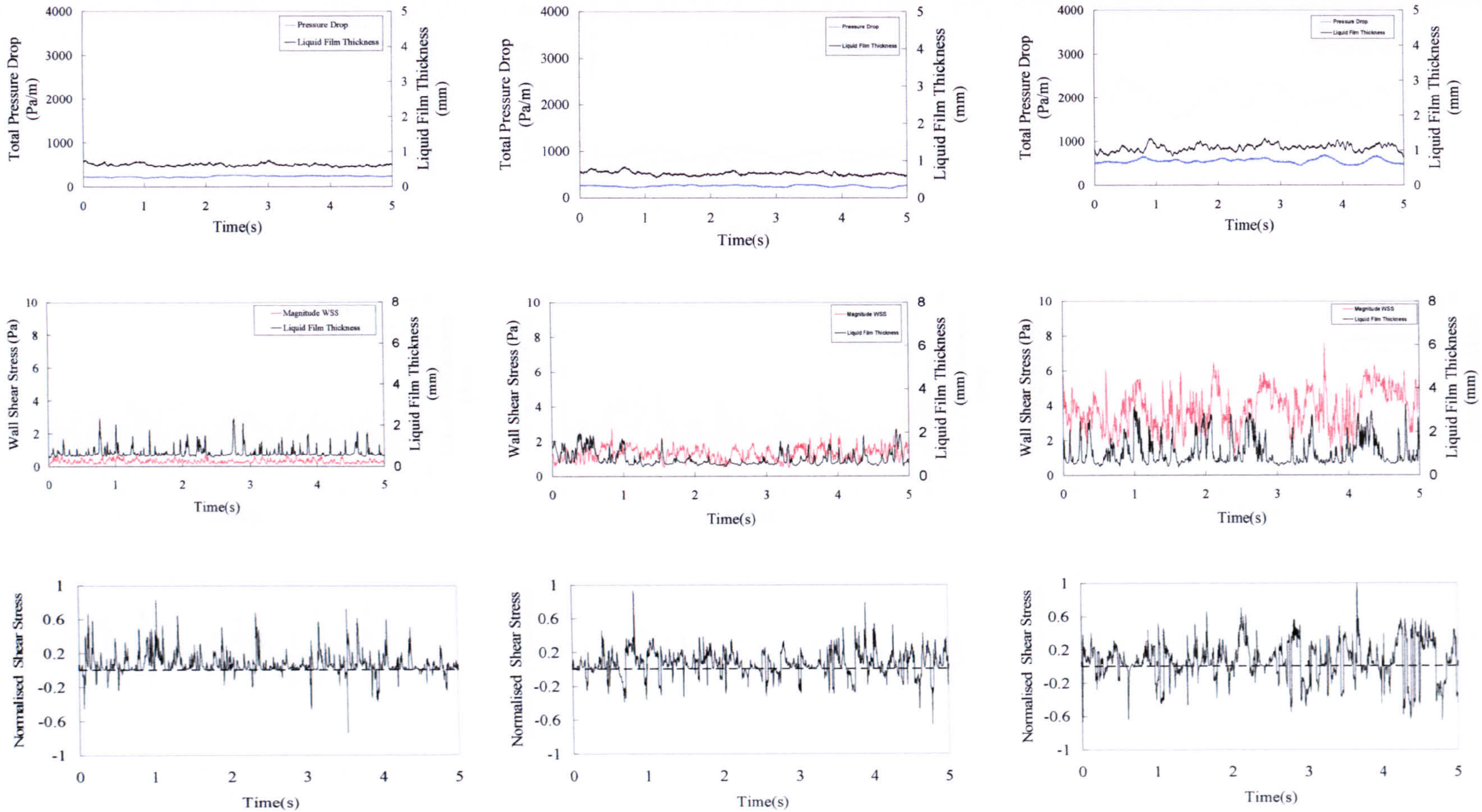

Figure 6.14 Time-varying data at Uls = 0.02m/s and Ugs = 16.5, 12.2 and 7.6 m/s from left to right respectively of: (Top) total pressure drop and liquid film thickness from conductance ring probe at (Middle) Magnitude wall shear stress and locally measured film thickness (bottom) directional wall shear stress.

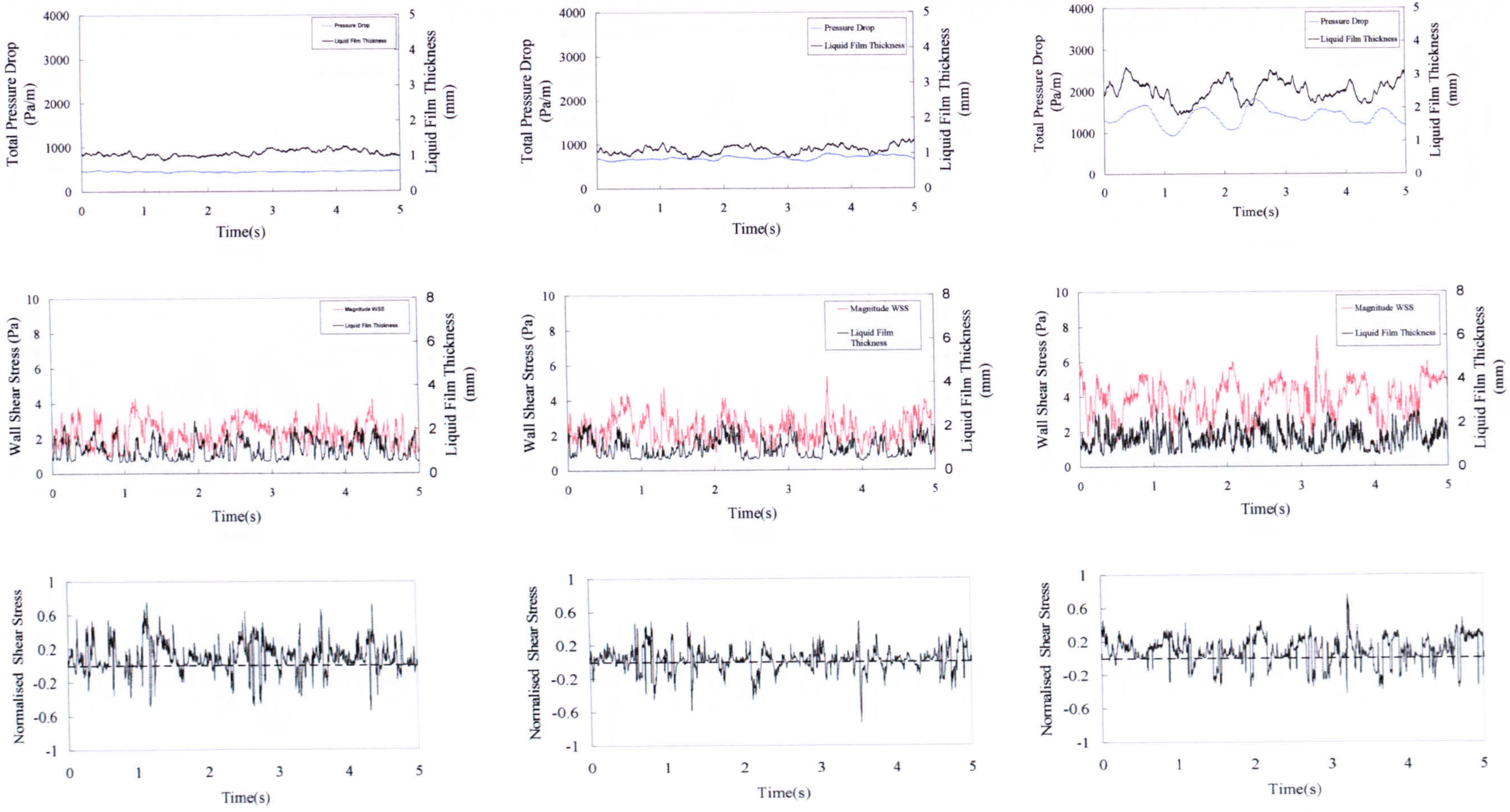

Figure 6.15 Time-varying data at Uls = 0.05m/s and Ugs = 16, 11.8 and 6.2 m/s from left to right respectively of: (Top) total pressure drop and liquid film thickness from conductance ring probe at (Middle) Magnitude wall shear stress and locally measured film thickness (bottom) directional wall shear stress.

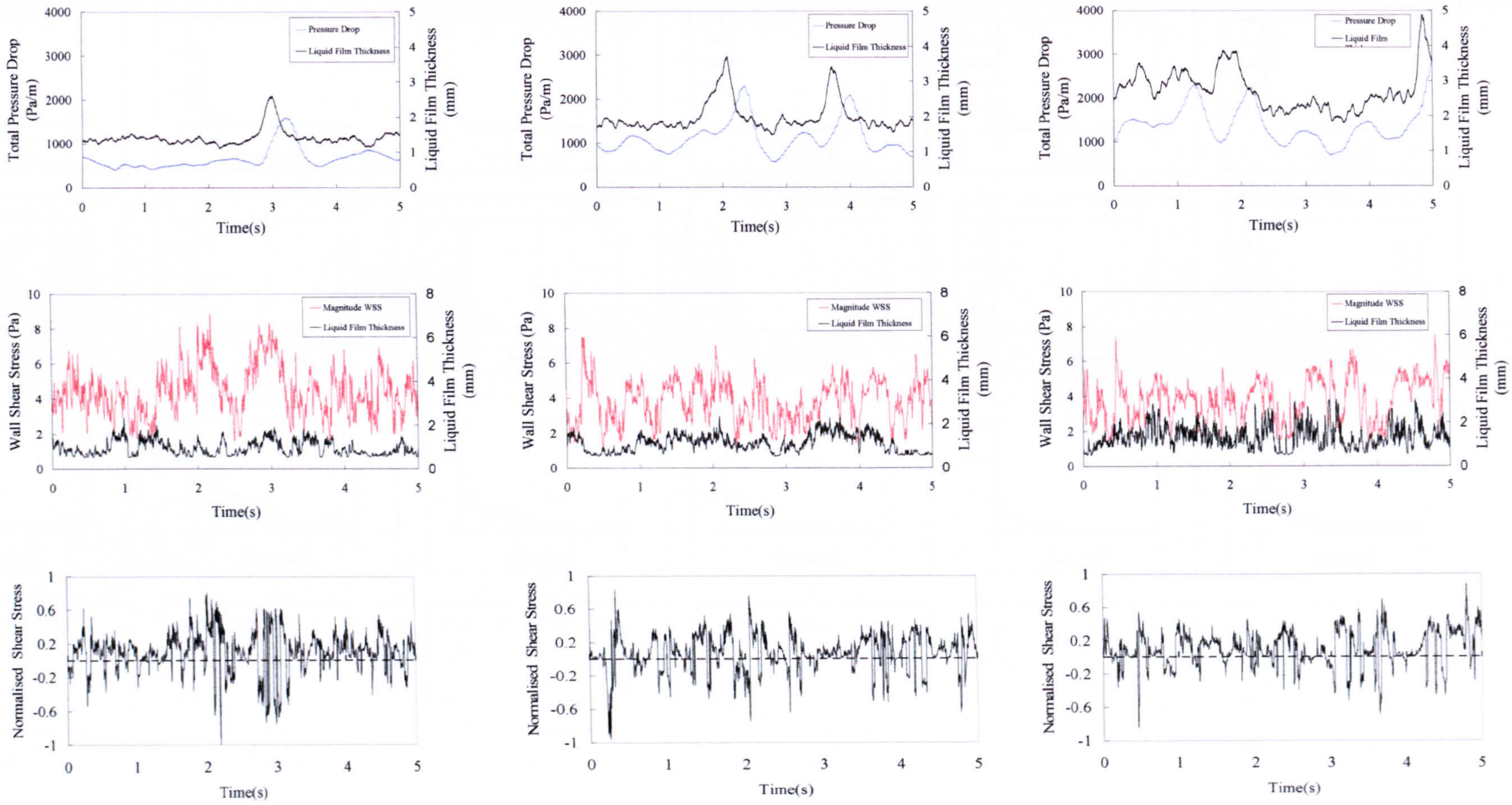

Figure 6.16 Time-varying data at Uls =0.1m/s and Ugs = 15.1, 10.8 and 6.6 m/s from left to right respectively of: (Top) total pressure drop and liquid film thickness from conductance ring probe at (Middle) Magnitude wall shear stress and locally measured film thickness (bottom) directional wall shear stress.

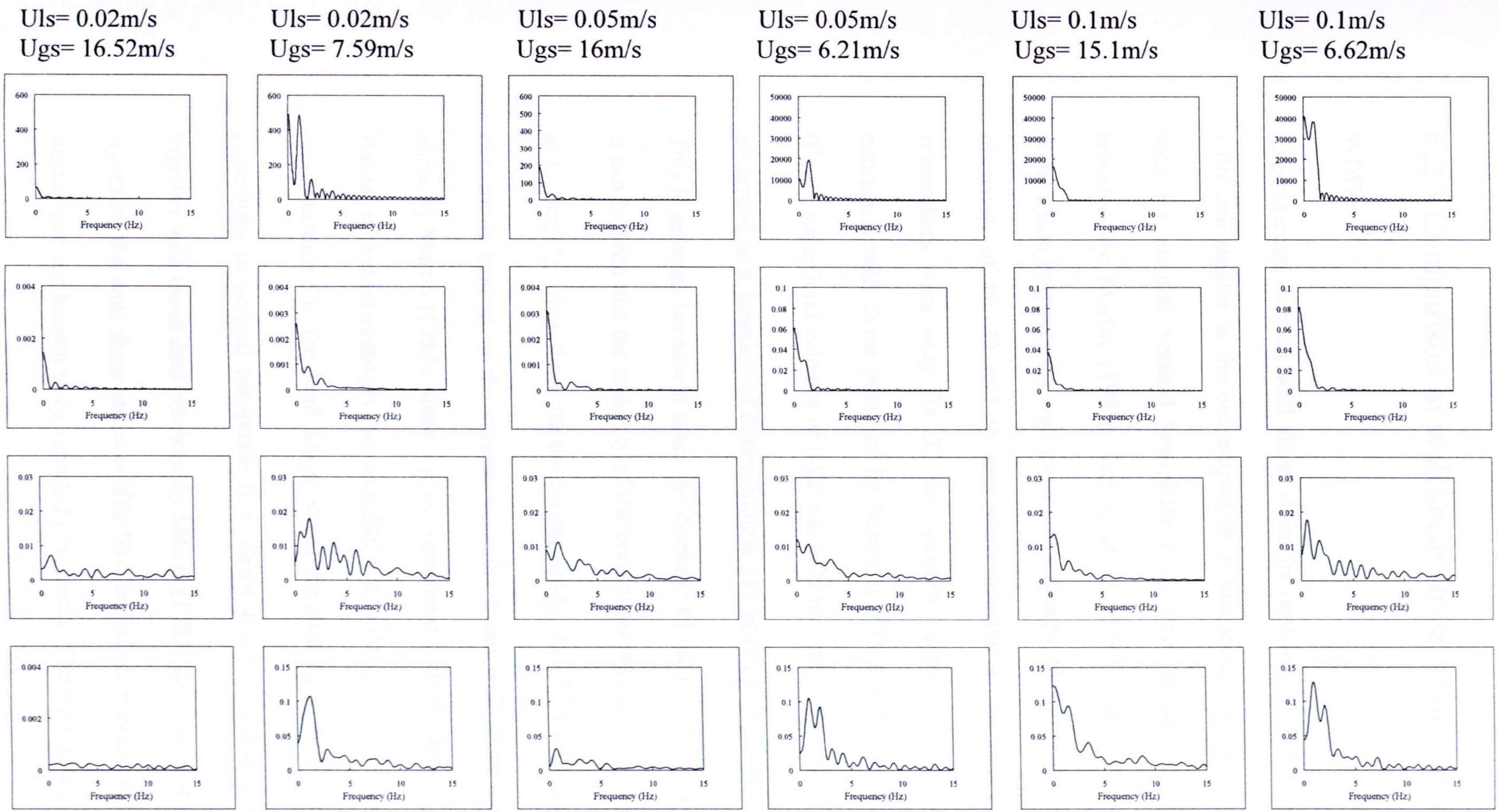

Figure 6.17 The power spectral density (PSD) of time-varying data: (A) total pressure drop; (B) liquid film thickness from the conductance ring probes; (C) liquid film thickness from the local pin probes; and (D) wall shear stress.

6.2.3 Comparison of wall shear stress results with previous work

Experimental data on wall shear stress in vertical two-phase flow for pipes with size similar to the one employed in this study are not available. Some data for annular vertical two-phase flow from smaller pipes have been reported by Martin (1983); Govan et al (1989); and Wolf (1995). For comparison purposes the wall shear stress data by Martin (1983) of pipes with diameters of 10, 32 and 58 mm were selected as the data by two other researchers were only for 32 mm diameter pipes. The present data are compared with those obtained by Marin (1983), see Figures 6.18 and 6.19 (liquid superficial velocity of 0.02 and 0.05 m/s respectively). The graphs are presented as a function of dimensionless gas velocity for reversal flow (U_g^*). This is selected because it takes the diameter of the pipe into account. Overall it can be seen that the majority of the conditions studied by Martin (1983) are at higher, U_g^*, than these for the current study. At U_g^* that in the range of the conditions studied in the current work the mean wall shear stress from the work by Martin (1983) show a good agreement with the data of present work Based on that interestingly the data obtained in this study can be considered as an extension for the wall shear stress measurement to a wider range of conditions in vertical two-phase flow down to a U_g^* value of just 0.33 and together with those data obtained by Martin (1983) the results of this study can represent the wall shear stress profile like the pressure drop profile which the former one not known to be reported previously. The over all trend of the wall

shear stress profile is as the gas velocity increases the wall shear stress decreases before it starts to increase at $U_g^* > 1$ which can be linked to the total pressure drop profile as described in Chapter 4. The effect of pipe diameter on wall shear stress is also noticeable (Table 6.1), as the pipe diameter increases the wall shear stress becomes lower, thus lowering the frictional pressure drop hence the total pressure drop.

Table 6.1 Mean wall shear stress at Liquid Mass Flux of 20 kg/m2s for different diameter vertical pipes

Pipe Diameter (mm)	Gas Mass Flux (kg/m^2s)	Wall Shear Stress (N/m^2)
10	20	2.2
10	40	5.8
10	60	10.1
10	80	15.1
32	20	0.5
32	40	2.3
32	60	10.4
32	80	13.3
58	20	1.3
58	40	1.8
58	50	4.3
58	60	6.5
58	70	10.7
58	80	11
127	27	1.42
127	36	0.97
127	43	0.67
127	48	0.51
127	53	0.3
127	59	0.25

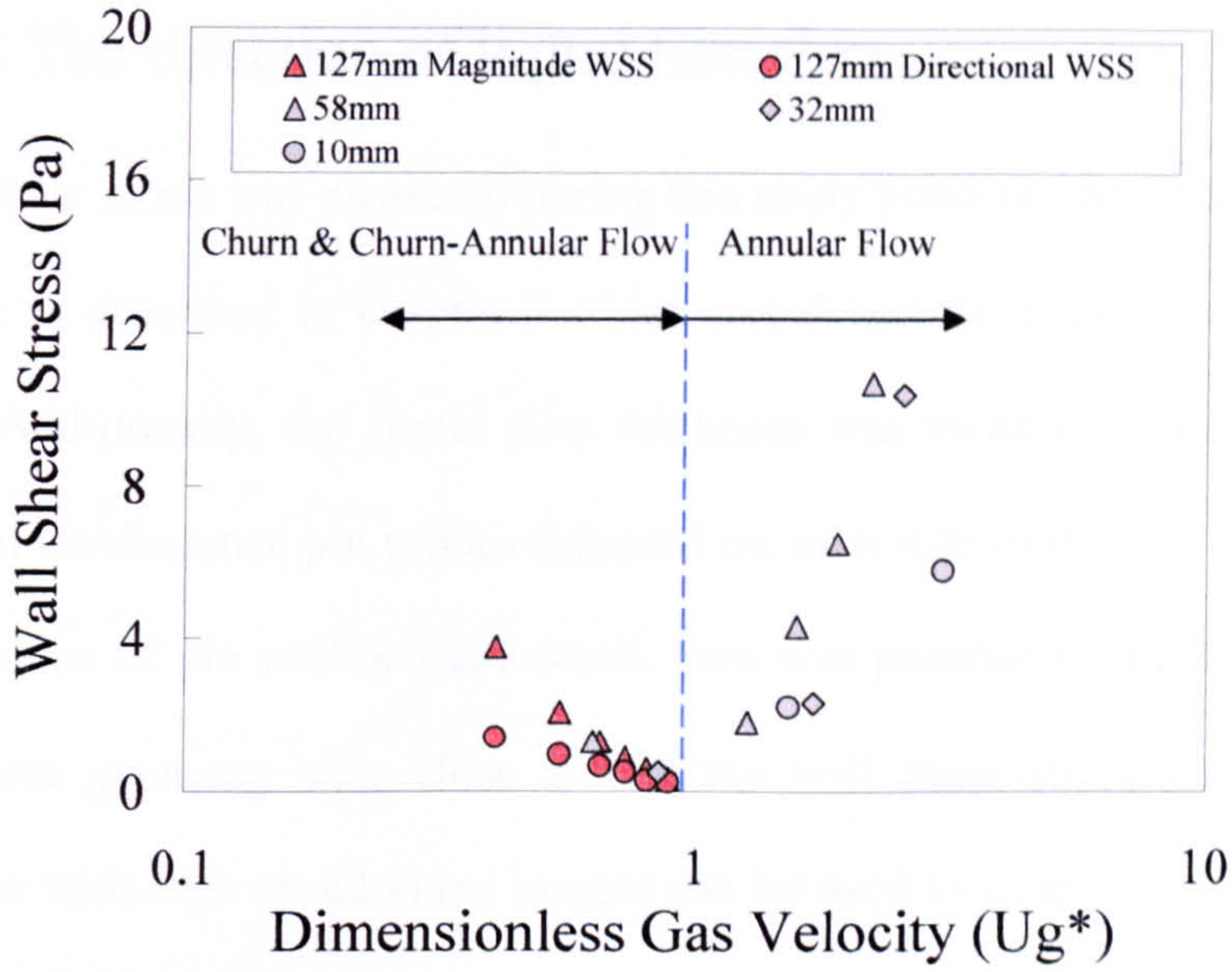

Figure 6.18 Time-averaged wall shear stress at liquid velocity of 0.02 m/s for different pipe diameters and as a function of dimensionless gas velocity.

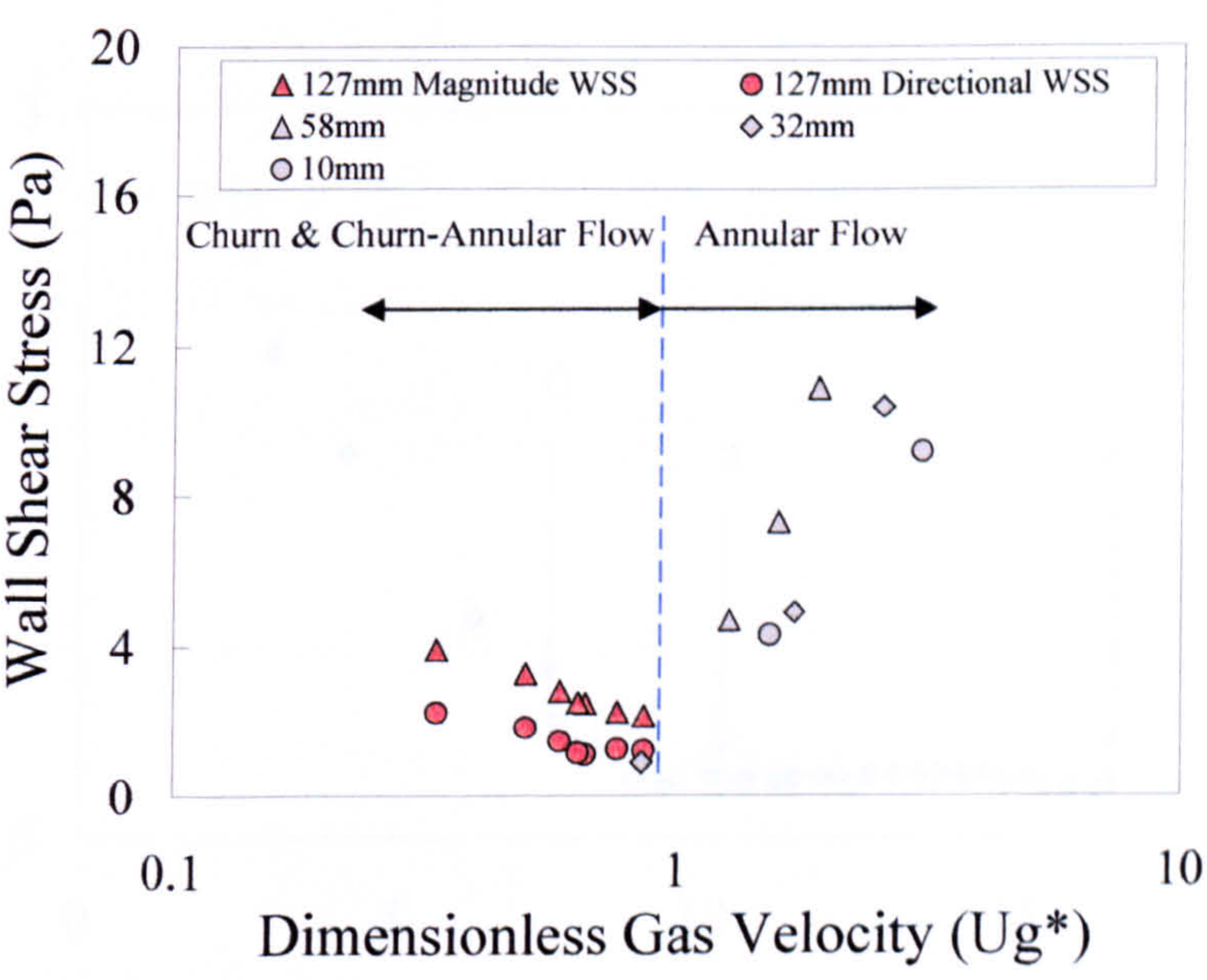

Figure 6.19 Time-averaged wall shear stress at liquid velocities of 0.05-0.06 m/s for different pipe diameters and as a function of dimensionless gas velocity.

6.2.4 The direction of liquid film flow

Wall shear stress was measured during this study using the directional hot film probes as described in chapter 5 which can detect the axial direction of the flow. Additionally, the liquid film thickness was measured locally using 4 pairs of conductance pin probes mounted on each side of the test section. The dimensions of pin probes were small, thus was possible to locate them in a cruciform geometry very close around the wall shear stress probes. These together with high speed video images can be used to determine the direction of the liquid film flow. A liquid superficial velocity of 0.02 m/s was selected at three gas superficial velocities of 16.5, 10 and 7.6 m/s which are termed as conditions A, B and C respectively (Figure 6.20):

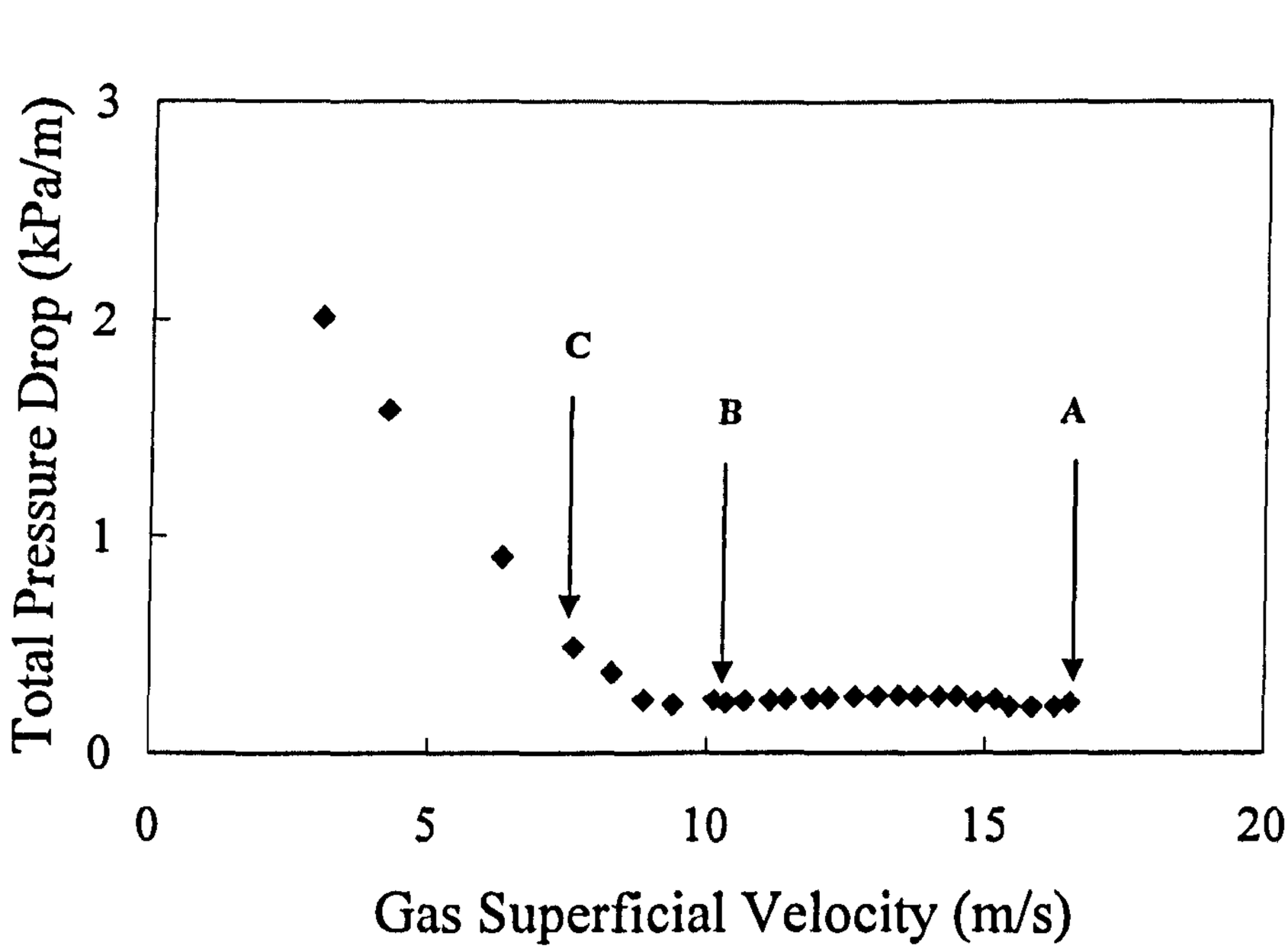

Figure 6.20 Time-averaged total pressure drop at liquid superficial velocity of 0.02 m/s as a function of gas superficial velocity.

Directional wall shear stress: Time-varying results of conditions above from the directional wall shear probe are illustrated in Figure 6.21. At condition A the wall shear stress is positive for most of the time. However, from time to time it switches to a negative value. As the gas superficial velocities decreases, i.e., at conditions B and C, the wall shear stress becomes more random in the fluctuation between negative and positive values. Therefore no completely unidirectional flow was observed over the conditions studied.

Local liquid film thickness: Liquid film thickness around the wall shear stress probe were collected locally from 4 conductance pin probes as described previously in this chapter. The time-varying data for condition A and over just 0.2 sec is presented in Figure 6.22. At that period of time the film is unidirectional moving upward, therefore the roughness of the film surface showing the probes at their correct order as they were located in the test section, i.e., probe number 3 in the bottom (upstream), probes 1 and 4 in the middle and probe 2 in the top (downstream), [see Figure 3.11a and b for the probes locations].

Figure 6.23 showing time series of liquid film thickness over a longer period of time (4 sec) and for conditions A, B and C. It can be seen that the probes not always can be determined at their correct order due to the frequent changes in the direction of the flow.

To investigate the film flow direction the time-varying results of the locally measured film thickness were cross-correlated at Conditions A, B and C. This was carried out between probes 3 and 1, 3 and 2, 3 and 4, 1 and 2, 4 and 2 and 1 and 4, as illustrated in Figure 6.24. Besides, the structural velocity between

each pair of these probes was calculated as shown in Figure 6.25. The results of Figures 6.24 and 6.25 can be summarized as:

- Overall, positive and negative values in the cross correlation functions can be seen which represent the direction change of the flow over the conditions studied.
- According to the location of each probe the cross correlation results and the structural velocity suggest that the film not only moving in the axial direction however two dimensional flows are also might be expected.
- Positive and negative values of structural velocities for conditions A and C respectively might represent an over all upward flow of the film over 15 sec for the former condition and in contrast to the turbulent complicated churn flow for the later condition. However the structural velocity mostly close to zero for condition B, which means, that the film flow has slowed down, bearing in mind, condition B is near the transition region of total pressure drop from sudden to gradual decrease.

High speed images: During this study a visualization campaign was performed using a high speed video camera as described in Chapter 3. Images extracted from the high speed videos for liquid superficial velocity of 0.014 m/s at gas superficial velocities of 16, 10 and 3.4 m/s as presented in Figures 6.26, 6.27 and 6.28 respectively. At gas superficial velocity of 16 m/s the flow of the film downward is not clear however, the movement of the waves are more clear which are circumferentially localized as reported also by Azzopardi

et al (1983). It can be observed that the waves moving at different velocity and in two dimensional directions, i.e., not only in the axial direction. So when two waves at different velocities moving upward they will collide to produce a bigger wave and as a result: firstly, the liquid film appears to be shock and as a result might move in two dimensional directions for a short period of time. Secondly: due to the gravity that new wave moves downward until becomes small enough to start moving upward again. This might explain the negative values of wall shear stress in high gas flow rate, i.e., at condition A. Besides, it may be concluded that in large diameter pipes, waves may move upwards or downwards in contrast to the case for smaller pipes where the film movement is uni-directionally upward.

At other two conditions, i.e., at gas superficial velocities of 10 and 3.4 m/s, the random flow of the film is apparent and becomes more complicated when the gas velocity decreases.

Based on the discussion above following conclusions can be drawn:

- From the directional wall shear stress probe, no completely unidirectional upward flow has been observed over the conditions studied.
- The negative values of wall shear stress at condition A might be linked to the wave characteristic as deduced from the high speed videos.
- On the basis of the information obtained from the local film thickness and the high speed video images, two dimensional film flows are expected rather than only an axial flow.

- Structural velocity results suggest that the liquid film slowed down at condition B that are in the transition region between sudden to gradual decreases of the pressure drop profile. However zero wall shear stress point not reached.

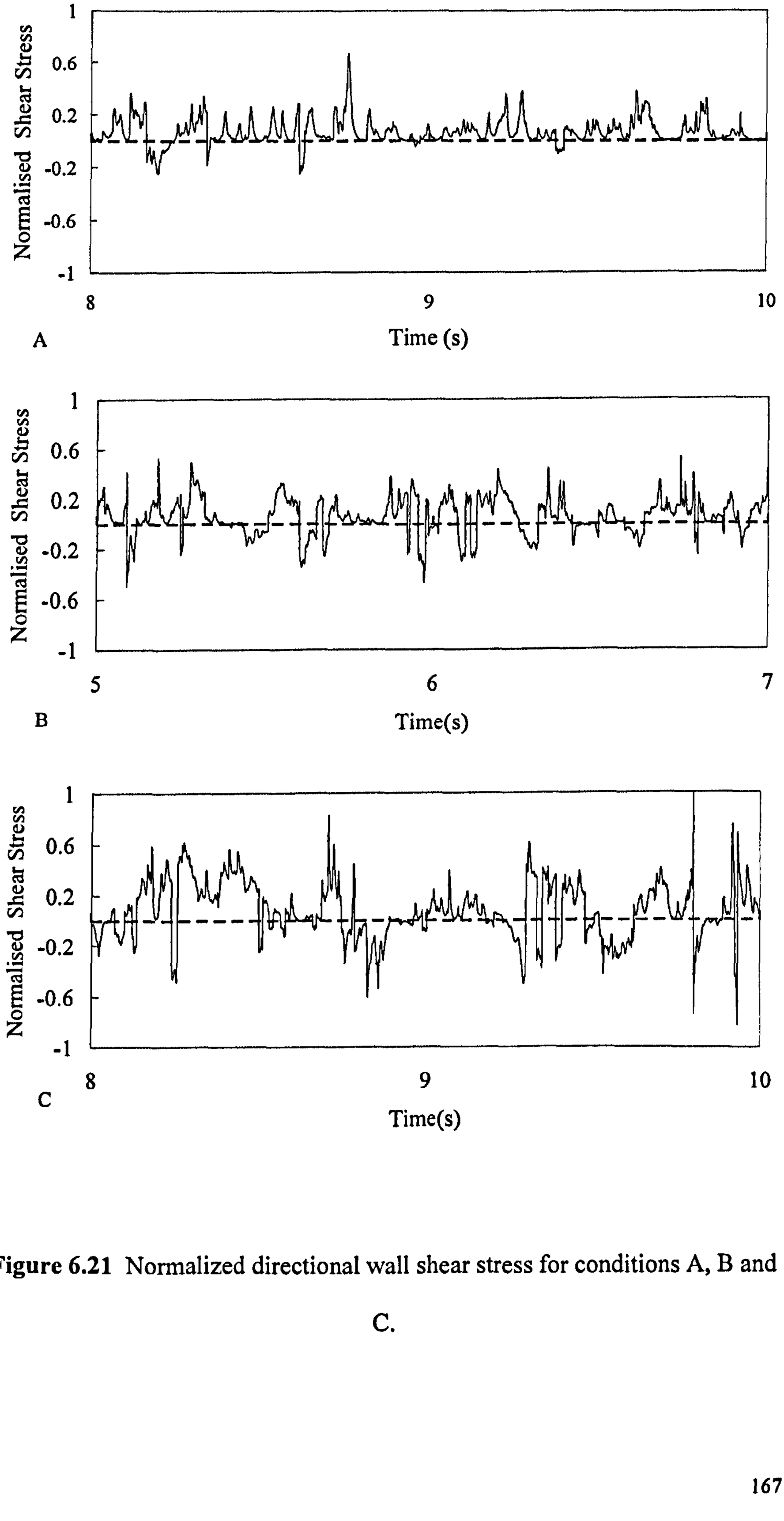

Figure 6.21 Normalized directional wall shear stress for conditions A, B and C.

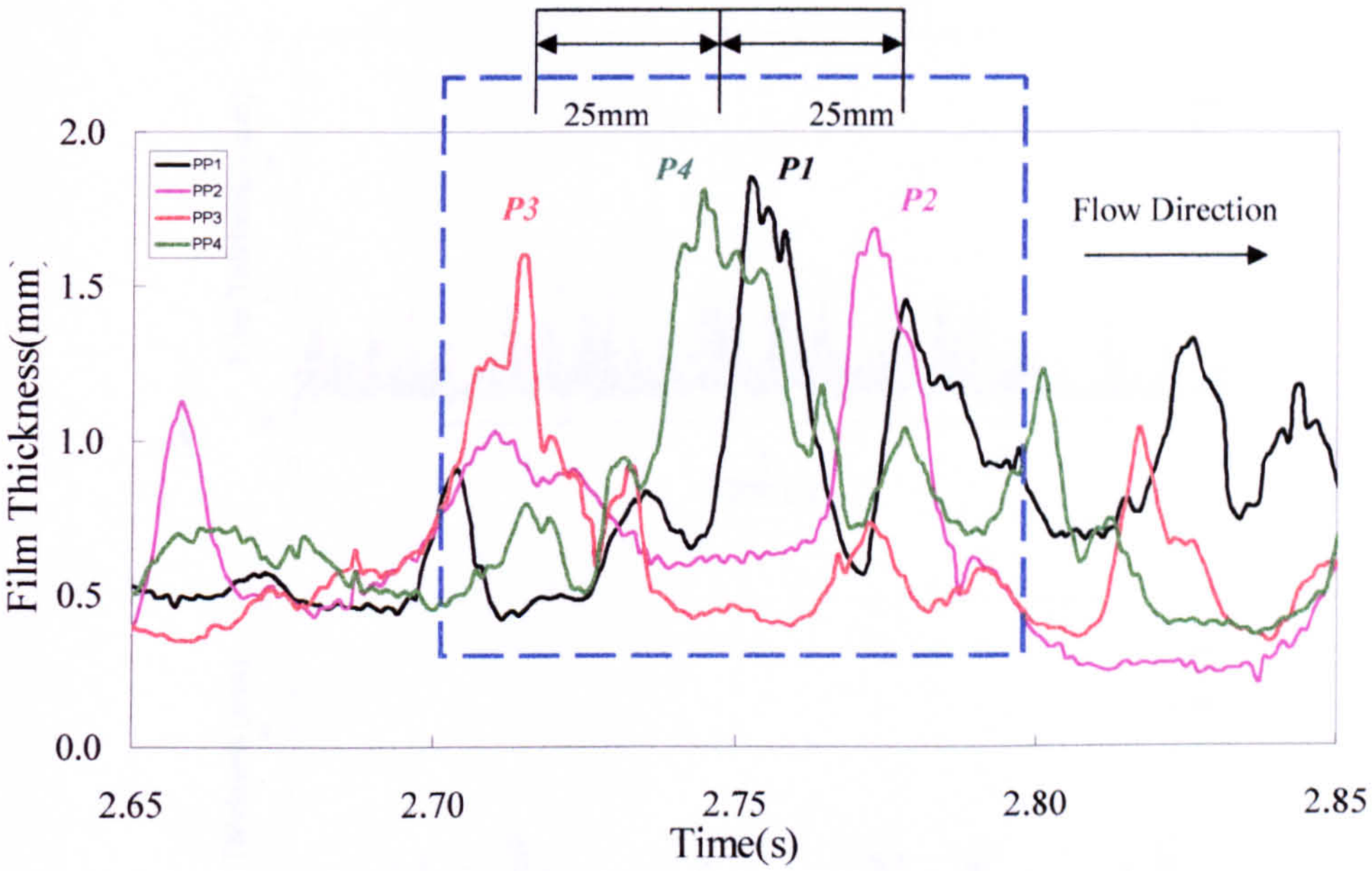

Figure 6.22 The liquid film surface roughness as detected by 4 conductance pin probes for condition A.

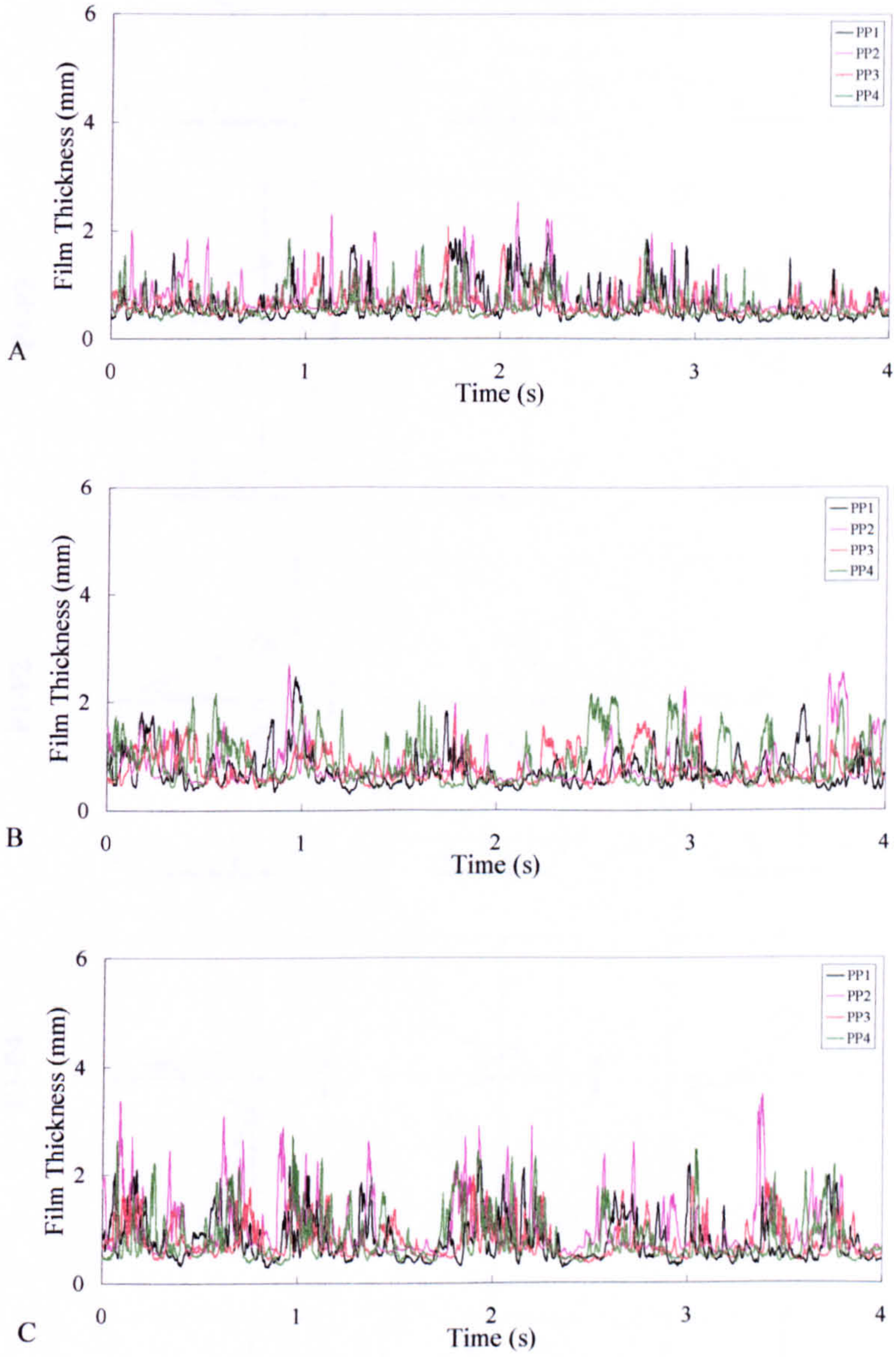

Figure 6.23 Time-varying results of film thickness obtained by 4 conductance pin probes for conditions A, B and C.

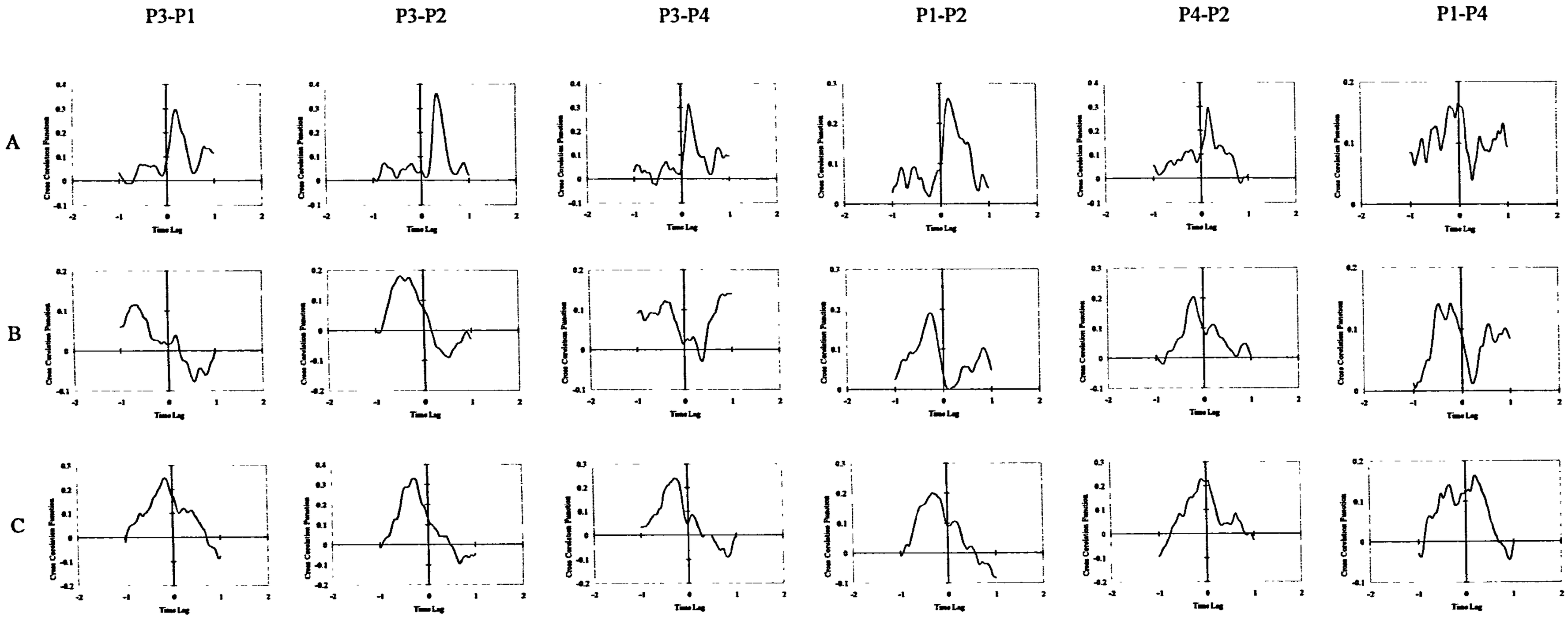

Figure 6.24 Cross correlation between conductance pin probes for the Conditions A, B and C.

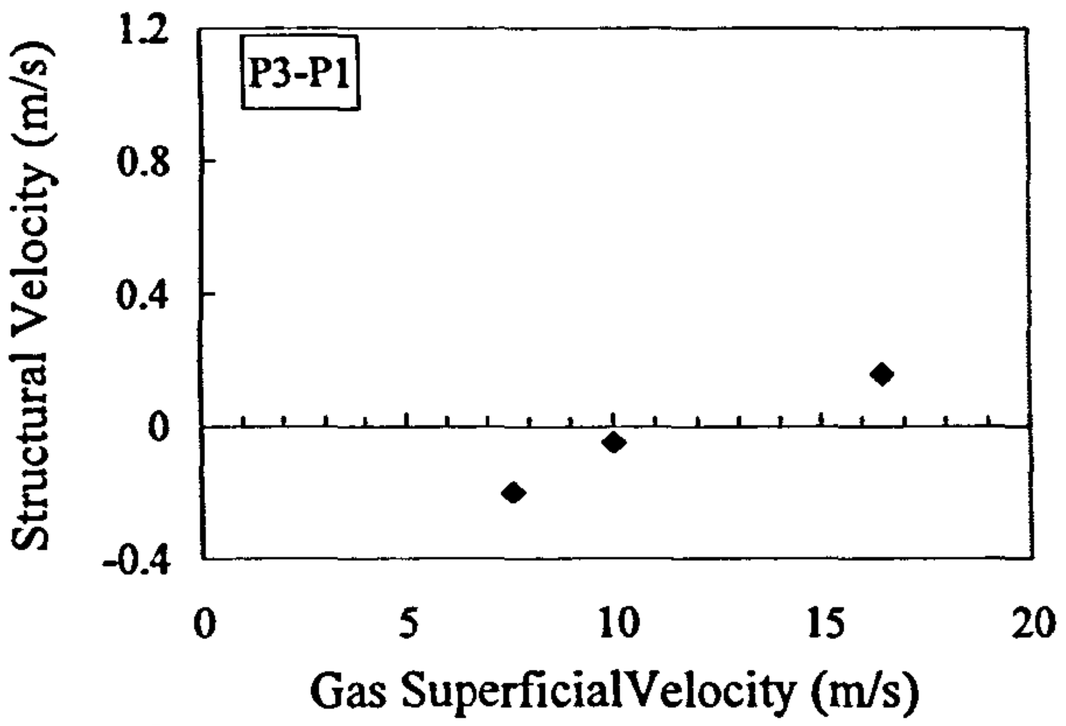

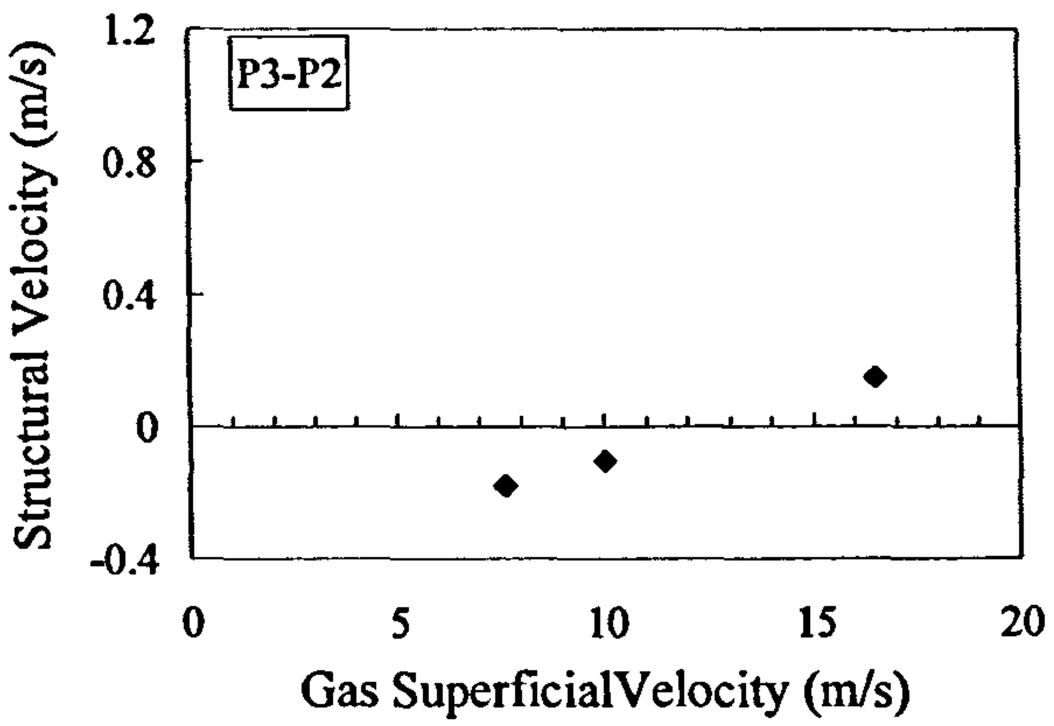

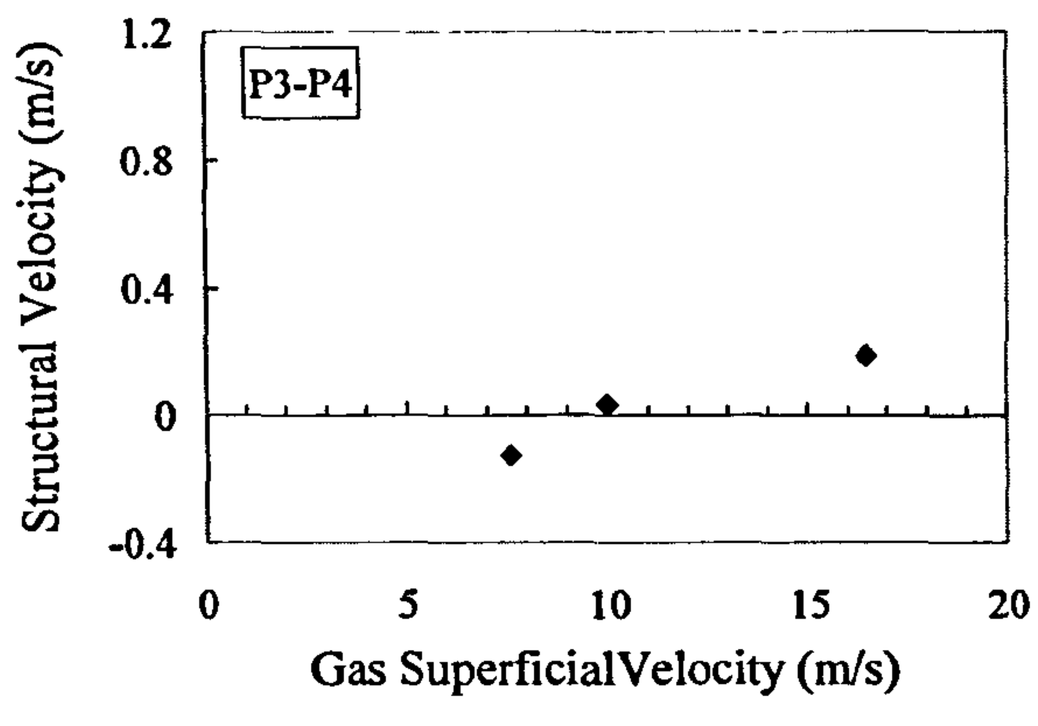

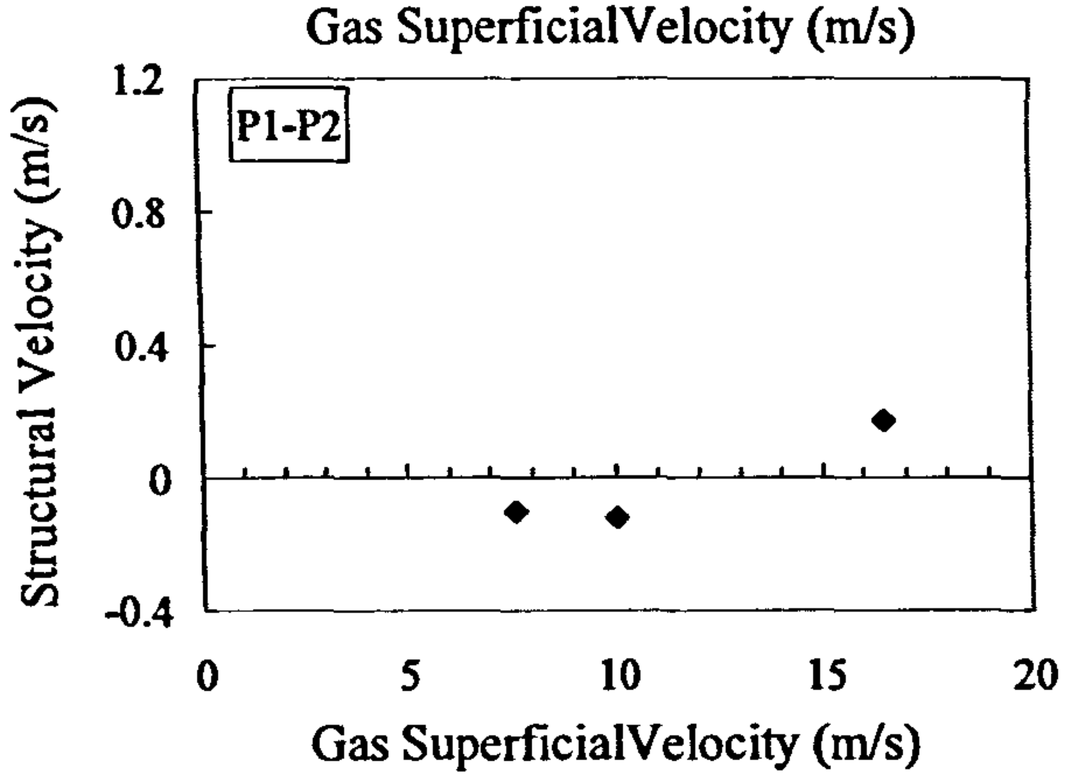

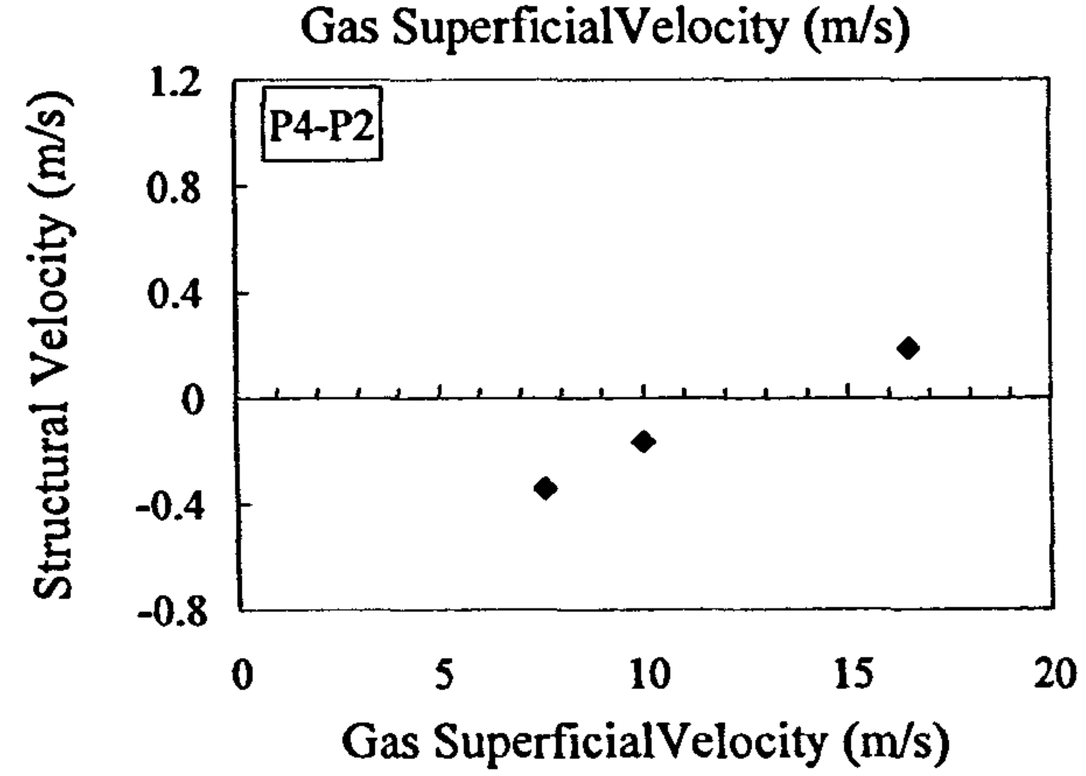

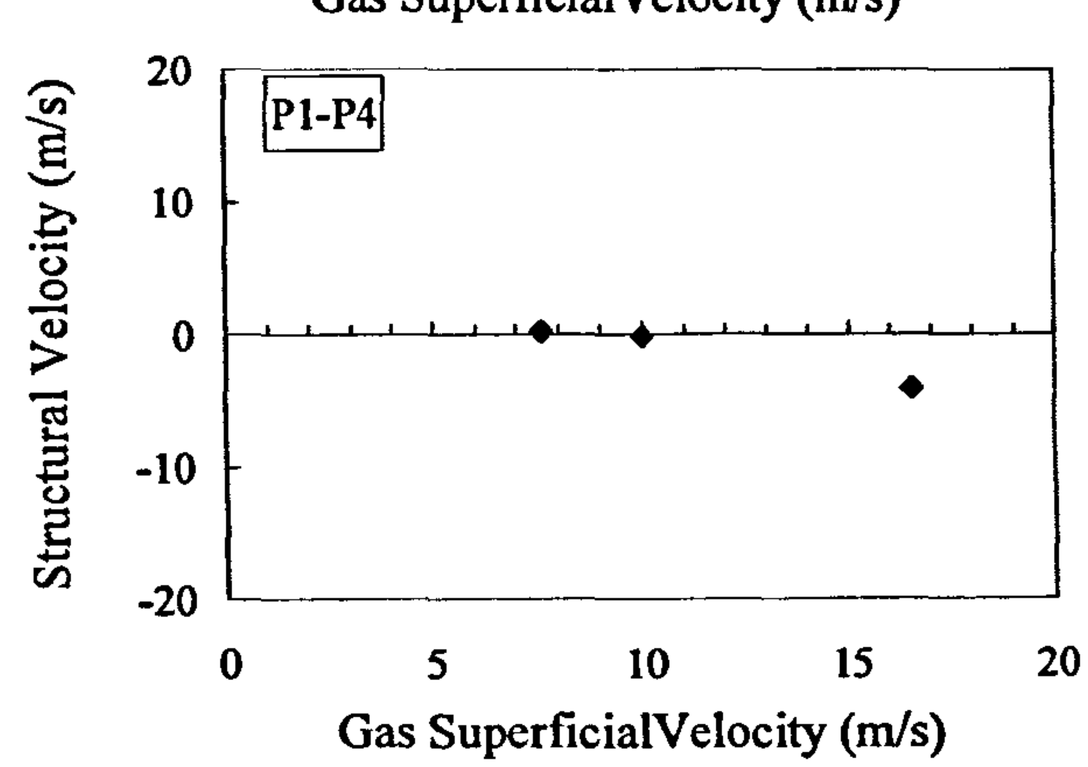

Figure 6.25 Structural velocities between the local film pin probes

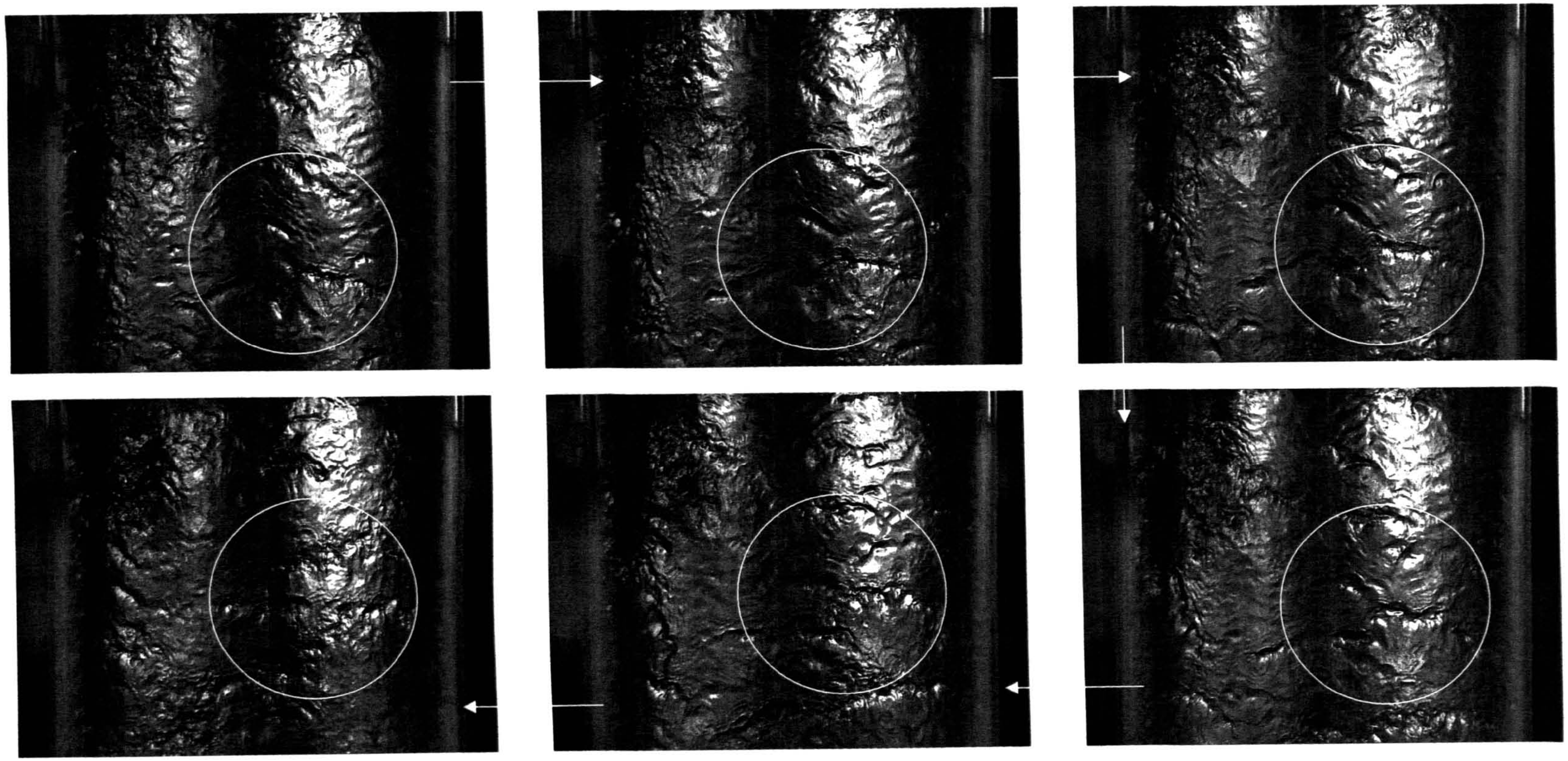

Figure 6.26 High speed video images for liquid superficial velocity of 0.014 m/s and gas superficial velocity of 16 m/s.

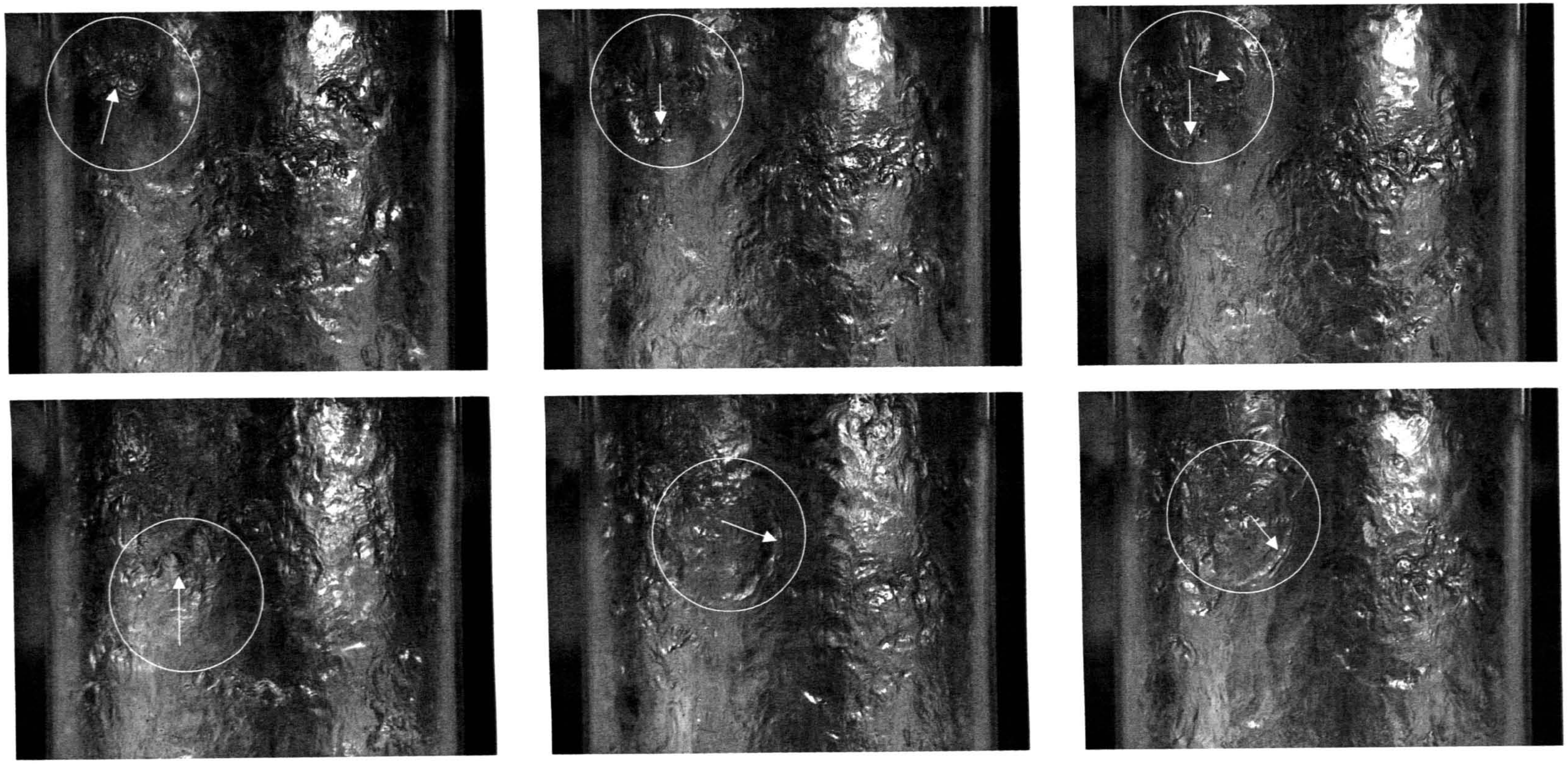

Figure 6.27 High speed video images for liquid superficial velocity of 0.014 m/s and gas superficial velocity of 10 m/s

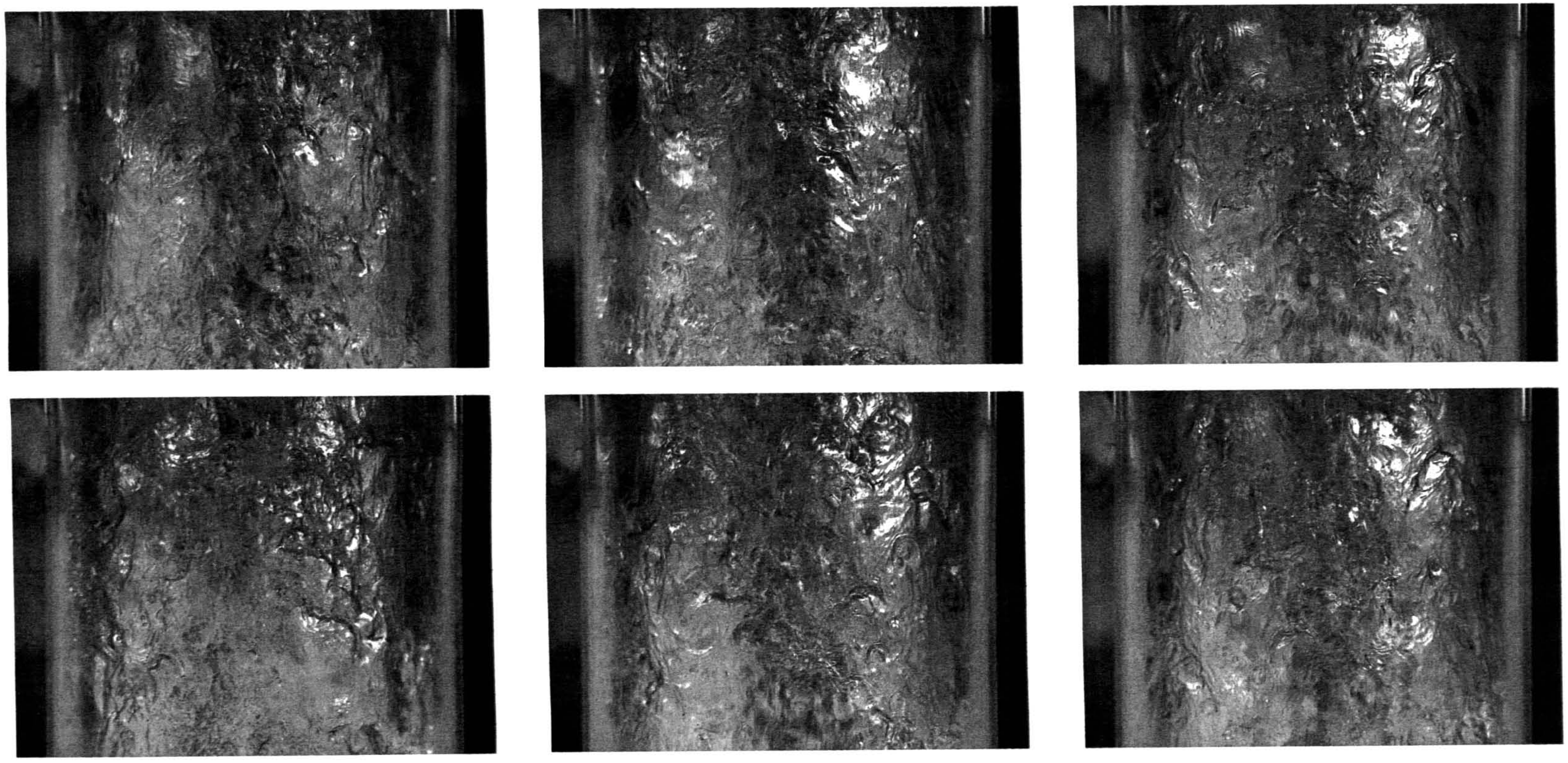

Figure 6.28 High speed video images for liquid superficial velocity of 0.014 m/s and gas superficial velocity of 3.4 m/s.

Chapter 7

Conclusions and future work

There is a lack of experimental data on gas-liquid two-phase flow in large diameter pipes; this is especially true for parameters such as pressure drop and liquid film properties. In this work a number of experimental campaigns were carried out to measure pressure drop, liquid film thickness and wall shear in 127mm vertical pipe. Total pressure drop were studied systematically through a data bank of 600 experimental runs. Magnitude and directional wall shear stress measurements have been made selectively using commercial non-directional probes and directional hot films. The latter technique is produced at Nottingham University during this study. Experimental data on liquid film properties was obtained by measuring total pressure drop, wall shear stress and film thickness simultaneously. The data were supported by some high speed images through a visualization campaign. Based on the parameters measured and the measurement techniques used, this work makes original contributions to the understanding of gas-liquid two-phase flow characteristics in large diameter vertical pipes as such study had not been carried out previous to the present work. From the analysis of its results the main conclusions that can be drawn from this work and suggestions for further work are as the following:

7.1 Conclusions

The main points and conclusions that may be drawn from this work are as the following:

1) The effect of liquid superficial velocity on time-averaged total pressure drop in the range of the conditions studied during this work can be identified in three major areas, namely low liquid velocity, 0.01, 0.02, 0.03 and 0.04 m/s, intermediate area, 0.05 and 0.06 m/s, and high liquid velocity area, from 0.07 to 0.7m/s. In the first area a sudden decrease in total pressure drop has been seen as the gas velocity increase before the trend to be changed to a gradual decrease. The trend of two-phase pressure drop with the gas velocity changes in the second area has a smoother nature however it becomes more complicated in the third area.

2) There are clear effects of gas and liquid velocity changes on time-varying total pressure drop. Fluctuations are apparent in its time series at high liquid flow rates. The extent of those fluctuations grows as the gas velocity reduced at lower liquid flow rates. That can be also observed from the standard deviations obtained.

3) Pipe diameter has a significant effect on total pressure drop. Generally, the total pressure drop for given liquid and gas superficial velocities

fall as the pipe diameter increases. However, there are some exceptions to this trend due to the differing balance between the frictional and gravitational components of the pressure drop.

4) The maxima and minima characteristics in pressure drop profile of 32 mm pipe can be described as a maxima set between two minima, however no minima or maxima has been found clearly for 127mm pipe.

5) For a 32 mm pipe, a clear link has been established between the variation of pressure drop with gas velocity and the successive occurrence of the bubble, slug, churn and annular flow regimes (Owen, 1986). For the large diameter (127 mm) pipe used in the present work, the sequence of regimes is less visible. The changes in pressure drop associated with the bubble/slug transition are absent, probably reflecting the absence of slug flow in larger diameter pipes. At higher gas velocity, the pressure drop falls continuously with gas velocity for a fixed liquid velocity. In this region there is a liquid film with a fluctuating flow direction (as evidenced by the directional shear stress measurements); this region has many of the characteristics of the churn flow region as described by Hewitt et al (1985). However, data at higher gas velocity would be required to confirm this.

6) Together with the data by Omebere-Iyari (2006) the current work can represent a very important two-phase pressure drop profile for large

diameter pipes covering a wide range of gas flow rates as such profile is visibly different from smaller pipes and not appear to be reported so far in the literature.

7) Kutateladze number has indicated the changes in the trend of pressure drop profile in the churn-annular transition region for the present work, especially, for low liquid flow rates, however, the reversal flow point not reached according to the flow reversal phenomenon. Bearing in mind that in the calculation of former parameter the effect of diameter pipe not taken into account however that effect has been considered in the dimensionless gas velocity (U_g^*).

8) The separated flow model based on Chisholm (1967) algebraic correlations was the best among other correlations that tested against current data. The Beggs and Brill (1973) correlation gives a significant over-prediction of pressure drop compared to the present data whereas the homogeneous model and the correlation of Friedel (1979) gave a significant under-prediction.

9) Glue-on hot film probes are flexible enough to take the shape of the curvature of the inner diameter of the pipe and hence they do not disturb the flow. Besides, it is not noticeably interferes with other measurement techniques of other parameters, However it requires a high level of care to be taken during the measurement.

10) Mean values of wall shear stress obtained using commercial glue-on hot films can be affected since it can not detect the direction of the flow, therefore the term magnitude wall shear stress is more accurate to be used.

11) Multiple hot films can be manufactured to detect the axial direction of the flow as well as the magnitude of the wall shear stress.

12) According to the time-varying wall shear stress results no completely unidirectional upward flow was observed over the range of the conditions studied, and as the gas velocity decreased, the flow became more oscillatory.

13) The magnitude mean wall shear stress from the commercial glue-on hot film probes shown an acceptable agreement with those obtained from the directional hot film probes, however, the directional mean wall shear was lower due to the negative signs from the direction changes of the flow over the range of the conditions studied.

14) Micro pillar sensors (MPS) with some further developments can be used for the detection of two-dimensional time varying and mean wall shear stress in two phase flow.

15) The comparison between the conductance ring probes and conductance pin probes shown that both techniques can capture the

low frequency structures but only the pin probes for the local film thickness measurement can provide the smaller scale, high frequency data. Some details of the film roughness can be missing in the data by conductance ring probes due to the averaging nature.

16) The sudden change that has been observed at low liquid flow rate in the pressure drop file to a gradual decrease with increase of gas flow rate is suggested to be linked to a transition of flow regime from churn to annular flow, however, the time-averaged total pressure not shown a clear minimum. Besides the time-averaged wall shear stress not reached the zero point.

17) The variation of time-averaged liquid film thickness with the gas and liquid superficial velocity has almost a similar trend as the total pressure drop. Over all, the liquid film thickness decreases with increasing gas velocity and decreasing liquid velocity.

18) Time-averaged wall shear stress increases as the liquid velocity increases and decrease as the gas velocity increases at low and intermediate liquid flow rates however not clearly sensible to the variation of gas velocity at high liquid flow rate.

19) A noticeable relationship between the time-varying total pressure drop and the liquid film thickness that obtained from the conductance ring probes has been observed and a closer relationship between the time-

varying wall shear stress and the liquid film thickness that obtained locally from the pin probes and this may be accounted to the fact that first two parameters have been averaged however the last two parameters have measured locally. Over all the parameters measured simultaneously were related to each other as can be seen in the power spectrum density (PSD) results.

20) The time-varying data of film thickness shown that the roughness in the interface between the gas and the liquid is affected noticeably by variation of liquid and gas velocities which consequently effected the time-varying data of both the wall shear stress and the total pressure drop.

21) The mean wall shear stress data by Martin (1983) have shown a good agreement with the data of present work at available U_g^* from the two sources. Based on that the data obtained in this study can be considered as an extension for the wall shear stress measurement to a wider range of conditions in vertical two-phase flow down to a U_g^* value of 0.33 and together with those data obtained by Martin (1983) the results of this study can represent the wall shear stress profile in vertical pipes.

22) According to the visualization study the waves observed were localized circumferentially as reported previously by Azzopardi et al (1983).

23) From the results of directional wall shear stress and local liquid film thickness measurements and the visualization study the direction of the liquid film were investigated and following conclusions have been made:

- From the directional wall shear stress probes as stated also in point 4, no completely unidirectional upward flow has been observed over the conditions studied.
- The negative values of wall shear stress at gas superficial velocities > 15 m/s might be linked to the wave's characteristics on the liquid film according to the high speed videos recorded.
- On the basis of the information obtained from the local film thickness and the high speed images, two dimensional film flows are expected rather than only an axial flow.
- Structural velocity results suggest that the liquid film slowed down at gas velocities that are in the transition region between sudden to gradual decreases of the pressure drop profile. However zero wall shear stress point not reached.

7.2 Future work

It is clear that the room is still widely open for more investigations in large diameter vertical pipes. Based on the results of present work some of these

areas can be suggested as a further work:

- Extend current work by studying fluids which are closer in terms of physical properties to those typical for oil and gas production industry.

- Studying higher gas flow rates will help to elucidate further the annular flow in large diameter vertical pipes.

- Two-dimensional directional wall shear stress to be studied using the micro pillar sensors (MPS) with taking the improvements suggested during this study into consideration.

Nomenclature

A	Constant in Equation 5.4	
A	Cross sectional area	m^2
a	Overheating ratio	
a_i	Value of element i	
AM	Average or the arithmetic mean	
B	Constant in Equation 5.4	
C	Empirical constant in Equation 1.1	
D, d, d_o	Diameter of pipe	m
D_P	Mean diameter of the pillar	m
ΔP_f	Frictional Pressure drop	Pa
Δp^*	Dimensionless pressure drop given by Equation 2.5	
f_{LF}	Friction factor	
g	Gravitational acceleration	m/s^2
G_e^*	The dimensionless conductance of the two-phase flow	
h	Heat transfer coefficient from heated wall to the fluid	w/m^2 k
k	Thermal conductivity of the liquid	w/m k
Ku_g	Kutateladze number	
L_p	Height of the pillar	m
l	Distance between the pressure drop tapping holes	m
M_L	Mass flow rate of the liquid phase	kg/s
n	Number of values	
p	pressure (N/m^2)	N/m^2
P_i	periphery of the interface	m
R_c	Resistance of the cable to the hot film probes	ohm
Re_{LF}	Renold number	
R_0	Sensor resistance at ambient (reference) temperature	ohm
R_{ps}	Resistance of the probe support	ohm
R_1 and R_{int}	Internal resistances in the anemometer bridge	ohm
R_{var}	Variable resistance in the bridge	ohm
R_W	Resistance of the probe at its operating temperature	ohm

r_i^*	Dimensionless radius	
T_0	Ambient (reference) temperature	°C
T_W	Operating temperature	°C
U_g	Gas superficial velocity	m/s
U_g^*	Dimensionless gas velocity	
V	Voltage	Volts
v	Anemometer output voltage	Volts
v_5	5th lowest anemometer output voltage	Volts
v_m	Maximum anemometer output voltage	Volts
V_{max}	Maximum allowable erosional velocity	ft/s
x	Width of the probe	m
y	Momentum boundary laminar sub-layer	m
y	Distance from the wall	m
y^+	Dimensionless distance from the wall of the pipe	

Greek Symbols

α_0	Sensor temperature coefficient of resistance at T_0	1/°C
α	Thermal diffusivity of the liquid	m^2/s
δ	Liquid film thickness	m
δ_T	Thermal boundary layer	m
$\varepsilon_G, \varepsilon_g$	Gas void fraction	
μ, μ_L	Liquid viscosity	Ns/m^2
μ_E	Effective liquid viscosity for turbulent flow	Ns/m^2
ρ_c	Homogenous gas/droplets core density	kg/m^3
ρ, ρ_l	Liquid density	kg/m^3, (Ibm/ft^3)
ρ_g	Gas density	kg/m^3, (Ibm/ft^3)
ρ_m	Density of the gas-liquid mixture	kg/m^3, (Ibm/ft^3)
ρ^*	Dimensionless density	
σ	Surface tension	N/m
τ_i	Interfacial shear stress	N/m^2
τ_o	wall shear stress	N/m^2
τ_w	Wall shear stress	Pa
τ_{wn}	Normalized wall shear stress	

Subscripts

c	Cable
c	Core
f	Frictional
G , *g*	Gas phase
i	Interface
int	Internal
LF	Liquid film
m	Maximum
m	Mixture
0	Ambient (reference) conditions
p	Pillar
ps	Probe support
T	Thermal
var	Variable
W	Working conditions
w	Wall
wn	Normalized

Superscripts

*	Symbol of dimensionless
+	Symbol of dimensionless

Appendix A

Summary of the Experimental Campaigns

Table A.1 Pressure drop and liquid film thickness measurement campaign

Liquid Superficial Velocity, m/s	Gas Superficial Velocity, m/s	Liquid Superficial Velocity, m/s	Gas Superficial Velocity, m/s	Liquid Superficial Velocity, m/s	Gas Superficial Velocity, m/s
0.02	16.25	0.03	10.92	0.05	3.47
0.02	15.84	0.03	10.72	0.07	15.21
0.02	15.44	0.03	10.19	0.07	14.89
0.02	15.17	0.03	9.95	0.07	14.50
0.02	14.83	0.03	9.51	0.07	14.18
0.02	14.49	0.03	9.08	0.07	13.78
0.02	14.16	0.03	8.65	0.07	13.40
0.02	13.77	0.03	8.02	0.07	12.81
0.02	13.44	0.03	7.38	0.07	12.66
0.02	13.05	0.03	6.69	0.07	12.27
0.02	12.65	0.03	5.94	0.07	11.86
0.02	12.20	0.03	3.93	0.07	11.50
0.02	11.88	0.05	15.54	0.07	11.13
0.02	11.43	0.05	15.25	0.07	10.66
0.02	11.13	0.05	14.94	0.07	10.23
0.02	10.68	0.05	14.49	0.07	9.86
0.02	10.35	0.05	14.17	0.07	9.56
0.02	9.40	0.05	13.71	0.07	9.07
0.02	8.86	0.05	13.30	0.07	8.65
0.02	8.29	0.05	13.07	0.07	8.10
0.02	6.30	0.05	12.53	0.07	7.54
0.02	4.23	0.05	12.25	0.07	7.01
0.02	3.04	0.05	11.89	0.07	6.46
0.03	15.85	0.05	11.48	0.07	5.84
0.03	15.45	0.05	11.12	0.07	4.42
0.03	15.17	0.05	10.65	0.07	3.41
0.03	14.86	0.05	10.32	0.09	15.07
0.03	14.43	0.05	9.87	0.09	14.76
0.03	14.11	0.05	9.42	0.09	14.42
0.03	13.74	0.05	8.93	0.09	14.02
0.03	13.34	0.05	8.35	0.09	13.60
0.03	12.94	0.05	7.74	0.09	13.30
0.03	12.52	0.05	7.22	0.09	12.95

0.03	12.22	0.05	6.71	0.09	12.49
0.03	11.75	0.05	6.20	0.09	12.13
0.03	11.47	0.05	4.62	0.09	11.74
0.09	11.34	0.13	5.72	0.21	10.72
0.09	11.01	0.13	4.54	0.21	10.36
0.09	10.61	0.16	14.53	0.21	9.94
0.09	10.20	0.16	14.22	0.21	9.53
0.09	9.79	0.16	13.87	0.21	9.15
0.09	9.38	0.16	13.52	0.21	8.64
0.09	8.94	0.16	13.18	0.21	8.15
0.09	8.49	0.16	12.78	0.21	7.67
0.09	8.00	0.16	12.40	0.21	7.24
0.09	7.37	0.16	12.03	0.21	6.73
0.09	6.85	0.16	11.58	0.21	6.13
0.09	6.27	0.16	11.29	0.21	4.95
0.09	5.40	0.16	10.94	0.21	3.77
0.09	4.06	0.16	10.54	0.21	3.09
0.09	3.32	0.16	10.16	0.06	15.31
0.13	14.65	0.16	9.82	0.06	14.96
0.13	14.35	0.16	9.32	0.06	14.68
0.12	14.00	0.16	8.93	0.06	14.29
0.12	13.63	0.16	8.53	0.06	13.98
0.13	13.30	0.16	8.00	0.06	13.60
0.13	12.94	0.16	7.57	0.06	13.26
0.13	12.50	0.16	7.07	0.06	12.94
0.13	12.17	0.16	6.49	0.06	12.54
0.12	11.79	0.16	5.80	0.06	12.17
0.12	11.41	0.16	4.73	0.06	11.79
0.12	11.07	0.16	3.47	0.06	11.36
0.13	10.65	0.21	14.29	0.06	10.97
0.13	10.30	0.21	14.02	0.06	10.63
0.13	9.80	0.21	13.61	0.06	10.15
0.13	9.46	0.21	13.27	0.06	9.71
0.13	9.02	0.21	12.89	0.06	9.52
0.13	8.59	0.21	12.52	0.06	8.77
0.13	8.11	0.21	12.14	0.06	8.38
0.13	7.59	0.21	11.77	0.06	7.73
0.13	7.06	0.21	11.42	0.06	7.22
0.13	6.58	0.21	11.06	0.06	6.51
0.06	5.73	0.10	11.84	0.15	6.49
0.06	4.37	0.10	11.49	0.15	5.49
0.06	3.39	0.10	11.04	0.15	4.30
0.09	14.97	0.10	10.69	0.19	13.97
0.09	14.69	0.10	10.30	0.19	13.66
0.09	14.37	0.10	9.94	0.19	13.33
0.09	13.98	0.10	9.46	0.19	13.05
0.09	13.67	0.10	9.00	0.19	12.64

0.09	13.30	0.10	8.63	0.19	12.32
0.09	12.93	0.10	8.15	0.19	12.02
0.09	12.56	0.10	7.71	0.19	11.74
0.09	12.14	0.10	7.25	0.19	11.42
0.09	11.73	0.10	6.70	0.19	11.13
0.09	11.35	0.10	5.84	0.19	10.77
0.09	10.94	0.10	4.60	0.19	10.34
0.09	10.59	0.10	3.53	0.19	9.94
0.09	10.20	0.15	14.48	0.19	9.56
0.09	9.75	0.15	14.15	0.19	9.07
0.09	9.37	0.15	13.83	0.19	8.60
0.09	8.86	0.15	13.48	0.19	8.10
0.09	8.46	0.15	13.16	0.19	7.60
0.09	7.93	0.15	12.77	0.19	7.15
0.09	7.42	0.15	12.40	0.19	6.69
0.09	6.92	0.15	11.99	0.19	6.20
0.09	6.32	0.15	11.64	0.19	5.70
0.09	5.30	0.15	11.29	0.19	5.18
0.09	3.92	0.15	10.86	0.24	14.12
0.09	3.20	0.15	10.51	0.24	13.77
0.10	14.74	0.15	10.08	0.24	13.45
0.10	14.38	0.15	9.67	0.24	13.12
0.10	14.07	0.15	9.30	0.24	12.74
0.10	13.71	0.15	8.89	0.24	12.32
0.10	13.35	0.15	8.40	0.24	11.92
0.10	13.01	0.15	7.97	0.24	11.60
0.10	12.65	0.15	7.48	0.24	11.24
0.10	12.25	0.15	6.97	0.24	10.80
0.24	10.45	0.30	13.81	0.33	8.44
0.24	10.09	0.30	13.47	0.33	8.06
0.24	9.68	0.30	13.18	0.33	7.60
0.24	9.25	0.30	12.72	0.33	7.17
0.24	8.84	0.30	12.37	0.33	6.68
0.24	8.48	0.30	11.98	0.33	6.10
0.24	8.02	0.30	11.62	0.33	5.26
0.24	7.54	0.30	11.28	0.33	3.68
0.24	7.13	0.30	10.95	0.33	3.08
0.24	6.61	0.30	10.58	0.37	13.40
0.24	5.78	0.30	10.15	0.37	13.09
0.24	4.29	0.30	9.80	0.37	12.74
0.24	3.42	0.30	9.38	0.37	12.32
0.27	13.95	0.30	9.02	0.37	11.94
0.27	13.64	0.30	8.63	0.37	11.63
0.27	13.36	0.30	8.19	0.37	11.30
0.27	13.00	0.30	7.79	0.37	10.96
0.27	12.56	0.30	7.30	0.37	10.57
0.27	12.17	0.30	6.78	0.37	10.29

0.27	11.77	0.30	6.09	0.37	9.83
0.27	11.45	0.30	5.26	0.37	9.49
0.27	11.09	0.30	3.93	0.37	9.06
0.27	10.78	0.33	13.54	0.37	8.65
0.27	10.39	0.33	13.23	0.37	8.29
0.27	10.04	0.33	12.88	0.37	7.77
0.27	9.62	0.33	12.56	0.37	7.46
0.27	9.27	0.33	12.12	0.37	6.96
0.27	8.86	0.33	11.80	0.37	6.37
0.27	8.33	0.33	11.42	0.37	5.72
0.27	7.94	0.33	11.09	0.37	4.58
0.27	7.54	0.33	10.73	0.41	13.15
0.27	7.01	0.33	10.37	0.42	12.82
0.27	6.50	0.33	9.98	0.42	12.43
0.27	5.82	0.33	9.66	0.42	12.03
0.27	4.59	0.33	9.23	0.42	11.71
0.27	3.40	0.33	8.84	0.42	11.37
0.42	11.06	0.51	11.65	0.56	6.01
0.42	10.66	0.51	11.33	0.55	5.48
0.41	10.29	0.51	11.00	0.56	4.21
0.42	9.96	0.51	10.63	0.55	3.27
0.42	9.56	0.51	9.90	0.62	12.27
0.42	9.24	0.51	9.51	0.63	11.97
0.42	8.88	0.51	9.13	0.63	11.66
0.42	8.47	0.51	8.81	0.62	11.29
0.42	8.01	0.51	8.46	0.61	11.01
0.41	4.57	0.51	8.06	0.61	10.64
0.41	3.57	0.51	7.56	0.62	10.27
0.41	3.26	0.51	7.56	0.62	9.94
0.46	12.84	0.51	7.21	0.62	9.49
0.46	12.51	0.51	6.75	0.62	9.25
0.46	12.31	0.51	6.25	0.62	8.86
0.46	11.70	0.51	5.72	0.62	8.50
0.47	11.42	0.51	4.68	0.61	8.08
0.47	11.10	0.51	3.51	0.61	7.69
0.46	10.78	0.51	2.58	0.61	7.38
0.46	10.41	0.56	12.35	0.62	6.95
0.47	10.00	0.56	12.01	0.62	6.49
0.46	9.66	0.56	11.71	0.61	6.04
0.47	9.37	0.57	11.33	0.61	5.55
0.46	9.03	0.57	11.00	0.61	4.57
0.46	8.65	0.57	10.64	0.62	3.43
0.47	8.22	0.57	10.31	0.70	11.70
0.47	7.87	0.56	9.94	0.70	11.37
0.46	7.43	0.56	9.54	0.70	11.00
0.47	6.99	0.56	9.22	0.70	10.78
0.47	6.51	0.56	8.93	0.70	10.43

0.47	6.01	0.56	8.49	0.70	10.08
0.46	5.28	0.56	8.17	0.70	9.70
0.47	3.92	0.57	7.76	0.70	9.27
0.51	12.69	0.56	7.40	0.70	8.91
0.51	12.34	0.56	6.99	0.70	8.62
0.51	11.97	0.56	6.64	0.70	8.24
0.70	7.95	0.01	12.08	0.04	9.83
0.70	7.53	0.01	12.33	0.04	10.26
0.70	7.20	0.01	12.71	0.04	10.81
0.70	6.84	0.01	13.03	0.04	11.10
0.70	6.40	0.01	13.43	0.04	11.47
0.70	5.87	0.01	13.66	0.04	11.85
0.70	5.32	0.01	14.13	0.04	12.32
0.70	4.30	0.01	14.34	0.04	12.55
0.70	3.14	0.01	14.84	0.04	13.09
0.01	6.07	0.01	15.03	0.04	13.28
0.01	8.33	0.01	15.47	0.04	13.74
0.01	8.25	0.01	15.69	0.04	13.96
0.01	9.23	0.04	4.62	0.04	14.42
0.01	9.27	0.04	6.60	0.04	14.66
0.01	10.02	0.04	7.02	0.04	15.16
0.01	10.53	0.04	7.88	0.04	15.27
0.01	10.90	0.04	8.33	0.04	15.86
0.01	11.22	0.04	9.05		
0.01	11.56	0.04	9.43		

Table A.2 Pressure drop and locally measured liquid film thickness campaign

Liquid Superficial Velocity, m/s	Gas Superficial Velocity, m/s	Liquid Superficial Velocity, m/s	Gas Superficial Velocity, m/s	Liquid Superficial Velocity, m/s	Gas Superficial Velocity, m/s
0.008	16.13	0.02	15.45	0.05	12.36
0.008	15.67	0.02	15.09	0.05	11.97
0.008	15.37	0.02	14.77	0.05	11.25
0.008	15.07	0.02	14.48	0.05	10.40
0.008	14.78	0.02	14.06	0.05	9.50
0.008	14.40	0.02	13.77	0.05	8.56
0.008	14.11	0.02	13.38	0.05	7.39
0.008	13.78	0.02	12.95	0.05	6.16
0.008	13.46	0.02	12.74	0.05	3.33
0.008	13.13	0.02	11.75	0.10	14.89
0.008	12.79	0.02	11.14	0.10	14.55
0.008	12.02	0.02	10.29	0.10	14.25
0.008	11.36	0.02	9.50	0.10	13.87
0.008	10.63	0.02	7.80	0.10	13.50
0.008	9.80	0.02	6.30	0.10	13.18

0.008	8.66	0.04	15.93	0.10	12.79
0.01	15.59	0.04	15.11	0.10	12.44
0.01	15.32	0.04	14.49	0.10	11.94
0.01	15.01	0.04	13.42	0.10	11.62
0.01	14.66	0.04	12.88	0.10	11.27
0.01	14.38	0.04	11.73	0.10	10.51
0.01	14.04	0.04	11.41	0.10	9.63
0.01	13.72	0.04	9.93	0.10	8.82
0.01	13.41	0.04	9.56	0.10	7.74
0.01	13.07	0.04	8.49	0.10	6.57
0.01	12.70	0.04	7.75	0.10	4.77
0.01	12.31	0.04	6.24	0.14	14.85
0.01	11.58	0.05	15.44	0.14	14.06
0.01	10.88	0.05	15.15	0.14	13.16
0.01	10.03	0.05	14.83	0.14	12.35
0.01	9.19	0.05	14.49	0.14	11.66
0.01	7.94	0.05	14.09	0.14	10.84
0.01	6.59	0.05	13.80	0.14	10.16
0.01	3.43	0.05	13.49	0.14	9.30
0.02	16.20	0.05	13.17	0.14	8.43
0.02	15.85	0.05	12.75	0.14	7.67
				0.14	6.62
				0.14	4.99

Table A.3 Pressure drop, wall shear stress and liquid film thickness campaign

Liquid Superficial Velocity, m/s	Gas Superficial Velocity, m/s	Liquid Superficial Velocity, m/s	Gas Superficial Velocity, m/s	Liquid Superficial Velocity, m/s	Gas Superficial Velocity, m/s
0.01	16.30	0.04	13.42	0.10	11.51
0.01	15.44	0.04	12.88	0.10	11.09
0.01	14.76	0.04	11.73	0.10	10.27
0.01	14.00	0.04	11.41	0.10	9.59
0.01	13.27	0.04	9.93	0.10	8.78
0.01	12.61	0.04	9.56	0.10	7.79
0.01	10.90	0.04	8.49	0.10	6.79
0.01	9.39	0.04	7.75	0.10	5.73
0.01	5.97	0.04	6.24	0.14	14.85
0.01	3.42	0.05	15.57	0.14	14.06
0.02	16.52	0.05	15.12	0.14	13.16
0.02	15.46	0.05	14.20	0.14	12.35
0.02	15.04	0.05	13.44	0.14	11.66
0.02	14.13	0.05	12.24	0.14	10.84
0.02	13.64	0.05	11.63	0.14	10.16
0.02	12.62	0.05	10.91	0.14	9.30

0.02	12.18	0.05	10.03	0.14	8.43
0.02	11.14	0.05	9.31	0.14	7.67
0.02	10.13	0.05	8.47	0.14	6.62
0.02	8.97	0.05	7.40	0.14	4.99
0.02	7.59	0.05	6.29		
0.02	4.92	0.10	14.90		
0.04	15.93	0.10	14.36		
0.04	15.11	0.10	13.35		
0.04	14.49	0.10	12.45		

Table A.4 High speed visualization campaign

Liquid Superficial Velocity, m/s	Gas Superficial Velocity, m/s	Liquid Superficial Velocity, m/s	Gas Superficial Velocity, m/s	Liquid Superficial Velocity, m/s	Gas Superficial Velocity, m/s
0.014	16	0.04	11.73	0.21	9.93
0.014	14.38	0.04	11.41	0.21	8.14
0.014	13.07	0.04	9.93	0.21	6.13
0.014	11.58	0.04	9.56	0.41	13.14
0.014	10.03	0.04	8.49	0.41	11.71
0.014	3.43	0.04	7.75	0.41	10.28
0.04	15.93	0.04	6.24	0.41	8.87
0.04	15.11	0.04	3.81	0.41	3.56
0.04	14.49	0.21	14.28	0.41	3.02
0.04	13.42	0.21	12.88		
0.04	12.88	0.21	11.41		

Appendix B

Standard Operating Procedure and safety features of the Large Scale Two-phase Flow Closed Loop Test Facility

The gas-liquid two-phase flow experiments conducted in this study were carried out on the large scale closed loop test facility in the department of Chemical and Environmental engineering at Nottingham University. Figure 3.1 showing a data schematic flow diagram of the rig. Before the start of the experiments the operator must be familiar with the Process Assessment and Laboratory safety procedures and is required to wear sensible shoes and protective clothing including safety glasses. The standard operating procedure and safety features of the test facility used during this work can be summarized as the following:

A.1 Preliminary Procedure

Check equipments to ensure it is safe to operate:

- Ensure power is not turned on
- Locate and identify all valves, lines, compressor, separator and pumps.
- Ensure that all walkways and ladders are free of obstruction and all valves are easily accessible.

- Ensure that the Separator, S1 and Tank, T1 are approximately half full of water.

A.2 Start-up Procedure

- Choose the gas flow meter to be used and open the appropriate valves (VF1a and VF1b, or VF3a and VF3b) to create a pathway for the gas.
- Ensure valve VR is open
- Open valves VH1 and VH2 and ensure there is steady flow of cooling water
- Partially open Valves VP2, VC1 and VC2
- Open Valves VC3 – VC6
- Open VP1 and close partially VB1
- From the main air supply unit pressurize the system
- Switch on P2
- Start the compressor motors, M1 and M2
- Adjust the compressor motor speeds using the control panel (Figure B.1).
- Choose the liquid flowmeter (F2 or F4) to be used and open the appropriate valves (VF2a and VF2b, or VF4a and VF4b) to create a pathway for the liquid.
- Start P1

A.3 Shut-down Procedure

- Switch liquid pump P1 off using by the on/off switch and stop the compressor motors from the control panel.
- Switch off P2
- Depressurize the system by opening the safety valve on T1

A.4 Safety Features

Emergency stop buttons for the compressor and water pump are located on all three levels of the facility. The tank in the compressor section and the separator are fitted with a relief valve and bursting disc respectively, for emergency pressure relief. Air/water mixtures at low pressures present no toxic hazards.

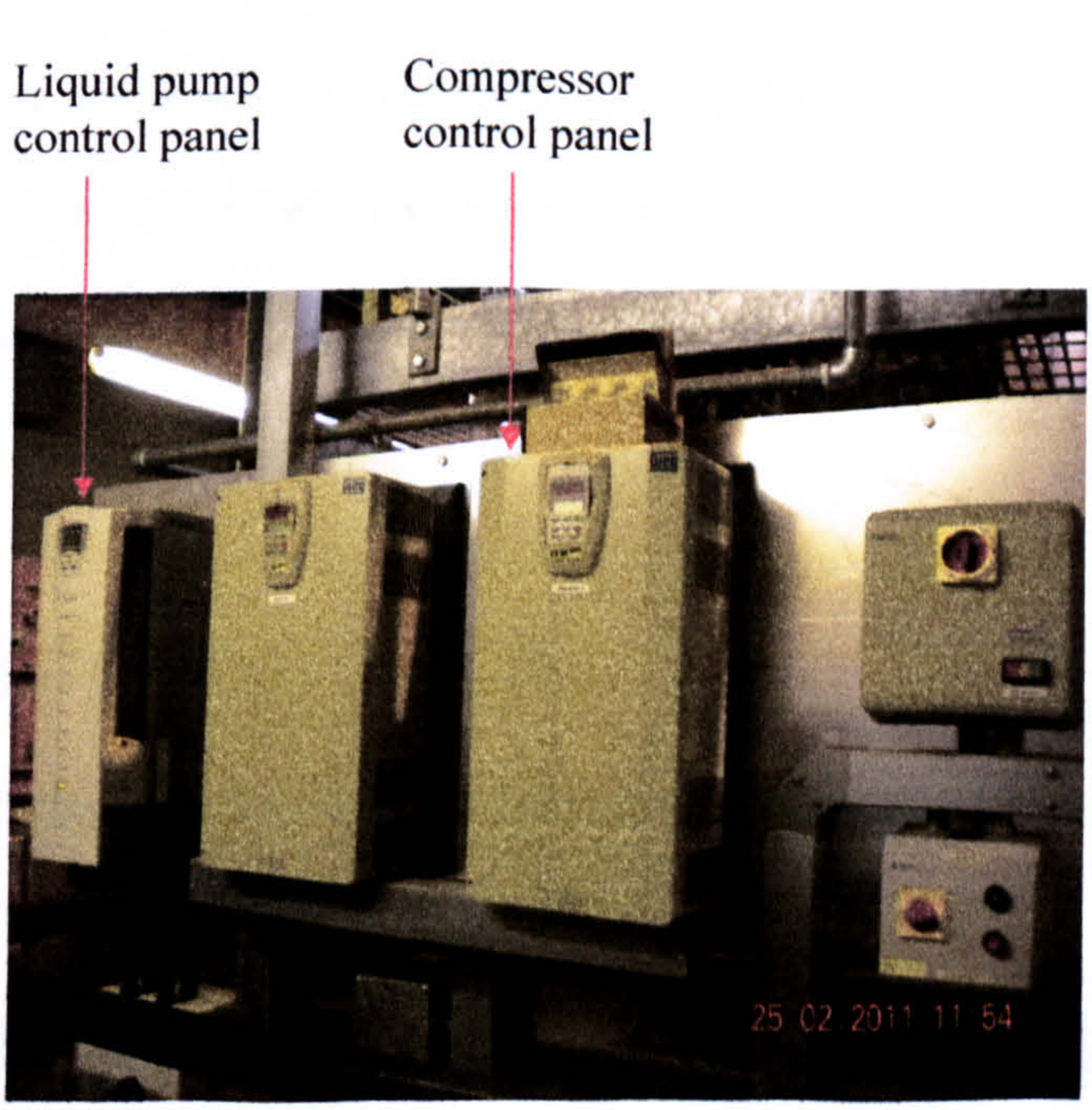

Figure A.1 showing the compressor and the liquid pump control panels

Appendix C

Operating Instructions for DISA Anemometer

Following is the operating instructions for DISA 55M system with 55M10 CTA, standard bridge (DISA type 55M10 instruction manual-1977):

C.1 Selecting and Installing Compensation Units:

When the 55M system is connected to the power supply and the correct line voltage been selected according to the local line voltage ,then check that the probe cable length indicated in the cable length window of the 55M10 standard bridge is suited for the measurement to be carried out (5 meters,20 meters, or 100 meters),if it is ,select a cable of the proper length ,if it is not ,replace the cable compensation unit accordingly.

C.2 Initial Setting of the Controls:

The controls should be set as the Following, before first applying power:

SQUARE WAVE	**OFF**
HF FILTER	**1**
VOLTS	**1**
FUNCTION	**STD.BY**
PROBE TYPE	**Depend (here FILM)**

GAIN	**1**
DECADE RESISTANCE	**00.00**

This initial procedure need not be repeated once the setup has been turned up. Thereafter it's only necessary to set the **FUNCTION** switch to **STD.BY** before removing power from the equipment. After power has been reapplied; the setup will be ready for operation when, after sufficient warm-up time has been allowed, the **FUNCTION** switch is set to **OPERATE**.

C.3 Applying Power:

Switch the power ON (on the back of the 55 M 05 units), and check the lamp when power applied, to make sure that shows the **POWER ON**, then the meter will deflect to the left to below zero.

Before beginning any measurement the instrument should be allowed to warm up. At least for 15 minutes (without loading it with probe current).temperature balance will be reached after approx. two hours operation at constant load (that is; with the probe current turned on). The length of the warm up time should choose on a basis of how much drift can be tolerated.

C.4 Measurement of Sensor Resistance:

When the probe is plugged to the probe socket, a lead resistance is introduced in the active arm of the bridge, in addition to the sensor resistance. The sensor lead resistance depends on the probe type and on the several of connection that are possible with it. It is composed of the probe cable used, the resistance of the probe support, and the resistance of the leads in the probe body (between

the connection and the sensor film). The last mentioned resistance is stated on the probe test card.

If the probe to be used is to be soldered to the support (as in the present study), the resistance of the probe support should be measured and the probe thereafter to the Support. To measure the mentioned resistance following steps must be followed:

- Plug the probe cable to be used into the probe socket and the free end of the probe cable should be terminated in reliable short-circuit.
- Turn the function switch to the RES.MEAS. Position. This should cause a change in meter reading) verify that the hand (needle) covers the red mark in the middle of the scale.
- Set the *ZERO OHMS screw until* the needle covers the red mark.
- Switch back to STAND.BY and connect the probe to the cable (replace it with the short circuit) [this will cause the meter reading to go below the ZERO.
- Set the resistance decade for the needle to move to cover the red mark in the middle. (The decade now indicates the resistance of the sensor and the lead at the temperature of medium the probe is exposed to.
- Now reduce the lead resistance from the resistance decade; this will change the meter again, by setting the ZERO OHMS, for the needle to move to cover the red mark again.
- Switch the function to STD.BY.

C.5 Calculation and Adjustment of Overheating Ratio:

Over heat ratio can be found from the following equation:

$R=R_O(1+a)$

R_O = Sensor cold resistance at ambient temperature (from the decade).

a= overheat Ratio.

NOW the decade resistance should be set at this value.

C.6 Closing the Servo Loop:

Turning the function switch to the operate position will close the servo loop, the probe will be heated, and the anemometer is in operation.

C.7 Balancing the Bridge:

Balancing the bridge is very important to optimize the dynamic response of the circuit, to balance the bridge:

- Expose the probe to a constant flow velocity (flow at lower velocity or even zero).
- Connect to oscilloscope with one of OUT sockets.
- Switch on the square waves (SQUARE WAVE switch) there are three frequencies depend on the type of oscilloscope pattern.
- Stepwise increase the GAIN switch until the response signal on the oscilloscope screen shows damped oscillations on the base line.
- Stepwise increase the HF FILTER switch setting, this will first reduce the oscillations will appear at the skirts of the signal, these oscillations can be compensated, by adjustment of CABLE COMPENATION Q

and L ,beginning with L ,if this doesn't completely eliminate the oscillations, different setting of Q should be tried ,thereafter again compensating with L. now the GAIN and HF FILTER switches may be advanced until damped oscillations reappear, these should be compensated as described above ,repeat this procedure until you reach the point where ,at certain settings of the GAIN and HF FILTER switches ,adequate compensation of the oscillation cannot be accomplished. Then back off one of the two switches or them both, if necessary until the oscillations disappear, the system consisting of probe, support, cable and anemometer is now adjusted to optimum frequency response for the measuring job to be performed.

If a measuring job makes no particular demands on band width, it is suggested that the HF FILTER and GAIN switches be backed **off** on completion of the adjustment procedure to the setting where only the required band width is obtained as the system will then be capable of exceedingly stable operation even under conditions of not quite optimum balance.

- Return the SQUARE WAVE switch to the OFF position and the FUNCTION switch to STD.BY.

C.8 Cover Plate:

This will ensure that the main unit controls will not be touched unintentionally, besides clearness will be improved.

Appendix D

Time-Varying Directional wall Shear Stress in 127mm Vertical pipe

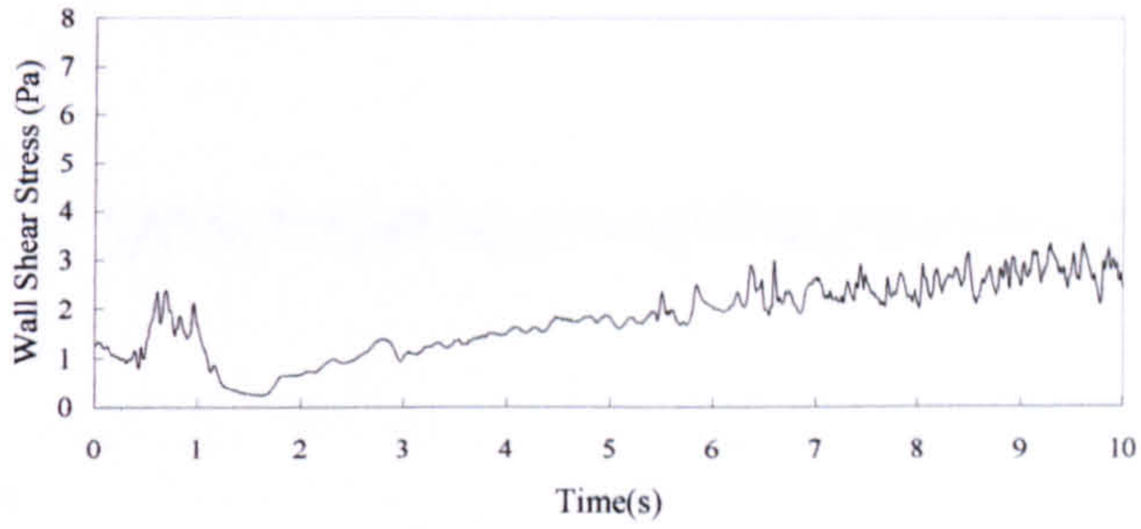

a

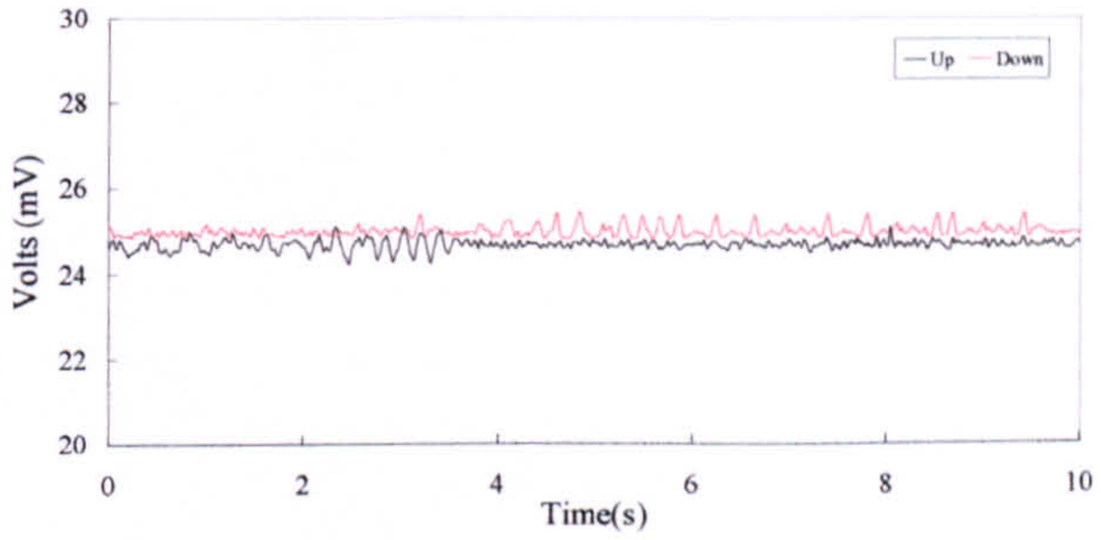

b

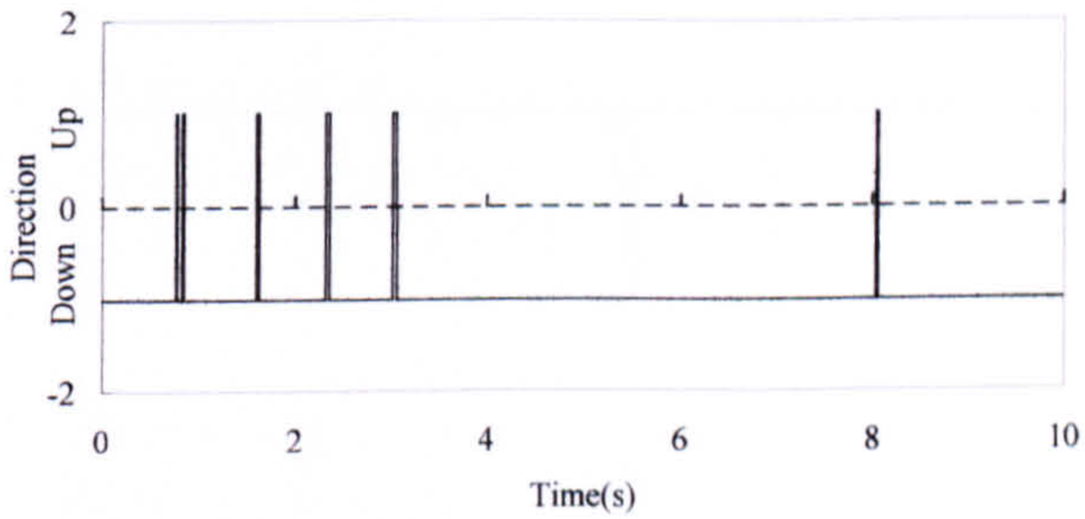

c

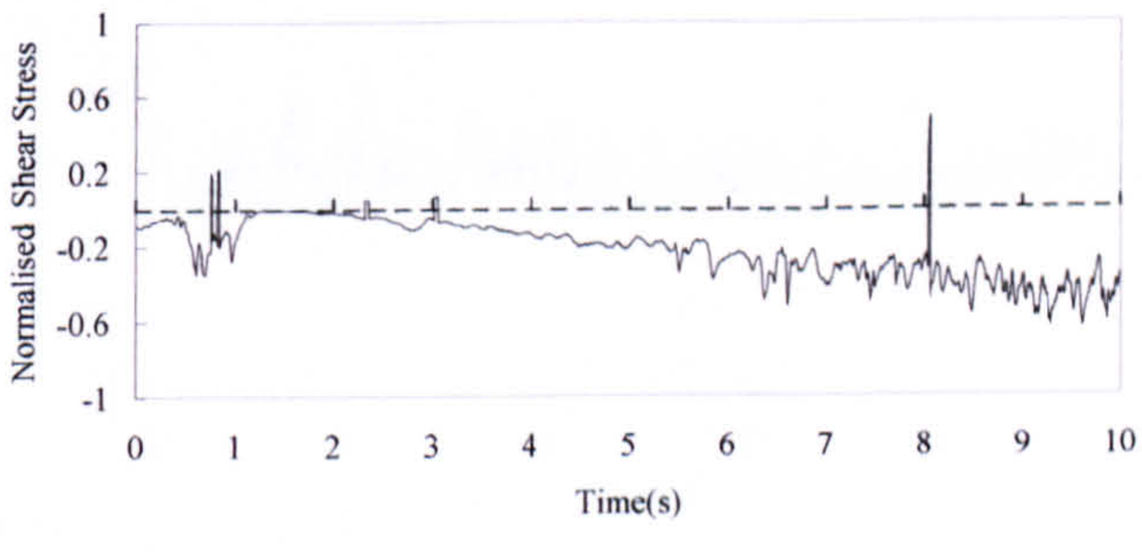

d

Figure D.1 The magnitude and direction of wall shear stress in single phase flow with change of direction

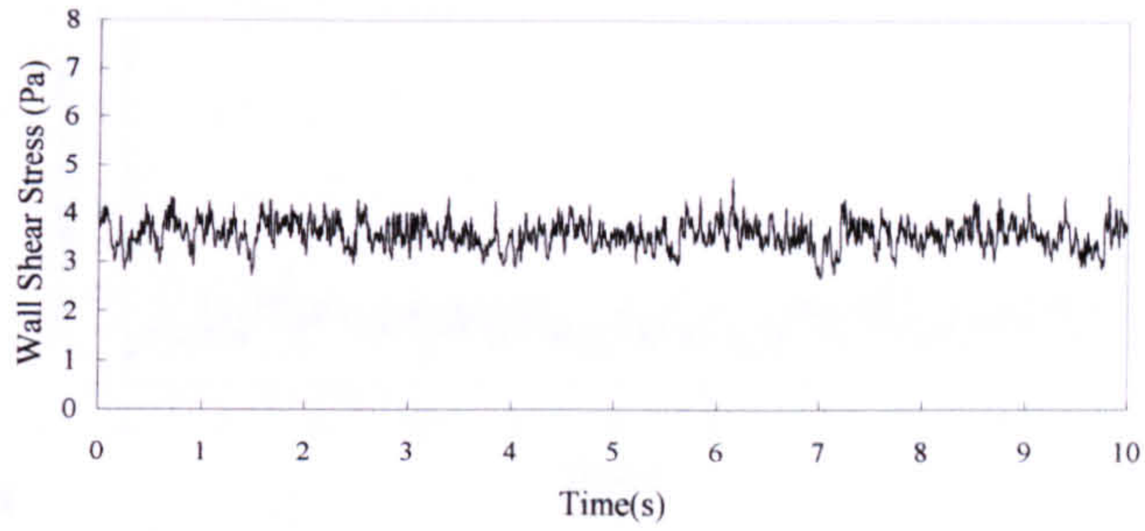

a

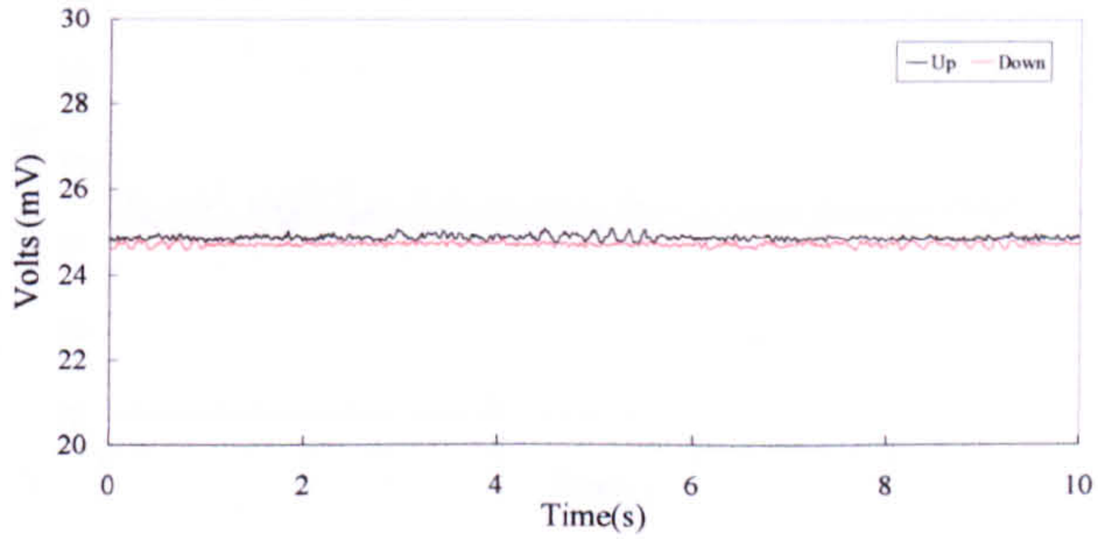

b

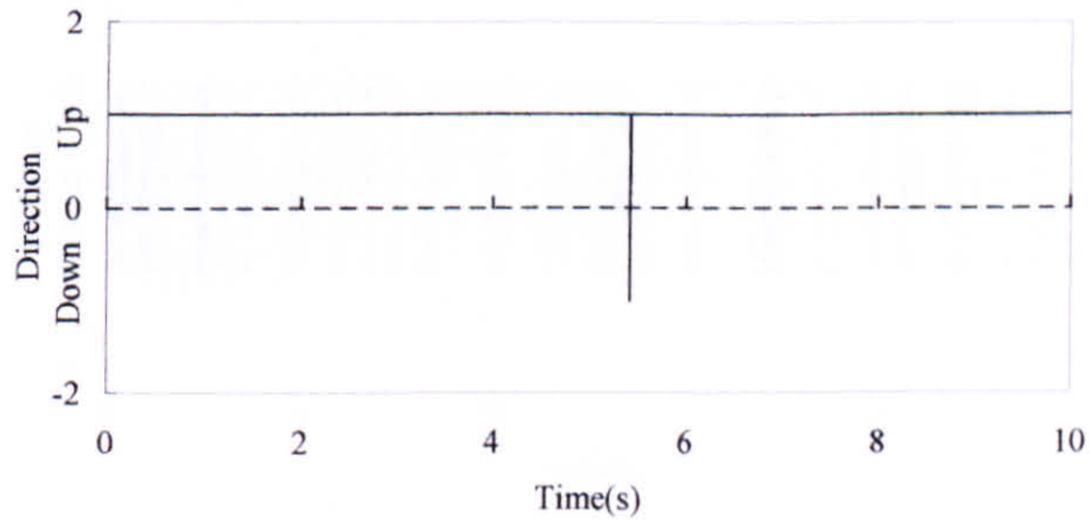

c

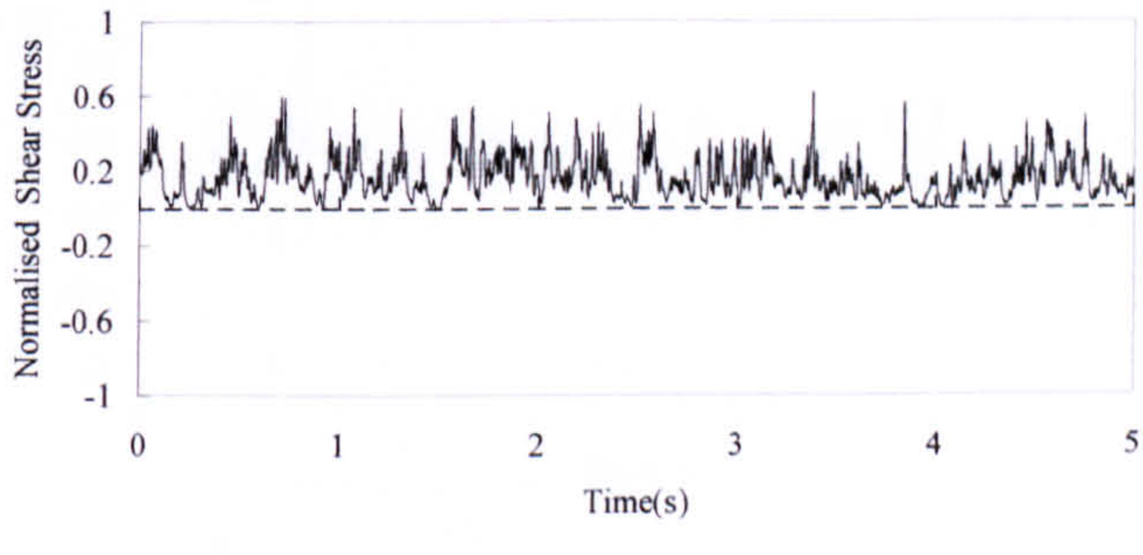

d

Figure D.2 The magnitude and direction of wall shear stress in single phase upward flow (U_L = 1.09 m/s).

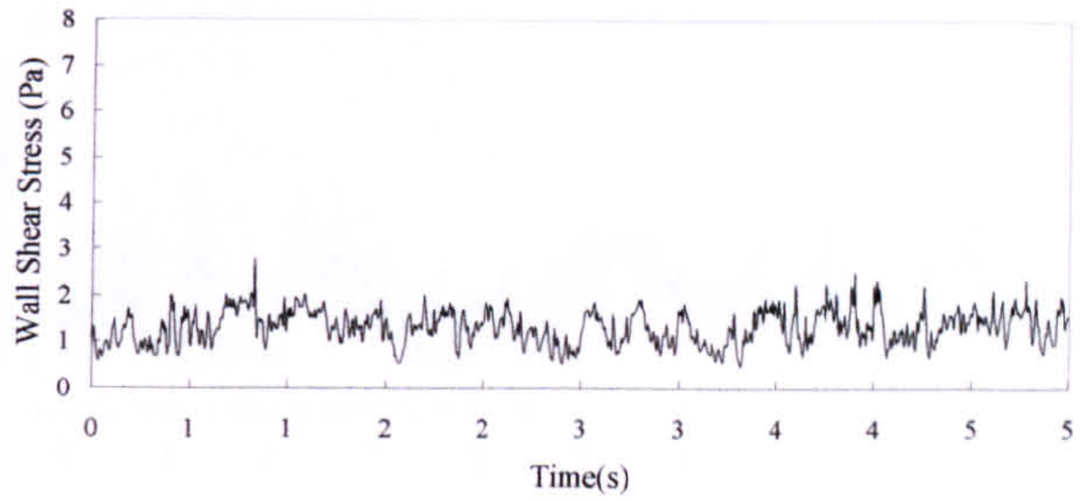

a

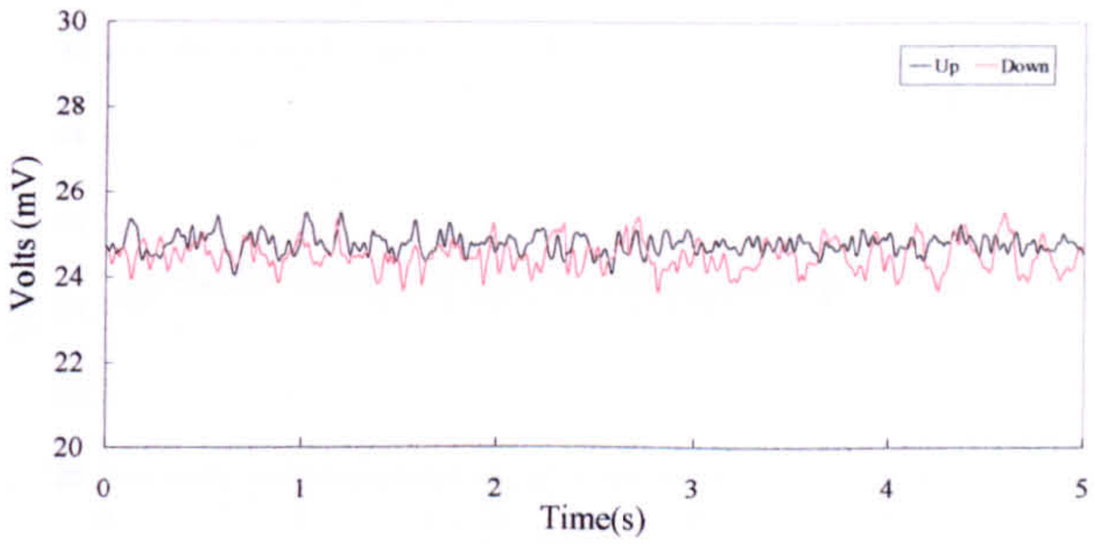

b

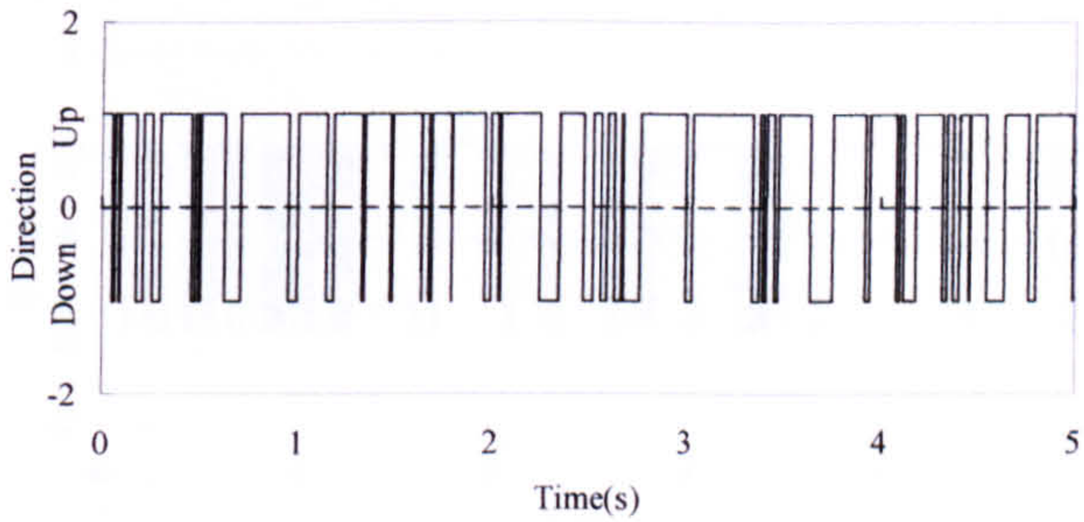

c

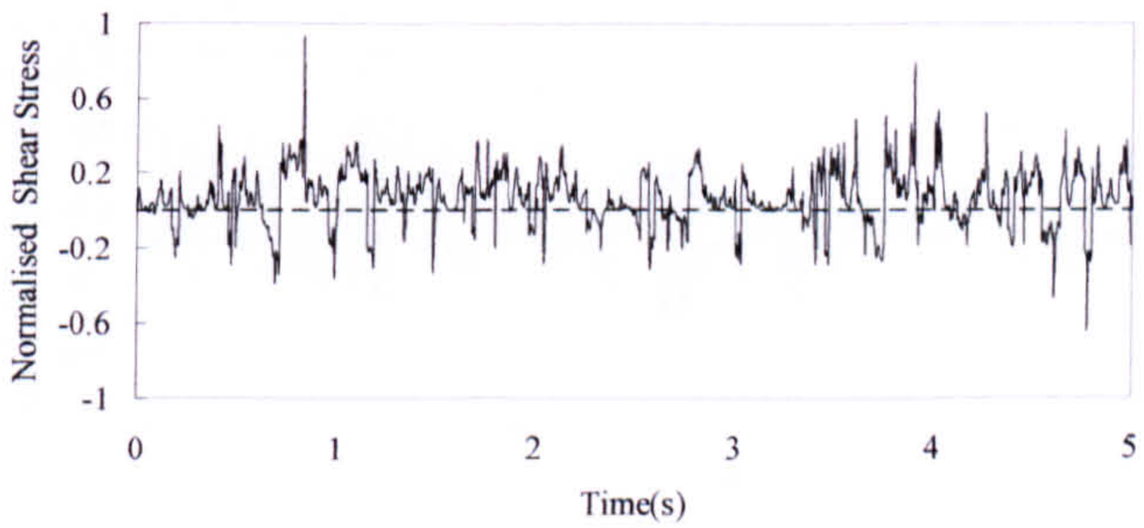

d

Figure D.3 The magnitude and direction of wall shear stress in two phase flow (U_{GS} = 12.2 m/s and U_{LS} =0.02m/s).

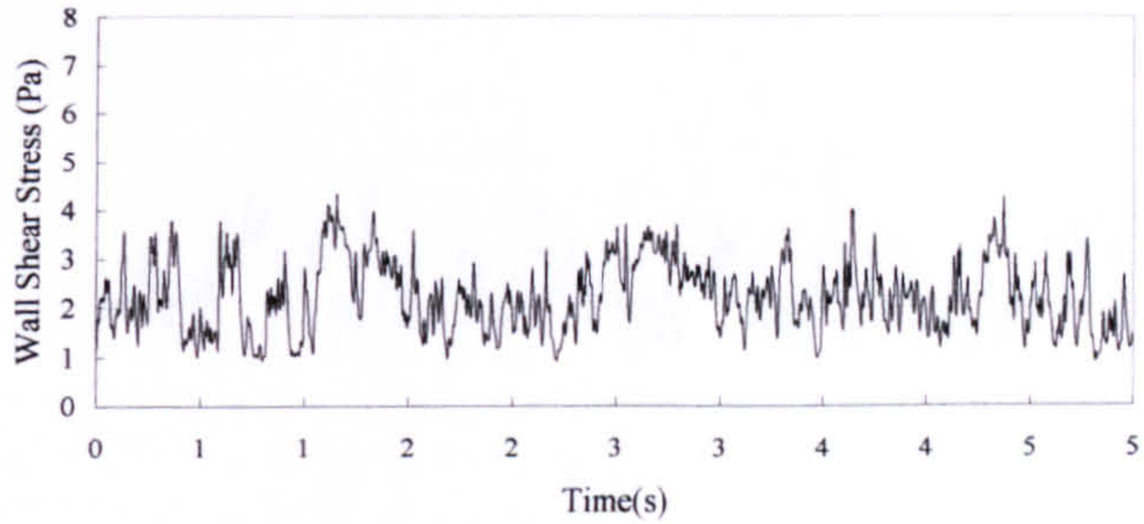

a

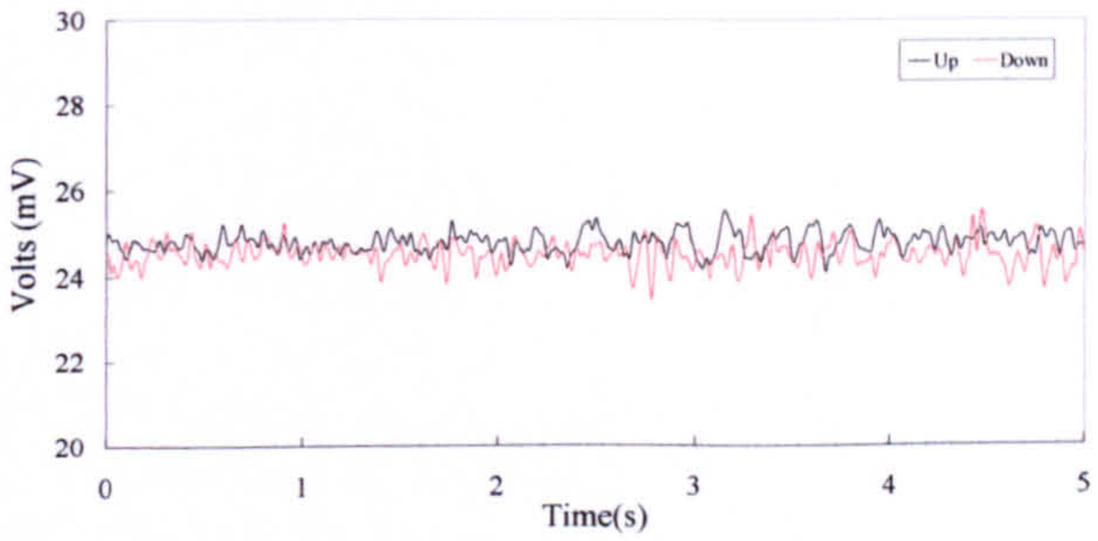

b

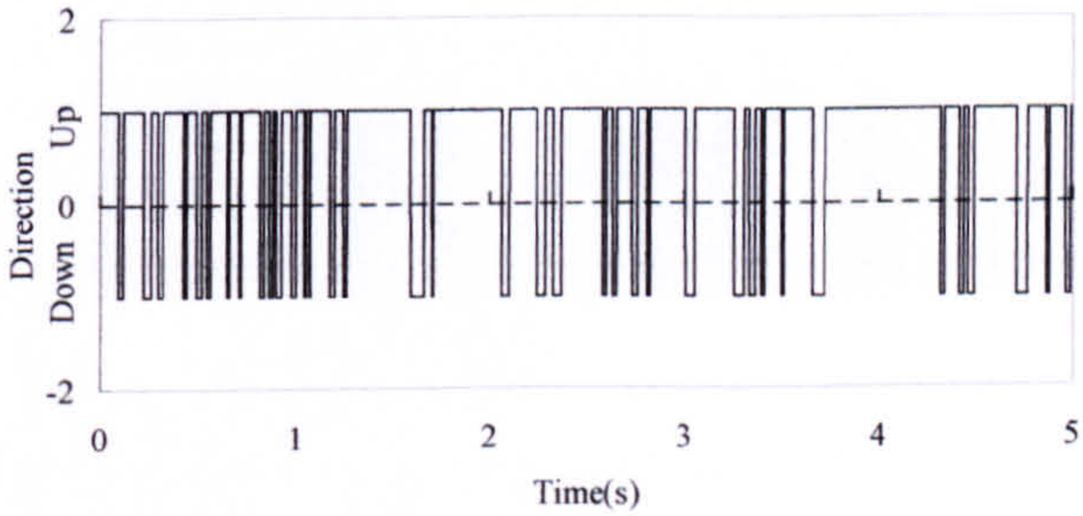

c

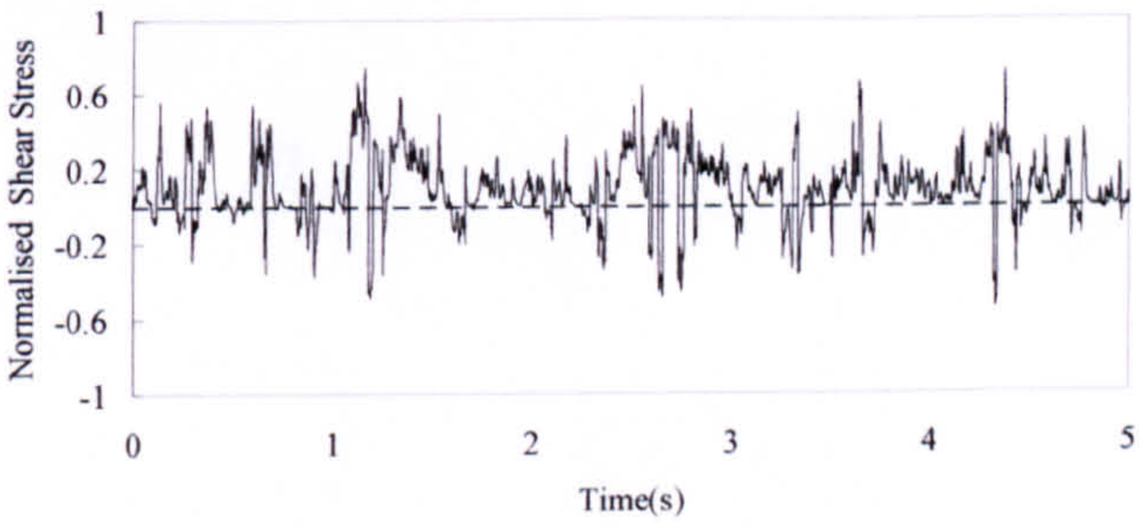

d

Figure D.4 The magnitude and direction of wall shear stress in two phase flow (U_{GS} = 16 m/s and U_{LS} =0.05m/s).

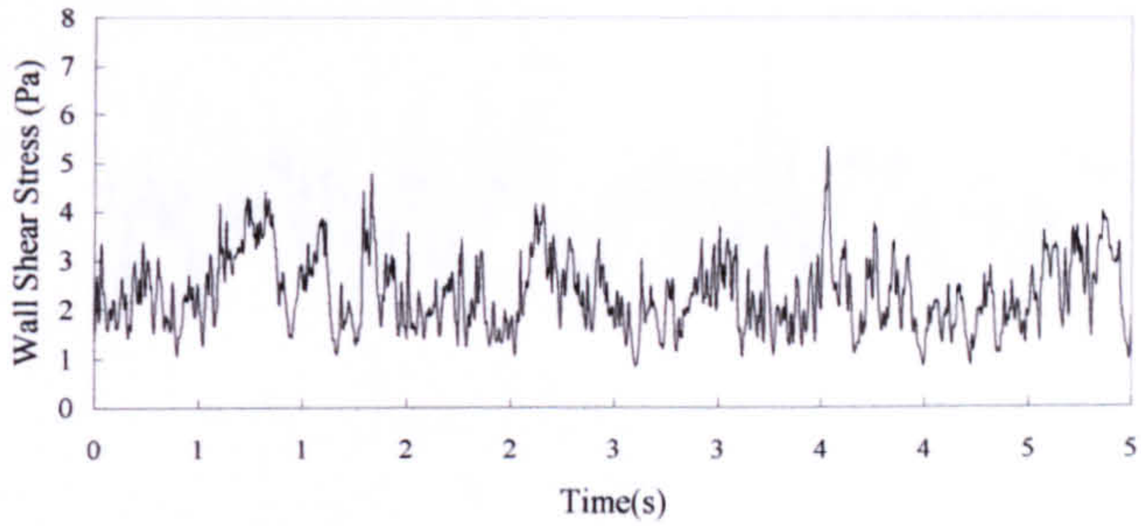

a

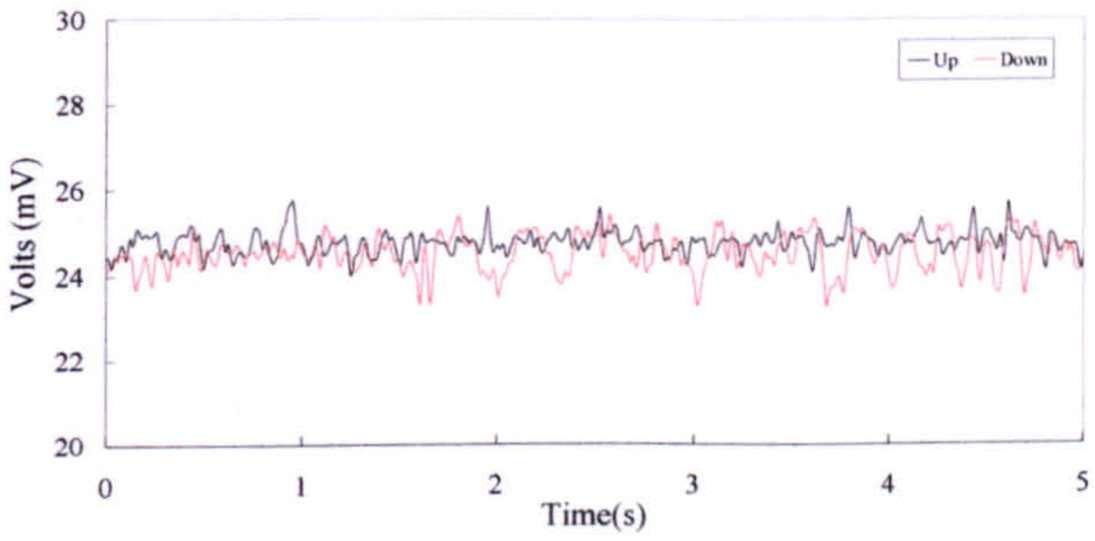

b

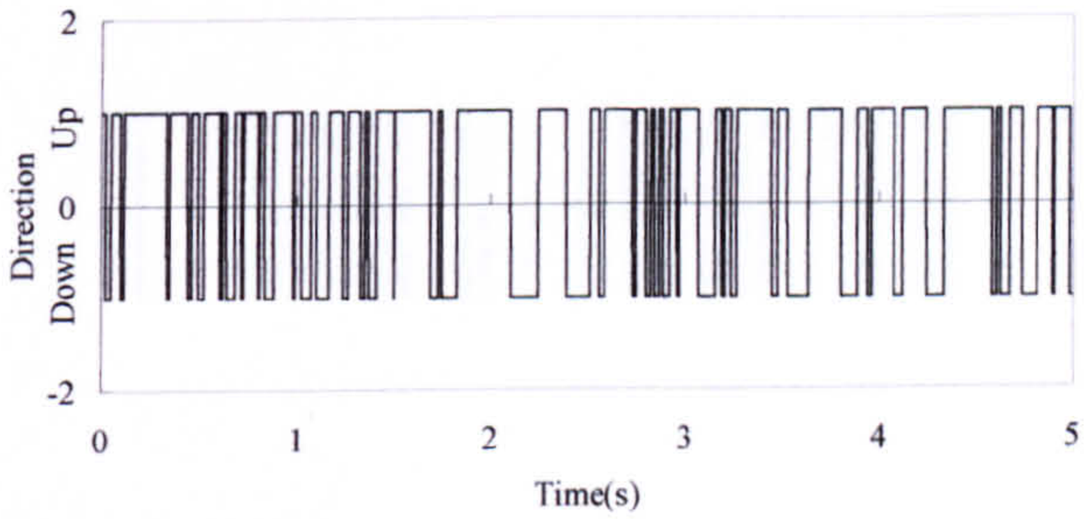

c

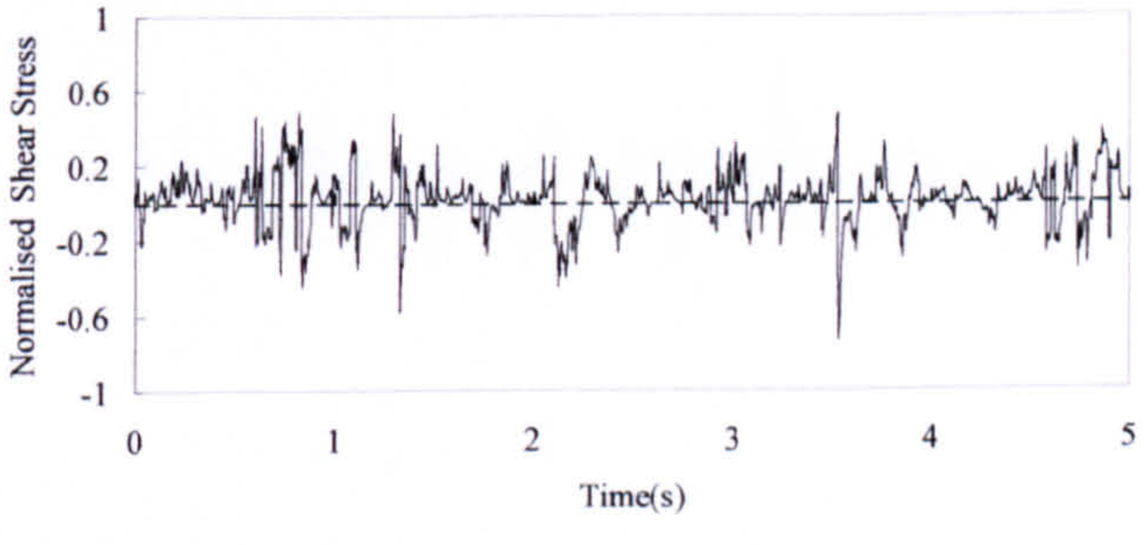

d

Figure D.5 The magnitude and direction of wall shear stress in two phase flow (U_{GS}= 11.8 m/s and U_{LS}=0.05m/s).

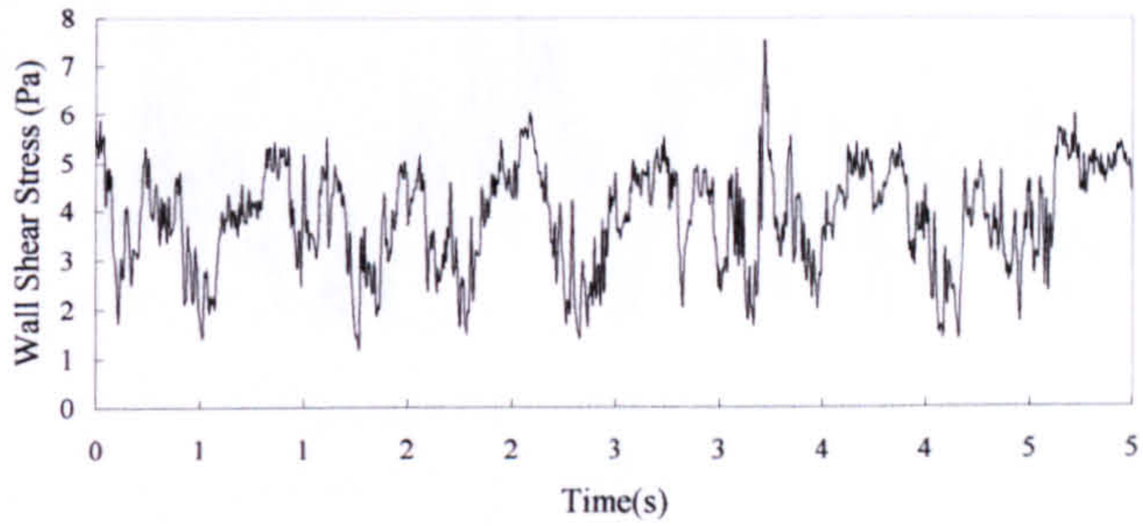

a

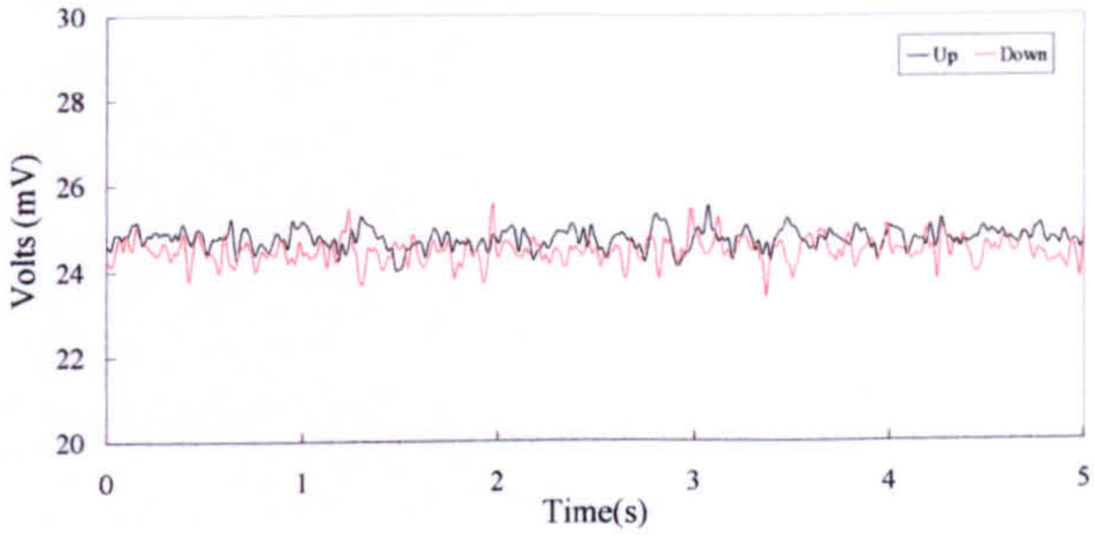

b

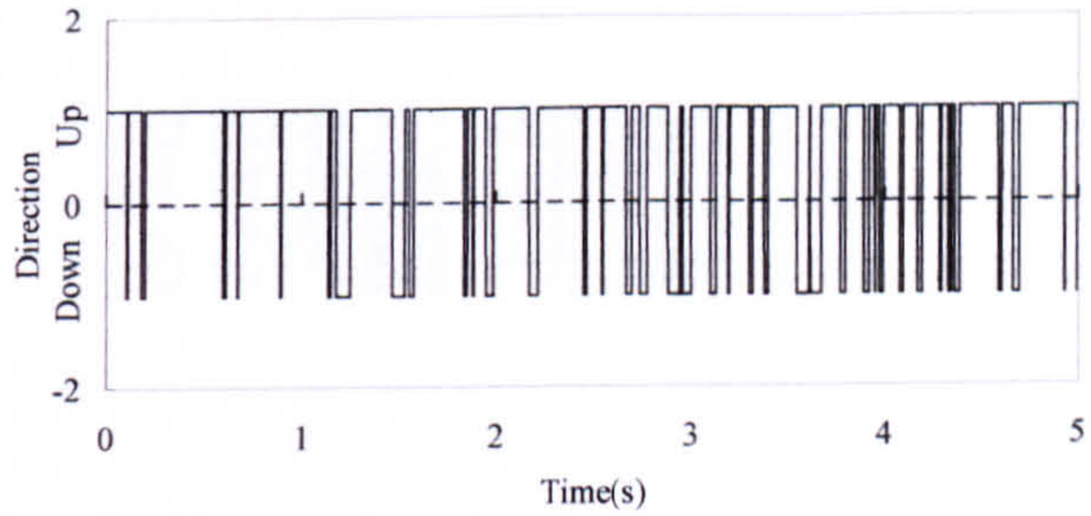

c

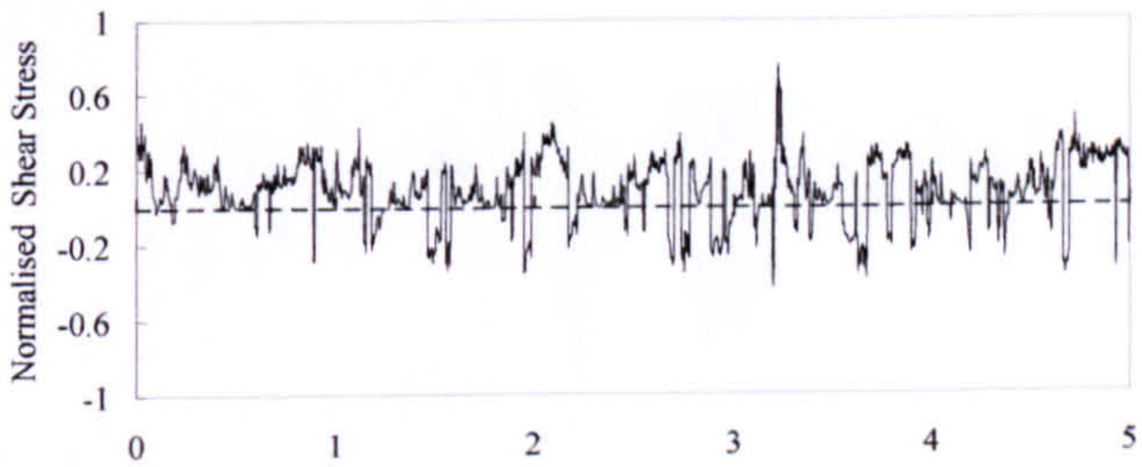

d

Figure D.6 The magnitude and direction of wall shear stress in two phase flow (U_{GS} = 6.2 m/s and U_{LS}=0.05m/s).

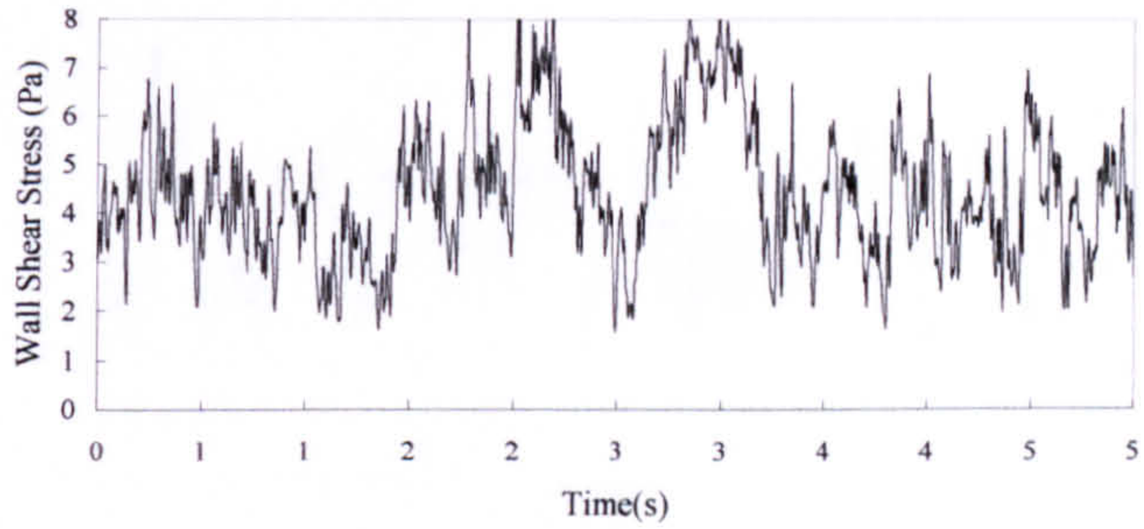

a

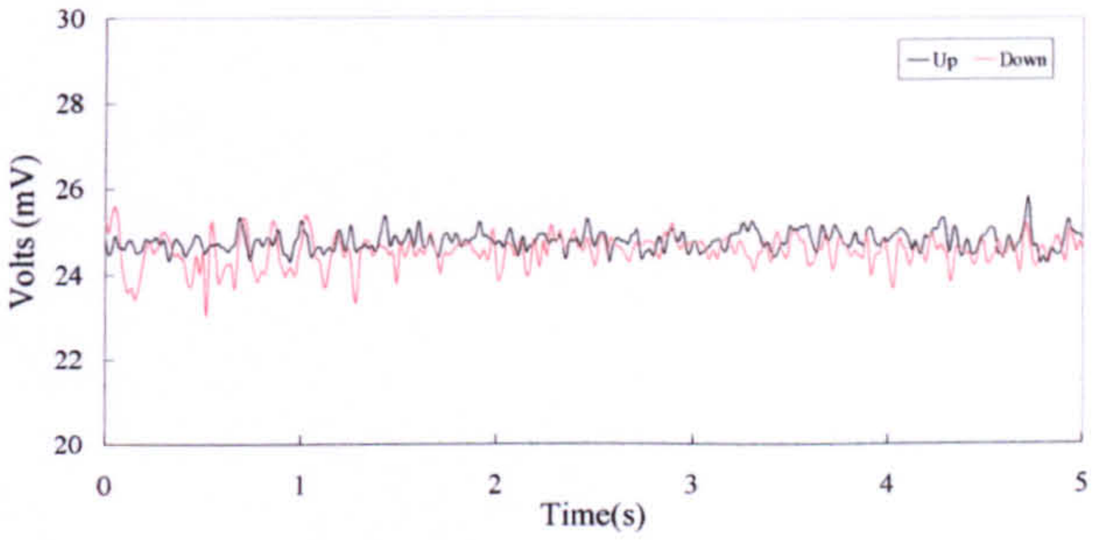

b

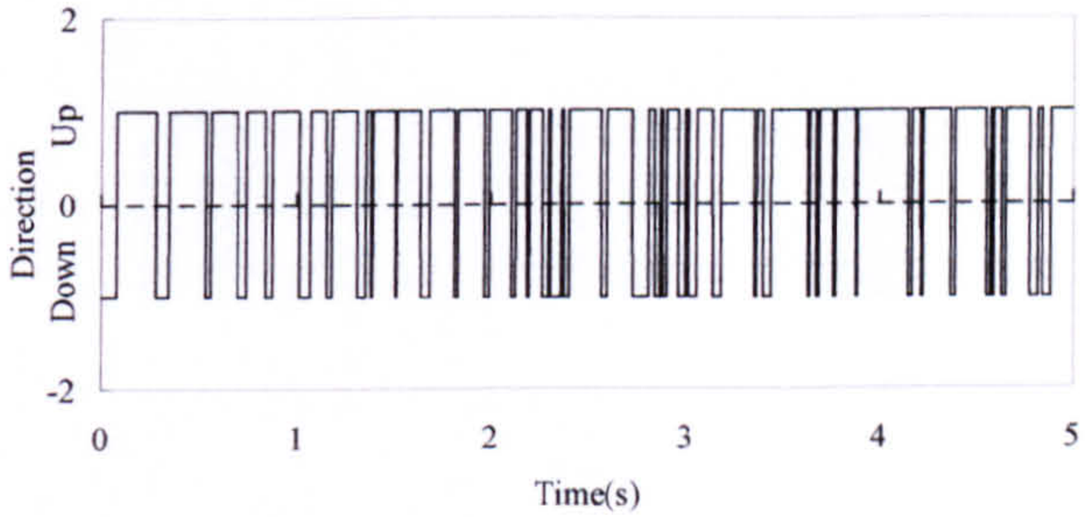

c

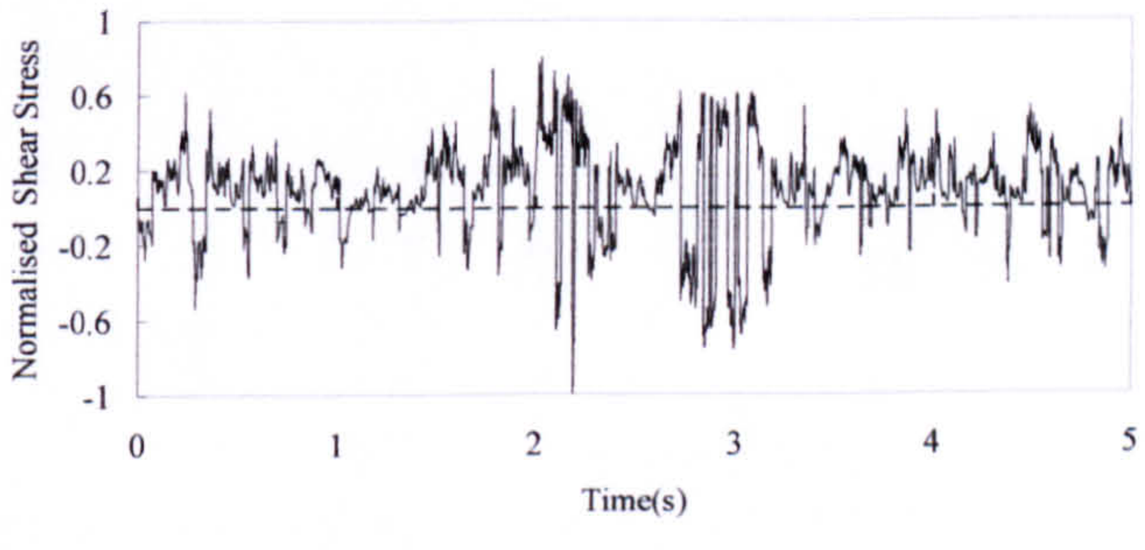

d

Figure D.7 The magnitude and direction of wall shear stress in two phase flow (U_{GS} = 15.1 m/s and U_{LS} =0.1m/s).

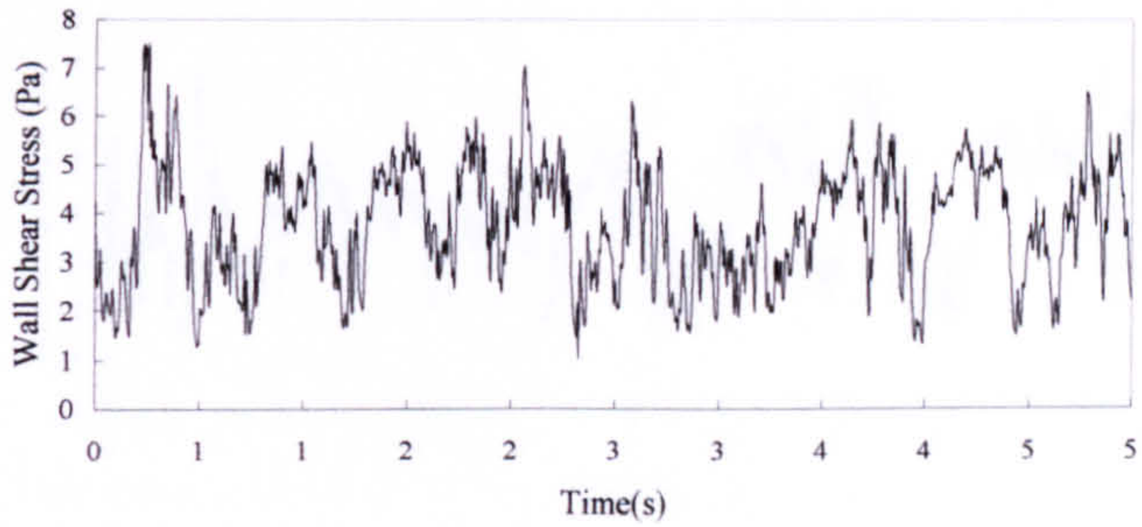

a

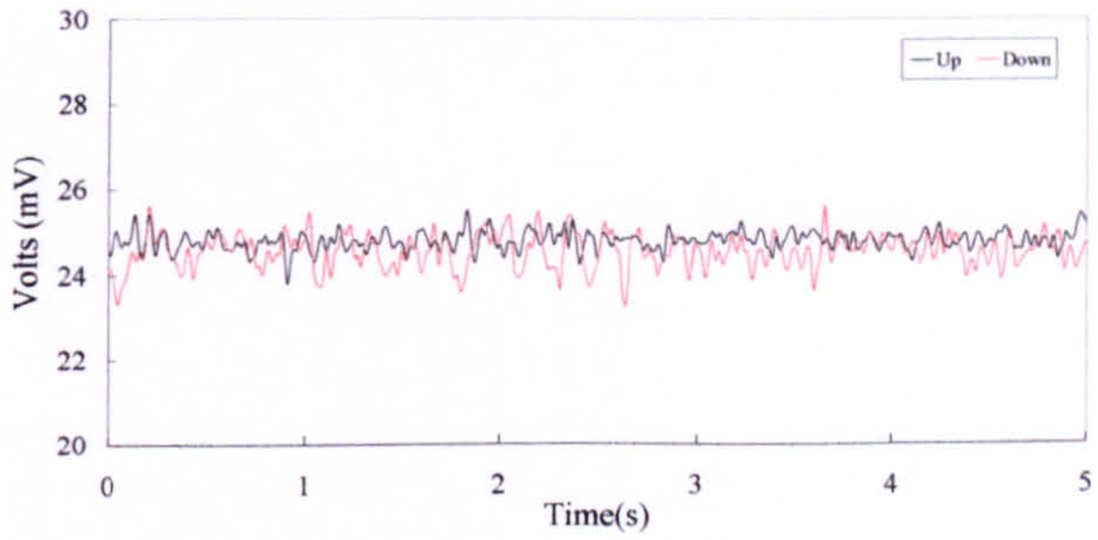

b

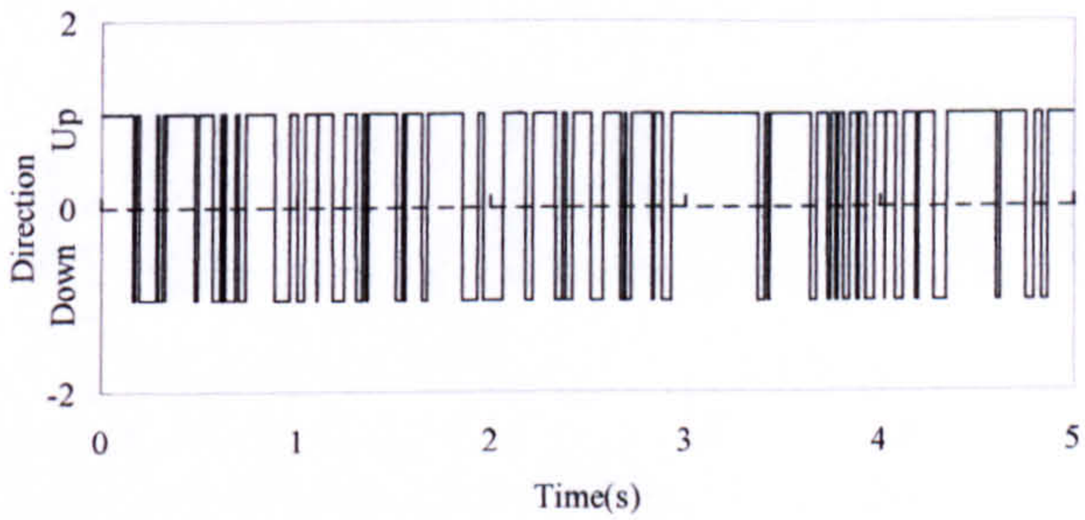

c

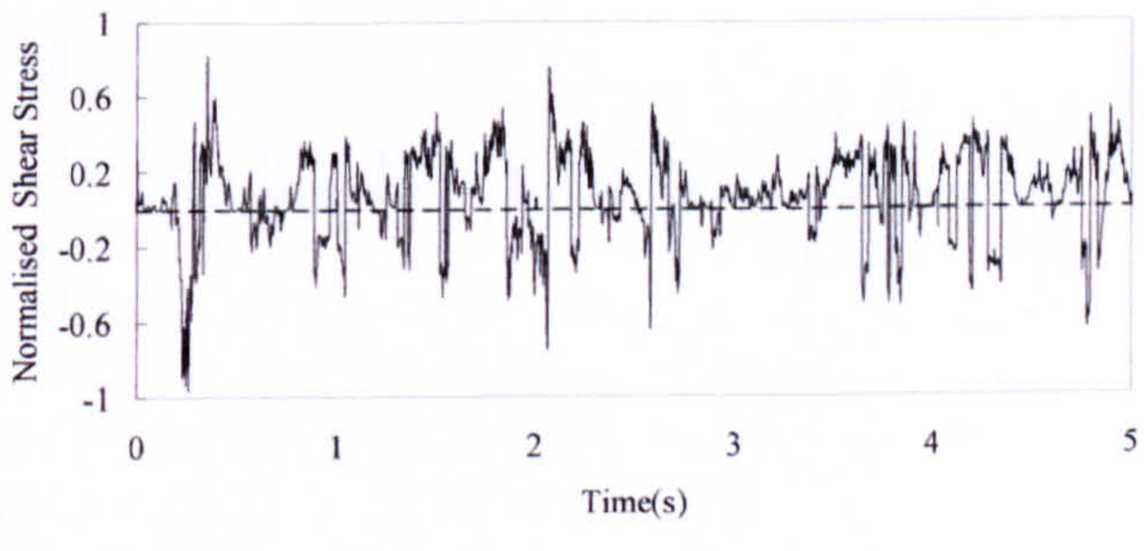

d

Figure D.8 The magnitude and direction of wall shear stress in two phase flow (U_{GS} = 10.6 m/s and U_{LS} =0.1m/s).

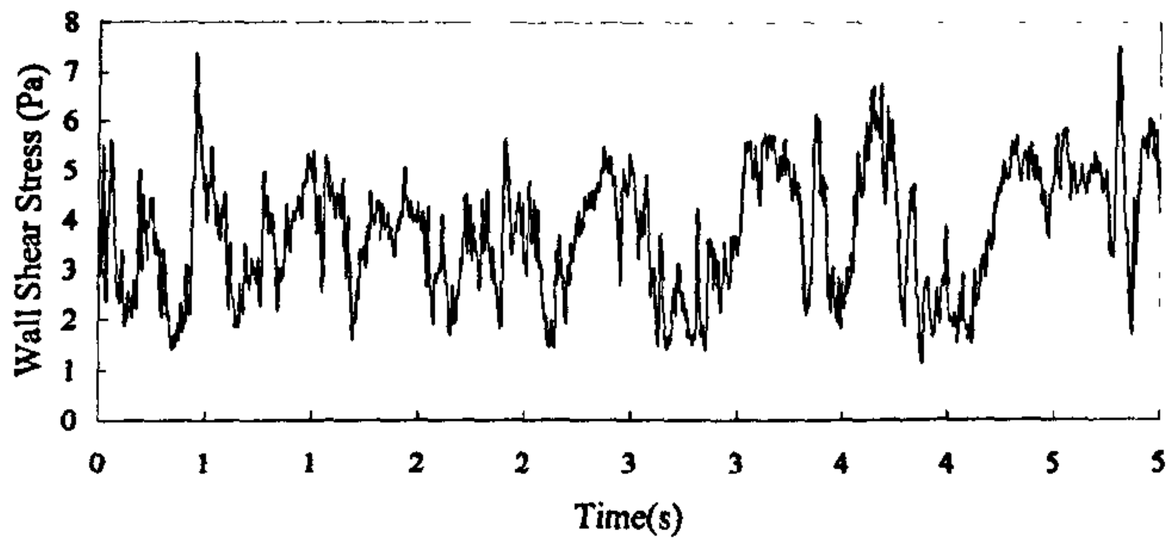

Figure D.9 The magnitude and direction of wall shear stress in two phase flow (U_{GS} = 6.6 m/s and U_{LS} =0.1m/s).

References

Azzopardi, B. J., Wren, E., (2004), "**What Is Entrainment In Vertical Two-Phase Churn Flow?**", *International Journal of Multiphase Flow, Vol. 30*, **pp.89–103**.

Azzopardi, B. J., (2006), "**Gas-Liquid Flows**", *Pub. Begell House, Inc.*

Azzopardi, B. J., Taylor, S., and Gibbons, D. B., (1983), "**Annular Two Phase Flow in a Large Diameter Tube**", *Int. conference on the physical modeling of multiphase flow, Coventry, England.*

Azzopardi, B. J. and, Whalley, P. B., (1980), "**Artificial Waves In Annular Two Phase Flow**" *ASME winter annual meeting, Chicago-published in Basic Mechanics in Two phase flow and Heat transfer.*

Badie, S., (2000) "**Horizontal Stratifying/Annular Gas-Liquid Flow**", *PhD Thesis, University of London.*

Belt, R. J., (2007), "**On the Liquid Film in Inclined Annular Flow**", *Ph.D. Thesis, Delft University of Technology.*

Boyer, C., Duquenne, A., Wild, G., (2002), "**Measuring Techniques in Gas–Liquid and Gas–Liquid–Solid Reactors**", *Chem. Eng. Sci., 57:3185–3215.*

Brill, J. P., and Beggs, H. D., (1991), "**Two Phase Flow in Pipes**", *6th edition, University of Tulsa.*

Brill, J. P., and Mukherjee, H., (1999), "**Multiphase Flow in Wells**", *Henry L.Doherty Memorial fund of AIME, Society of petroleum engineers Inc. Richardson, Texas.*

Brucker, C., Spatz, J., and Schroder, W., (2005), "**Feasibility Study of Wall Shear Stress Imaging Using Microstructured Surfaces With Flexible Micropillars**", *Exp. Fluids, 39, 464-474.*

Bruun, H. H., (1995), "**Hot-Wire Anemometry–Principles and Signal Analysis**", *New York: Oxford University Press.*

Bruun, H. H., (1996), "**Hot Film Anemometry in Liquid Flows**", *Meas. Sci. Technol., Vol.7, pp.1301-1312.*

Cheng, H., Hills, J. H., and Azzopardi, B. J., (1998), "**A Study of The Bubble To Slug Transition In Vertical Gas Liquid Flow In Columns Of Different Diameter**", *Int. J. Multiphase Flow, Vol. 24, No. 3, pp.431-452.*

Chisholm, D. A., (1967), "**Theoretical Basis For The Lockhart–Martinelli Correlation For Two-Phase Flow**" *Int. J. Heat Mass Transfer, Vol. 10, 1767–1778.*

Cicchitti, a., Lombardi, c., Silvestri, m., Soldani, g., and Zavatarelli, r. (1960), "**Two-phase cooling experiments - pressure drop, heat transfer and burnout experiments**". *energia nucleare* vol. 7, **pp 407-425.**

Cognet, G., Lbouche, M., and Souhar, M., (1984), "**Wall Stress Measurement By Electrochemical Probe For Gas-Liquid Two Phase Flow In Vertical Duct**", *AICHE Journal, Vol.30, No.2, pp.338-341.*

Coney, M.W.E., (1973), "**The Theory and Application Of Conductance Probes For The Measurement Of Liquid Film Thickness In Two-Phase Flow**", *J. Phys. E: Scient. Instrum., 6: 903-910.*

Conte, G., Azzopardi, B. J., (2003), "**Film Thickness Variation about a T-Junction**" *International Journal of Multiphase Flow 29, 305–328.*

Costigan, G., and Whalley, P. B., (1997), "**Slug Flow Regime Identification From Dynamic Void Fraction Measurements In Vertical Air-Water Flows**", *International Journal of Multiphase Flow*, Vol. 23, No. 2, **pp. 263-282.**

Cravarolo, L., Giorgini, A., Hassid, A., and Fedrocchi, E., (1964), " **A Device For The Measurement Of Shear Stress On The Wall Of A Conduit- Its Applications In The Mean Density Determination In Two-Phase Flow Shear Stress Data In Two-Phase Adiabatic Vertical Flow**", *CISE (Milan) Report No.R-82, (February 1964), pp.70.*

Descamps, M., Oliemans, R., Ooms, G., Mudde, R., (2008), "**Air–Water Flow in A Vertical Pipe: Experimental Study of Air Bubbles In The Vicinity Of the Wall**", *Experiments in Fluids, Vol. 45, No.2, pp. 357-370.*

Dijkstra, M., Van Baar, J. J., Wiegerink, R. J., Lammerink, T. S., De Boer, J. H., and Krijnen, G. J. M., (2005), " **Artificial Sensory Hairs Based On The Flow Sensitive Receptor Hairs Of Crickets**", *J. Micromech. Microeng., S132-S138.*

Engel, J., Chen, J., Liu, C., Bullen, D., (2006), "**Polyurethane Rubber All-Polymer Artificial Hair Cell Sensor**", *Journal of Microelectromechanical sysytems, 15 (5), 729-736.*

Etebari, A., (2008), "**Recent Innovations In Wall Shear Stress Sensor Technologies**", *Recent patents on mechanical engineering., Vol.1, No.1, pp.22-28.*

Fan, Z., Chen, J., Zou, J., (2002), "**Design And Fabrication Of Artificial Lateral Line Flow Sensors**", *J.Micromech.Microeng., Vol.12, pp.655-661.*

Fernholtz, H. H., Janke, G., Schober, M., Wagner, P.M., and Warnack, D., (1996), "**New Developments And Applications Of Skin-Friction Measuring Techniques**", *Meas. Sci. Technol., Vol. 7, pp. 1396–1409.*

Fortuna, G., and Hanratty, T. J., (1971), "**Frequency Response Of The Boundary Layer On Wall Transfer Probes**", *Int. J. Heat and Mass transfer, Vol.14, pp.1499-1507.*

Fossa, M., (1988), "**Design And Performance Of A Conductivity Probe For Measuring The Liquid Fraction In Two-Phase Gas–Liquid Flows**", *Flow Meas. Instrum., 9, 103–109.*

Friedel, L. (1979), "**Improved friction pressure drop correlations for horizontal and vertical two-phase pipe flow**", *European Two-phase Flow Group Meeting,* Ispra, Italy, Paper E2.

Govan, A. H., (1990), "**Modelling Of Vertical Annular And Dispersed Two-Phase Flows**", *Ph.D. Thesis, Imperial College London, UK.*

Govan, A. H., Hewitt, G. F., Owen, D. G., and Burnett, G., (1989), "**Wall Shear Stress Measurement In Vertical Air-Water Annular Two Phase Flow**", *Int. J. Multiphase Flow, Vol.15, No.3, pp.307-325.*

Grobe, S., and Shroder, W., (2008), "**Dynamic Wall Shear Stress Measurements In Turbulent Pipe Flow Using The Micro Pillar Sensor MPS**", *Int. J. Heat fluid flow, Vol.29, pp.830-840.*

Grobe, S., and Shroder, W., (2008), "**Mean Wall-Shear Stress Measurements Using The Micro Pillar Shear Stress Sensor MPS**" *Meas.Sci.Technol. Vol.19, pp.1-12.*

Guo Boyun, Lyons, C., W., Ghalambor, A., (2007), "**Petroleum Production Engineering: A Computer-Assisted Approach**", *Book Type : Hardback. Pages: 288.*

Hanratty, T. J., and Campbell, J. A., (1996), "**Measurements Of Wall Shear Stress**", *Fluid Mech.Measurements, (Ed. Goldstein R.J.), 2nd edition Pub. Taylor and Francis, Chapter 9,* ***pp. 575-648.***

Hernandez-Perez, V., Zangana, M., Kaji, R., and Azzopardi, B., J., (2010), "**Effect Of Pipe Diameter On Pressure Drop In Vertical Two-Phase Flow**", *7th Int. Conf. Multiphase Flow, ICMF 2010, Tampa, FL USA.*

Hernandez-Perez, V., (2007), "**Gas-Liquid Two-Phase Flow In Inclined Pipes**", *PhD thesis, University of Nottingham.*

Hewitt, G. F., Lacy, P. M. C., Nicholls, B.,(1965), "**Transition In Film Flow In A Vertical Tube**" *symposium on two phase flow, Exeter, 2 pp.* ***B401-B429.***

Hewitt, G. F., King, I., and Lovegrove, P. C., (1961), "**Holdup And Pressure Drop Measurement In The Two Phase Annular Flow Of Air-Water Mixtures**", *UKAEA Research Group. AERE R-3764.*

Hewitt, G. F., Martin, C.J., and Wilkes, N.S., (1985), "**Experimental And Modeling Studies Of Annular Flow In The Region Between Flow Reversal And The Pressure Drop Minimum**", *PCH PhysicoChemical Hydrodynamics, Vol.6, No.1/2,* ***pp.69-86.***

Hewitt, G. F., and Hall-Taylor, N. S., (1970), "**Annular two phase flow**", *pub.Pergamon.*

Hewitt, G. F., and Lovergrove, P. C., (1969), "**Frequency and Velocity Measurements of Disturbance Waves in Annular Two-Phase Flow**", *UKAEA Report AERE R-4304.*

Hewitt, G. F., and Wallis, G. B., (1963), "**Flooding And Associated Phenomena In Falling Film Flow In A Vertical Tube**", *UKAEA Report AERE R-4022.*

Hewitt, G. F., and Whalley, P. B., (1989), "**Vertical Annular Two Phase Flow**", *Multiphase Science and Technology, Vol.4, Chap.2, Hemisphere Publishing, New York.*

Hewitt, G. F., (1961), "**Analysis of Annular Two-Phase Flow; Application Of The Dukler Analysis To Upward Vertical Flow In A Tube**" *AERE-R3680.*

Hewitt, G. F., (1982a), "**Empirical Relationships For Frictional Pressure Gradient**", *Section 2.2.3 of "handbook of multiphase system", Ed. G.Hetsroni, Hemishpere publishing corporation, New York.*

Holt, A. J., (1996), "**Two Phase Pressure Drop and Void Fraction in Narrow Channels**", *Ph.D. Thesis, University of Nottingham.*

Jaeyoung Lee, P. E., (2009), "**Introduction to Offshore Pipelines and Risers**" *Lecture note, Houston, Texas.*

Jayanti, S., and Hewitt, G. F., (1992), "**Prediction Of The Slug-To-Churn Transition In Vertical Two-Phase Flow**", *Int. J. Multiphase Flow, Vol. 18, No. 6, pp.847-860.*

Jayanti, S., Tokarz, A., Hewitt, G. F., (1996), "**Theoretical Investigation of The Diameter Effect on Flooding in Counter-Current Flow**", *Int. J. Multiphase Flow, Vol. 22, pp.307-324.*

Jorgensen, F. E., (2002), "**How To Measure Turbulence With Hot-Wire Anemometers - A Practical Guide**", *by Dantec Dynamics, Publication no.: 9040U6151. Feb. 2002.*

Kaji, R., and Azzopardi, B. J., (2010), "**The Effect Of Pipe Diameter On The Structure Of Gas/Liquid Flow In Vertical Pipes**" *International Journal of Multiphase Flow, Vol.36, pp.303–313.*

Kaji, R., (2008), "**Characteristics Of Two-Phase Structures And Transitions In Vertical Upflow**", *Ph.D. Thesis, University of*

Nottingham.

Kaji, R., Omebere-Iyari, N. K., Hernandez-Perez, V., and Azzopardi, B. J., (2007), "**The Effect of Pipe Diameter on Flow Pattern in Vertical Upflow**", *6th Int. Conf. Multiphase Flow, Leipzig, Germany.*

Kirillov, P. L., Smogalev, I. P., Suvorov, M. Y., Shumsky, R.V., and Stein, Y., (1978), "**Investigation Of Steam-Water Flow Characteristics At High Pressures**", *Proc.* 6th Int. Heat Transfer Conf., Toronto, 1, **315-320.**

Koskie, J. E., Mudawar, I., and Tiederman, W.G., (1989), "**Parallel Wire Probes For Measurements Of Thick Liquid Films**", Int. J. Multiphase Flow, 15, **521–530.**

Kowalski, J. E., (1987), "**Wall And Interfacial Shear Stress In Stratified Flow In A Horizontal Pipe**", *AIChE J., Vol. 33, No. 2, pp. 274-281.*

Kutateladze, S. S., Burdukov, A. P., Nakoryakov, V., and Kuzmin, V. Z., (1969), "**Application Of An Electrochemical Method For The Measurement Of Shear Stress In Two Phase Flow**", *Heat Transfer Soviet Research, Vol.1, No.1, pp.66-73.*

Martin, C. J., (1984), " **The Non Intrusive Measurement Of Wall Shear Stress And Velocity Profiles In Vertical Annular Two Phase Flow**" *American Society of Mechanical Engineers, Heat Transfer Division HTD, Vol. 31, pp. 47-54.*

Martin, C. J., and Whalley, P. B., (1983), "**Wall Shear Stress Measurement In Annular Two-Phase Flow**", *BHRA First International Conference on the Physical modeling of multi-phase flow, Coventry, England, Paper G1.*

Martin, C. J., (1983), "**Annular Two-Phase Flow**", *Ph.D. Thesis, University of Oxford.*

McQuallin, K. W., (1985), "**Flooding In Annular Two Phase Flow**", *PhD thesis, Oxford University.*

Miller, G. E., (1980), "**Position Sensitivity Of Hot Film Shear Probes**", *J. Phys. E. Sci. Instrum., Vol.13., pp.973-976.*

Mishima, K., Hibiki, T., and Nishihara, H., (1995), "**Some Characteristics Of Air/Water Two-Phase Flow In Small Diameter Tubes**", *Proceeding of the 2nd international conference on multiphase flow, 95, 39-46, Kyoto, Japan.*

Ohnuki, A., Akimoto, H., and Sudo, Y., (1995), "**Flow Pattern And Its Transition In Gas-Liquid Two Phase Flow Along A Large Vertical Pipe**", *In: Proc. Of second Int. Conf. on Multiphase flow, 95-Kyoto, Vol.3, FT1-17-FT1-23.*

Ohnuki, A., and Akimoto, H., (2000), "**Experimental Study On Transition Of Flow Pattern And Phase Distribution In Upward Air Water Two Phase Flow Along A Large Vertical Pipe**", *Int. J. Multiphase Flow, Vol. 26, pp.367-386.*

Ombebere-Iyari, N. K., (2006), "**The Effect Of Pipe Diameter And Pressure In Vertical Two Phase Flow**", *PhD thesis, university of Nottingham.*

Omebere-Iyari, N.K., Azzopardi, B.J., Lucas D., Prasser H.M., (2008), "**The Characteristics Of Gas/Liquid Flow In Large Risers At High Pressures**", *International Journal of Multiphase Flow, Vol.34, pp.461–476.*

Owen, D.G., (1986), "**An Experimental and Theoretical Analysis of Equilibrium Annular Flows**" *PhD Thesis, University of Birmingham.*

Qing-F., Fu, Yang, L., Qu., y., (2010), "**Measurement Of Annular Liquid Film Thickness In Open End Swirl Injector**", *Aerospace Science and Technology,* doi:10.1016/j.ast.210.06.006.

Richter, H. J., (1981), "**Flooding In Tubes and Annuli**" *Int. J. Multiphase Flow, Vol. 7, pp. 647-658.*

Sawai, T., Kaji, M., Kasugai, T., Nakashima, H., and Mori, T., (2004), "**Gas-Liquid Interfacial Structure And Pressure Drop Characteristics Of Churn Flow**" *Experimental Thermal and Fluid Science, Vol. 28, 597-606.*

Sekoguchi, K., Takeishi, M., and Ishimatsu, T., (1985), "**Interfacial Structure In Vertical Upward Annular Flow**", *PhysicoChem. Hydrodynam., 6, 239-255.*

Shaha, J., (1999), "**Phase Interactions In Transient Stratified Flow**" *PhD Thesis, Imperial college of science, Technology of medicine, University of London.*

Sheplak, M., Cattafesta, L., Nishida, T., and McGinleys, C., (2004), "**MEMS Shear Stress Sensors: Promise And Progress**", *24th AIAA Aerodynamic Measurment Technology and Ground Testing Conference, AIAA2004-2606.*

Spedding, P. L., Woods, G.. S., Raghunathan, R. S., and Watterson, J. K., (1998), "**Vertical Two- Phase Flow; Part 111:** Pressure Drop" *Trans. IChemE., Vol. 76, Part A.*

Taitel, Y., (1999), "**Flow Pattern Transition In Two Phase Flow**" *an extended summary prepared for the 2nd Annual Meeting of the Institute of Multifluid Science And Technology, March 18-20.*

Taitel, Y., Barnea, O., and DUKLER, A. E., (1980), "**Modelling of glow pattern transitions for steady upward gas-liquid flow in vertical tubes**" ,*AIChE Jornal , Vol.26, No.3, pp.345-354.*

Tucker, C., Chen N., (2006), "**High-Sensitivity Bi Directional Flow Sensor Based on Biological Inspiration of Animal Hair-Cell Sensors**", *In: proceeding of the 5th IEEE sensors conference 2006.*

Van der Meulen, G. P., Zangana, M., Zhao, D., and Azzopardi, B. J., (2009), **"Phase Distribution Measurements By Conductance Probes And Pressure Drop In Gas-Liquid Flows"**, *7th World Conference on Experimental Heat Transfer, Fluid Mechanics and Thermodynamics, Krakow, Poland on June 28 - July 03.*

Vijayan, M., Jayanti, S., Balakrishnan, A. R., (2001), **"Effect of Tube Diameter on Flooding"**, *Int. J. Multiphase Flow, Vol. 27, pp. 797–816.*

Wallis, G.. B., (1961), **"Flooding Velocities For Air And Water In Vertical Tubes"**, *A.E.E.W.-R 123.*

Whalley, P.B., and McQuillan, K.W., (1985), **"The Development And Use Of Directional Wall Shear Stress Probe"** *Presented at 2nd Int. conf. on multiphase flow, London paper G2.*

Whalley, P.B., (1987), **"Boiling, Condensation and Gas-Liquid Flow"**, *Clarendon Press, Oxford.*

Wicaksanaa, F., Fanea, A., Law, A., (2009), **"The Use Of Constant Temperature Anemometry For Permeate Flow Distribution Measurement In A Submerged Hollow Fibre System"** *Journal of Membrane Science, 339, pp.195–203.*

Winter, K.G., (1977), **"An Outline of the Techniques Available For the Measurement of Skin Friction In Turbulent Boundary Layers"**, *Prog. Aerospace. Sci., vol.18, pp.1-57.*

Wolf, A. D., (1995), **"Film Structure Of Vertical Annular Flow"** *PhD thesis, Imperial college of Science, Technology and Medicine, London University.*

Yong Bai, and Qiang Bai, (2005), **"Subsea Pipelines and Risers"**, *1st Edition, Elsevier.*

Zabaras, G.,Dukler, A. E., and Moalem-Maron, D., (1986) "**Vertical Upward Co Current Gas-Liquid Annular Flow**", *AIChE Journal, Vol.32, No.5 pp.829-843.*